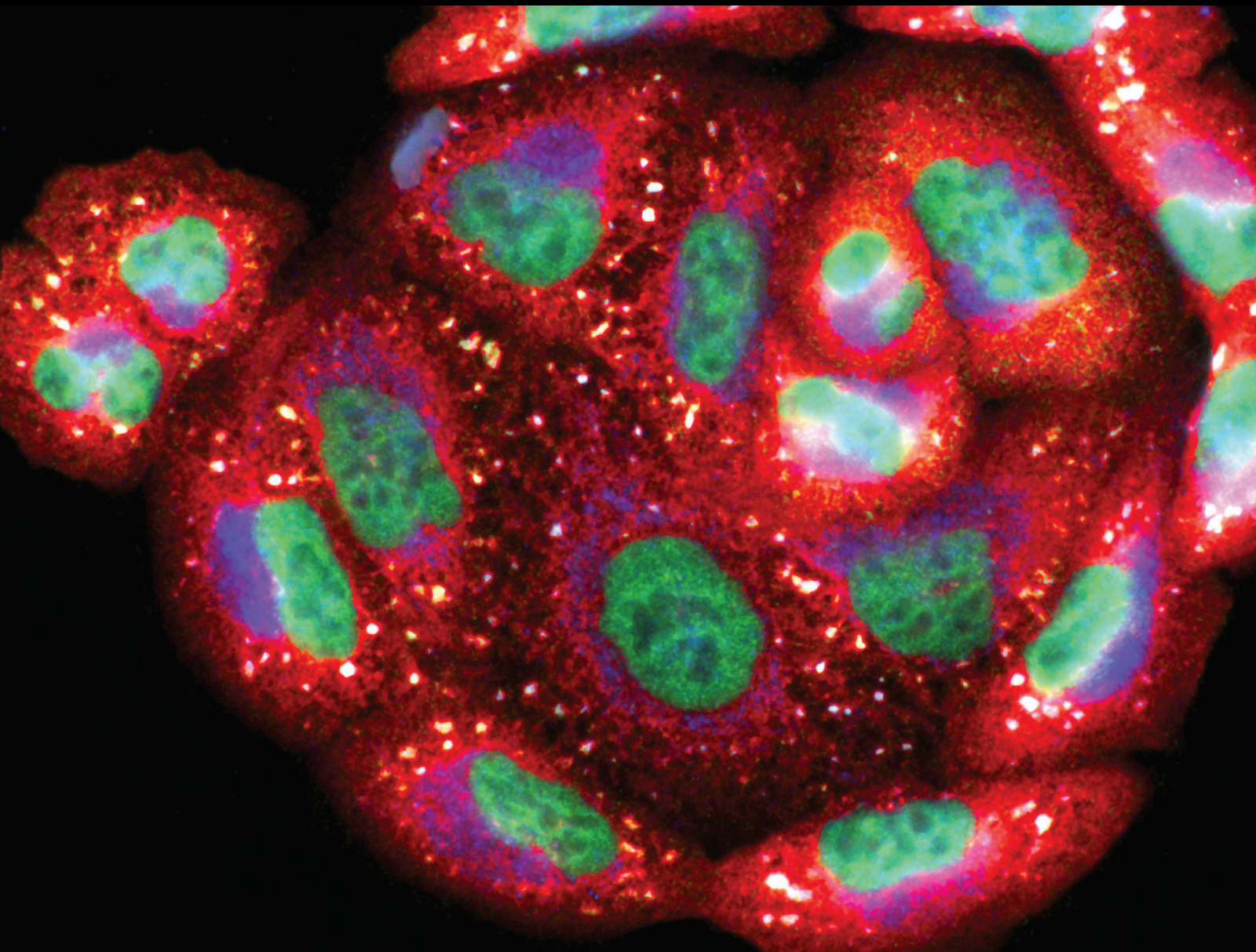# Oxidative Stress and Heart Failure: Mechanisms, Signalling Pathways, and Therapeutics

Lead Guest Editor: Luana Urbano Pagan
Guest Editors: Mariana Janini Gomes, Paula Felippe Martinez, and Marina Politi Okoshi

Oxidative Stress and Heart Failure: Mechanisms, Signalling Pathways, and Therapeutics

Oxidative Stress and Heart Failure: Mechanisms, Signalling Pathways, and Therapeutics

Lead Guest Editor: Luana Urbano Pagan
Guest Editors: Mariana Janini Gomes, Paula Felippe Martinez, and Marina Politi Okoshi

Chief Editor

Jeannette Vasquez-Vivar, USA

Editorial Board

Contents

LCZ696 Ameliorates Oxidative Stress and Pressure Overload-Induced Pathological Cardiac Remodeling by Regulating the Sirt3/MnSOD Pathway

Shi Peng (iD), Xiao-feng Lu, Yi-ding Qi, Jing Li, Juan Xu, Tian-you Yuan, Xiao-yu Wu, Yu Ding, Wen-hua Li, Gen-qing Zhou, Yong Wei, Jun Li, Song-wen Chen (iD), and Shao-wen Liu (iD)

Impact of Modality and Intensity of Early Exercise Training on Ventricular Remodeling after Myocardial Infarction

Diego Fernando Batista, Bertha Furlan Polegato, Renata Candido da Silva, Renan Turini Claro, Paula Shmidt Azevedo, Ana Angélica Fernandes, Katashi Okoshi, Sergio Alberto Rupp de Paiva, Marcos Ferreira Minicucci, and Leonardo Antônio Mamede Zornoff (iD)

Editorial

Oxidative Stress and Heart Failure: Mechanisms, Signalling Pathways, and Therapeutics

Luana Urbano Pagan [iD],[1] **Mariana Janini Gomes** [iD],[2] **Paula Felippe Martinez** [iD],[3] **and Marina Politi Okoshi** [iD][1]

[1]*Botucatu Medical School, Sao Paulo State University, UNESP, Botucatu, Brazil*
[2]*Brigham and Women's Hospital, Harvard Medical School, Boston, USA*
[3]*Integrated Institute of Health, Federal University of Mato Grosso do Sul, UFMS, Campo Grande, Brazil*

Correspondence should be addressed to Luana Urbano Pagan; luanapagan@alunos.fmb.unesp.br

Heart failure is an important public health issue due to its poor prognosis and high prevalence, morbidity, and mortality [1]. Heart failure is clinically characterized by a reduced capacity for physical exercise and daily activities as a result of the early occurrence of fatigue and dyspnea.

Oxidative stress, defined as an imbalance between oxygen radical production and scavenging, plays an important role in the pathophysiology of cardiac remodeling and heart failure [2, 3]. Clinical and experimental studies have provided substantial evidences that oxidative stress is increased in the myocardium and at a systemic level during heart failure [4, 5]. Although at physiological levels, reactive oxygen species (ROS) play important roles in intracellular pathways and redox signaling, they may induce cellular dysfunction and damage at higher levels. Despite extensive investigation, the molecular pathways involved in heart failure-associated oxidative stress are still not completely understood.

Common causes of heart failure include myocardial infarction, systemic arterial hypertension, valve disease, and cardiomyopathy [6]. This Special Issue consists of nine original articles that investigated cellular and molecular processes involved in the oxidative stress associated with heart failure. The manuscripts approached distinctive causes of heart failure in both humans and animals, improving our understanding of signaling pathways and mechanisms of novel targets for heart failure prevention and therapy. In this Editorial, we provide an overview of these articles highlighting the major finds of each one.

Several animal models that mimic heart failure have been used to gain insight into the complex biology of this disease [7–9]. Three studies included in this Special Issue investigated cardiotoxicity-induced heart failure caused by chemotherapy drugs widely used in cancer treatment. Zhang et al. [10] evaluated by peptidomics changes in peptide profiles related to doxorubicin- (DOX-) induced cardiotoxicity and successfully identified differentially expressed peptides in mouse cardiac tissue. Through bioinformatics analyses, the authors identified a candidate peptide for protecting the myocardium against DOX-induced cell apoptosis, thus providing a new approach for the treatment of DOX-induced cardiotoxicity. Modesto et al. [11] reinforced the oxidative stress role on the mechanisms involved in DOX-induced cardiotoxicity in rats. DOX leads to lipid peroxidation and lowered activity of antioxidant enzymes, which were combined with inflammation, energy metabolism changes, and cytotoxicity. Similarly, Gholami et al. [12] also demonstrated evidence to support the involvement of oxidative stress in the pathogenesis of cardiotoxicity induced by another chemotherapy drug, the arsenic trioxide. At least in part, green tea attenuated oxidative stress and cytotoxic damage. The authors revealed a link between the antioxidant effects of pentoxifylline and its therapeutic potential against cardiac oxidative damage.

Besides cardiotoxicity, this Special Issue presents manuscripts that investigated pressure overload-induced cardiac remodeling in different animal models. Horvath et al. [13]

investigated the cardioprotective effect of BGP-15, an insulin signaling-related molecule, in an animal model of hypertension-induced heart failure. Their major findings include a BGP-15 positive effect on cardiac function and the remodeling process by inhibition of profibrotic signaling factors and promotion of mitochondrial biogenesis. Zhang et al. [14] used a mouse model of pathological cardiac hypertrophy caused by transverse aortic constriction. The authors verified that the newfound proliferator-activated receptor-gamma coactivator (PGC)-1α/activating transcription factor 5 (ATF5) axis can partly activate mitochondrial unfolding protein response and mediate the protective role of tetrahydrocurcumin against pressure overload-induced cardiac hypertrophy and oxidative stress. The results demonstrate a possible therapeutic action of tetrahydrocurcumin in heart failure caused by pressure overload. Also in the transverse aortic constriction model, Peng et al. [15] studied the effects of oxidative stress in inducing heart failure and unraveled a specific action mechanism underlying the role of LCZ696, a drug recommended for the treatment of heart failure with reduced ejection fraction. The authors showed that Sirt3 may be a therapeutic target in the heart failure treatment, as the cardioprotective effects of LCZ696 were partly mediated by the Sirt3-dependent pathway.

Considering inflammation associated with oxidative stress plays a role in the pathophysiology of many chronic diseases [16], including heart failure, animal models of sepsis have been often used to investigate molecular mechanisms involved in cardiac injury. Interleukin- (IL-) 16 is an important inflammatory mediator and a potential pharmacologic target in heart failure. The study by Zhang et al. [17] evaluated whether IL-16 participates in sepsis-induced cardiac injury and dysfunction in mice through the regulation of oxidative stress. The study demonstrated that IL-16 neutralization may positively regulate the Nrf2 pathway, reduce oxidative stress, and inhibit the transfer of mitochondrial apoptosis-inducing factor from mitochondria to the nucleus, and thus reduce cardiomyocyte apoptosis and myocardial injury and improve cardiac function in sepsis rats.

Pharmacological treatment recommended by guidelines for heart failure has progressed over the past decades and has improved the patient prognosis [18]. However, the importance of tailoring the treatment has been emphasized as different groups of patients benefit more from specific therapies. Wojciechowska et al. [19] analyzed the influence of the redox balance parameters on the prognosis of 707 patients with heart failure with reduced ejection fraction, taking into account ischemic and nonischemic etiology. The authors showed an association between different oxidative biomarkers in the heart failure progression depending on its etiology, therefore strengthening the importance of personalizing the heart failure treatment.

Beyond pharmacological treatment, physical exercise has been recommended as a nonpharmacological therapy for heart failure. Batista et al. [20] analyzed the impact of different modalities and intensities of exercise training on cardiac remodeling started early after experimental myocardial infarction. The authors showed that both high-intensity interval and continuous low-intensity modalities improved

cardiac energetic metabolism in comparison with control infarcted rats. In addition, high-intensity interval training decreased cardiac oxidative stress, which was associated with improved diastolic function.

We hope that this Special Issue has provided new insights into the pathways and mechanisms involved in oxidative stress associated with heart failure and stimulated new research ideas and collaborations that can benefit advances in the heart failure treatment.

Conflicts of Interest

We declare that none of the Guest Editors has a conflict of interest.

Acknowledgments

Luana Urbano Pagan
Mariana Janini Gomes
Paula Felippe Martinez
Marina Politi Okoshi

References

[1] C. W. Tsao, A. W. Aday, Z. I. Almarzooq et al., "Heart disease and stroke statistics-2022 update: a report from the American Heart Association," *Circulation*, vol. 145, no. 8, pp. e153–e639, 2022.

[2] H. Tsutsui, S. Kinugawa, and S. Matsushima, "Oxidative stress and heart failure," *American Journal of Physiology. Heart and Circulatory Physiology*, vol. 301, no. 6, pp. H2181–H2190, 2011.

[3] L. U. Pagan, M. J. Gomes, M. Gatto, G. A. F. Mota, K. Okoshi, and M. P. Okoshi, "The role of oxidative stress in the aging heart," *Antioxidants*, vol. 11, no. 2, article 336, 2022.

[4] P. F. Martinez, C. Bonomo, D. M. Guizoni et al., "Modulation of MAPK and NF-kappaB signaling pathways by antioxidant therapy in skeletal muscle of heart failure rats," *Cellular Physiology and Biochemistry*, vol. 39, no. 1, pp. 371–384, 2016.

[5] C. M. Rosa, R. Gimenes, D. H. Campos et al., "Apocynin influence on oxidative stress and cardiac remodeling of spontaneously hypertensive rats with diabetes mellitus," *Cardiovascular Diabetology*, vol. 15, no. 1, p. 126, 2016.

[6] R. H. G. Schwinger, "Pathophysiology of heart failure," *Cardiovascular Pathology*, vol. 11, no. 1, pp. 263–276, 2021.

[7] A. R. R. Lima, P. F. Martinez, R. L. Damatto et al., "Heart failure-induced diaphragm myopathy," *Cellular Physiology and Biochemistry*, vol. 34, no. 2, pp. 333–345, 2014.

[8] J. F. Guimaraes, B. P. Muzio, C. M. Rosa et al., "Rutin administration attenuates myocardial dysfunction in diabetic rats," *Cardiovascular Diabetology*, vol. 17, no. 14, p. 90, 2015.

[9] P. F. Martinez, C. Bonomo, D. M. Guizoni et al., "Influence of N-acetylcysteine on oxidative stress in slow-twitch soleus muscle of heart failure rats," *Cellular Physiology and Biochemistry*, vol. 35, no. 1, pp. 148–159, 2015.

[10] L. Zhang, X. Wang, M. Feng et al., "Peptidomics analysis reveals peptide pdcryab1 inhibits doxorubicin-induced

cardiotoxicity," *Oxidative Medicine and Cellular Longevity*, vol. 2020, Article ID 7182428, 23 pages, 2020.

[11] P. N. Modesto, B. F. Polegato, P. P. Dos Santos et al., "Green tea (Camellia sinensis) extract increased topoisomerase II β, improved antioxidant defense, and attenuated cardiac remodeling in an acute doxorubicin toxicity model," *Oxidative Medicine and Cellular Longevity*, vol. 2021, Article ID 8898919, 10 pages, 2021.

[12] A. Gholami, S. Ataei, D. Ahmadimoghaddam, N. Omidifar, and A. Nili-Ahmadabadi, "Pentoxifylline attenuates arsenic trioxide-induced cardiac oxidative damage in mice," *Oxidative Medicine and Cellular Longevity*, vol. 2021, Article ID 6406318, 10 pages, 2021.

[13] O. Horvath, K. Ordog, K. Bruszt et al., "BGP-15 protects against heart failure by enhanced mitochondrial biogenesis and decreased fibrotic remodelling in spontaneously hypertensive rats," *Oxidative Medicine and Cellular Longevity*, vol. 2021, Article ID 1250858, 13 pages, 2021.

[14] B. Zhang, Y. Tan, Z. Zhang et al., "Novel PGC-1 α/ATF5 axis partly activates UPR mt and mediates cardioprotective role of tetrahydrocurcumin in pathological cardiac hypertrophy," *Oxidative Medicine and Cellular Longevity*, vol. 2020, Article ID 9187065, 21 pages, 2020.

[15] S. Peng, X. F. Lu, Y. D. Qi et al., "LCZ696 ameliorates oxidative stress and pressure overload-induced pathological cardiac remodeling by regulating the Sirt3/mnSOD pathway," *Oxidative Medicine and Cellular Longevity*, vol. 2020, Article ID 9815039, 15 pages, 2020.

[16] Y. Ranneh, F. Ali, A. M. Akim, H. A. Hamid, H. Khazaai, and A. Fadel, "Crosstalk between reactive oxygen species and proinflammatory markers in developing various chronic diseases: a review," *Applied Biological Chemistry*, vol. 60, pp. 327–338, 2017.

[17] J. Zhang, Z. Yang, Z. Liang et al., "Anti-interleukin-16 neutralizing antibody treatment alleviates sepsis-induced cardiac injury and dysfunction via the nuclear factor erythroid-2 related factor 2 pathway in mice," *Oxidative Medicine and Cellular Longevity*, vol. 2021, Article ID 6616422, 11 pages, 2021.

[18] T. A. McDonagh, M. Metra, M. Adamo et al., "2021 ESC guidelines for the diagnosis and treatment of acute and chronic heart failure," *European Heart Journal*, vol. 42, no. 36, pp. 3599–3726, 2021.

[19] C. Wojciechowska, W. Jacheć, E. Romuk et al., "Serum sulfhydryl groups, malondialdehyde, uric acid, and bilirubin as predictors of adverse outcome in heart failure patients due to ischemic or nonischemic cardiomyopathy," *Oxidative Medicine and Cellular Longevity*, vol. 2021, Article ID 6693405, 14 pages, 2021.

[20] D. F. Batista, B. F. Polegato, R. C. Da Silva et al., "Impact of modality and intensity of early exercise training on ventricular remodeling after myocardial infarction," *Oxidative Medicine and Cellular Longevity*, vol. 2020, Article ID 5041791, 6 pages, 2020.

Research Article

Green Tea (*Camellia sinensis*) Extract Increased Topoisomerase IIβ, Improved Antioxidant Defense, and Attenuated Cardiac Remodeling in an Acute Doxorubicin Toxicity Model

Pamela N. Modesto [ID],[1] **Bertha F. Polegato** [ID],[1] **Priscila P. dos Santos**,[1] **Leticia D. V. Grassi**,[1] **Leticia C. C. Molina**,[1] **Silmeia G. Z. Bazan**,[1] **Elenize J. Pereira**,[1] **Ana Angelica H. Fernandes**,[2] **Alexandre T. Fabro**,[3] **Vickeline N. Androcioli**,[4] **Meliza G. Roscani**,[5] **Sergio A. R. de Paiva**,[1] **Leonardo A. M. Zornoff**,[1] **Marcos F. Minicucci**,[1] **and Paula S. Azevedo**[1]

[1]*Internal Medicine Department, Botucatu Medical School, São Paulo State University (UNESP), Botucatu, Brazil*
[2]*Department of Chemical and Biological Sciences, São Paulo State University (UNESP), Botucatu, Brazil*
[3]*Department of Pathology and Legal Medicine, Ribeirão Preto Medical School, University of São Paulo (UNESP), Ribeirão Preto, Brazil*
[4]*Experimental Research Unit (UNIPEX), Botucatu Medical School, São Paulo State University (UNESP), Botucatu, Brazil*
[5]*Medicine Department, São Carlos Federal University, São Paulo State, Brazil*

Correspondence should be addressed to Pamela N. Modesto; pamela.nutri@hotmail.com

Experimental studies have shown the action of green tea in modulating cardiac remodeling. However, the effects of green tea on the cardiac remodeling process induced by doxorubicin (DOX) are not known. Therefore, this study is aimed at evaluating whether green tea extract could attenuate DOX-induced cardiac remodeling, assessed by cardiac morphological and functional changes and associated with the evaluation of different modulators of cardiac remodeling. The animals were divided into four groups: the control group (C), the green tea group (GT), the DOX group (D), and the DOX and green tea group (DGT). Groups C and GT received intraperitoneal sterile saline injections, D and DGT received intraperitoneal injections of DOX, and GT and DGT were fed chow supplemented with green tea extract for 35 days prior to DOX injection. After forty-eight hours, we performed an echocardiogram and euthanasia and collected the materials for analysis. Green tea attenuated DOX-induced cardiotoxicity by increasing cardiac function and decreasing the concentric remodeling. Treatment with DOX increased oxidative stress in the heart, marked by a higher level of lipid hydroperoxide (LH) and lower levels of antioxidant enzymes. Treatment with green tea increased the antioxidant enzymes' activity and decreased the production of LH. Green tea extract increased the expression of Top2-β independent of DOX treatment. The activity of ATP synthase, citrate synthase, and complexes I and II decreased with DOX, without the effects of green tea. Both groups that received DOX presented with a lower ratio of P-akt/T-akt and a higher expression of CD45, TNFα, and intermediate MMP-2, without the effects of green tea. In conclusion, green tea attenuated cardiac remodeling induced by DOX and was associated with increasing the expression of Top2-β and lowering oxidative stress. However, energy metabolism and inflammation probably do not receive the benefits induced by green tea in this model.

1. Introduction

Doxorubicin-induced toxicity is a severe cardiooncology problem in children and adults. Doxorubicin (DOX) is a chemotherapeutic drug with a broad spectrum of activity against various hematological and solid tumors [1]. But its adverse effects limit the use of this drug [2]. One of the most critical side effects is acute or chronic cardiotoxicity. The number of cancer survivors has been increasing, which means there is a larger pool of people who are suitable to become cardiac patients [1, 3]. For example, it is estimated that 70% of breast cancer patients will survive at least five years [3].

There are four types of cardiotoxicity caused by DOX: acute, subacute, chronic, and late toxicity [4]. Arrhythmia, ventricular dilation, and diastolic and systolic dysfunction characterize DOX-induced cardiotoxicity [5]. Considering the variety of clinical presentations, it is not easy to precisely specify the incidence and prevalence. But researchers have reported an incidence of lower ejection fraction (<50%) at 9%, within one year after DOX administration [1, 6]. In addition, 32% of adult survivors of childhood cancer had evidence of cardiac dysfunction by global longitudinal strain [7].

Although there has been increasing interest and substantial research conducted regarding DOX-induced cardiotoxicity, a definitive picture of the mechanisms involved in it remains unclear [8]. Studies have suggested that DOX-induced mitochondrial dysfunction is a crucial cause of cardiotoxicity [9]. In addition, the interaction of DOX with iron, generation of reactive oxygen species (ROS), and the binding of DOX with topoisomerase II (Top2-β) have proven to be central mechanisms [10]. Therefore, plant-derived polyphenols, well known as rich sources of antioxidants, could have a potential role in preventing or, at least, attenuating the cardiotoxicity in this clinical setting [11].

Green tea (*Camellia sinensis*) is one of the most widely consumed beverages in the world. The common bioactive compounds found in green teas have a polyphenol structure, including flavan-3-ols (catechins), proanthocyanidins (tannins), and flavonols, the biological properties of which are antioxidant, anticancer, antithrombotic, and anti-inflammatory activities [12, 13].

Experimental studies have shown the action of green tea in modulating cardiac remodeling. For example, in the experimental model of myocardial infarction, green tea attenuated cardiac remodeling through the modulation of metabolism, oxidative stress, and apoptosis [14]. But the effects of green tea on the cardiac remodeling process induced by DOX are not known. Therefore, this study is aimed at evaluating whether green tea extract could attenuate DOX-induced cardiac remodeling, as assessed by cardiac morphological and functional changes and associated with the evaluation of different modulators of cardiac remodeling, including Top2-β, oxidative stress, energy metabolism, inflammation, and extracellular matrix components.

2. Materials and Methods

The study was approved by The Ethics Committee on Animal Experiments of our institution, and we provided care according to the *Guide for the Care and Use of Laboratory Animals* published by the National Institutes of Health (NIH publication 85–23, revised 1996). We used male Wistar rats weighing between 250 and 300 g, which were acquired from the central animal facility of our institution. The animals were divided into four groups: the control group (C; $n = 15$), which consumed standard chow and received intraperitoneal sterile saline injections; the green tea group (GT; $n = 15$), which consumed food supplemented with green tea extract and received intraperitoneal sterile saline injections; the DOX group (D; $n = 15$), which consumed standard chow and received intraperitoneal injections of

DOX; and the DOX/green tea group (DGT; $n = 15$), which consumed food supplemented with green tea extract and received intraperitoneal injections of DOX, and the animals that had food added with green tea received the same for 35 days, prior to DOX injection. The green tea extract used was Polyphenon 60 (Sigma-Aldrich Canadá, Oakville, ON, Canadá). Considering a Wistar rat's feed intake, about 30 g/day, each animal had an intake equivalent to six or seven cups of green tea per day in 60 kg humans [14]. All groups received intraperitoneal injections of DOX or intraperitoneal injections of sterile saline measuring 20 mg/kg weight, respectively. This dose of DOX in rats is equivalent to 250 mg in a 70 kg human [15]. In Figure 1, it is possible to identify how the present study was carried out.

2.1. Echocardiography. All animals were submitted to echocardiographic evaluation prior to and forty-eight hours after the DOX injection. The rats were anesthetized with an intramuscular injection of a mixture of ketamine (50 mg/kg) and xylazine (0,5 mg/kg). The apparatus used for evaluation was the HDI 5500 (Philips), equipped with a multifrequency transducer of 7–12 MHz. The examinations were performed by the same examiner (an experienced cardiologist), who did not know which of the previously established groups the animals belonged to. The method was previously set in our group [16, 17].

2.2. Morphometric Analysis. Forty-eight hours after the echocardiographic study, we euthanized the animals with a high dose of pentobarbital, dissected their hearts, and collected the blood. Part of the heart was stored in a freezer at −80°C for later analysis. Transverse sections of the left ventricle were fixed in 4% buffered formalin and embedded in paraffin.

2.3. Oxidative Stress and Energy Metabolism. We used samples from the left ventricle for protein quantification. Samples of approximately 200 g from the left ventricle were homogenized in sodium phosphate buffer (0,1 M, pH 7,0) and centrifuged at 10,000 rpm for 15 minutes at -4°C, and supernatant helped to determine the concentration of lipid hydroperoxide (LH) and the activity of antioxidant enzymes, because the lipid hydroperoxide in the myocardium served as an oxidation marker of oxidation. We also evaluated the activity of the antioxidant enzymes catalase (CAT), superoxide dismutase (SOD), and glutathione peroxidase (GPx) in the myocardium and determined the concentrations according to previously described methods [18, 19]. On the energetic metabolism, we evaluated the activity of phosphofructokinase (PFK), 3-hydroxyacyl coenzyme A dehydrogenase (3-OHADH), lactate dehydrogenase (LDH), pyruvate dehydrogenase (PDH), and citrate synthase (CS). We also evaluated the activity of the enzymatic complex of the mitochondrial respiratory chain I, complex II, and ATP synthase activity according to the method described above [19, 20].

2.4. Western Blot. We extracted left ventricle samples using RIPA buffer for detection of TNFα, collagen I and III, AMPKα, PPARα, phosphorylated/nonphosphorylated AKT, and Top2-β. We then centrifuged the samples at 12,000 rpm at 4°C for 20 minutes and collected the supernatant. We
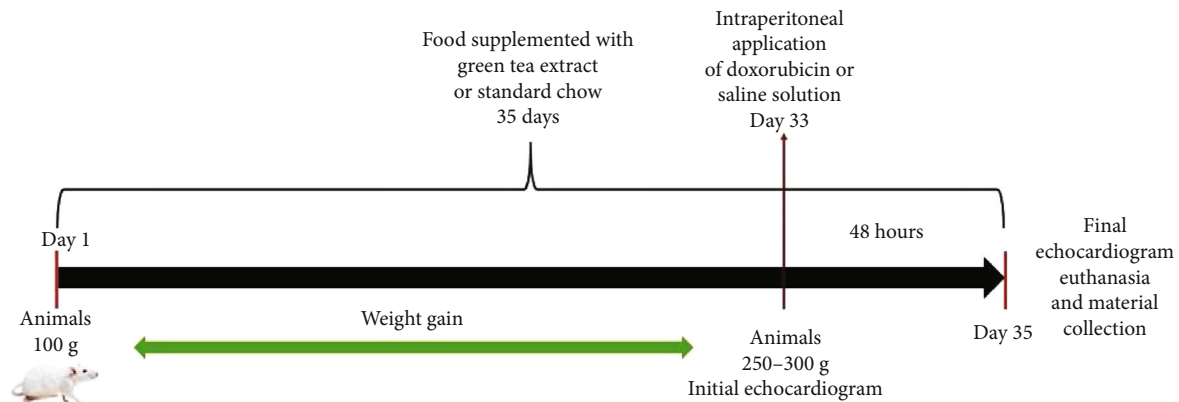
FIGURE 1: Study development. On day one, we received the animals at approximately 100 g. Since then, they started to received their respective chow. When they reached a weight between 250 g and 300 g, we performed the first echocardiogram and intraperitoneal injection of DOX or saline solution according to which group the animals belonged to. On the thirty-fifth day, at forty-eight hours after administering the DOX or saline solution, we euthanized the animals and collected the blood and cardiac samples for analysis.

quantified the proteins present in the supernatant using the Bradford method. The SDS-polyacrylamide gel and the protein were transferred to a nitrocellulose membrane. The membrane was blocked with 5% skimmed milk powder in Tris buffer containing 1 M Tris, pH 8,0, 5 M NaCl, and Tween 20 at room temperature for 1 hour 30 minutes. The membranes were incubated with their respective primary antibodies (Table 1) for 12 hours. We then washed the membrane with Tris-buffered saline (TBS) and Tween 20 and incubated it with the peroxidase-conjugated secondary antibody (Table 2) for 1 hour 30 minutes. We also performed the same procedures to determine GAPDH, which we used as a normalizer for the described proteins. With the data generated by the Carestream Molecular Imaging Analyzer (Carestream, Inc., USA), the quantification was performed as follows: we normalized the proteins of interest for one standard sample of one animal and repeated on all the gels; we normalized the GAPDH in the same way by the animal and repeated in all the gels; the proteins (already normalized) were then normalized by the GAPDH (already normalized), to obtain the result of the expression by western blot.

2.5. Determination of Cardiac Metalloproteinase Activity: Zymography.

We performed the zymography according to the method described previously [21, 22]. Briefly, we used 30 mg of cardiac tissue, added it to an extraction buffer, macerated and centrifuged it, and collected the supernatant. We used the Bradford method to quantify the proteins [23]. We identified three bands corresponding to metalloprotease 2 (MMP-2): inactive MMP-2 (pro-MMP-2), with a molecular weight of approximately 75 kDa, and the active form (active MMP-2), with a molecular weight of approximately 62 kDa, and an intermediate band with a molecular weight 66 kDa [24]. We normalized the quantification of MMP-2 activity by the control animal, which was repeated in all gels [25]. In addition, we determined the activity rate using the proportion of active/inactive bands.

2.6. Morphological Study.

We dissected the hearts and sectioned the left ventricle at 4 mm from the apex in a 3 mm thick fragment, which was fixed in a 4% buffered formalin solution for 48 hours, according to previous reports [26]. After fixation, we included the tissue in paraffin blocks and obtained coronal sections for posterior histological analysis. We prepared the blades with coronal histological sections and stained them using the Picro Sirius red technique, used specifically for the visualization of collagen. We analyzed 30 to 40 fields per ventricle, excluding perivascular collagen. We made readings using a 40x objective, polarized light, LEICA DM LS microscope, which was coupled to a video camera that sent digital images to a computer equipped with the image analysis program Image-Pro Plus (Media Cybernetics, Silver Spring, Maryland, USA). We calculated the average of the collagen fractional area by the percentage of red color (collagen) per field [26].

2.7. Immunohistochemistry.

In brief, we dewaxed cardiac tissue in xylene and alcohols, then recovered the antigens using sodium citrate tribasic dihydrate (SIGMA, S4641) in a steamer at 60°C for 20 minutes, followed by peroxidase blockage (3% hydrogen peroxide). Next, we incubated the primary antibody, anti-CD45 (1 : 50, 550539; BD Biosciences), overnight, then incubated it with Histofine Simple Stain Rat MAX PO polymer (MULTI; Nichirei/414191F), which is a combining amino acid polymer with peroxidase (PO) and a secondary antibody, for 1 hour. Then, we applied diamine benzidine chromogen (DAB; Thermo Scientific kit—UltraVision Quanto Detection System; TA-060-HDX) for 30 seconds, followed by a counterstain with hematoxylin (Mayer's hematoxylin solution, SIGMA MHS16-500 ml). We captured digitized images (200 magnification) using a video camera attached to a microscope (Leica Microsystems, Germany). We quantified CD45 in a way similar to the procedure for the collagen fractional area. We measured it by the sum of the percentage of brown cells (CD45) per field [27].

2.8. Statistical Analysis.

We evaluated the results by comparing groups using a two-way ANOVA. The statistical analysis considered the interaction between the two factors, DOX and green tea, showing a P value for this comparison (P_i). If P_i

TABLE 1: Concentrations of primary antibodies used for western blot.

Antibody		Dilution (μl)
TNFα	Cell Signaling Technology; cs 11948S	1/1000
Collagen I	Santa Cruz, sc 293182	1/100
Collagen III	Santa Cruz, sc 271249	1/100
AMPKα	Cell Signaling Technology; cs 2532S	1/1000
PPARα	Santa Cruz; sc-9000 (H-98)	1/100
Phosphorylated AKT	Cell Signaling Technology (Ser473); cs 4060S	1/2000
AKT	Cell Signaling Technology; cs 9272	1/1000
Top2-β	Abcam; ab109524	1/10000
GAPDH	Santa Cruz; sc 32233	1/10000

TABLE 2: Secondary antibody concentrations used for western blot.

Analyzed protein	Antibody	Dilution (μl)
TNFα	Mouse anti-rabbit sc-2357	1/5000
Collagen I	Mouse anti-rabbit sc-2357	1/2000
Collagen III	Mouse anti-mouse sc-2005	1/1000
AMPKα	Mouse anti-rabbit sc-2357	1/5000
PPARα	Mouse anti-mouse sc-2005	1/10000
Phosphorylated AKT	Mouse anti-rabbit sc-2357	1/5000
AKT	Mouse anti-rabbit sc-2357	1/5000
Top2-β	Mouse anti-rabbit sc-2357	1/5000
GAPDH	Mouse anti-mouse sc-2005	1/10000

was less than 0,05, the two-way ANOVA was completed by the Holm-Sidak test to find which group was different from the others.

If there was no interaction among the groups, the statistical test compared both groups treated with DOX (D and DGT) versus the groups not treated with DOX (C and GT), showing a P value for the presence of the DOX factor (P_{d}). The same was stated for the presence or absence of the green tea factor, where GT and DGT were compared with C and D, showing a P value (P_{gt}).

The level of significance was 5%. The variables were presented as a mean ± standard deviation. Data with nonnormal distributions were normalized for comparison.

3. Results

We performed an echocardiogram prior to DOX injection to assess whether there was homogeneity among the groups. There were no differences between the groups (data not shown).

Table 3 shows the echocardiographic evaluation after forty-eight hours of treatment with DOX, which decreased the heart rate and increased left atrium (LA). Green tea attenuated DOX-induced remodeling by increasing the heart rate and decreasing LA, posterior wall thickness (PWT), and relative wall thickness (RWT).

Treatment with DOX increased oxidative stress in the heart, marked by a higher level of LH and lower levels of CAT, SOD, and GPx. Treatment with green tea extract (DGT) increased the antioxidant enzymes' activity (SOD, GPx) and decreased the production of LH, as shown in Table 4. Considering energy metabolism, in the D group, the activity of glycolytic enzymes PFK and LDH increased and the activity of 3-OHADH, from FA oxidation, decreased. Green tea attenuated DOX effects on glycolytic and FA oxidation pathways. The activity of ATP synthase, from electron transport chains, decreased in the D group, but green tea could not recover this. DOX reduced the activity of CS, from the citrate cycle and complexes I and II in both groups D and DGT, as shown in Table 5.

In relation to proteins analyzed by western blot, green tea extracts increased the expression of AMPKα and PPARα in only animals that did not receive DOX. Green tea extracts increased the expression of Top2-β independent of DOX treatment. Both groups that received DOX presented with a lower ratio of P-akt/T-akt, a higher expression of TNFα, and intermediate activity of MMP-2, regardless of the presence of green tea, as shown in Figure 2 and Table 6.

In the present study, CD45 expression was higher in animals receiving DOX (D and DGT) when compared with groups that did not receive DOX (C and GT), regardless of the presence of green tea. When analyzed for interstitial collagen and expression of collagen I and III, there was no statistical difference between the groups, as shown in Figure 3.

4. Discussion

The aim of this study was to evaluate the effects of green tea on cardiac remodeling induced by DOX. Our data suggest that green tea attenuated the remodeling process. Among the mechanisms involved in DOX-induced cardiotoxicity, we observed that participation of oxidative stress, leading to lipid peroxidation and lowered activity of antioxidant enzymes, which corresponded with higher inflammation, abnormalities in energy metabolism, and cytotoxicity. At least in part, green tea attenuated oxidative stress and cytotoxic damage.

There are different experimental models to study DOX-induced cardiotoxicity. We chose an acute injury pattern, as described previously [25]. In fact, after a few hours of DOX infusion, the presence of inflammation and myocardial damage has already been detected [28]. Electrocardiogram abnormalities have been evidenced within twenty-four hours after DOX infusion in up to 30% of patients [29]. In the present

TABLE 3: Echocardiography forty-eight hours after doxorubicin injection.

	C ($n = 15$)	GT ($n = 15$)	D ($n = 15$)	DGT ($n = 15$)	P_i	P_{gt}	P_d
HR (bpm)	$367 \pm 9, 50$	$335 \pm 10, 5$	$290 \pm 9, 82$	$305 \pm 9, 82$	0,02	0,39	<0,001
LVDD/c (mm)	$20, 5 \pm 0, 66$	$19, 9 \pm 0, 73$	$20, 9 \pm 0, 67$	$21, 0 \pm 0, 67$	0,55	0,69	0,29
LVSD/c (mm)	$10, 1 \pm 0, 72$	$9, 26 \pm 0, 79$	$10, 7 \pm 0, 74$	$9, 96 \pm 0, 74$	0,94	0,28	0,39
PWT/c (mm/g)	$4, 39 \pm 0, 17$	$4, 15 \pm 0, 19$	$4, 76 \pm 0, 17$	$3, 97 \pm 0, 17$	0,01	0,006	0,58
RWT	$0, 42 \pm 0, 02$	$0, 42 \pm 0, 02$	$0, 46 \pm 0, 02$	$0, 38 \pm 0, 02$	0,03	0,08	0,93
LA/c (mm/g)	$10, 1 \pm 0, 45$	$11, 1 \pm 0, 48$	$12, 3 \pm 0, 45$	$11, 3 \pm 0, 48$	0,004	0,93	0,01
LA/AO (mm)	$1, 03 \pm 0, 05$	$1, 15 \pm 0, 05$	$1, 14 \pm 0, 05$	$01, 15 \pm 0, 05$	0,26	0,22	0,27
A (cm/s)	$78, 0 \pm 4, 63$	$78, 4 \pm 4, 88$	$49, 0 \pm 4, 63$	$68, 4 \pm 4, 88$	0,05	0,03	<0,001
E (cm/s)	$88, 1 \pm 9, 23$	$82, 7 \pm 4, 46$	$72, 8 \pm 4, 22$	$74, 2 \pm 4, 48$	0,44	0,65	0,001
E/A	$1, 18 \pm 0, 11$	$1, 11 \pm 0, 12$	$1, 60 \pm 0, 11$	$1, 09 \pm 0, 12$	0,07	0,02	0,09
IRTc (m/s)	$4, 08 \pm 0, 06$	$3, 99 \pm 0, 06$	$4, 11 \pm 0, 06$	$4, 08 \pm 0, 06$	0,60	0,30	0,35
SF	$0, 51 \pm 0, 02$	$0, 53 \pm 0, 03$	$0, 49 \pm 0, 02$	$0, 53 \pm 0, 02$	0,72	0,24	0,74
LVMI	$1, 75 \pm 0, 33$	$1, 71 \pm 0, 39$	$1, 92 \pm 0, 39$	$1, 72 \pm 0, 39$	0,37	0,19	0,35

Groups: C: control; GT: green tea; D: doxorubicin; DGT: doxorubicin+green tea. HR: heart rate in beats per minute; LVDD/c: left ventricular diastolic diameter corrected for body weight; LVSD/c: left ventricular systolic diameter corrected for body weight; PWT: posterior wall thickness; LA/c: left atrium diameter corrected for body weight; LA/AO: left atrium diameter corrected for aorta; A: wave ratio (represents the peak velocity of transmitral flow during atrial contraction); E: wave ratio (represents the peak velocity of early ventricular filling); IRTc: isovolumetric relaxation time; SF: shortening fraction. Values are expressed in mean ± standard deviation. P value: two-way ANOVA. P_i: P value of interaction; P_{gt}: P value of green tea; P_d: P value of doxorubicin. When we observed the interaction between factors doxorubicin and green tea, we considered $P_i < 0, 05$. HR: C ≠ GT, C ≠ D, and DGT ≠ D. PWT/c: D ≠ DGT. LA/c: D ≠ C, DGT ≠ D. RWT: D ≠ DGT. Comparisons without interaction: a wave and E/A: (GT + DGT) ≠ (C + D), A and E waves: (C + GT) ≠ (D + DGT).

TABLE 4: Cardiac oxidative stress forty-eight hours after doxorubicin injection.

	C ($n = 8$)	GT ($n = 8$)	D ($n = 6$)	DGT ($n = 6$)	P_i	P_{gt}	P_d
LH (nmol/g of tissue)	$206 \pm 34, 2$	$181 \pm 6, 30$	$265 \pm 18, 0$	$166 \pm 8, 97$	<0,001	0,002	0,22
CAT (μmol/g of tissue)	$59, 1 \pm 10, 5$	$37, 4 \pm 7, 01$	$34, 8 \pm 7, 18$	$41, 4 \pm 5, 24$	0,002	0,30	<0,001
SOD (nmol/g of tissue)	$17, 1 \pm 1, 40$	$16, 7 \pm 2, 46$	$13, 4 \pm 0, 10$	$11, 2 \pm 2, 82$	0,01	0,01	<0,001
GPx (nmol/g of tissue)	$27, 6 \pm 9, 10$	$28, 3 \pm 1, 72$	$13, 7 \pm 6, 05$	$20, 5 \pm 2, 00$	0,01	0,70	<0,001

Groups: C: control; GT: green tea; D: doxorubicin; DGT: doxorubicin+green tea. LH: lipid hydroperoxide; CAT: catalase; SOD: superoxide dismutase; GPx: glutathione peroxidase. Values are expressed in mean ± standard deviation. P value: two-way ANOVA. P_i: P value of interaction; P_{gt}: P value of green tea; P_d: P value of doxorubicin. We observed the interaction between factors in all the variables evidenced by $P_i < 0, 05$. LH: D ≠ DGT, D ≠ C. CAT: C ≠ GT, CP ≠ D. SOD: C ≠ GT, C ≠ D, and GT ≠ DGT. GPx: D ≠ DGT, C ≠ D.

TABLE 5: Cardiac energy metabolism forty-eight hours after doxorubicin injection.

	C ($n = 8$)	GT ($n = 8$)	D ($n = 6$)	DGT ($n = 6$)	P_i	P_{gt}	P_d
PFK (nmol/g tissue)	$0, 90 \pm 0, 28$	$1, 28 \pm 0, 34$	$1, 86 \pm 0, 31$	$1, 16 \pm 0, 41$	<0,001	0,23	0,003
LDH (nmol/mg tissue)	$3, 51 \pm 0, 25$	$3, 50 \pm 0, 15$	$7, 69 \pm 1, 41$	$5, 05 \pm 0, 51$	<0,001	<0,001	<0,001
PDH (nmol/g tissue)	$1, 03 \pm 0, 21$	$0, 97 \pm 0, 10$	$1, 03 \pm 0, 14$	$0, 88 \pm 0, 13$	0,46	0,10	0,42
CS (nmol/mg tissue)	$48, 22 \pm 8, 58$	$45, 52 \pm 5, 05$	$29, 05 \pm 5, 68$	$35, 48 \pm 6, 22$	0,08	0,46	<0,001
3-OHADH (nmol/mg tissue)	$20, 91 \pm 2, 10$	$19, 79 \pm 2, 74$	$10, 60 \pm 1, 56$	$18, 89 \pm 2, 24$	<0,001	0,55	<0,001
Complex I (nmol/mg tissue)	$44, 38 \pm 5, 97$	$45, 9 \pm 5, 20$	$34, 2 \pm 4, 42$	$30, 20 \pm 6, 14$	0,19	0,55	<0,001
Complex II (nmol/mg tissue)	$9, 16 \pm 1, 97$	$8, 53 \pm 1, 75$	$4, 80 \pm 1, 23$	$5, 57 \pm 0, 88$	0,26	0,91	<0,001
ATPs (nmol/mg tissue)	$25, 39 \pm 3, 00$	$21, 86 \pm 2, 89$	$16, 55 \pm 2, 02$	$18, 83 \pm 5, 15$	0,03	0,63	<0,001

Groups: C: control; GT: green tea; D: doxorubicin; DGT: doxorubicin+green tea. PFK: phosphofructokinase; LDH: lactate dehydrogenase; PDH: pyruvate dehydrogenase; CS: citrate synthase; β-OHADH: L-3-hydroxyacyl CoA dehydrogenase; complex I (NADH dehydrogenase): nicotinamide adenine nucleotide dehydrogenase; complex II: succinate oxide reductase; ATPs: adenosine triphosphate synthase. Values are expressed in mean ± standard deviation. P value: two-way ANOVA. P_i: P value of interaction; P_{gt}: P value of green tea; P_d: P value of doxorubicin. When we observed the interaction between factors ($P_i < 0, 05$), we compared the groups. PFK: C ≠ D, C ≠ GT, and D ≠ DGT; LDH: C ≠ DX, C ≠ GT, and D ≠ DGT; β-OHADH: C ≠ D, C ≠ GT, and D ≠ DGT; ATPs: C ≠ D, C ≠ GT. Comparisons without interactions: CS, complex I, complex II: (C + GT) ≠ (D + DGT).
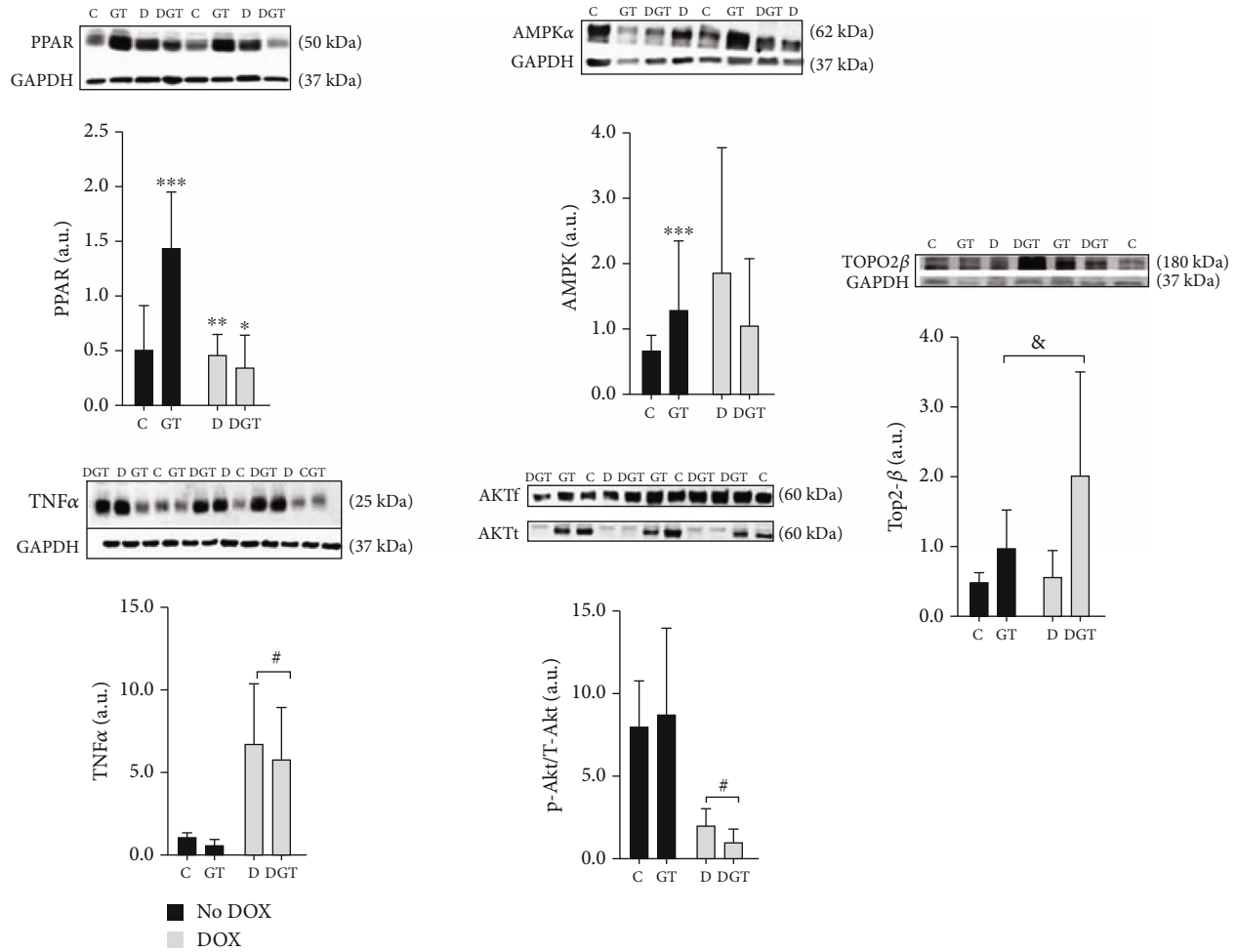
FIGURE 2: Plot and western blot images showed the expression of proteins in the heart forty-eight hours after injection with doxorubicin (DOX). Groups: C: control; GT: green tea; D: doxorubicin; DGT: doxorubicin+green tea. PPARα: peroxisome proliferator-activated receptor; AMPKα: activated protein kinase; TNFα: tumor necrosis factor-alpha; P-akt/T-akt: protein kinase B phosphorylated; Top2-β: topoisomerase IIβ. P_i: P value for interaction between factors GT and DOX. P_{gt}: P value for the differences between the groups with GT and without GT; P_d: P value for the differences between the groups with DOX and without DOX. For PPARα: $P_i = 0,001$ and AMPKα: $P_i = 0,04$, there were interactions between GT and DOX. Thus, for PPARα and AMPKα, we considered *DGT ≠ C, **D ≠ GT, ***C ≠ GT, and ****D ≠ GT. Comparisons without interaction considered the groups #DOX (D + DGT) ≠ no DOX (C + GT); &GT (GT + DGT) ≠ (C + D). For TNFα, $P_d = 0,01$ and for P-akt/T-akt, $P_d = 0,02$. For Top2-β, $P_{gt} = 0,03$.

TABLE 6: Matrix metalloproteinase (MMP-2) activation in myocardial tissue forty-eight hours after injection of doxorubicin.

	C ($n = 6$)	GT ($n = 6$)	D ($n = 6$)	DGT ($n = 6$)	P_i	P_{gt}	P_d
MMP-2at	9412 ± 6060	7690 ± 3939	11413 ± 10306	8468 ± 12171	0,85	0,49	0,68
MMP-2int.	21907 ± 10304	23576 ± 11532	54553 ± 26211	32163 ± 32206	0,16	0,23	0,02
MMP-2inat	35800 ± 21485	34116 ± 32446	48421 ± 29076	48677 ± 32498	0,93	0,95	0,24
MMP-2at/inat	$2,41 \pm 0,62$	$1,14 \pm 0,74$	$1,94 \pm 1,76$	$1,11 \pm 1,80$	0,81	0,79	0,72
MMP-2int/inat	$0,89 \pm 0,62$	$0,86 \pm 0,43$	$1,94 \pm 1,58$	$0,57 \pm 0,21$	0,09	0,13	0,53

Groups: C: control; GT: green tea; D: doxorubicin; DGT: doxorubicin+green tea. MMP-2a: active matrix metalloproteinase; MMP-2int: intermediary matrix metalloproteinase; MMP-2inat: inactive matrix metalloproteinase. Values are expressed in mean ± standard deviation. P value: two-way ANOVA. P_i: P value of interaction; P_{gt}: P value of green tea; P_d: P value of doxorubicin. When we observed the interaction between factors ($P_i < 0,05$), we compared the groups. MMP-2int: D ≠ C, D ≠ GT, DGT ≠ C, and DGT ≠ GT.
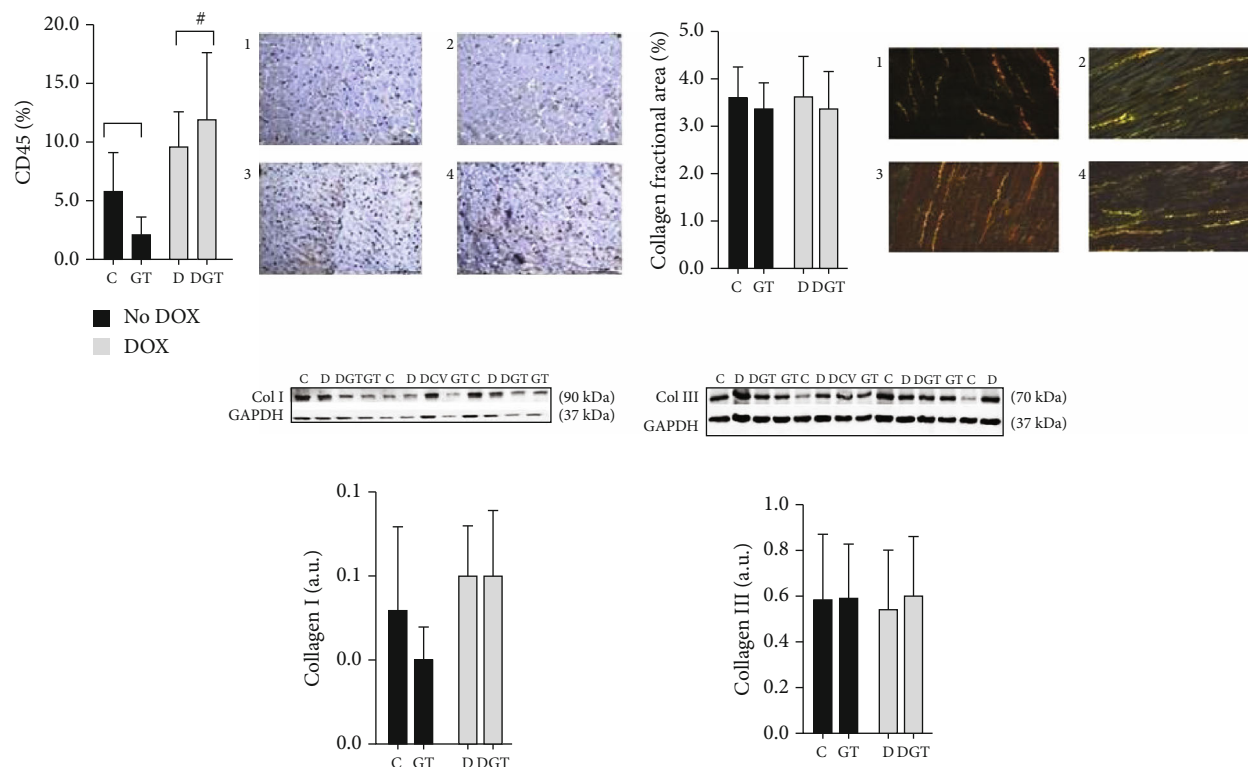
Figure 3: Inflammatory cells and interstitial collagen fraction. Groups: C: control; GT: green tea; D: doxorubicin; DGT: doxorubicin+green tea. In the microscopic images, animal 1 corresponds to group C; 2, GT; 3, DGT; and 4, D. Col I: collagen I; Col III: collagen III; box and bars are expressed in mean ± standard deviation. P_i: P value of interaction; P_{gt}: P value of green tea; P_d: P value of doxorubicin. After the statistical analysis using two-way ANOVA, no interactions were observed for these data. CD45: #comparisons without interaction considered the differences between: DOX (D + DGT) ≠ no DOX (C + GT): P_d value < 0,001. Collagen fractional area: Col I, Col III: all the comparisons presented $P > 0, 05$.

study, after forty-eight hours of DOX infusion, the main findings were an increase in RWT without an increase in ventricular mass, suggesting concentric remodeling and enlargement of LA, which may represent diastolic dysfunction. Both were attenuated by green tea. We also observed lower HR in the DOX group. Despite the fact that systolic dysfunction has been considered a hallmark of DOX-induced cardiotoxicity, the fractional shortening was not affected. However, in the rat model, a lower heart rate may represent systolic dysfunction [30]. Therefore, green tea attenuated morphological changes and improved diastolic and systolic dysfunction as well.

Top2-β is a protein that helps DNA fix topological difficulties and protects cells from being destroyed. DOX interacts with DNA and topoisomerase, forming the Top2-DOX-DNA complex, which increases the double-strand breakage, leading to cytotoxic effects [10]. This mechanism is in part responsible for the destruction of cancer cells and the drug's toxicity as well. Regarding the toxicity, the deletion of the Top2-β gene protected the heart from damage, confirming that this interaction in part mediates cardiotoxicity [31]. In addition, dexrazoxane, a drug that reduces Top2-β levels, protected the heart from cardiac damage [3, 32]. The contradictions here are remarkable, because in general topoisomerase is beneficial to cell survival, but it may

also exert a genotoxic role, depending upon the situation. Therefore, the role of topoisomerase levels and its interaction with DOX remains to be elucidated [10]. In the present study, the expression of nuclear Top2-β increased in both groups treated with green tea extract. On the other hand, the Top2-β expressions were similar in rats treated with DOX when compared with the control group. To our knowledge, this is the first study that investigates the expression of Top2-β within the green tea and DOX model. Therefore, our data shows that in the presence of green tea, higher levels of Top2-β are not associated with cardiac toxicity. Importantly, green tea has entered as a compound with synergic properties with DOX and other chemotherapy drugs, without increasing cardiotoxicity [33].

Oxidative stress plays a central role in DOX-induced cardiotoxicity. DOX is a substrate for oxireductase enzymes, resulting in a semiquinone radical that binds to iron, resulting in an iron-anthracycline complex that reduces oxygen by forming superoxide. Superoxide, alternatively, has a high affinity with cardiolipin, the main component of the internal membrane of mitochondria that is necessary for oxidative phosphorylation. Cardiolipin is rich in phospholipids and therefore, when interacting with superoxide or DOX, is susceptible to lipoperoxidation. The lipid peroxidation of the inner membrane of mitochondria impairs the transit of

ionic transporters, causing damage to energy transfer and increasing the production of ROS. In fact, researchers observed lower concentrations of antioxidants during cardiotoxicity induced by DOX [28, 30, 34]. The present study evidenced higher levels of lipid hydroperoxide (LH), a product of lipoperoxidation, and low levels of antioxidant enzymes induced by DOX. Importantly, green tea reversed those changes. Therefore, we can suggest that the attenuation of oxidative stress was one of the mechanisms involved in the beneficial effects of green tea.

Another potential mechanism involved in the action of green tea on cardiac remodeling is related to cardiac energy metabolism. Under normal conditions, fatty acids are the main substrates mitochondria use to supply energy to the heart. Between 60 and 90% of the heart's ATP is generated by the oxidation of fatty acids, and 10–40% is generated by glucose metabolism. Acetil coenzyme A is the common product of metabolism of FA and glucose, which enters the citrate cycle by generating electron carriers to the electron transport chain from complex I to V in the mitochondrial inner membrane. In complex V, adenosine diphosphate binds to phosphorus (ADP+P) to transform into adenosine triphosphate (ATP) under the action of ATP synthase [35].

In situations of cardiac remodeling, the heart exhibits several changes in energy metabolism, including a fuel preference shift, decreased fuel amount, mitochondrial abnormalities, and impaired transport of energy from mitochondria to the site of utilization [30]. In the present study, the energy metabolism was also involved in the DOX's effects, evidenced by the increased activity of PFK and LDH, suggesting that the anaerobic glycolytic pathway is stimulated. In addition, the decreased activity of 3-OHADH suggests an impairment in FA oxidation. The activity of CS from the citrate cycle, followed by complexes I and II and ATP synthase, was reduced in the D group, but the green tea extract failed to recover this imbalance. Although green tea increased the rate of lipid oxidation, this product did not interfere with the final process of energy production. Therefore, our results suggest that changes in energy metabolism are probably not one of the beneficial effects induced by green tea in this model.

Finally, DOX promotes the release of inflammatory cytokines that are involved in various conditions, including cardiotoxicity. In our study, we observed the elevation of inflammation by the increased activity of intermediate MMP-2, TNFα expression, and CD45, which is a common lymphocyte antigen, in both groups treated with DOX. But green tea had no influence on these inflammatory mediators. Therefore, our study did not demonstrate anti-inflammatory effects of green tea, at least with the analyzed variables. While the inflammatory process can produce oxidative stress, oxidative stress induces inflammation, as well. Therefore, they are closely linked, but it is challenging to define which one occurred first. While the inflammatory process can produce oxidative stress, oxidative stress induces inflammation, as well. Therefore, inflammation and oxidative stress are closely linked, but it is challenging to define which one occurred first. It is not possible to explain the lack of green tea anti-inflammatory effects in the presence of an antioxi-

dant attenuation in the present study. We might only hypothesize that green tea might have reduced oxidative stress first, via other reactive oxygen species sources [36].

5. Conclusion

In summary, the acute administration of DOX-induced cardiac remodeling, modulated by decreased Top2-β, increased oxidative stress and an imbalance in inflammation and energy metabolism. Animals previously fed with green tea extract-enriched chow and treated with DOX presented with greater measurements of cardiac remodeling and function associated with increasing Top2-β and lowering oxidative stress. Energy metabolism and anti-inflammation were not some of the beneficial effects induced by green tea in this model, though.

The present experimental study raises the hypothesis of green tea's beneficial effects on preventing cardiac toxicity, which might support future larger research in the clinical setting.

Data Availability

The data that support this study are available from the corresponding author upon reasonable request.

Conflicts of Interest

The authors declare that they have no conflicts of interest.

References

[1] D. Cappetta, F. Rossi, and E. Piegari, "Doxorubicin targets multiple players: a new view of an old problem," *Pharmacological Research*, vol. 127, pp. 4–14, 2017.

[2] A. Cuomo, A. Rodolico, A. Galdieri et al., "Heart failure and cancer: mechanisms of old and new cardiotoxic drugs in cancer patients," *Cardiac Failure Review*, vol. 5, no. 2, pp. 112–118, 2019.

[3] B. Kalyanaraman, "Teaching the basics of the mechanism of doxorubicin-induced cardiotoxicity: have we been barking up the wrong tree?," *Redox Biology*, vol. 29, article 101394, 2020.

[4] A. Ghigo, M. Li, and E. Hirsch, "New signal transduction paradigms in anthracycline-induced cardiotoxicity," *Biochimica et Biophysica Acta*, vol. 1863, no. 7, pp. 1916–1925, 2016.

[5] J. Yu, C. Wang, Q. Kong, X. Wu, J. J. Lu, and X. Chen, "Recent progress in doxorubicin-induced cardiotoxicity and protective potential of natural products," *Phytomedicine*, vol. 40, pp. 125–139, 2018.

[6] D. Cardinale, A. Colombo, G. Bacchiani et al., "Early detection of anthracycline cardiotoxicity and improvement with heart failure therapy," *Circulation*, vol. 131, no. 22, pp. 1981–1988, 2015.

[7] G. T. Armstrong, V. M. Joshi, K. K. Ness et al., "Comprehensive echocardiographic detection of treatment-related cardiac dysfunction in adult survivors of childhood cancer," *Journal of the American College of Cardiology*, vol. 65, no. 23, pp. 2511–2522, 2015.

[8] D. Cappetta, A. de Angelis, L. Sapio et al., "Oxidative stress and cellular response to doxorubicin: a common factor in the complex milieu of anthracycline cardiotoxicity," *Oxidative Medicine and Cellular Longevity*, vol. 2017, Article ID 1521020, 13 pages, 2017.

[9] M. A. Mitri and J. G. Edward, "Doxorubicin-induced heart failure: phenotype and molecular mechanisms," *International Journal of Cardiology, Heart and Vasculature*, vol. 10, pp. 17–24, 2015.

[10] W. Shi, H. Deng, J. Zhang, Y. Zhang, X. Zhang, and G. Cui, "Mitochondria-targeting small molecules effectively prevent cardiotoxicity induced by doxorubicin," *Journal Molecules*, vol. 23, no. 6, p. 1486, 2018.

[11] S. Shabalala, C. J. F. Muller, J. Louw, and R. Johnson, "Polyphenols, autophagy and doxorubicin-induced cardiotoxicity," *Life Sciences*, vol. 180, pp. 160–170, 2017.

[12] F. Malongane, L. J. Mcgraw, and F. N. Mudau, "The synergistic potential of various teas, herbs and therapeutic drugs in health improvement: a review," *Journal of the Science of Food and Agriculture*, vol. 97, no. 14, pp. 4679–4689, 2017.

[13] M. S. Butt, R. S. Ahmad, M. T. Sultan, M. M. N. Qayyum, and A. Naz, "Green tea and anticancer perspectives: updates from last decade," *Critical Reviews in Food Science and Nutrition*, vol. 55, no. 6, pp. 792–805, 2015.

[14] B. B. Lustosa, B. Polegato, M. Minicucci et al., "Green tea (*Cammellia sinensis*) attenuates ventricular remodeling after experimental myocardial infarction," *International Journal of Cardiology*, vol. 225, pp. 147–153, 2016.

[15] C. Tian, Q. Huang, L. Yang et al., "Green tea consumption is associated with reduced incident CHD and improved CHD-related biomarkers in the Dongfeng-Tongji cohort," *Nature Scientific Reports*, vol. 6, no. 1, pp. 1–7, 2016.

[16] M. Akhlagui and B. Bandy, "Dietary green tea extract increases phase 2 enzyme activities in protecting against myocardial ischemia-reperfusion," *Nutrition Research*, vol. 30, no. 1, pp. 32–39, 2010.

[17] M. L. Gazzana, J. J. Souza, and M. P. Okoshi, "Prospective echocardiographic evaluation 3 of right ventricle and pulmonary arterial 4 pressure in hyperthyroid patients," *Heart, Lung & Circulation*, pp. 1–7, 2018.

[18] R. M. Lang, M. Bierig, R. B. Devereux et al., "Recommendations for chamber quantification: a report from the American Society of Echocardiography's Guidelines and Standards Committee and the Chamber Quantification Writing Group, developed in conjunction with the European Association of Echocardiography, a branch of the European Society of Cardiology," *Journal of the American Society of Echocardiography*, vol. 18, no. 12, pp. 1440–1463, 2005.

[19] J. F. Ewing and D. R. Janero, "Microplate superoxide dismutase assay employing a nonenzymatic superoxide generator," *Analytical Biochemistry*, vol. 232, no. 2, pp. 243–248, 1995.

[20] V. G. Desai, R. Weindruch, R. W. Hart, and R. J. Feuers, "Influences of age and dietary restriction on gastrocnemius electron transport system activities in mice," *Archives of Biochemistry and Biophysics*, vol. 333, no. 1, pp. 145–151, 1996.

[21] F. R. F. Seiva, L. G. A. Chuffa, G. M. X. Ebaid, T. Silva, A. A. H. Fernandes, and E. L. B. Novelli, "Calorimetry, morphometry, oxidative stress, and cardiac metabolic response to growth hormone treatment in obese and aged rats," *Hormone Metabolic Response*, vol. 43, no. 6, pp. 397–403, 2011.

[22] S. C. Tyagi, L. Matsubara, and K. T. Weber, "Direct extraction and estimation of collagenase(s) activity by zymography in microquantities of rat myocardium and uterus," *Clinical Biochemistry*, vol. 26, no. 3, pp. 191–198, 1993.

[23] E. Castardeli, D. R. Duarte, M. F. Minicucci et al., "Tobacco smoke-induced left ventricular remodelling is not associated with metalloproteinase-2 or -9 activation," *European Journal of Heart Failure*, vol. 9, no. 11, pp. 1081–1085, 2007.

[24] M. M. Bradford, "A rapid and sensitive method for the quantitation of microgram quantities of protein utilizing the principle of protein-dye binding," *Analytical Biochemistry*, vol. 72, no. 1-2, pp. 248–254, 1976.

[25] F. S. Costa, M. J. L. Cardoso, L. M. R. Muniz et al., "Avaliação das metaloproteinases de matriz -2 e -9 em gatos com desmineralização óssea secundária à tirotoxicose induzida," *Arquivos brasileiro de medicina veterinária e zootecnia*, vol. 60, no. 5, pp. 1053–1060, 2008.

[26] B. F. Polegato, M. F. Minicucci, P. S. Azevedo et al., "Acute doxorubicin-induced cardiotoxicity is associated with matrix metalloproteinase-2 alterations in rats," *Cellular Physiology and Biochemistry*, vol. 35, no. 5, pp. 1924–1933, 2015.

[27] Y. Zhang, Y. Huang, A. Cantalupo et al., "Endothelial nogo-B regulates sphingolipid biosynthesis to promote pathological cardiac hypertrophy during chronic pressure overload," *JCI Insight*, vol. 1, no. 5, 2016.

[28] P. S. Azevedo, D. R. Duarte, M. F. Minicucci et al., "Papel da lipoperoxidação na intensificação da remodelação causada pelo betacaroteno após o infarto," *Arquivos Brasileiros de Cardiologia*, vol. 93, no. 1, pp. 34–38, 2009.

[29] M. Songbo, H. Lang, C. Xinyong, X. Bin, Z. Ping, and S. Liang, "Oxidative stress injury in doxorubicin-induced cardiotoxicity," *Toxicology Letters*, vol. 307, pp. 41–48, 2019.

[30] M. A. M. Lourenço, M. G. Braz, A. G. Aun et al., "Spondias mombinsupplementation attenuated cardiac remodelling process induced by tobacco smoke," *Journal of Cellular and Molecular Medicine*, vol. 22, no. 8, pp. 3996–4004, 2018.

[31] S. Zhang, X. Liu, T. Bawa-Khalfe et al., "Identification of the molecular basis of doxorubicin-induced cardiotoxicity," *Natural Medicine*, vol. 18, no. 11, pp. 1639–1642, 2012.

[32] S. Deng, T. Yan, C. Jendrny et al., "Dexrazoxane may prevent doxorubicin-induced DNA damage via depleting both topoisomerase II isoforms," *BMC Cancer*, vol. 14, no. 1, p. 842, 2014.

[33] E. Lecumberri, M. Y. Dupertuis, R. Miralbell, and C. Pichard, "Green tea polyphenol epigallocatechin-3-gallate (EGCG) as adjuvant in cancer therapy," *Clinical Nutrition*, vol. 32, no. 6, pp. 894–903, 2013.

[34] N. Wenningmann, M. Knapp, A. Ande, T. R. Vaidya, and S. Ait-Oudhia, "Insights into doxorubicin-induced

cardiotoxicity: molecular mechanisms, preventive strategies, and early monitoring," *Molecular Pharmacology*, vol. 96, no. 2, pp. 219–232, 2019.

[35] M. Lamberti, G. Giovane, E. M. Garzillo et al., "Animal models in studies of cardiotoxicity side effects from antiblastic drugs in patients and occupational exposed workers," *BioMed Research International*, vol. 2014, Article ID 240642, 8 pages, 2014.

[36] S. K. Biswas, "Does the interdependence between oxidative stress and inflammation explain the antioxidant paradox?," *Oxidative Medicine and Cellular Longevity*, vol. 2016, Article ID 5698931, 9 pages, 2016.

Research Article

Serum Sulfhydryl Groups, Malondialdehyde, Uric Acid, and Bilirubin as Predictors of Adverse Outcome in Heart Failure Patients due to Ischemic or Nonischemic Cardiomyopathy

Celina Wojciechowska [iD],[1] **Wojciech Jacheć** [iD],[1] **Ewa Romuk** [iD],[2] **Anna Ciszek** [iD],[3] **Patryk Bodnar** [iD],[3] **Tomasz Chwalba** [iD],[3] **Martyna Waliczek** [iD],[4] **Mariusz Gąsior** [iD],[5] **and Piotr Rozentryt** [iD][4,5]

[1]*Second Department of Cardiology, Faculty of Medical Sciences in Zabrze, Medical University of Silesia, M. C. Skłodowskiej 10 Street, 41-800 Zabrze, Poland*

[2]*Department of Biochemistry, Faculty of Medical Sciences in Zabrze, Medical University of Silesia, Jordana 19 Street, 41-808 Zabrze, Poland*

[3]*Student Research Team at the Department of Cardiology, Faculty of Medical Sciences in Zabrze, Medical University of Silesia, M. C. Skłodowskiej 10 Street, 41-800 Zabrze, Poland*

[4]*Department of Toxicology and Health Protection, Faculty of Health Sciences in Bytom, Medical University of Silesia, 41-902 Bytom, Poland*

[5]*3rd Department of Cardiology, SMDZ in Zabrze, Medical University of Silesia, Silesian Centre for Heart Disease, 41-800 Zabrze, Poland*

Correspondence should be addressed to Ewa Romuk; eromuk@gmail.com

Oxidative stress plays a significant role in the pathogenesis of heart failure (HF). The aim of the study was to investigate the prognostic value of oxidation-reduction (redox) markers in patients with HF due to ischemic and nonischemic cardiomyopathy. The study included 707 patients of HF allocated into two groups depending on ethology: ischemic cardiomyopathy (ICM) ($n = 435$) and nonischemic cardiomyopathy (nICM) ($n = 272$), who were followed up for one year. The endpoint occurrence (mortality or heart transplantation) in a 1-year follow-up was similar in the ICM and nICM group. The predictive value of endpoint occurrence of oxidative stress biomarkers such as the serum protein sulfhydryl groups (PSH), malondialdehyde (MDA), uric acid (UA), bilirubin, and MDA/PSH ratio and other clinical and laboratory data were assessed in both groups (ICM and nICM) separately using univariate and multivariate Cox regression analyses. In multivariate analysis, the higher concentrations of UA ($p = 0.015$, HR = 1.024, 95% CI (1.005-1.044)) and MDA ($p = 0.004$, HR = 2.202, 95% CI (1.296-3.741)) were significantly associated with adverse prognosis in patients with ICM. Contrastingly, in patients with nICM, we observed that higher bilirubin concentration ($p = 0.026$, HR = 1.034, 95% CI (1.004-1.064)) and MDA/PSH ratio ($p = 0.034$, HR = 3.360, 95% CI (1.096-10.302)) were significantly associated with increased risk of death or HT. The results showed the association of different oxidative biomarkers on the unfavorable course of heart failure depending on etiology.

1. Introduction

The prognosis of patients with heart failure with reduced left ventricular ejection fraction is particularly poor. Dysregu-lated reduction-oxidation status, along with neurohormonal abnormalities and inflammation, is one of the common drivers of disease progression [1]. Increased formation of reactive oxygen species, a by-product of reduction-oxidation

reactions, can lead to lipid peroxidation, protein carboxylation, cytoskeletal disruption, and DNA damage. Many clinical and laboratory parameters reflecting disturbed pathophysiological pathways in heart failure are used to identify patients at higher risk of unfavorable prognosis. Due to the extremely short half-life of ROS, it is not feasible to assess it directly. The compromised choice may be the assessment of stable by-products, modified under oxidative conditions associated with elevated ROS formation, which have been released into the circulation. Malondialdehyde (MDA) is a low molecular weight aldehyde that is formed by free radical attacks on polyunsaturated fatty acids. MDA testing as a biomarker of oxidative damage was useful as a favorable prognostic tool, e.g., sepsis or nephrotic syndrome [2, 3]. Protein sulfhydryl groups (PSH) predominate in serum in contrast to the intracellular space, which mainly consists of low molecular weight thiols [4]. Since reduced thiols are readily oxidized by reactive oxygen species, once oxidized, the thiols are less readily reduced in serum compared to their intracellular counterparts. Thus, free thiol depletion in serum reflects relatively stable systemic redox status. Recently published data revealed a prognostic role of serum free thiols in the general population [5]. The risk assessment in the outpatient population, despite stability of symptoms, is important to escalate the therapy in the appropriate time. The data analyzing the dependence prognosis on ischemic or nonischemic cardiomyopathy causes of heart failure come from many years ago [6]. In the Studies of Left Ventricular Dysfunction (SOLVD) including patients with heart failure, the etiology of the disease (ischemic or nonischemic) did not influence mortality in a one-year follow-up [7]. However, in most studies, the ischemic group had poorer prognosis [8, 9].

The mechanisms of oxidative stress and antioxidant defense are partially different in the ICM and the nICM patients [10]. Therefore, the aim of this study was to examine the prognostic value of clinical factors, oxidation-reduction (redox) biomarkers with special consideration of MDA and PSH, in two large cohorts of HF patients depending on ischemic or/and nonischemic etiology in a 1-year follow-up.

2. Study Group and Methods

2.1. The Inpatient. A clinic cohort with reduced ejection fraction heart failure (HFrEF) and chronic heart failure symptoms was considered potential candidates for heart transplantation and follow-up in the Prospective Registry of Heart Failure since 2003. Patients were stable and received optimal medical pharmacotherapy according to contemporary guidelines for at least 3 months before inclusion. Exclusion criteria were as follows: inability or unwillingness to provide informed consent, alcohol abuse or known antioxidant supplementation, and noncardiac diseases that affect life expectancy as judged by the treating physician. The data of 707 participants who had completed clinical laboratory assessment were included into the final analysis.

2.2. Endpoint of the Study. The endpoint of the study was all-cause mortality or urgent heart transplantation.

2.3. Clinical Assessments. Patients were characterized as an ischemic or nonischemic cardiomyopathy group according to the definition proposed by Felker et al. [11]. Besides any history of myocardial infarction or coronary revascularization, the basis for the qualification was the results of angiography performed within the last six months. At the time of study entry, detailed clinical data were obtained using a questionnaire. History of smoking was defined as current or previous use of tobacco products. Comorbidities such as hypertension, diabetes mellitus, or hypercholesterolemia were recognized based on actual measurements of respective variables, current medication, and clinical history. The body mass index (BMI) was calculated from mass and height measured on the day of inclusion visit. The functional capacity was assessed by NYHA classification and exercise maximum O_2 uptake in the cardiopulmonary testing (MaxVO$_2$) [12]. Two-dimensional transthoracic echocardiography was performed in all patients, and echocardiographic parameters were acquired in standard views as in the recommendation of the American Society of Echocardiography Committee [13]. A follow-up on patients was obtained via direct or phone contact with patients or their family every 6 months by a research personnel. For some patients not contacted through this mechanism, the exact data of death were obtained from the national identification number database. Prior to enrolment in the study, all participants provided written informed consent.

2.4. Biochemical Methods. Venous blood samples were obtained from each patient at the enrollment process. Each serum sample was separated by centrifugation at 1500 g for 10 minutes at 4°C. UA, bilirubin, lipid parameters, blood hemoglobin, and serum iron, sodium, creatinine, glucose, and albumin concentrations were measured with the use of the colorimetric method (Roche, Cobas 6000 e 501). The chemiluminescence method was used to determine NT-proBNP concentration (Roche, Cobas 6000 e 501). The serum for determining the oxidant parameters was frozen at -70°C until assayed. Total oxidant status (TOS) was measured by a spectrophotometric method by Erel. This method is based on the oxidation of Fe^{2+} ions to form Fe^{3+} in acidic environment and consists of measuring the color intensity of Fe^{3+} ion complexes with xylenol orange. The measurements were performed using EM280 biochemical analyzer. TOS was expressed in mmol/L. [14]. TAC was measured by Erel's colorimetric methods with the use of 2,2$'$-azino-bis (3-ethylbenzothiazoline-6-sulfonate) (ABTS+) [15]. In this reaction, reduced ABTS, a colorless molecule, is oxidized to blue-green ABTS+. The oxidized form of ABTS is reduced to the original colorless reduced form as a result of reactions with oxidizable substances. TAC was expressed in mmol/L. The sulfhydryl groups (PSH) were determined with the use of 5,5$'$-dithiobis (2-nitrobenzoic acid) (DTNB) in the method described by Koster. In this method, DTNB, after reduction by the sulfhydryl group-containing compounds, forms a yellow-colored anionic 5-thio-2-nitrobenzoic acid. The absorbance was measured with a Shimadzu 1700 UVVIS spectrophotometer at a wavelength of 412 nm [16]. PSH concentration was expressed in μmol/g protein. Malondialdehyde (MDA) was

TABLE 1: Baseline characteristic of the examined group and comparison of subgroups separated on the basis of prognosis.

	ICM			nICM					
	A (n = 78), death or HT	B (n = 357), without endpoint	A vs. B, p	C (n = 44), death or HT	D (n = 228), without endpoint	C vs. D, p	A vs. C, p	B vs. D, p	ANOVA (A-D)
General characteristics, median (25th-75th percentiles) and *n (%)									
Male*	65 (83.33)	308 (86.27)	0.621	38 (86.36)	191 (87.77)	0.837	0.855	0.475	0.813
Age (years)	56.50 (52.00-61.00)	56.00 (52.00-61.00)	0.958	50.00 (43.00-57.50)	49.00 (38.00-55.50)	0.278	<0.001	0.129	<0.001
BMI (kg/m²)	26.05 (22.09-29.07)	26.45 (24.14-29.30)	0.142	23.44 (20.89-26.43)	26.07 (22.70-29.33)	0.007	0.030	0.285	<0.001
Duration of symptoms (months)	40.58 (13.50-70.43)	33.30 (14.13-64.73)	0.402	59.03 (23.38-86.45)	29.57 (9.58-66.57)	0.004	0.083	0.730	0.018
NYHA class (III-IV)*	65 (83.33)	181 (50.70)	<0.001	39 (88.64)	115 (50.44)	<0.001	0.598	0.982	<0.001
T6M (m)	320.0 (233.0-363.0)	378.0 (312.0-407.5)	0.004	346.5 (291.0-409.0)	401.0 (341.0-454.0)	0.090	0.169	0.009	<0.001
Max VO₂ (mL/min/kg)	12.30 (9.80-14.00)	15.20 (12.40-18.70)	<0.001	11.90 (9.70-14.10)	16.00 (13.30-20.10)	<0.001	0.878	0.135	<0.001
LVEDD (mm)	70.00 (65.00-76.00)	68.00 (63.00-75.00)	0.054	73.00 (63.00-78.0)	70.00 (65.00-77.00)	0.525	0.605	0.000	0.059
LVEDV (mL)	232.5 (195.0-314.0)	204.0 (156.0-264.0)	0.002	263.8 (222.0-340.0)	236.0 (179.0-307.0)	0.038	0.041	0.011	<0.001
LVEF (%)	19.00 (16.00-23.00)	25.00 (20.00-33.00)	<0.001	22.50 (17.00-26.00)	23.50 (20.00-29.00)	0.063	0.069	0.034	<0.001
Basic biochemistry, median (25th-75th percentiles)									
Hemoglobin (g/dL)	14.02 (12.89-14.99)	13.86 (13.05-14.83)	0.792	14.10 (12.81-15.39)	14.18 (13.14-15.29)	0.892	0.329	0.010	0.192
Iron (μmol/L)	14.85 (10.80-19.04)	17.33 (12.38-21.90)	0.005	16.35 (10.40-22.75)	17.95 (12.35-23.60)	0.287	0.301	0.500	0.013
Creatinine (μmol/L)	95.00 (81.0-123.0)	85.0 (72.00-104.0)	0.003	87.50 (78.00-114.5)	81.00 (70.00-97.00)	0.016	0.790	0.149	<0.001
Serum protein (g/L)	72.00 (67.00-76.00)	71.00 (66.00-75.00)	0.224	72.50 (65.00-78.50)	71.00 (67.00-75.00)	0.380	0.577	0.114	0.457
Albumin (g/L)	40.00 (37.00-44.00)	42.00 (39.00-44.00)	0.048	41.00 (38.00-44.00)	42.00 (40.00-45.00)	0.110	0.155	0.123	0.034
Fasting glucose (mmol/L)	5.70 (5.00-6.80)	5.60 (5.00-6.20)	0.227	5.30 (4.95-5.95)	5.50 (4.90-6.10)	0.879	0.226	0.597	0.127
Cholesterol (mmol/L)	4.26 (3.66-5.11)	4.24 (3.65-5.22)	0.576	4.21 (3.35-5.15)	4.35 (3.62-5.20)	0.344	0.110	0.252	0.705
Triglycerides (mmol/L)	1.16 (0.89-1.63)	1.20 (0.84-1.75)	0.675	1.11 (0.76-1.41)	1.25 (0.93-1.75)	0.022	0.678	0.523	0.134
HDL (mmol/L)	1.08 (0.83-1.35)	1.16 (0.97-1.42)	0.012	1.16 (0.79-1.42)	1.13 (0.93-1.39)	0.512	0.780	0.362	0.064
LDL (mmol/L)	2.52 (1.92-3.18)	2.34 (1.86-3.09)	0.505	2.31 (1.75-3.23)	2.49 (1.93-3.12)	0.854	0.012	0.129	0.878
NT-proBNP (pg/mL/100)	28.50 (15.04-48.10)	11.70 (5.49-23.99)	<0.001	47.24 (22.16-87.99)	13.63 (6.20-28.11)	<0.001	<0.001	0.285	<0.001
Comorbidities, n (%)									
Diabetes	35 (44.87)	111 (31.09)	0.28	11 (25.00)	43 (18.86)	0.466	0.048	0.002	<0.001
Arterial hypertension	42 (53.85)	221 (61.90)	0.946	20 (45.45)	106 (46.49)	0.969	0.483	0.001	0.002
Atrial fibrillation	17 (21.79)	58 (16.25)	0.313	16 (36.36)	73 (32.02)	0.072	0.127	0.043	<0.001
ICD presence	3 (3.85)	104 (29.13)	0.001	3 (6.82)	91 (39.91)	0.001	0.770	0.009	<0.001
Smoker	21 (26.92)	112 (31.37)	0.001	15 (34.09)	96 (42.11)	0.411	0.531	0.011	0.025
Treatment, n (%)									
Beta-blockers	77 (98.72)	352 (98.60)	0.650	41 (93.18)	223 (97.81)	0.240	0.942	0.694	0.104
ACE inhibitors, n (%)	63 (80.77)	317 (88.80)	0.081	31 (70.45)	199 (87.28)	0.009	0.282	0.673	0.004
ARB	5 (6.41)	38 (10.64)	0.100	5 (11.36)	25 (10.96)	0.853	0.539	0.988	0.687
Loop diuretics, n (%)	75 (96.15)	285 (79.83)	0.001	43 (97.73)	211 (92.54)	0.350	0.952	0.001	<0.001

TABLE 1: Continued.

| | ICM | | | nICM | | | | | |
	A (n = 78), death or HT	B (n = 357), without endpoint	A vs. B, p	C (n = 44), death or HT	D (n = 228), without endpoint	C vs. D, p	A vs. C, p	B vs. D, p	ANOVA (A-D)
Thiazide diuretics, n (%)	12 (15.38)	37 (10.36)	0.283	15 (34.09)	24 (10.53)	0.001	0.031	0.939	<0.001
MRA	73 (93.59)	319 (89.36)	0.355	39 (88.64)	219 (96.11)	0.096	0.539	0.006	0.017
Statins	55 (70.51)	274 (76.75)	0.010	17 (38.64)	120 (52.63)	0.125	0.001	0.001	<0.001
Fibrates	2 (2.56)	15 (4.20)	0.724	0 (0.00)	9 (3.95)	0.379	0.777	0.845	0.518
Digitalis	40 (51.28)	140 (39.22)	0.067	27 (61.36)	117 (51.32)	0.290	0.376	0.005	0.003
XO blockers	27 (34.62)	102 (28.57)	0.357	25 (56.82)	116 (57.14)	0.577	0.029	<0.001	<0.001

BMI: body mass index; NYHA: New York Heart Association functional class; max VO_2: maximum oxygen uptake; LVEDD: left ventricle end-diastolic diameter; LVEDV: left ventricle end-diastolic volume; LVEF: left ventricle ejection fraction; NT-proBNP: N-terminal pro-B-type natriuretic peptide; ICD: implantable cardioverter defibrillator; ACE inhibitor: angiotensin-converting enzyme inhibitor; ARB: angiotensin receptor blocker; MRA: mineralocorticoid receptor antagonists; NS: nonsignificant; XO: xanthine oxidase; A: ICM patients (EP+); B: ICM patients (EP-); C: nICM patients (EP+); D: nICM patients (EP-).

TABLE 2: Redox parameters of the examined group and comparison of subgroups separated on the basis of prognosis (median (25th-75th percentiles)).

	ICM A ($n = 78$), death or HT	ICM B ($n = 357$), without endpoint	A vs. B, p	nICM C ($n = 44$), death or HT	nICM D ($n = 228$), without endpoint	C vs. D, p	A vs. C, p	B vs. D, p	ANOVA (A-D)
TAC (mmol/L)	1.13 (1.02-1.27)	1.14 (1.040-1.25)	0.861	1.140 (1.060-1.250)	1.08 (0.98-1.21)	0.017	0.759	<0.001	<0.001
TOS (mmol/L)	5.15 (4.10-6.60)	4.70 (4.000-5.90)	0.227	5.40 (4.45-6.60)	5.10 (4.20-6.05)	0.105	0.298	0.126	0.069
Uric acid (μmol/L)	44.55 (36.20-59.90)	39.90 (32.30-49.30)	0.002	42.35 (35.90-56.95)	40.80 (31.40-48.45)	0.068	0.699	0.642	0.002
Bilirubin (μmol/L)	14.80 (10.10-24.70)	12.30 (9.10-18.60)	0.036	20.55 (13.80-33.00)	14.70 (10.00-20.60)	<0.001	0.007	0.014	<0.001
PSH (μmol/g of protein)	3.85 (3.10-5.00)	4.10 (3.100-5.300)	0.592	4.45 (3.100-5.450)	4.80 (3.80-5.60)	0.146	0.317	<0.001	<0.001
MDA (μmol/L)	2.00 (1.60-2.40)	1.80 (1.400-2.100)	<0.001	1.90 (1.500-2.250)	1.70 (1.30-2.00)	0.024	0.162	0.144	<0.001
MDA/PSH ratio	0.52 (0.36-0.74)	0.41 (0.308-0.622)	0.004	0.42 (0.291-0.705)	0.35 (0.26-0.50)	0.029	0.146	<0.001	<0.001

TAC: total antioxidant capacity; TOS: total oxidant status; MDA: malondialdehyde; PSH: sulfhydryl groups; A: ICM patients (EP+); B: ICM patients (EP-); C: nICM patients (EP+); D: nICM patients (EP-).

TABLE 3: Clinical and laboratory parameters as risk factors for death or OHT of patients with ICM in a 1-year follow-up. Uni- and multivariable Cox regression analysis.

	Univariable Cox regression analysis			Multivariable Cox regression analysis (complete data, $n = 387$)		
	p	HR	95% CI	p	HR	95% CI
General characteristics						
Female (yes/no)	0.721	1.113	0.618-2006			
Age (years)	0.861	0.998	0.972-1.024			
BMI (kg/m^2)	0.134	0.959	0.908-1.013			
Duration of symptoms before inclusion (months)	0.233	1.003	0.998-1.007			
NYHA class (by one)	<0.001	2.396	1.774-3.237	0.559	1.143	0.730-1.798
Max VO$_2$ (by 1 mL/min/kg)	<0.001	0.849	0.802-0.899	0.044	0.923	0.854-0.998
LVEDD (mm)	0.030	1.027	1.003-1.051			
LVEDV (mL)	<0.001	1.005	1.002-1.007			
LVEF (by 1%)	<0.001	0.868	0.835-0.903	<0.001	0.881	0.831-0.934
Basic biochemistry						
Hemoglobin (g/dL)	0.906	0.992	0.871-1.130			
Iron concentration (μmol/L)	0.012	0.960	0.930-0.991	0.052	0.957	0.915-1.000
Creatinine (μmol/L)	0.007	1.005	1.001-1.010	0.992	1.000	0.993-1.007
Serum protein (g/L)	0.226	1.021	0.987-1.056			
Albumin (g/L)	0.019	0.940	0.892-0.990	0.318	0.961	0.889-1.039
Fasting glucose (mmol/L)	0.060	1.098	0.996-1.212			
Total cholesterol (mmol/L)	0.738	0.970	0.814-1.157			
Triglycerides (mmol/L)	0.417	0.886	0.660-1.188			
Cholesterol HDL (mmol/L)	0.008	0.423	0.224-0.797	0.578	0.817	0.401-1.665
Cholesterol LDL (mmol/L)	0.369	1.094	0.899-1.332			
NT-proBNP (100 pg/mL)	<0.001	1.017	1.011-1.023	0.322	1.005	0.995-1.014
Comorbidities						
Diabetes (yes/no)	0.025	1.663	1.064-2.599	0.978	0.993	0.588-1.677
Arterial hypertension (yes/no)	0.196	0.745	0.477-1.163			
Atrial fibrillation (yes/no)	0.123	1.481	0.899-2.438			
ICD presence (yes/no)	<0.001	0.133	0.049-0.363	<0.001	0.130	0.040-0.422
Smoker (yes/no)	0.586	0.879	0.553-1.397			
Treatment						
Beta-blockers (yes/no)	0.840	1.226	0.171-8.801			
ACE inhibitors (yes/no)	0.033	0.542	0.308-0.951	0.493	0.795	0.412-1.532
ARB (yes/no)	0.467	0.751	0.347-1.625			
Loop diuretics (yes/no)	0.002	5.923	1.873-18.729	0.867	1.112	0.319-3.877
Thiazide diuretics (yes/no)	0.158	1.529	0.848-2.745			
MRA (yes/no)	0.166	1.893	0.767-4.667			
Statins (yes/no)	0.175	0.714	0.439-1.162			
Fibrates (yes/no)	0.500	0.617	0.152-2.509			
Digitalis (yes/no)	0.035	1.567	1.032-2.380	0.416	0.803	0.473-1.363
XO inhibitors (yes/no)	0.345	1.237	0.796-1.922			
Oxidative stress parameters						
TAC (mmol/L)	0.469	1.518	0.490-4.698			
TOS (mmol/L)	0.700	1.015	0.942-1.093			
OSI (TOS/TAC)	0.717	1.014	0.940-1.094			
Uric acid (10 μmol/L)	<0.001	1.003	1.002-1.004	0.015	1.024	1.005-1.044
Bilirubin (μmol/L)	<0.001	1.026	1.011-1.041	0.569	0.994	0.972-1.016
MDA (μmol/L)	<0.001	2.125	1.493-3.023	0.004	2.202	1.296-3.741

TABLE 3: Continued.

	Univariable Cox regression analysis			Multivariable Cox regression analysis (complete data, $n = 387$)		
	p	HR	95% CI	p	HR	95% CI
MDA/PSH ratio	0.036	1.617	1.032-2.532	0.334	0.671	0.298-1.508

BMI: body mass index; NYHA: New York Heart Association functional class; max VO$_2$: maximum oxygen uptake; LVEDD: left ventricle end-diastolic diameter; LVEDV: left ventricle end-diastolic volume; LVEF: left ventricle ejection fraction; NT-proBNP: N-terminal pro-B-type natriuretic peptide; ICD: implantable cardioverter defibrillator; ACE inhibitor: angiotensin-converting enzyme inhibitor; ARB: angiotensin receptor blocker; MRA: mineralocorticoid receptor antagonists; XO: xanthine oxidase; TAC: total antioxidant capacity; TOS: total oxidant status; MDA: malondialdehyde; PSH: sulfhydryl groups.

measured by Ohkawa et al.'s spectrofluorimetric method. In this method, lipid peroxides react with thiobarbituric acid at the excitation wavelength 515 nm and emission wavelength 552 nm. The standard curve, prepared for 1,1,3,3-tetraethoxypropane, was used to calculate MDA concentration in μmol/L [17].

2.5. *Statistical Analysis.* The subjects were allocated into groups according to the etiology of cardiomyopathy: ischemic (ICM) and nonischemic (nICM). Then, for the purposes of the analysis, in each group, the following patients were distinguished: the patient who achieved the endpoint (EP+) or without the endpoint (EP-) during one year of observation. Categorical data were displayed as proportions and were compared using the chi-square test with the Yates correction. Distribution of all continuous variables was evaluated by the Shapiro-Wilk test. Because of abnormal distribution of most continuous variables, the continuous data were presented as median with the first and third quartile. Data were tested with the Kruskal-Wallis ANOVA test; next, we assessed the differences between the selected groups using the nonparametric Mann Whitney U test and the chi^2 test.

The estimation of risk of death and urgent transplantation was performed using a Cox proportional hazards model for the ICM and nICM group. All demographic, clinical, echocardiography, and laboratory variables and also medication data presented in Tables 1 and 2 were included in a univariate Cox analysis. A multivariate model was constructed separately for both groups based on the variables significantly associated with EP occurrence in each group (univariate analysis, $p < 0.05$). The results of the Cox analysis were reported as relative risks with corresponding 95% confidence intervals (CI). Cumulative survival over one year of follow-up was displayed using the Kaplan-Meier method, with comparison between groups depending on the cutoff value of concentrations of MDA, UA, and bilirubin or the MDA/PSH ratio calculated in Receiver Operation Characteristic (ROC) analysis, and the differences were tested for significance by the log-rank test. Results were considered statistically significant if $p < 0.05$. Statistical analysis was performed using Statistica 13.1 PL (TIBCO, Cracow, Poland).

3. Results

3.1. *Baseline Characteristics of Subgroups in Relation to Etiology and Endpoint.* In general, ischemic cardiomyopathy was more common than nonischemic cardiomyopathy (61.5% versus 38.5%). In the group of 435 patients of ICM etiology, 78 (17.9%) deaths and HT occurred over a one-year follow-up. 44 (16.2%) patients achieved an endpoint in 272 patients of the nICM group (chi^2, $p = 0.678$). Baseline characteristics for patients enrolled in the study are shown in Table 1. Patients of the ICM group were older than those of the nICM group, but there were no differences between EP+ and EP-.

The percentage of patients in NYHA class III-IV was greater, and patients with implanted ICD were lower in EP+ groups in the ICM and nICM population. In both ICM and nICM, EP+ groups characterized a more enlarged left ventricle in echocardiography and maximum VO$_2$ consumption in cardiopulmonary exercise testing and higher concentration of creatinine and NT-proBNP. In patients with ICM (EP+), lower ejection fraction in echocardiography, iron concentration, and higher HDL-cholesterol were observed.

The differences in redooxidative parameters are presented in Table 2. In patients with ICM (EP+), higher uric acid, bilirubin, and MDA concentrations and MDA/PSH ratio than those in patients with ICM (EP-) were indicated. Similarly, bilirubin and MDA concentrations and the MDA/PSH ratio but not uric acid were higher in the nICM (EP+) than in the nICM (EP-) group. Additionally, TAC was the most increased in nICM (EP+).

3.2. *Association between Redox Reaction Parameters and Risk of Endpoint*

3.2.1. *Uni- and Multivariate Cox Regression Analyses.* Demographic and clinical data, laboratory results, comorbidities, pharmacotherapy, and oxidative stress-related parameters were assessed as risk factors for death or urgent heart transplantation in a 1-year follow-up in uni- and multivariate Cox regression analyses as presented in Tables 3 and 4. In univariate Cox regression analysis, higher levels of uric acid, bilirubin, MDA, and MDA/PSA were associated with endpoint occurrence in ICM patients. All assessed oxidative stress biomarkers without PSH in univariate Cox regression analysis were associated with the risk of death and HT in nICM.

In order to evaluate oxidative stress parameters in the context of confounders, a final multivariate model was calculated including all significant clinical, laboratory, and medication predictors significant in univariate analysis. After adjusting for significant predictors, only maxVO$_2$ uptake in the cardiopulmonary testing, left ventricle ejection fraction, ICD presence, higher uric acid concentration (increase of risk

TABLE 4: Clinical and laboratory parameters as risk factors for death or OHT of patients with nICM in a 1-year follow-up. Uni- and multivariable Cox regression analysis.

	Univariable Cox regression analysis			Multivariable Cox regression analysis (complete data, $n = 247$)		
	p	HR	95% CI	p	HR	95% CI
General characteristics						
Male (yes/no)	0.699	1.184	0.502-2.793			
Age (years)	0.286	1.014	0.988-1.041			
BMI (kg/m^2)	0.012	0.923	0.867-0.982	0.772	1.013	0.928-1.106
Duration of symptoms before inclusion (months)	0.033	1.005	1.001-1.009	0.179	1.005	0.998-1.012
NYHA class	<0.001	3.879	2.517-5.978	0.144	1.687	0.837-3.400
Maximum measured VO$_2$ (by 1 mL/min/kg b.m.)	<0.001	0.826	0.762-0.896	0.121	0.919	0.825-1.023
LVEDD (mm)	0.714	0.995	0.969-1.022			
LVEDV (mL)	0.101	1.003	1.000-1.006			
LVEF (by 1%)	0.886	0.997	0.961-1.035			
Basic biochemistry						
Hemoglobin (mmol/L)	0.987	1.001	0.841-1.193			
Iron concentration (μmol/L)	0.651	0.993	0.962-1.024			
Creatinine (μmol/L)	0.039	1.008	1.000-1.016	0.703	0.997	0.982-1.012
Serum protein (g/L)	0.256	1.027	0.981-1.074			
Albumin (g/L)	0.053	0.938	0.879-1.001			
Fasting glucose (mmol/L)	0.491	1.059	0.899-1.248			
Total cholesterol (mmol/L)	0.918	0.988	0.778-1.254			
Triglycerides (mmol/L)	0.329	0.844	0.601-1.187			
Cholesterol HDL (mmol/L)	0.645	0.865	0.468-1.601			
Cholesterol LDL (mmol/L)	0.588	1.086	0.805-1.466			
NT-proBNP (100 pg/mL)	<0.001	1.021	1.015-1.027	<0.001	1.019	1.008-1.031
Comorbidities						
Diabetes (yes/no)	0.405	1.334	0.677-2.626			
Arterial hypertension (yes/no)	0.885	0.958	0.536-1.711			
Atrial fibrillation (yes/no)	0.586	1.181	0.649-2.149			
ICD presence (yes/no)	<0.001	0.080	0.019-0.331	0.009	0.180	0.050-0.645
Smoker (yes/no)	0.342	0.745	0.406-1.367			
Treatment						
Beta-blockers (yes/no)	0.037	0.287	0.089-0.926	0.895	0.838	0.060-11.629
ACE inhibitors (yes/no)	<0.001	0.334	0.178-0.627	0.446	0.657	0.223-1.935
ARB (yes/no)	0.662	1.211	0.513-2.856			
Loop diuretics (yes/no)	0.249	3.206	0.442-23.253			
Thiazide diuretics (yes/no)	<0.001	3.685	2.023-6.713	0.027	2.702	1.117-6.535
MRA (yes/no)	0.034	0.368	0.146-0.929	0.884	0.876	0.150-5.132
Statins (yes/no)	0.100	0.605	0.333-1.102			
Fibrates (yes/no)	0.526	0.527	0.073-3.823			
Digitalis (yes/no)	0.306	1.363	0.754-2.463			
XO inhibitors (yes/no)	0.767	0.992	0.939-1.048			
Oxidative stress parameters						
TAC (mmol/L)	0.019	5.454	1.325-22.444	0.547	0.334	0.009-11.841
TOS (mmol/L)	0.037	1.099	1.006-1.201	0.221	0.883	0.723-1.078
OSI (TOS/TAC)	0.590	1.019	0.953-1.089			
Uric acid (10 μmol/L)	0.010	1.025	1.006-1.045	0.268	1.019	0.985-1.054
Bilirubin (μmoL/L)	<0.001	1.034	1.019-1.049	0.026	1.034	1.004-1.064
PSH (μmol/g of protein)	0.146	0.851	0.685-1.058			

TABLE 4: Continued.

	Univariable Cox regression analysis			Multivariable Cox regression analysis (complete data, $n = 247$)		
	p	HR	95% CI	p	HR	95% CI
MDA (μmol/L)	0.032	1.823	1.052-3.160	0.326	1.665	0.603-4.602
MDA/PSH ratio	<0.001	3.414	2.047-5.695	0.034	3.360	1.096-10.302

BMI: body mass index; NYHA: New York Heart Association functional class; max VO$_2$: maximum oxygen uptake; LVEDD: left ventricle end-diastolic diameter; LVEDV: left ventricle end-diastolic volume; LVEF: left ventricle ejection fraction; NT-proBNP: N-terminal pro-B-type natriuretic peptide; ICD: implantable cardioverter defibrillator; ACE inhibitor: angiotensin-converting enzyme inhibitor; ARB: angiotensin receptor blocker; MRA: mineralocorticoid receptor antagonists; XO: xanthine oxidase; TAC: total antioxidant capacity; TOS: total oxidant status; MDA: malondialdehyde; PSH: sulfhydryl groups.

Follow-up (days)
AUC 0.642, 95%CI (0.576−0.708), $p < 0.001$

—— MDA ≤ 1.9 μmol/l

- - - MDA > 1.9 μmol/l

FIGURE 1: Kaplan-Meier curve of survival for the ICM group stratified by the MDA cutoff value of 1.9 μmol/L. Log rank test ($p = 0.034$).

(IoR) by 2.4% per 10 μmol/L, $p = 0.015$), and higher serum MDA concentration (IoR by 220% per mmol/L, $p = 0.004$) were independent risk factors for death or heart transplantation in ICM. On the other hand, NT-proBNP, left ventricle ejection fraction, ICD presence, higher bilirubin concentration (increase of risk (IoR) by 3.4% per 1 μmol/L, $p = 0.026$), and higher MDA/PSH ratio (IoR by 336%, $p = 0.034$) were independently related to endpoint occurrence in nICM.

The Kaplan-Meier plot with a log-rank test for the outcome in ICM is shown in Figures 1 and 2. MDA and UA concentrations above the cutoff value obtained in ROC analysis were associated with poor outcome in ICM ($p = 0.034$ and $p < 0.001$, respectively). The Kaplan-Meier plot with a log-rank test for the endpoint occurrence in nICM is shown in

Figures 3 and 4. The MDA/PSH ratio ($p = 0.032$) and bilirubin concentration ($p = 0.003$) above the cutoff value were related to risk of death and HT.

4. Discussion

While many clinical and biochemical variables have not only diagnostic but also prognostic value in heart failure, the question is whether these variables are of similar value in patients with ischemic and nonischemic heart failure. The observational studies, randomized clinical trials, and retrospective analyses of hospital records revealed inconsistent data on the impact of the etiology of heart failure on prognosis [7–9, 18].
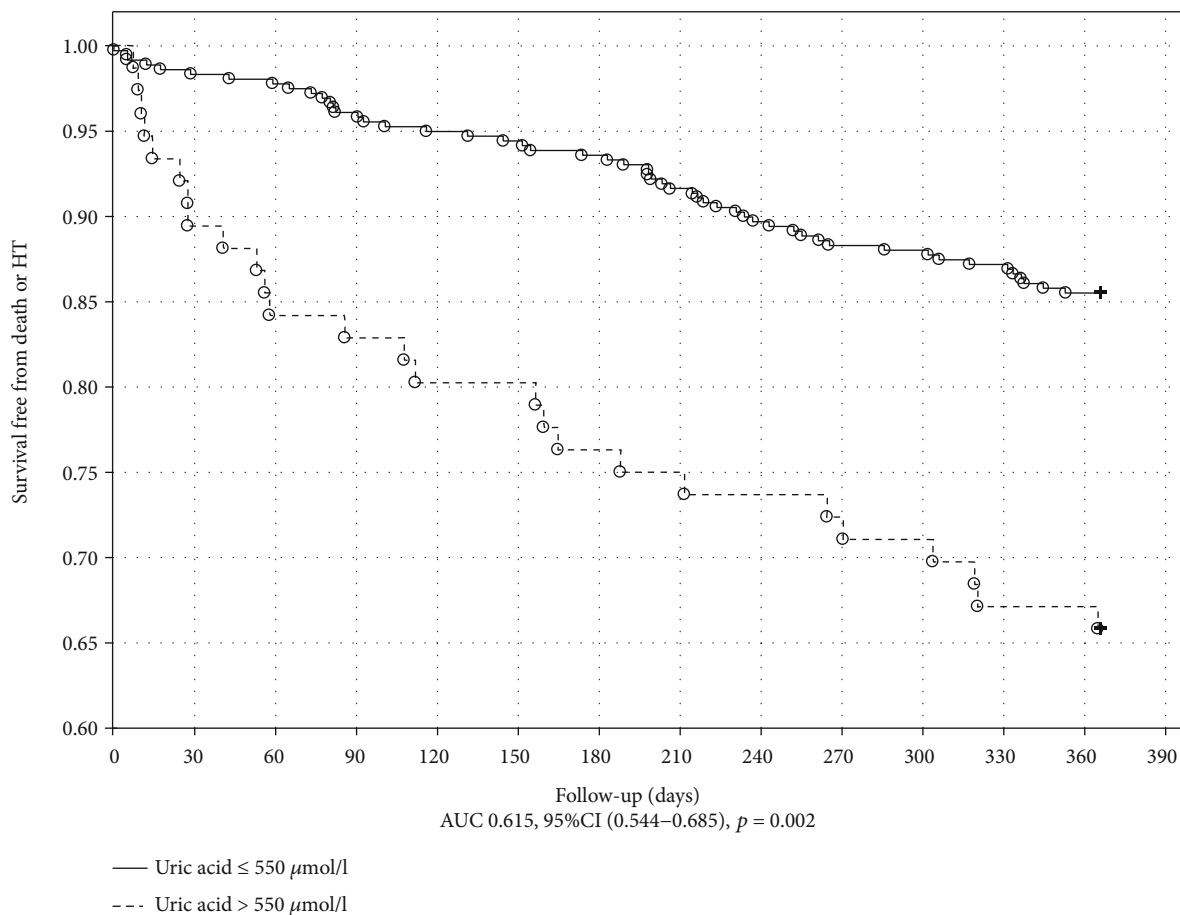
FIGURE 2: Kaplan-Meier curve of survival for the ICM group stratified by the uric acid cutoff value of 550 μmol/L. Log rank test ($p < 0.001$).

In most of reports, a higher risk of death in patients with ICM compared with patients with nICM was indicated. In our study, the endpoint occurrence (all-cause mortality and HT) in a one-year follow-up was similar in ICM and nICM groups. A previous study has shown that oxidative stress is related to the severity of heart failure, although the results have been different in patients with ischemic and nonischemic cardiomyopathy [10]. According to our knowledge, this is the first study analyzing the influence of the reduction-oxidative balance parameters on the prognosis in patients with systolic heart failure, taking into account ischemic and nonischemic etiology. Independent redox biomarkers related to increased all-cause mortality and heart transplantation in a one-year follow-up were higher concentrations of uric acid and MDA in ICM. In contrast, higher levels of bilirubin and MDA/PSH were predictors of the endpoint in the nICM group. Surprisingly, NT-proBNP was a predictor only in the nICM and the maxVO$_2$ and left ventricle ejection fraction only in the ICM group.

The results of our study showed that the sex and age of the patients did not affect the achievement of the one-year endpoint in both groups ICM and nICM. Anker et al. indicated that uric acid, age, and left ventricle ejection fraction, but not peak VO$_2$, were predictive of impaired survival in European heart failure patients (60% of ischemic etiology) [19]. Similarly, UA was a prognostic marker of all-cause mor-

tality after adjustment to NYHA class and creatinine clearance in the population of heart failure patients (70% of ischemic etiology) as described by Jankowska et al. [20]. Sakai et al. confirmed the important prognostic role of UA in a Japanese population. Both increased UA and BNP were associated with mortality independently from etiology, sex, age, NYHA class, and LVEF [21]. Hyperuricemia may reflect raised xanthine oxidase activity in heart failure; this enzyme system is an important source of oxygen free radicals [22, 23]. Uric acid concentration is affected by using a xanthine oxidase inhibitor (allopurinol). Allopurinol was used more often in the nICM groups (EP+ and EP-) than, respectively, in the ICM groups (EP+ and EP-). The median uric acid concentration did not differ statistically between ICM and nICM; however, uric acid concentration was statistically significantly higher in the ICM EP+ than in ICM EP- ($p < 0.002$). Higher uric acid level was a marker associated with increased mortality in this group;

Our results indicating malondialdehyde, a by-product of polyunsaturated fatty acid lipid peroxidation, as a predictor of death and heart transplantation only in ICM, are consistent with observation published by Radovanovic et al. that malondialdehyde predicted mortality in patients with chronic ischemic heart failure during 13-month observation [24]. The previous reports demonstrated increase in MDA concentration in patients with HF of different etiologies,
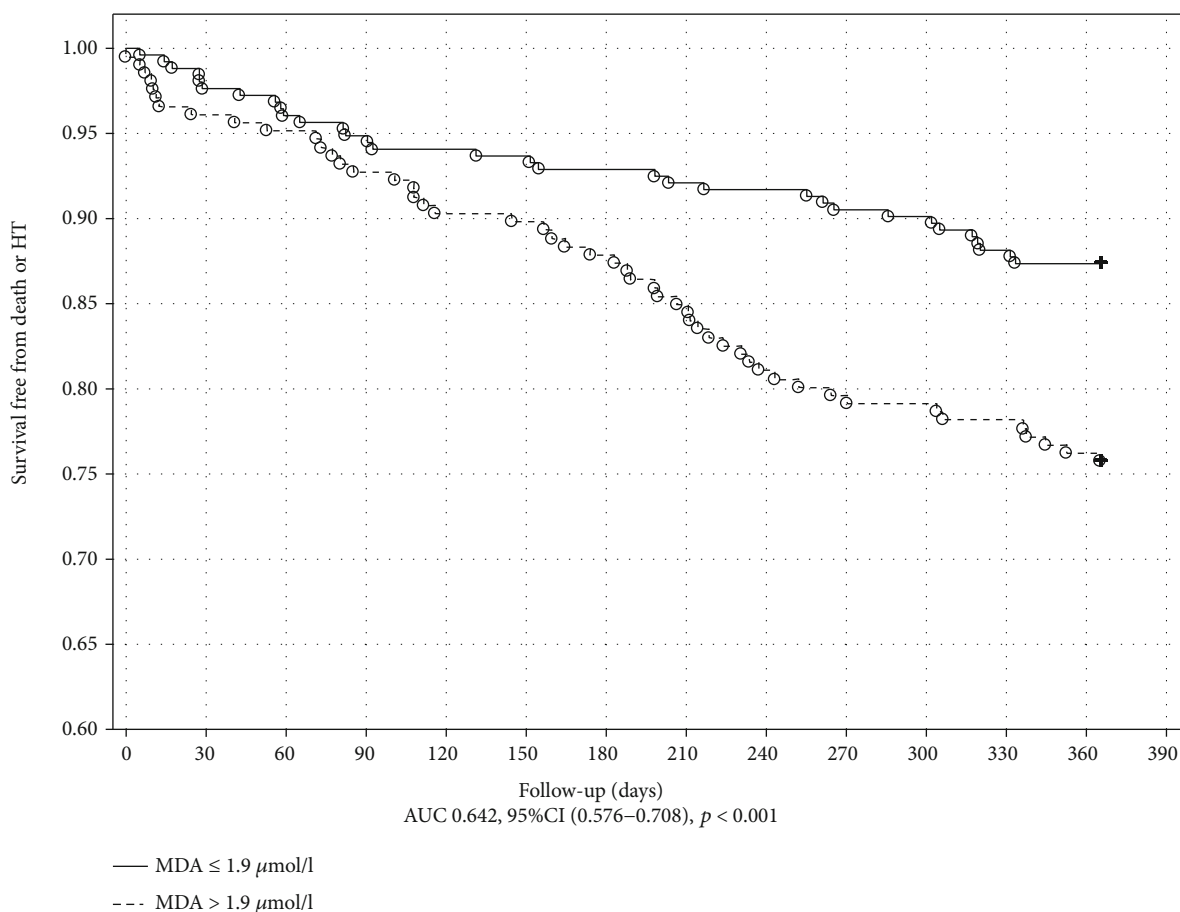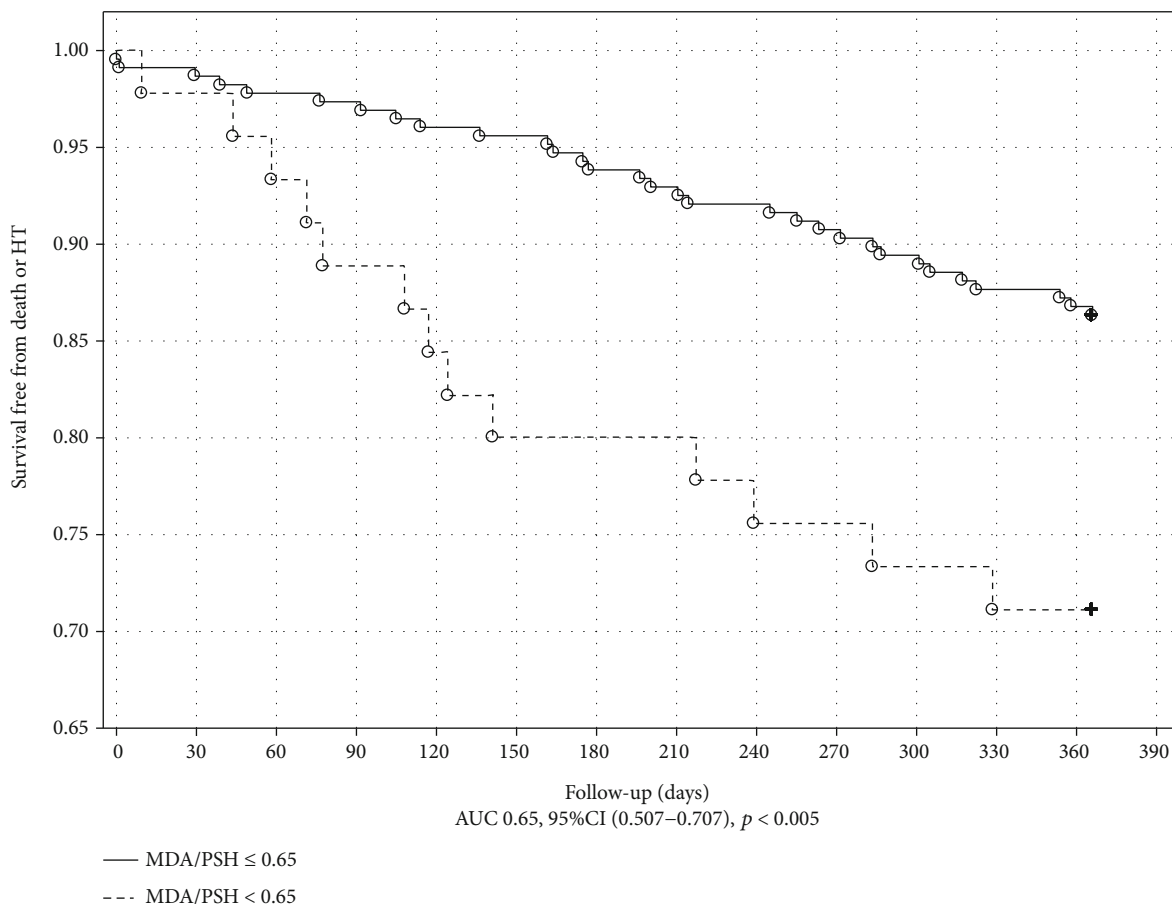
FIGURE 3: Kaplan-Meier curve of survival for the nICM group stratified by the MDA/PSH cutoff value of 0.65. Log rank test ($p = 0.032$).

but the relationship between MDA and the severity of heart failure assessed as NYHA class, exercise intolerance LVEF, and invasive hemodynamic measurements is inconsistent [25–30]. The last papers do not confirm such a relationship perhaps due to the use of standardized treatment with inhibitors of the renin-angiotensin system and beta-blockers [29, 30]. MDA, the highest quartile concentration, was an independent risk factor for a cardiovascular event (myocardial infarction—fatal, nonfatal, stroke, and unstable angina) as compared to the lowest quartile. The prognostic value was independent of interleukin-6, C-reactive protein, and classical risk factors for atherosclerosis [31]. The above observations draw our attention to the lipid profile of patients with ICM. In lipid parameters, it was surprising that only the high concentration of HDL cholesterol in univariable analysis had a protective effect on survival in the ischemic group. However, the ICM EP+ group had a significantly higher LDL than the nICM EP+ group despite more frequent use of statins. It should be emphasized that patients were enrolled in the study before the current very strict LDL target recommendations [32]. This fact may confirm the large role of LDL in the pathogenesis of coronary diseases in general. LDL cholesterol is oxidized by MDA to MDA-LDL molecules. These combinations have been shown to be particularly atherogenic [33, 34]. Tani et al. proved that the concentration of MDA-LDL is independent of the overall LDL. It may depend on the oxi-

dative state of a patient individually. Their study showed that patients with coronary artery disease have increased levels of MDA-LDL. It has been suggested that this may be a promising indicator in assessing the risk of coronary artery disease [35].

In the ICM group, the PSH, MDA/PSH index, and NT-proBNP in multivariable Cox regression analysis indices showed no prognostic significance in predicting the endpoint. The situation is different in the case of patients with nICM, in whom the MDA/PSH ratio and NT-proBNP were indicated as risk factors for death or OHT. Increasing attention, for the last years, has been paid to the role of oxidative stress in CVD, since it may lead to endothelial dysfunction [36]. Frenay et al. show that high serum concentrations of PSH are associated with a favorable cardiovascular risk profile and better survival for patients with the transplanted kidney [37]. In acute myocardial infarction, it was shown that thiols are an oxidative stress marker [38] and that plasma thiols are significantly lower in subjects with congestive heart failure, as compared to healthy subjects [39]. Recently, Abdulle et al. found that protein-adjusted serum free thiol concentrations were able to predict the risk of all-cause mortality and cardiovascular events after adjustment for confounders in the general population. In the subgroup of subjects with a known history of cardiovascular disease ($n = 217$), regression analyses revealed age- and sex-
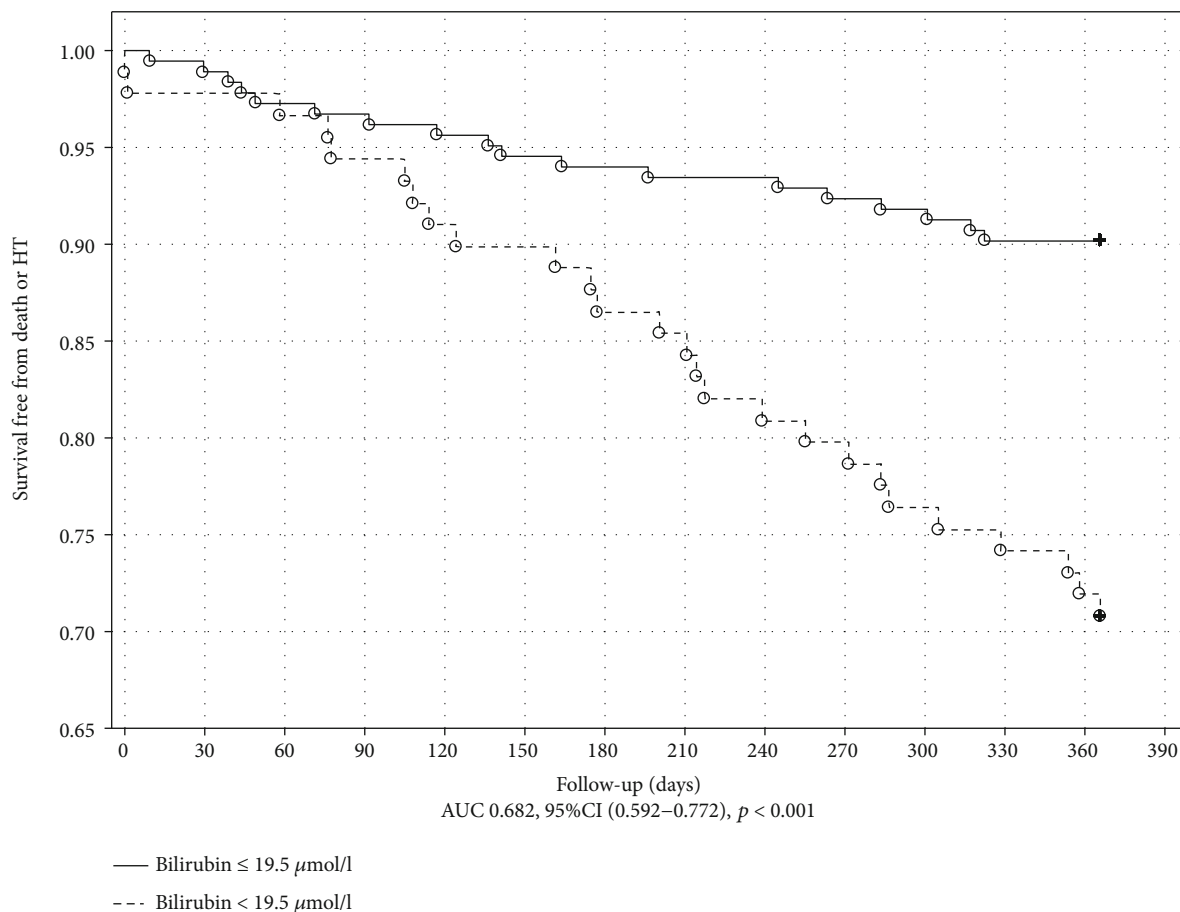
Figure 4: Kaplan-Meier curve of survival for the nICM group stratified by the bilirubin cutoff value of 19.5 μmol/L. Log rank test ($p = 0.003$).

adjusted associations between protein-adjusted serum free thiol concentrations and all-cause mortality when comparing the upper two tertiles with the lowest tertile and lack of significant associations with the risk of cardiovascular events [5]. In the study by Koning et al., they found in a group of 101 patients with stable heart failure that free serum thiols are associated independently with age, cholesterol, and parathyroid hormone. Free thiols and age were inversely related. In multivariable analysis, an association of PSH with NT-proBNP was not identified. Both serum free thiols per gram of protein below the mean and NT-proBNP above the median were predictors of a composite endpoint: HF-related rehospitalisation and all-cause mortality. However, further analysis adjusting PSH to establish prognostic factors in HF (age, eGFR, and NT-proBNP) revealed no longer significant association with the endpoint [40]. 72% of patients in this study characterized ischemic etiology. The participants were older compared to our nICM group and had less reduced ejection fraction. Despite free thiols (PSH, sulfhydryl groups) are more accurately reflecting the systemic in vivo redox status as compared to many other individual oxidant or antioxidant factors and their derivatives [41], in our study, the MDA/PSH ratio but not PSH was a valuable predictor of adverse outcome in nICM.

The positive association of reduced thiol concentration with increased circulating bilirubin was indicated in uncon-jugated hyperbilirubinemia (Gilbert syndrome). The modulation by bilirubin lipid status may be the explanation of protection from ischemic heart disease in Gilbert syndrome [42]. The epidemiological studies indicate that mildly elevated bilirubin concentrations were protective against cardiovascular disease and all-cause mortality [43–45]. However, we did not observe significance of bilirubin concentration with endpoint prediction in heart failure of ischemic etiology. Moreover, higher bilirubin was associated with adverse outcome in the nICM group.

It is disappointing to find that using allopurinol did not improve patients' prognosis in any group of our study, although previous studies indicated that allopurinol may have the ability to decrease mortality in HF. [46, 47]. The explanation may be that the dose was too low, because higher doses of allopurinol have a greater impact on cardiovascular outcomes than lower doses [47, 48]. Oxidation-reduction systems play an important role in the progression of heart failure. It has been proven that some of the commonly used drugs in HF, such as ACE inhibitors or beta-blockers, affect this system [49, 50]. Pharmacological treatment of HF recommended by guidelines has progressed over the past decades and has improved the prognosis in this group of patients. Recently, the importance of personalizing treatment has been emphasized because the population enrolled to the randomized trials does not always represent the patients we

treat. In most HF clinical trials, patients predominantly were male with ischemic etiology. Thus, we decided for separate analysis of each group and we indicated that only the ICD presence was a common prognostic factor for both groups. The others (max VO_2, LVEF, uric acid, and MDA) were risk factors for the endpoint in ischemic etiology whereas thiazide diuretic therapy, concentration of NT-proBNP, bilirubin, and MDA/PSH ratio in the nonischemic group. Our results proved influence of different redox biomarkers on one-year prognosis in HF cohorts of ischemic and nonischemic etiology. Nowadays, it is usually difficult to predict which patients will benefit most from the different therapy; maybe when we pay attention on deviations in redox biomarkers, it would help us in qualifying patients for the use of, e.g., allopurinol, as donors of SH groups.

Data Availability

The original data is available after contact with the corresponding author.

Conflicts of Interest

The authors declare that there is no conflict of interests regarding the publication of this paper.

Acknowledgments

References

[1] M. Seddon, Y. H. Looi, and A. M. Shah, "Oxidative stress and redox signalling in cardiac hypertrophy and heart failure," *Heart*, vol. 93, no. 8, pp. 903–907, 2007.

[2] L. Lorente, M. M. Martín, and P. Abreu-González, "Prognostic value of malondialdehyde serum levels in severe sepsis: a multicenter study," *PLoS One*, vol. 8, no. 1, article e53741, 2013.

[3] S. Mao, A. Zhang, and S. Huang, "Serum levels of malondialdehyde, vitamin C and E in idiopathic nephrotic syndrome: a meta-analysis," *Renal Failure*, vol. 36, no. 6, pp. 994–999, 2014.

[4] L. Turell, R. Radi, and B. Alvarez, "The thiol pool in human plasma: the central contribution of albumin to redox processes," *Free Radical Biology & Medicine*, vol. 65, pp. 244–253, 2013.

[5] A. E. Abdulle, A. R. Bourgonje, L. M. Kieneker et al., "Serum free thiols predict cardiovascular events and all-cause mortality in the general population: a prospective cohort study," *BMC Medicine*, vol. 18, no. 1, p. 130, 2020.

[6] K. F. Adams Jr., S. H. Dunlap, C. A. Sueta et al., "Relation between gender, etiology and survival in patients with symptomatic heart failure," *Journal of the American College of Cardiology*, vol. 28, no. 7, pp. 1781–1788, 1996.

[7] SOLVD Investigators, "Effect of enalapril on survival in patients with reduced left ventricular ejection fractions and congestive heart failure," *New England Journal of Medicine*, vol. 325, no. 5, pp. 293–302, 1991.

[8] D. Gajanana, M. Shah, P. Junpapart, A. Romero-Corral, V. M. Figueredo, and B. Bozorgnia, "Mortality in systolic heart failure revisited: ischemic versus non-ischemic cardiomyopathy," *International Journal of Cardiology*, vol. 224, pp. 15–17, 2016.

[9] R. Corbalan, J.-P. Bassand, L. Illingworth et al., "Analysis of outcomes in ischemic vs nonischemic cardiomyopathy in patients with atrial fibrillation," *JAMA Cardiology*, vol. 4, no. 6, pp. 526–548, 2019.

[10] E. Romuk, C. Wojciechowska, and W. Jacheć, "Comparison of oxidative stress parameters in heart failure patients depending on ischaemic or nonischaemic aetiology," *Oxidative medicine and cellular longevity*, vol. 2019, Article ID 7156038, 2019.

[11] G. M. Felker, L. K. Shaw, and C. M. O'Connor, "A standardized definition of ischemic cardiomyopathy for use in clinical research," *Journal of the American College of Cardiology*, vol. 39, no. 2, pp. 210–218, 2002.

[12] The Criteria Committee of the New York Heart Association, *Nomenclature and Criteria for Diagnosis of Diseases of the Heart and Blood Vessels*, Little Brown, Boston, Mass, USA, 1964.

[13] R. M. Lang, M. Bierig, R. B. Devereux et al., "Recommendations for chamber quantification: a report from the American Society of Echocardiography's Guidelines and Standards Committee and the Chamber Quantification Writing Group, developed in conjunction with the European Association of Echocardiography, a branch of the European Society of Cardiology," *Journal of the American Society of Echocardiography*, vol. 18, no. 12, pp. 1440–1463, 2005.

[14] O. Erel, "A new automated colorimetric method for measuring total oxidant status," *Clinical Biochemistry*, vol. 38, no. 12, pp. 1103–1111, 2005.

[15] O. Erel, "A novel automated method to measure total antioxidant response against potent free radical reactions," *Clinical Biochemistry*, vol. 37, no. 2, pp. 112–119, 2004.

[16] J. F. Koster, P. Biemond, and A. J. Swaak, "Intracellular and extracellular sulphydryl levels in rheumatoid arthritis," *Annals of the Rheumatic Diseases*, vol. 45, no. 1, pp. 44–46, 1986.

[17] H. Ohkawa, N. Ohishi, and K. Yagi, "Assay for lipid peroxides in animal tissues by thiobarbituric acid reaction," *Analytical Biochemistry*, vol. 95, no. 2, pp. 351–358, 1979.

[18] C. Lourenço, F. Saraiva, H. Martins et al., "Ischemic versus non-ischemic cardiomyopathy: are there differences in prognosis? Experience of an advanced heart failure center," *Revista Portuguesa de Cardiologia*, vol. 30, no. 2, pp. 181–197, 2011.

[19] D. Anker, W. Doehner, M. Rauchhaus et al., "Uric acid and survival in chronic heart failure: validation and application in metabolic, functional, and hemodynamic staging," *Circulation*, vol. 107, no. 15, pp. 1991–1997, 2003.

[20] E. A. Jankowska, B. Ponikowska, J. Majda et al., "Hyperuricaemia predicts poor outcome in patients with mild to moderate chronic heart failure," *International Journal of Cardiology*, vol. 115, no. 2, pp. 151–155, 2007.

[21] H. Sakai, T. Tsutamoto, T. Tsutsui, T. Tanaka, C. Ishikawa, and M. Horie, "Serum level of uric acid, partly secreted from the failing heart, is a prognostic marker in patients with congestive heart failure," *Circulation Journal*, vol. 70, no. 8, pp. 1006–1011, 2006.

[22] M. M. Givertz, D. L. Mann, K. L. Lee et al., "Xanthine oxidase inhibition for hyperuricemic heart failure patients: design and rationale of the EXACT-HF study," *Circulation. Heart Failure*, vol. 6, no. 4, pp. 862–868, 2013.

[23] L. S. Terada, D. M. Guidot, J. A. Leff et al., "Hypoxia injures endothelial cells by increasing endogenous xanthine oxidase

activity," *Proceedings of the National Academy of Sciences of the United States of America*, vol. 89, no. 8, pp. 3362–3366, 1992.

[24] S. Radovanovic, A. Savic-Radojevic, M. Pljesa-Ercegovac et al., "Markers of oxidative damage and antioxidant enzyme activities as predictors of morbidity and mortality in patients with chronic heart failure," *Journal of Cardiac Failure*, vol. 18, no. 6, pp. 493–501, 2012.

[25] C. R. Díaz-Vélez, S. García-Castiñeiras, E. Mendoza-Ramos, and E. Hernández-López, "Increased malondialdehyde in peripheral blood of patients with congestive heart failure," *American Heart Journal*, vol. 131, no. 1, pp. 146–152, 1996.

[26] Y. Nishiyama, H. Ikeda, N. Haramaki, N. Yoshida, and T. Imaizumi, "Oxidative stress is related to exercise intolerance in patients with heart failure," *American Heart Journal*, vol. 135, no. 1, pp. 115–120, 1998.

[27] J. McMurray, J. McLay, M. Chopra, A. Bridges, and J. J. F. Belch, "Evidence for enhanced free radical activity in chronic congestive heart failure secondary to coronary artery disease," *The American Journal of Cardiology*, vol. 65, no. 18, pp. 1261-1262, 1990.

[28] M. Keith, A. Geranmayegan, M. J. Sole et al., "Increased oxidative stress in patients with congestive heart failure," *Journal of the American College of Cardiology*, vol. 31, no. 6, pp. 1352–1356, 1998.

[29] E. Tingberg, A. K. Ohlin, A. Gottsäter, and H. Ohlin, "Lipid peroxidation is not increased in heart failure patients on modern pharmacological therapy," *International Journal of Cardiology*, vol. 112, no. 3, pp. 275–281, 2006.

[30] C. Wojciechowska, E. Romuk, A. Tomasik et al., "Oxidative stress markers and C-reactive protein are related to severity of heart failure in patients with dilated cardiomyopathy," *Mediators of Inflammation*, vol. 2014, Article ID 147040, 2014.

[31] M. F. Walter, R. F. Jacob, B. Jeffers et al., "Serum levels of thiobarbituric acid reactive substances predict cardiovascular events in patients with stable coronary artery disease: a longitudinal analysis of the PREVENT study," *Journal of the American College of Cardiology*, vol. 44, no. 10, pp. 1996–2002, 2004.

[32] F. Mach, C. Baigent, A. L. Catapano et al., "2019 ESC/EAS Guidelines for the management of dyslipidaemias: lipid modification to reduce cardiovascular risk," *European Heart Journal*, vol. 41, no. 1, pp. 111–188, 2020.

[33] T. Amaki, T. Suzuki, F. Nakamura et al., "Circulating malondialdehyde modified LDL is a biochemical risk marker for coronary artery disease," *Heart*, vol. 90, no. 10, pp. 1211–1213, 2004.

[34] K. Tajika, K. Okamatsu, M. Takano et al., "Malondialdehyde-modified low-density lipoprotein is a useful marker to identify patients with vulnerable plaque," *Circulation Journal*, vol. 76, no. 9, pp. 2211–2217, 2012.

[35] S. Tani, I. Watanabe, T. Anazawa et al., "Effect of *Pravastatin* on Malondialdehyde-Modified Low-Density Lipoprotein Levels and Coronary Plaque Regression as Determined by Three-Dimensional Intravascular Ultrasound," *The American Journal of Cardiology*, vol. 96, no. 8, pp. 1089–1094, 2005.

[36] K. C. Gracia, D. Llanas-Cornejo, and H. Husi, "CVD and oxidative stress," *Journal of Clinical Medicine*, vol. 6, no. 2, 2017.

[37] A. S. Frenay, M. H. de Borst, M. Bachtler et al., "Serum free sulfhydryl status is associated with patient and graft survival in renal transplant recipients," *Free Radical Biology & Medicine*, vol. 99, pp. 345–351, 2016.

[38] H. Kundi, I. Ates, E. Kiziltunc et al., "A novel oxidative stress marker in acute myocardial infarction; thiol/disulphide homeostasis," *The American Journal of Emergency Medicine*, vol. 33, no. 11, pp. 1567–1571, 2015.

[39] J. J. Belch, A. B. Bridges, N. Scott, and M. Chopra, "Oxygen free radicals and congestive heart failure," *British Heart Journal*, vol. 65, no. 5, pp. 245–248, 1991.

[40] A. M. Koning, W. C. Meijers, A. Pasch et al., "Serum free thiols in chronic heart failure," *Pharmacological Research*, vol. 111, pp. 452–458, 2016.

[41] M. M. Cortese-Krott, A. Koning, G. G. C. Kuhnle et al., "The reactive species interactome: evolutionary emergence, biological significance, and opportunities for redox metabolomics and personalized medicine," *Antioxidants & Redox Signaling*, vol. 27, no. 10, pp. 684–712, 2017.

[42] A. C. Boon, C. L. Hawkins, K. Bisht et al., "Reduced circulating oxidized LDL is associated with hypocholesterolemia and enhanced thiol status in Gilbert syndrome," *Free Radical Biology & Medicine*, vol. 52, no. 10, pp. 2120–2127, 2012.

[43] L. J. Horsfall, G. Rait, K. Walters et al., "Serum bilirubin and risk of respiratory disease and death," *JAMA*, vol. 305, no. 7, pp. 691–697, 2011.

[44] L. Vitek, "The association of elevated serum bilirubin levels and coronary heart disease," *Journal of Hepatology*, vol. 39, no. 5, pp. 881-882, 2003.

[45] A. Lingenhel, B. Kollerits, J. P. Schwaiger et al., "Serum bilirubin levels, UGT1A1 polymorphisms and risk for coronary artery disease," *Experimental Gerontology*, vol. 43, no. 12, pp. 1102–1107, 2008.

[46] A. Noman, D. S. Ang, S. Ogston, C. C. Lang, and A. D. Struthers, "Effect of high-dose allopurinol on exercise in patients with chronic stable angina: a randomised, placebo controlled crossover trial," *The Lancet*, vol. 375, no. 9732, pp. 2161–2167, 2010.

[47] J. George, E. Carr, J. Davies, J. J. F. Belch, and A. Struthers, "High-dose allopurinol improves endothelial function by profoundly reducing vascular oxidative stress and not by lowering uric acid," *Circulation*, vol. 114, no. 23, pp. 2508–2516, 2006.

[48] A. D. Struthers, P. T. Donnan, P. Lindsay, D. McNaughton, J. Broomhall, and T. MacDonald, "Effect of allopurinol on mortality and hospitalisations in chronic heart failure: a retrospective cohort study," *Heart*, vol. 87, no. 3, pp. 229–234, 2002.

[49] I. T. Mak, A. M. Freedman, B. F. Dickens, and W. B. Weglicki, "Protective effects of sulfhydryl-containing angiotensin converting enzyme inhibitors against free radical injury in endothelial cells," *Biochemical Pharmacology*, vol. 40, no. 9, pp. 2169–2175, 1990.

[50] K. Nakamura, M. Murakami, D. Miura et al., "Beta-blockers and oxidative stress in patients with heart failure," *Pharmaceuticals*, vol. 4, no. 8, pp. 1088–1100, 2011.

Research Article

Anti-Interleukin-16 Neutralizing Antibody Treatment Alleviates Sepsis-Induced Cardiac Injury and Dysfunction via the Nuclear Factor Erythroid-2 Related Factor 2 Pathway in Mice

Jianwei Zhang,[1] Zicong Yang,[2] Zhishan Liang,[2] Mengjie Wang,[2] Changxing Hu,[2] Chao Chang,[3] Lei Shi,[2] Qingwei Ji [ID],[2] and Ling Liu [ID][2]

[1]*Department of Cardiology, Beijing Anzhen Hospital, Capital Medical University, Beijing Institute of Heart Lung and Blood Vessel Diseases, Beijing Key Laboratory of Precision Medicine of Coronary Atherosclerotic Disease, Clinical Center for Coronary Heart Disease, Capital Medical University, Beijing 100029, China*
[2]*Department of Cardiology, The People's Hospital of Guangxi Zhuang Autonomous Region, Nanning, China*
[3]*Department of Cardiology, Handan First Hospital, Handan, Hebei, China*

Correspondence should be addressed to Qingwei Ji; jqw124@163.com and Ling Liu; gxliu@126.com

Received 18 October 2020; Revised 12 January 2021; Accepted 18 January 2021; Published 13 February 2021

Academic Editor: Marina Politi Okoshi

Several interleukin (IL) members have been reported to participate in sepsis. In this study, the effects of IL-16 on sepsis-induced cardiac injury and dysfunction were examined, and the related mechanisms were detected. IL-16 expression in septic mice was first measured, and the results showed that both cardiac and serum IL-16 expression levels were increased in mice with sepsis induced by LPS or cecal ligation and puncture (CLP) compared with control mice. Then, IL-16 was neutralized, and the effects on lipopolysaccharide- (LPS-) induced cardiac injury were detected. The results showed that an anti-IL-16 neutralizing antibody (nAb) significantly reduced mortality and increased serum lactate dehydrogenase (LDH), creatine kinase myocardial bound (CK-MB), and cardiac troponin T (cTnT) levels while improving cardiac function in mice with LPS-induced sepsis. Neutralization of IL-16 also increased the activation of antioxidant pathways and the expression of antioxidant factors in septic mice while decreasing the activation of prooxidant pathways and the expression of prooxidants. Treatment with the anti-IL-16 nAb increased mitochondrial apoptosis-inducing factor (AIF) expression, decreased nuclear AIF and cleaved poly-ADP-ribose polymerase (PARP) expression, and decreased TUNEL-positive cell percentages in LPS-treated mice. Additionally, treatment with CPUY192018, the nuclear factor erythroid-2 related factor 2 (Nrf2) pathway, significantly increased mortality and reversed the above effects in mice treated with LPS and the anti-IL-16 nAb. Our results showed that the anti-IL-16 nAb regulates oxidative stress through the Nrf2 pathway and participates in the regulation of cardiac injury in septic mice. Neutralization of IL-16 may be a beneficial strategy for the prevention of cardiac injury and dysfunction in sepsis patients.

1. Introduction

Sepsis is a complex set of clinical syndromes that can lead to the failure of multiple vital organs. The most dangerous effects are cardiac injury and subsequent cardiac dysfunction, which is one of the most important complications affecting prognosis [1–3]. Due to its high incidence rate and its strong correlations with intensive care unit (ICU) admission and in-hospital mortality, sepsis was listed as a global health priority at the 2017 World Health Assembly [3, 4]. Further understanding of the pathogenesis of sepsis is crucial for sepsis treatment.

Interleukins (ILs) are a class of pluripotent cytokines that mediate multiple biological effects, and data from clinical and animal studies have demonstrated the involvement of multiple members of the interleukin family in sepsis. In an earlier study, circulating IL-26 levels were found to be significantly elevated in sepsis patients and to be correlated with severity and survival, and peritoneal inflammatory responses were found to be increased in septic mice treated

with recombinant human IL-26 [5]. In another study, IL-33 deficiency aggravated sepsis-induced lung injury, while supplementation with IL-5 reversed this effect in IL-33 knockout mice, suggesting that IL-33 participates in the process of sepsis-induced lung injury by regulating IL-5 release [6]. In mice with cecal ligation and puncture- (CLP-) induced sepsis, treatment with IL-34 has been found to significantly reduce macrophage infiltration, protect against organ injury, and improve survival, while neutralization of IL-34 exerts the opposite effects [7]. Serum IL-38 levels are elevated in both septic adults and septic children, and neutralization of IL-38 significantly amplifies inflammatory responses and reduces survival in mice with both lipopolysaccharide- (LPS-) and CLP-induced sepsis [8].

IL-16, an important chemokine, is widely expressed in a variety of immune and nonimmune cells [9, 10]. In addition to regulating the infiltration and differentiation of immune cells, IL-16 has also been reported to regulate biological effects such as the inflammatory response and apoptosis [10–14]. To date, IL-16 has been shown to be involved in a variety of diseases, and its related mechanisms involve mainly the regulation of the inflammatory response [11–14]. IL-16 also plays roles in carotid atherosclerosis and angiotensin II- (Ang II-) induced cardiac fibrosis by amplifying inflammatory responses [15, 16]. However, the role of IL-16 in sepsis and its regulatory effects on oxidative stress are unknown. In this study, we determined whether IL-16 participates in sepsis-induced cardiac injury and dysfunction through the regulation of oxidative stress.

2. Experimental Materials and Methods

2.1. Mice, Treatments, and Sepsis Model Construction.

The use of the mice and the procedure for the experiment were approved by the Ethics Committee of the People's Hospital of Guangxi Zhuang Autonomous Region (approval no. 2015-16). Male wild-type (WT) mice purchased from Beijing Vital River Laboratory Animal Technology were used in this study. WT mice aged 10 weeks and weighing 25-27 g were used for the following experiments. First, mice were intraperitoneally injected (i.p.) with 10 mg/kg LPS (Sigma) or subjected to CLP for 6 hours. Some mice were given 400 μ/kg polyethylene glycol- (PEG-) superoxide dismutase (SOD) within 1 hour of sepsis [17]. Control mice received saline or underwent sham surgery and were treated with PBS (parts 1-2, $n = 6$). IL-16 expression was detected in these mice. Furthermore, WT mice were pretreated with 200 μg of a mouse anti-IL-16 neutralizing antibody (nAb, BD Biosciences) or the same amount of isotype IgG (BD Biosciences) for 1 hour and then treated with LPS or saline for 6 hours (part 3, $n = 10$). Some mice were observed for 8 days (part 4, $n = 9$-13), and the mortality rates were recorded [16]. Additionally, mice that received the anti-IL-16 nAb or IgG were also given 50 μl of dimethyl sulfoxide (DMSO, Sigma) or 5 mg/kg CPUY192018 (Sigma), a nuclear factor erythroid-2 related factor 2 (Nrf2) pathway inhibitor, and were treated with LPS (part 5, $n = 10$) [18]. The mortality rates of the different groups of mice were recorded during an 8-day follow-up

(part 6, $n = 9$-12). The treatment of mice and the establishment of the sepsis model are shown in Figure 1.

In addition to LPS, CLP was used to establish a mouse sepsis model. According to the descriptions in previous literature, the general process was as follows: after anesthesia via inhalation of 1.5% isoflurane, the mice were laid flat on the operating table, and the entire abdomen of each rat was shaved. After alcohol disinfection, the abdominal skin was cut open, and the abdominal cavity was exposed. The cecum was found and ligated at half the distance between the distal pole and the base of the cecum, and then the cecum was punctured once from the mesenteric toward the antimesenteric direction using 26 G needles. The operation was considered complete after the skin was sutured and the abdominal skin was again disinfected [19].

2.2. Cell Culture Study.

The mouse HL-1 cardiomyocytes used in this study were purchased from the American Type Culture Collection (ATCC, USA). HL-1 cardiomyocytes were plated in a 10 cm petri dish and cultured in the RPMI 1640 medium with 10% fetal bovine serum (both from Gibco, USA) in batches. HL-1 cardiomyocytes were transferred to 6 cm petri dishes once enough cells were obtained. After covering the 6 cm petri dish, the cells were synchronized for 24 hours and divided into 3 groups as follows: a group treated with 1 μmol/ml LPS for 6 hours, a group treated with LPS+100 U/l PEG-SOD for 6 hours, and a control group treated with PBS [20, 21]. The culture medium was changed, and the stimulation was repeated every six hours. Twelve hours later, both the HL-1 cardiomyocytes and the culture supernatant were collected for IL-16 expression analysis.

2.3. Analysis of Cardiac Function.

The mice were anesthetized with 1.5% isoflurane and laid flat on the operating table, and echocardiography was performed using a MyLab 30CV (Esaote) ultrasound system with a 15 MHz probe to measure left ventricular function in the mice. The left ventricular end-diastolic diameter (LVEDD), left ventricular end-systolic diameter (LVESD), left ventricular ejection fraction (LVEF, LVFS (%) = (LVEDD − LVESD)/LVEDD × 100%), and fractional shortening (FS) data were collected from 10 cardiac cycles and averaged.

2.4. Detection of Serum Levels of IL-16 and Cardiac Injury Markers.

A mouse IL-16 enzyme-linked immunosorbent assay (ELISA) kit was purchased from BioLegend, and assay kits for cardiac injury markers, including lactate dehydrogenase (LDH), creatine kinase myocardial bound (CK-MB), and cardiac troponin T (cTnT), were purchased from Beyotime Biotechnology. Serum was collected after blood samples were centrifuged at 3000 × g for 20 minutes, and then the serum levels of IL-16, LDH, CK-MB, and cTnT were detected based on the manufacturer's instructions.

2.5. Separation of Mitochondria and Nuclei and Detection of Protein.

Mitochondria were isolated from the left ventricle (LV) using a mitochondrial isolation kit (Cayman) as described in our previous study [22]. In brief, fresh LV tissue was lysed using a mitochondrial separation solution and then centrifuged at 700 × g for 10 minutes. Then, the supernatant

FIGURE 1: Establishment and pretreatment of the mouse sepsis model. WT: wild-type; PBS: phosphate-buffered saline; SOD: superoxide dismutase; LPS: lipopolysaccharide; CLP: cecal ligation and puncture; nAb: anti-IL-16 neutralizing antibody; CPU: CPUY192018; DMSO: dimethyl sulfoxide.

was obtained and further centrifuged at $6000 \times g$ for 10 minutes. The granular material at the bottom of the EP tube was collected as the mitochondrial fraction.

Nuclei were collected using a nuclear separation kit (Njjcbio) as previously described [22]. First, fresh LV tissue was lysed using the lysis buffer contained in the kit, and the homogenate was obtained and centrifuged at $1000 \times g$ for 10 minutes. The granular material at the bottom of the EP tube was collected as the nuclear fraction.

Furthermore, western blotting was performed to detect protein expression as described in our previous study [23]. Briefly, mitochondria, nuclei, and LV tissue were lysed using the RIPA lysis buffer containing protease inhibitors and phosphatase inhibitors (both from Roche), and the total protein in each sample was collected after centrifugation ($4000 \times g$) at 4°C and quantified using a BCA Protein Assay Kit (Thermo Fisher Scientific). Then, the proteins in $20\,\mu g$ total protein samples were separated by 10% gel electrophoresis and transferred to PVDF membranes (Millipore). After blocking with 5% nonfat milk, the membranes were incubated with the corresponding primary antibodies, which were used to label the target protein at 4°C overnight. The protein expression levels of IL-16, Nrf2, heme oxygenase 1 (HO-1), nicotinamide adenine nucleotide phosphate (NADPH) oxidase 2 (Nox2), Nox4, and GAPDH (antibodies all purchased from Abcam) in the LV; mitochondrial apoptosis-inducing

factor (AIF) and cytochrome c oxidase IV (Cox IV) in mitochondria; and AIF, cleaved poly-ADP-ribose polymerase (PARP), and proliferating cell nuclear antigen (PCNA) in nuclei were labeled. Most of the blots originate from the same membrane in the figures. A small number of proteins are closer in molecular weight, so not all of them are in the same membrane. After incubation with the secondary antibody at room temperature for 1 hour, the blots were scanned using Odyssey (LI-COR Biosciences).

2.6. Analysis of Oxidative Stress Markers. In this study, appropriate kits (all purchased from Nanjing Jiancheng Bioengineering Institute) were used to detect serum SOD activity, glutathione (GSH) levels, NADPH oxidase activity, and malondialdehyde (MDA) levels according to the manufacturer's protocols. These molecules are all markers of oxidative stress.

2.7. Histological Analysis. After fixation, hearts were embedded in paraffin, cut into approximately $5\,\mu m$ thick sections, and mounted on slides. A mouse anti-4-hydroxynonenal (4-HNE) antibody (Abcam, UK) was used to perform 4-HNE staining to detect cardiac oxidative stress as described in our previous study [23]. Briefly, the sections were first deparaffinized and blocked and then incubated with the anti-4-HNE antibody (1:200) overnight at 4°C. Following
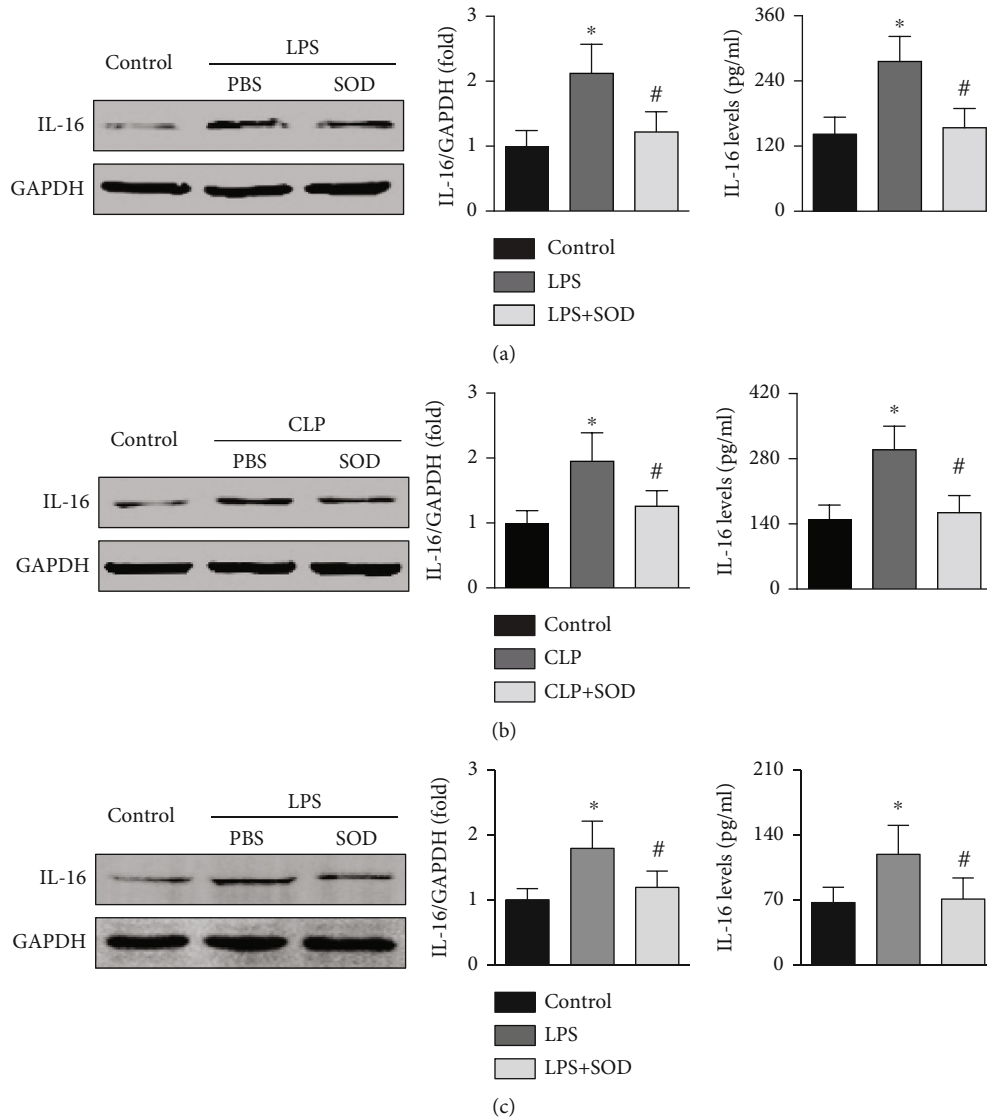
FIGURE 2: Effects of oxidative stress on IL-16 expression in sepsis. (a) Effects of SOD on cardiac IL-16 and serum IL-16 expression in LPS-treated mice (one-way ANOVA). (b) Effects of SOD on IL-16 expression in CLP-induced septic mice (nonparametric test). (c) Effect of SOD on IL-16 expression in LPS-treated HL-1 cardiomyocytes (nonparametric test). $n = 6$ in each group. $^*p < 0.05$ vs. the control group. $^#p < 0.05$ vs. the LPS- or CLP-induced sepsis group. LPS: lipopolysaccharide; CLP: cecal ligation and puncture; SOD: superoxide dismutase.

incubation with the anti-rabbit HRP reagent for 1 h at 25°C and development using a peroxide-based substrate DAB kit (Genentech), the sections were dehydrated in ethanol and cleared in xylene. A commercially available kit was used to perform terminal deoxynucleotidyl transferase-mediated dUTP nick end labeling (TUNEL) staining (Millipore, USA) for analysis of cardiac apoptotic cells.

2.8. Data Statistics and Analysis. Data contained in this study are expressed as the mean ± SD and were analyzed by GraphPad Prism 8. When the data had a normal distribution, the differences between 2 groups were compared by Student's t-test, while differences in the mean during multiple (≥3) groups were determined using two-way ANOVA, followed by Tukey's multiple comparison test. While the data had an abnormal distribution, the differences were analyzed

using a nonparametric test. The survival rates of mice during the 8-day follow-up were analyzed using the log-rank test. A p value less than 0.05 was considered statistically significant.

3. Results

3.1. Oxidative Stress Regulates IL-16 Expression in Sepsis. In mice with LPS-induced sepsis, both cardiac and serum IL-16 expression levels were increased, but these increases were reversed by PEG-SOD treatment (Figure 2(a)). Similar trends were found for IL-16 expression in mice with CLP-induced sepsis (Figure 2(b)). LPS treatment also increased IL-16 expression in cardiomyocytes and IL-16 levels in the culture supernatant, while IL-16 levels were reduced in both the cardiomyocytes and the culture supernatant after PEG-SOD
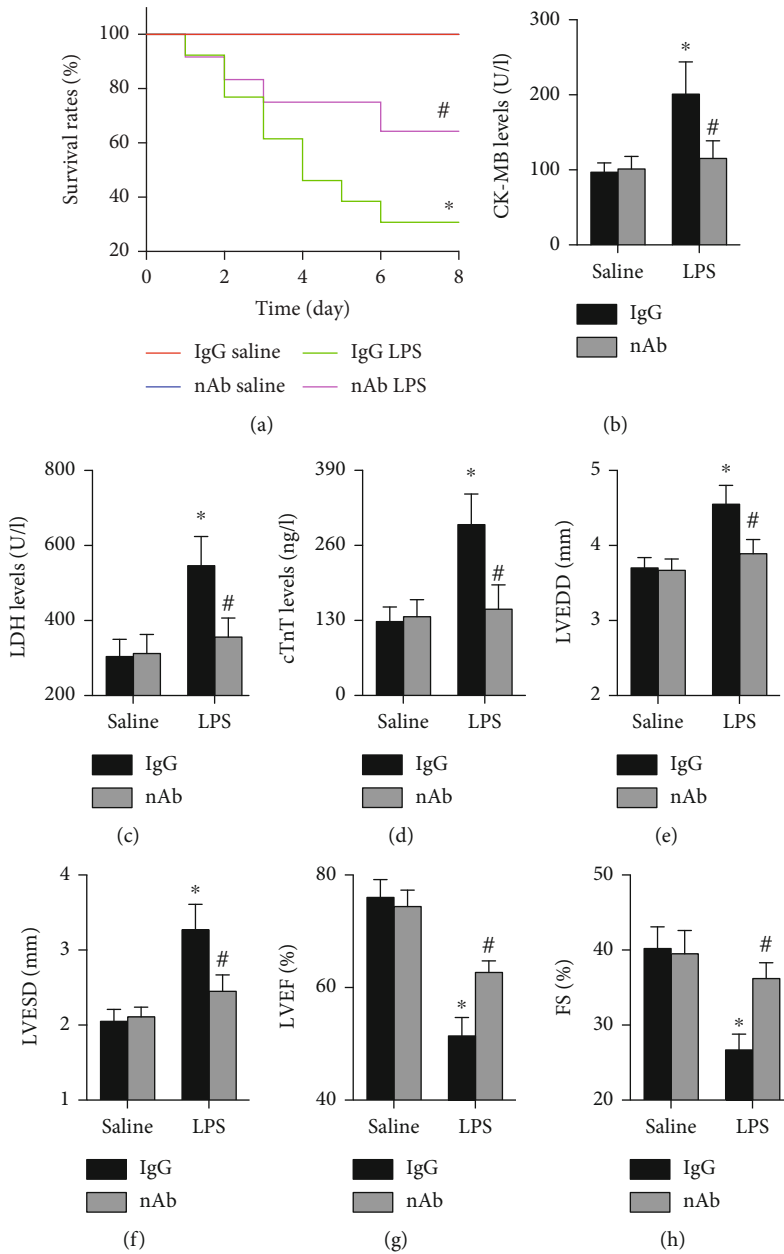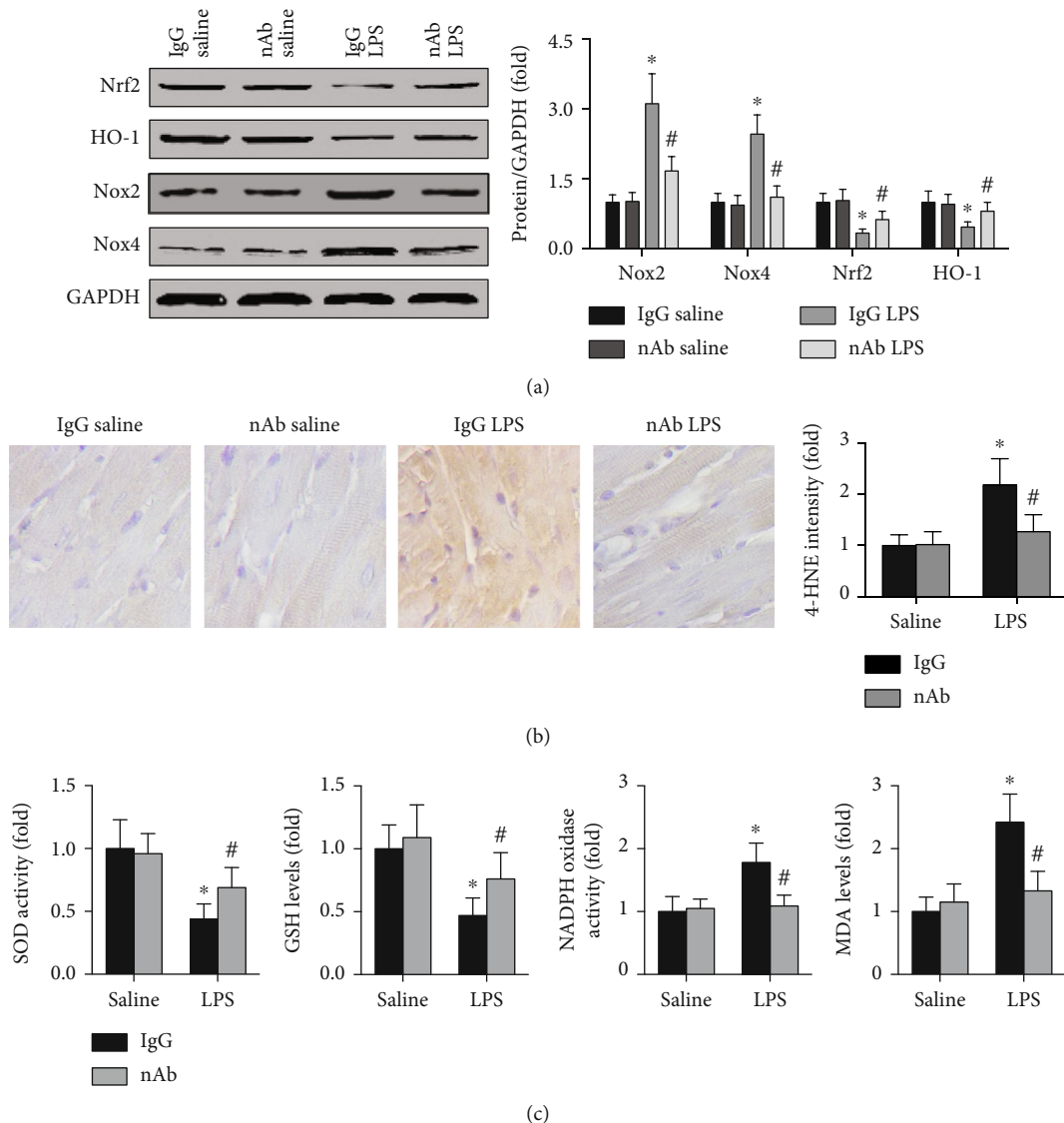
FIGURE 3: Effects of anti-IL-16 nAb on cardiac injury and function in septic mice. (a) Survival rates during the 8-day follow-up in each group (log-rank test). (b–d) Serum levels of oxidative stress markers in the four groups (two-way ANOVA). (e–h) Cardiac structure and function were determined by echocardiography (nonparametric test). $n = 5$-10 in each group. $^*p < 0.05$ vs. the IgG saline group. $^\#p < 0.05$ vs. the IgG LPS group. nAb: anti-IL-16 neutralizing antibody; LPS: lipopolysaccharide; LDH: lactate dehydrogenase; CK-MB: creatine kinase myocardial bound; cTnT: cardiac troponin T; LVEDD: left ventricular end-diastolic diameter; LVESD: left ventricular end-systolic diameter; LVEF: left ventricular ejection fraction; FS: fractional shortening.

treatment (Figure 2(c)). In this section, the blots of IL-16 and GAPDH originated from the same membrane.

3.2. Anti-IL-16 nAb Treatment Alleviates Sepsis-Induced Cardiac Injury and Dysfunction in Mice.
The effects of the anti-IL-16 nAb on survival rates in each group were first analyzed, and the results showed that the anti-IL-16 nAb significantly improved survival rates in mice with LPS-induced sepsis but did not affect survival rates in saline-treated mice (Figure 3(a)). LPS-treated mice also showed higher serum

CK-MB, LDH, and cTnT levels than control mice, and the LPS-induced increases were reversed by the anti-IL-16 nAb (Figures 3(b)–3(d)). In addition, neutralization of IL-16 reduced the LVEDD and LVESD and increased the percentages of both LVEF and FS in septic mice but did not affect LVEF or FS in mice without sepsis (Figures 3(e)–3(h)).

3.3. Anti-IL-16 nAb Treatment Reduces Oxidative Stress in Septic Mice.
Furthermore, the effects of the anti-IL-16 nAb on oxidative stress were detected. The results showed that

(a)

(b)

(c)

FIGURE 4: Effects of anti-IL-16 nAb on oxidative stress in septic mice. (a) Cardiac protein expression of Nrf2, HO-1, Nox2, Nox4, and GAPDH in each group was detected and analyzed (two-way ANOVA). (b) The cardiac 4-HNE intensity of the four groups was measured (nonparametric test). (c) The activities of SOD and NADPH oxidase and the levels of GSH and MDA in serum were determined (two-way ANOVA). $n = 5$ in each group. $^*p < 0.05$ vs. the IgG saline group. $^#p < 0.05$ vs. the IgG LPS group. Nrf2: nuclear factor erythroid-2 related factor 2; HO-1: heme oxygenase 1; Nox2/4: nicotinamide adenine nucleotide phosphate oxidase 2/4; nAb: anti-IL-16 neutralizing antibody; LPS: lipopolysaccharide; 4-HNE: 4-hydroxynonenal; SOD: superoxide dismutase; GSH: glutathione; NADPH: nicotinamide adenine nucleotide phosphate; MDA: malondialdehyde.

neutralization of IL-16 increased cardiac Nrf2 and HO-1 expression while decreasing cardiac Nox2 and Nox4 levels in septic mice (Figure 4(a)). In this section, the blots of Nrf2, HO-1, and Nox4 did not originate from the same membrane because their molecular weights are similar to those of Nox2 or GAPDH or Nrf2. Lower cardiac 4-HNE staining intensity was observed in anti-IL-16 nAb-treated septic mice than in IgG-treated septic mice (Figure 4(b)). In addition, anti-IL-16 nAb treatment also increased SOD activity and GSH levels while decreasing Nox activity and MDA levels in serum from septic mice (Figure 4(c)).

3.4. Anti-IL-16 nAb Treatment Decreases AIF-Related Cardiomyocyte Apoptosis in Septic Mice. AIF expression was detected in both mitochondria and nuclei from LV tissue. The results showed that neutralization of IL-16 significantly increased mitochondrial AIF expression while decreasing nuclear AIF and cleaved PARP expression in septic mice (Figure 5(a)). The blots of AIF and Cox IV in the mitochondria originated from the same membrane, and the blots of cleaved PARP, AIF, and PCNA in the nucleus originated from the same membrane. In addition, fewer TUNEL-positive cells were observed in nAb- and LPS-treated mice than in IgG- and LPS-treated mice (Figure 5(b)). The anti-
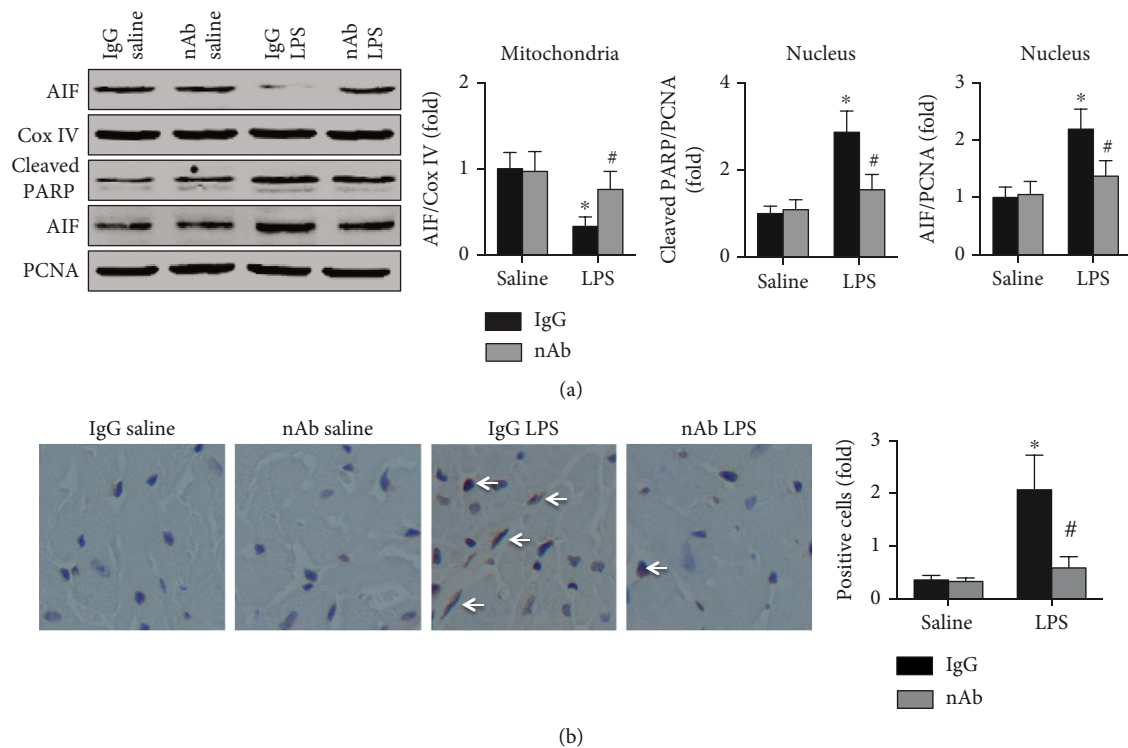
(a)

(b)

FIGURE 5: Effects of IL-16 nAb on AIF expression in LPS-treated mice. (a) Cardiac mitochondrial AIF and Cox IV expression and cardiac nuclear AIF, cleaved PARP, and PCNA expression in each group were detected (two-way ANOVA). (b) TUNEL-positive cells in the four groups were analyzed (nonparametric test). $n = 5$ in each group. $^*p < 0.05$ vs. the IgG saline group. $^\#p < 0.05$ vs. the IgG LPS group. AIF: apoptosis-inducing factor; Cox IV: cytochrome c oxidase IV; PARP: poly-ADP-ribose polymerase; PCNA: proliferating cell nuclear antigen; nAb: anti-IL-16 neutralizing antibody; LPS: lipopolysaccharide.

IL-16 nAb did not affect either the AIF expression or the number of TUNEL-positive cells (Figures 5(a) and 5(b)).

3.5. CPUY192018 Treatment Reverses the Effects of Anti-IL-16 nAb Treatment on Sepsis-Induced Cardiac Injury.
The effects of CPUY192018 on survival rates were determined, and the results showed that CPUY192018 treatment significantly increased mortality in anti-IL-16 nAb-treated septic mice (Figure 6(a)). Serum LDH, CK-MB, and cTnT levels were all elevated by CPUY192018 in anti-IL-16 nAb-treated septic mice (Figures 6(b)–6(d)). Higher LVEDD and LVESD and lower LVEF and FS percentages were observed in CPUY192018-treated septic mice than in CPUY192018-treated mice without LPS-induced sepsis (Figures 6(e)–6(h)).

3.6. The Nrf2 Pathway Mediates the Antioxidative and Antiapoptotic Effects of Anti-IL-16 nAb Treatment in Septic Mice.
Treatment with CPUY192018 decreased Nrf2 and HO-1 levels and increased Nox2 and Nox4 expression in anti-IL-16 nAb-treated septic mice (Figure 7(a)). The anti-IL-16 nAb-mediated reductions in Nox and MDA levels and the increases in SOD activity and GSH levels in mice with LPS-induced sepsis were reversed by CPUY192018 treatment (Figure 7(b)). Additionally, inhibition of the Nrf2 pathway with CPUY192018 decreased cardiac mitochondrial AIF expression while increasing cardiac nuclear AIF and cleaved PARP expression in septic mice pretreated with the anti-IL-16 nAb (Figure 7(c)).

4. Discussion

In this study, we examined the effect of IL-16 on sepsis-induced cardiac injury and dysfunction and focused on oxidative stress to elucidate the possible mechanisms. We found, for the first time, that both cardiac and serum IL-16 expression levels were elevated in both LPS- and CLP-induced mouse sepsis models. Moreover, neutralization of IL-16 significantly improved survival rates, ameliorated cardiac dysfunction, reduced the expression of multiple cardiac injury markers, alleviated oxidative stress, and protected cardiomyocytes from apoptosis. Inhibition of the Nrf2 pathway with CPUY192018 significantly reversed the above effects of the anti-IL-16 nAb in septic mice.

The mechanisms by which sepsis induces cardiac injury and dysfunction are very complex; data from animal studies have revealed that a variety of complex pathological effects, including inflammation, oxidative stress, and autophagy, are involved [24–26]. In recent years, an increasing number of studies have focused on oxidative stress because sepsis can lead to severe oxidative stress in a variety of different organs and tissues [26–28]. Our study revealed that the expression of IL-16 was significantly increased in septic mice and LPS-treated cardiomyocytes and that this upregulation could be reversed by SOD, a common antioxidant. These results suggest that IL-16 expression is regulated by oxidative stress levels during sepsis, although IL-16 release in other models is regulated by inflammatory responses. In a
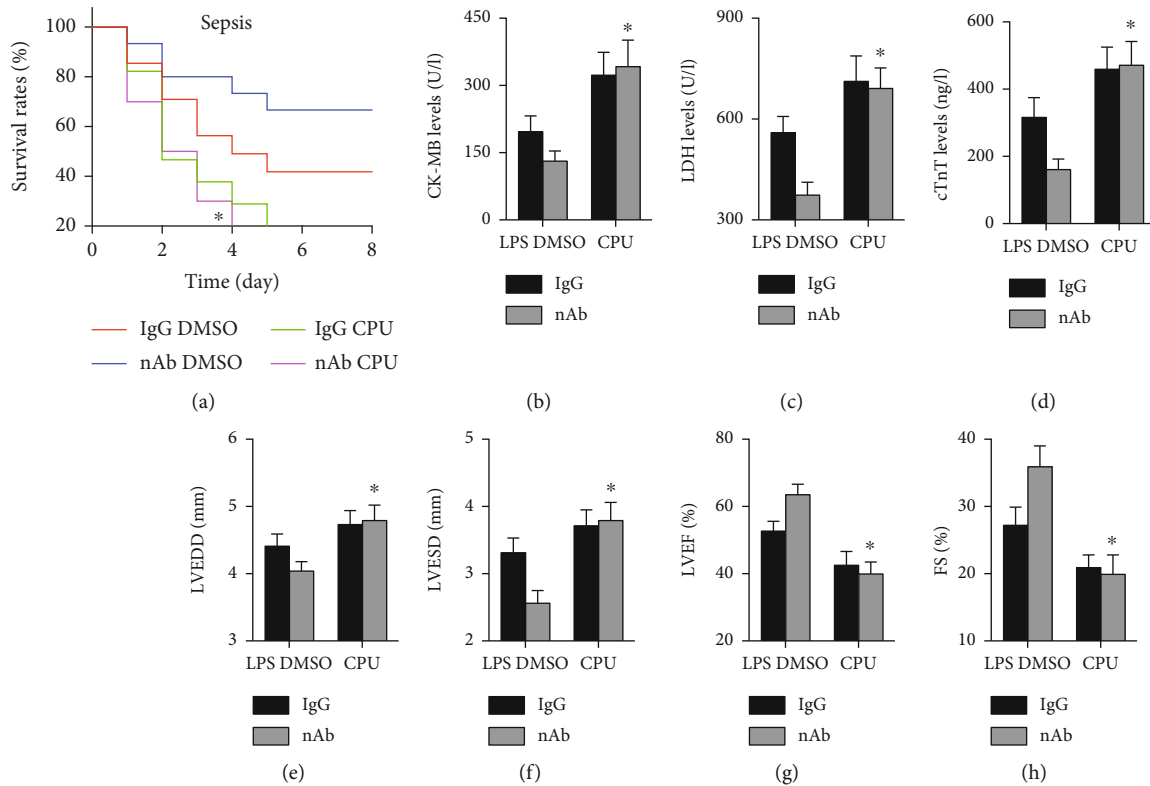
Figure 6: Effects of CPUY192018 on cardiac injury in septic mice. (a) Survival rates were measured for each group (log-rank test). (b–d) Serum levels of cardiac injury markers, including CK-MB, LDH, and cTnT, were measured (two-way ANOVA). (e–h) Cardiac structure and function in each group were measured (two-way ANOVA). $n = 5$ in each group. $*p < 0.05$ vs. the nAb DMSO+LPS group. LPS: lipopolysaccharide; DMSO: dimethyl sulfoxide; CPU: CPUY192018; nAb: anti-IL-16 neutralizing antibody; LDH: lactate dehydrogenase; CK-MB: creatine kinase myocardial bound; cTnT: cardiac troponin T; LVEDD: left ventricular end-diastolic diameter; LVESD: left ventricular end-systolic diameter; LVEF: left ventricular ejection fraction; FS: fractional shortening.

subsequent LPS-induced mouse sepsis model, neutralization of IL-16 significantly increased survival, reduced the expression of multiple markers of cardiac injury, and improved cardiac function. These data suggest that reducing the expression of IL-16 can attenuate sepsis-induced cardiac injury and dysfunction. Considering that oxidative stress is an important factor affecting the secretion of IL-16, we speculate that IL-16 may participate in the process of myocardial injury and dysfunction by regulating the level of oxidative stress.

Under normal physiological conditions, prooxidant and antioxidant substances maintain a dynamic balance, which is essential for the maintenance of normal physiological activities [28, 29]. Under the action of doxorubicin, Ang II, and other external pathogenic factors, this stable equilibrium relationship is broken, as evidenced by reductions in the levels of antioxidants, including NRf2, HO-1, and SOD, and increases in the levels of oxygen-promoting substances, including Nox2, Nox4, and MDA [30, 31]. To determine whether IL-16 is involved in sepsis-induced cardiac injury through the regulation of oxidative stress, pathways and markers related to oxidative stress were detected. The results showed that neutralization of IL-16 significantly reversed sepsis-induced oxidative stress imbalance in both the heart and the serum. These results support our hypothesis and pro-

vide the first evidence that IL-16 regulates oxidative stress in addition to inflammatory responses.

There are also regulatory effects among oxidative stress-related pathways. One such pathway, the Nrf2 signaling pathway, regulates the physiological response to oxidative stress and is very important for the maintenance of cellular redox balance. In a recent study, Kim et al. reported that sodium butyrate promoted inactivation of the nuclear factor kappa-B (NF-κB) pathway through the Nrf2 pathway, upregulated SOD levels, and inhibited Nox2 expression in a mouse Alzheimer's disease model [32].

In a mouse orthotopic liver transplantation model, Ke et al. found that deletion of the Nrf2 pathway significantly reduced HO-1 pathway activation [33]. In an earlier study, the authors reported that Nrf2 deficiency elevated ROS levels by upregulating both Nox2 expression and Nox4 expression [34]. These results indicate that the Nrf2 signaling pathway regulates the activation of other oxidative stress-related pathways and the expression of oxidative stress-related markers during oxidative stress regulation, which means that the Nrf2 pathway plays a leading role in the process of oxidative stress. To investigate whether the protective effect of the anti-IL-16 nAb against sepsis-induced cardiac injury was mediated by the Nrf2 pathway, CPUY192018 was used to inhibit the Nrf2 pathway in
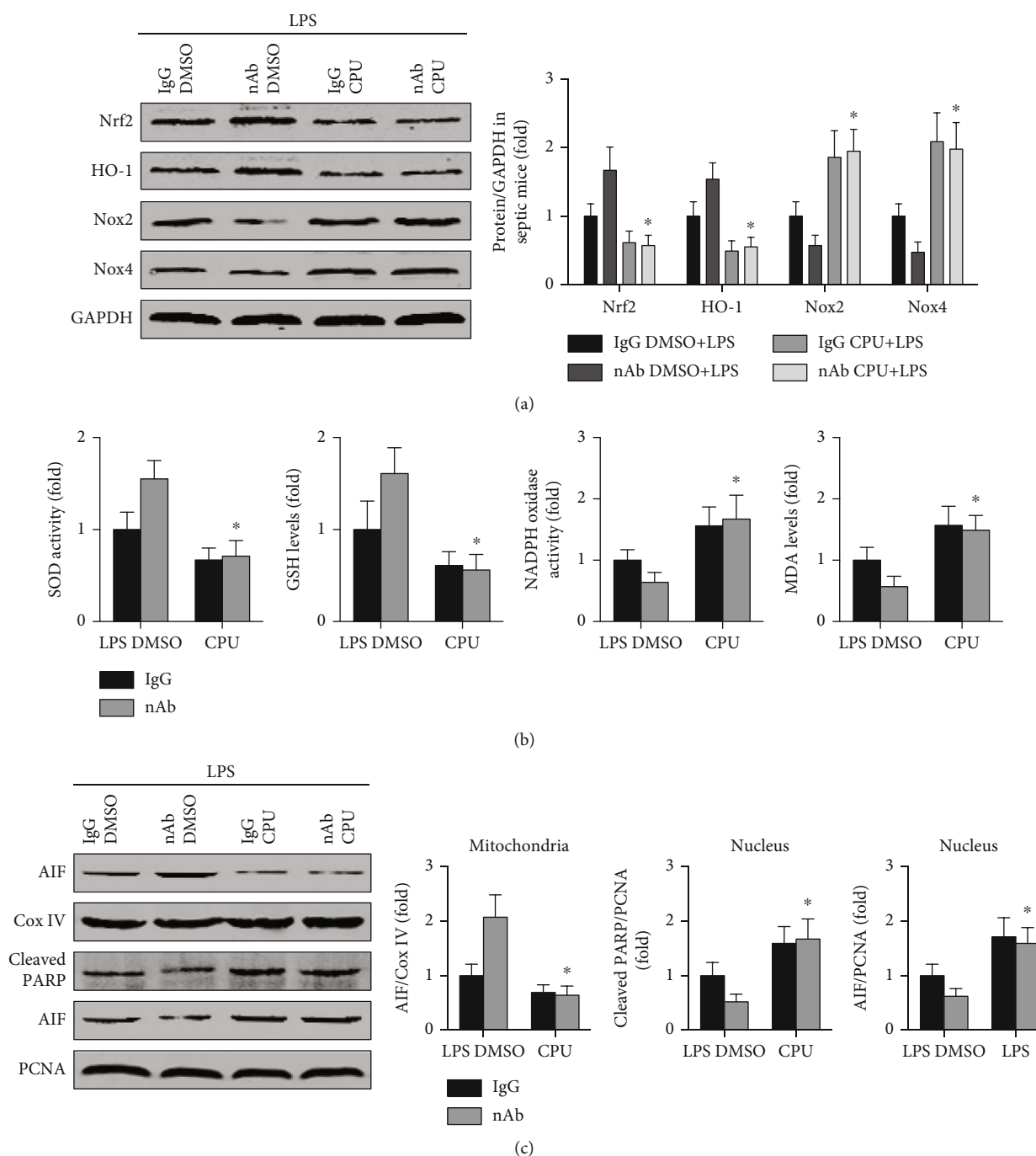
(a)

(b)

(c)

FIGURE 7: Effects of CPUY192018 on oxidative stress and cardiomyocyte apoptosis in septic mice. (a) Nrf2, HO-1, Nox2, Nox4, and GAPDH expression in LV tissue was detected (two-way ANOVA). (b) Serum activity of SOD and NADPH oxidase and levels of GSH and MDA were measured (two-way ANOVA). (c) AIF and Cox IV expression in mitochondria and AIF, cleaved PARP, and PCNA expression in nuclei were analyzed (two-way ANOVA). $n = 5$ in each group. $^*p < 0.05$ vs. the nAb DMSO+LPS group. Nrf2: nuclear factor erythroid-2 related factor 2; HO-1: heme oxygenase 1; Nox2/4: nicotinamide adenine nucleotide phosphate oxidase 2/4; nAb: anti-IL-16 neutralizing antibody; CPU: CPUY192018; LPS: lipopolysaccharide; SOD: superoxide dismutase; GSH: glutathione; NADPH: nicotinamide adenine nucleotide phosphate; MDA: malondialdehyde; AIF: apoptosis-inducing factor; Cox IV: cytochrome c oxidase IV; PARP: poly-ADP-ribose polymerase; PCNA: proliferating cell nuclear antigen.

mice with LPS-induced sepsis. The results showed that treatment with CPUY192018 significantly decreased cardiac HO-1 levels, increased Nox2 and Nox4 expression, and aggravated oxidative stress imbalance in septic mice with neutralized IL-16. These results are consistent with

previous conclusions and suggest that IL-16 regulates downstream oxidative stress through the Nrf2 pathway.

In a mouse sepsis model, increased oxidative stress is often accompanied by increased cardiomyocyte apoptosis, and reversing the increase in oxidative stress significantly

attenuates cardiomyocyte apoptosis [34, 35]. This suggests that oxidative stress is an important cause of cardiomyocyte apoptosis in the context of sepsis. Large numbers of apoptotic cardiomyocytes are found in septic animals; such extensive apoptosis can lead to declines in cardiac function. However, reducing cardiomyocyte apoptosis can significantly reverse cardiac dysfunction, suggesting that sepsis-induced excessive apoptosis of cardiomyocytes might be the most fundamental cause of cardiac injury [36]. AIF, which exists mainly in the mitochondrial inner membrane and is less prevalent or non-existent in the nucleus, is one of the important factors mediating non-Caspase-dependent apoptosis [22]. Under stimulation by external pathological factors, AIF is released in massive quantities by mitochondria and transferred to the nucleus through the cytoplasm [22]. Increases in nuclear AIF levels promote apoptosis, which can act through a feed-back mechanism to promote the nuclear expression of cleaved PARP, a DNA damage repair protein, to protect against apoptosis [22]. To further explore the mechanisms, cardiomyocyte apoptosis was detected in septic mice. The results showed that inhibition of the Nrf2 pathway with CPUY192018 significantly promoted the transfer of mito-chondrial AIF to the nucleus and increased the expression of nuclear cleaved PARP in septic mice that were pretreated with the anti-IL-16 nAb. In addition, more TUNEL-positive cells were found in septic mice with IL-16 neutralization than in septic mice without neutralization. These results indicate that inhibition of the Nrf2 pathway can significantly reverse the protective effect of the anti-IL-16 nAb against AIF-mediated cardiomyocyte apoptosis in septic mice.

In conclusion, our study demonstrates, for the first time, that neutralization of IL-16 can upregulate the Nrf2 pathway, reduce oxidative stress, inhibit the transfer of AIF from the mitochondria to the nucleus, and thus reduce cardiomyocyte apoptosis, alleviate cardiac injury, and improve cardiac func-tion in septic mice.

Data Availability

We declare that the materials described in the manuscript, including all relevant raw data, will be freely available to any scientist wishing to use them for noncommercial pur-poses without breaching participant confidentiality.

Conflicts of Interest

The authors declare that they have no conflicts of interest.

Acknowledgments

References

[1] M. Mirna, V. Paar, R. Rezar et al., "MicroRNAs in inflamma-tory heart diseases and sepsis-induced cardiac dysfunction: a potential scope for the future?," *Cell*, vol. 8, no. 11, p. 1352, 2019.

[2] R. Sato and M. Nasu, "A review of sepsis-induced cardiomyop-athy," *Journal of Intensive Care*, vol. 3, no. 1, article 48, 2015.

[3] A. Flynn, B. Chokkalingam Mani, and P. J. Mather, "Sepsis-induced cardiomyopathy: a review of pathophysiologic mech-anisms," *Heart Failure Reviews*, vol. 15, no. 6, pp. 605–611, 2010.

[4] K. Reinhart, R. Daniels, N. Kissoon, F. R. Machado, R. D. Schachter, and S. Finfer, "Recognizing sepsis as a global health priority-a WHO resolution," *The New England Journal of Medicine*, vol. 377, no. 5, pp. 414–417, 2017.

[5] H. Tu, X. Lai, J. Li, L. Huang, Y. Liu, and J. Cao, "Interleukin-26 is overexpressed in human sepsis and contributes to inflam-mation, organ injury, and mortality in murine sepsis," *Critical Care*, vol. 23, no. 1, article 290, 2019.

[6] H. Xu, J. Xu, L. Xu et al., "Interleukin-33 contributes to ILC2 activation and early inflammation- associated lung injury dur-ing abdominal sepsis," *Immunology and Cell Biology*, vol. 96, no. 9, pp. 935–947, 2018.

[7] X. Lin, H. Luo, X. Yan et al., "Interleukin-34 ameliorates sur-vival and bacterial clearance in polymicrobial sepsis," *Critical Care Medicine*, vol. 46, no. 6, pp. e584–e590, 2018.

[8] F. Xu, S. Lin, X. Yan et al., "Interleukin 38 protects against lethal sepsis," *The Journal of Infectious Diseases*, vol. 218, no. 7, pp. 1175–1184, 2018.

[9] J. Li, W. Wei, H. Shi, Y. Li, and W. Mo, "Cellular sources of interleukin 16 in benign and malignant pleural effusions," *Chi-nese Medical Journal*, vol. 124, no. 24, pp. 4160–4165, 2011.

[10] C. Li, J. Dai, G. Dong et al., "Interleukin-16 aggravates ovalbumin-induced allergic inflammation by enhancing Th2 and Th17 cytokine production in a mouse model," *Immunol-ogy*, vol. 157, no. 3, pp. 257–267, 2019.

[11] C. A. Mueller, H. J. Schluesener, S. Conrad, T. Pietsch, and J. M. Schwab, "Spinal cord injury-induced expression of the immune-regulatory chemokine interleukin-16 caused by acti-vated microglia/macrophages and CD8+ cells," *Journal of Neu-rosurgery. Spine*, vol. 4, no. 3, pp. 233–240, 2006.

[12] N. L. Mathy, W. Scheuer, M. Lanzendörfer et al., "Interleukin-16 stimulates the expression and production of pro-inflammatory cytokines by human monocytes," *Immunology*, vol. 100, no. 1, pp. 63–69, 2000.

[13] M. Benoit, F. Fenollar, D. Raoult, and J. L. Mege, "Increased levels of circulating IL-16 and apoptosis markers are related to the activity of Whipple's disease," *PLoS One*, vol. 2, no. 6, article e494, 2007.

[14] A. Elssner, A. I. Doseff, M. Duncan, M. Kotur, and M. D. Wewers, "IL-16 is constitutively present in peripheral blood monocytes and spontaneously released during apoptosis," *Journal of Immunology*, vol. 172, no. 12, pp. 7721–7725, 2004.

[15] C. Grönberg, E. Bengtsson, G. N. Fredrikson et al., "Human carotid plaques with high levels of interleukin-16 are associ-ated with reduced risk for cardiovascular events," *Stroke*, vol. 46, no. 10, pp. 2748–2754, 2015.

[16] S. Tamaki, T. Mano, Y. Sakata et al., "Interleukin-16 promotes cardiac fibrosis and myocardial stiffening in heart failure with preserved ejection fraction," *PLoS One*, vol. 8, no. 7, article e68893, 2013.

[17] B. Y. de Winter, L. van Nassauw, J. G. de Man et al., "Role of oxidative stress in the pathogenesis of septic ileus in mice," *Neurogastroenterology and Motility*, vol. 17, no. 2, pp. 251–261, 2005.

[18] M. Lu, J. Zhao, Y. Liu et al., "CPUY192018, a potent inhibitor of the Keap1-Nrf2 protein-protein interaction, alleviates renal inflammation in mice by restricting oxidative stress and NF-κB activation," *Redox Biology*, vol. 26, article 101266, 2019.

[19] D. Rittirsch, M. S. Huber-Lang, M. A. Flierl, and P. A. Ward, "Immunodesign of experimental sepsis by cecal ligation and puncture," *Nature Protocols*, vol. 4, no. 1, pp. 31–36, 2009.

[20] D. Xiao, D. Yuan, B. Tan, J. Wang, Y. Liu, and B. Tan, "The role of Nrf2 signaling pathway in Eucommia ulmoides flavones regulating oxidative stress in the intestine of piglets," *Oxidative Medicine and Cellular Longevity*, vol. 2019, Article ID 9719618, 9 pages, 2019.

[21] H. Nguyen, V. L. Chiasson, P. Chatterjee, S. E. Kopriva, K. J. Young, and B. M. Mitchell, "Interleukin-17 causes Rho-kinase-mediated endothelial dysfunction and hypertension," *Cardiovascular Research*, vol. 97, no. 4, pp. 696–704, 2013.

[22] J. Ye, Y. Wang, Z. Wang et al., "Interleukin-12p35 deficiency enhances mitochondrial dysfunction and aggravates cardiac remodeling in aging mice," *Aging*, vol. 12, no. 1, pp. 193–203, 2020.

[23] J. Ye, Y. Huang, B. Que et al., "Interleukin-12p35 knock out aggravates doxorubicin-induced cardiac injury and dysfunction by aggravating the inflammatory response, oxidative stress, apoptosis and autophagy in mice," *eBioMedicine*, vol. 35, pp. 29–39, 2018.

[24] N. Zhang, H. Feng, H. Liao et al., "Myricetin attenuated LPS induced cardiac injury *in vivo* and *in vitro*," *Phytotherapy Research*, vol. 32, no. 3, pp. 459–470, 2018.

[25] P. Xing, P. An, G. Hu, D. Wang, and M. Zhou, "LncRNA MIAT promotes inflammation and oxidative stress in sepsis-induced cardiac injury by targeting miR-330-5p/ TRAF6 /NF-κB axis," *Biochemical Genetics*, vol. 58, pp. 783–800, 2020.

[26] H. Yuan, C. Perry, C. Huang et al., "LPS-induced autophagy is mediated by oxidative signaling in cardiomyocytes and is associated with cytoprotection," *American Journal of Physiology Heart and Circulatory Physiology*, vol. 296, no. 2, pp. H470–H479, 2009.

[27] C. Poggi and C. Dani, "Sepsis and oxidative stress in the newborn: from pathogenesis to novel therapeutic targets," *Oxidative Medicine and Cellular Longevity*, vol. 2018, Article ID 9390140, 14 pages, 2018.

[28] D. Bar-Or, M. M. Carrick, C. W. Mains, L. T. Rael, D. Slone, and E. N. Brody, "Sepsis, oxidative stress, and hypoxia: are there clues to better treatment?," *Redox Report*, vol. 20, no. 5, pp. 193–197, 2015.

[29] A. Dandekar, R. Mendez, and K. Zhang, "Cross talk between ER stress, oxidative stress, and inflammation in health and disease," *Methods in Molecular Biology*, vol. 1292, pp. 205–214, 2015.

[30] A. Zimnol, K. Amann, P. Mandel, C. Hartmann, and N. Schupp, "Angiotensin II type 1a receptor-deficient mice develop angiotensin II-induced oxidative stress and DNA damage without blood pressure increase," *American Journal of Physiology Renal Physiology*, vol. 313, no. 6, pp. F1264–F1273, 2017.

[31] J. Ye, Y. Wang, Y. Xu et al., "Interleukin-22 deficiency alleviates doxorubicin-induced oxidative stress and cardiac injury via the p38 MAPK/macrophage/Fizz3 axis in mice," *Redox Biology*, vol. 36, article 101636, 2020.

[32] S. Y. Kim, C. W. Chae, H. J. Lee et al., "Sodium butyrate inhibits high cholesterol-induced neuronal amyloidogenesis by modulating NRF2 stabilization-mediated ROS levels: involvement of NOX2 and SOD1," *Cell Death & Disease*, vol. 11, no. 6, p. 469, 2020.

[33] B. Ke, X. Shen, Y. Zhang et al., "KEAP1-NRF2 complex in ischemia-induced hepatocellular damage of mouse liver transplants," *Journal of Hepatology*, vol. 59, no. 6, pp. 1200–1207, 2013.

[34] Y. Li, P. Liang, B. Jiang et al., "CARD9 inhibits mitochondria-dependent apoptosis of cardiomyocytes under oxidative stress via interacting with Apaf-1," *Free Radical Biology & Medicine*, vol. 141, pp. 172–181, 2019.

[35] M. Dong, N. Hu, Y. Hua et al., "Chronic Akt activation attenuated lipopolysaccharide-induced cardiac dysfunction _via_ Akt/GSK3 β-dependent inhibition of apoptosis and ER stress," *Biochimica et Biophysica Acta*, vol. 1832, no. 6, pp. 848–863, 2013.

[36] H. Li, Y. Xing, D. Yang, X. Tang, D. Lu, and H. Wang, "Alpha-1 adrenergic receptor agonist phenylephrine inhibits sepsis-induced cardiomyocyte apoptosis and cardiac dysfunction via activating ERK1/2 signal pathway," *Shock*, vol. 52, no. 1, pp. 122–133, 2019.

Research Article

BGP-15 Protects against Heart Failure by Enhanced Mitochondrial Biogenesis and Decreased Fibrotic Remodelling in Spontaneously Hypertensive Rats

Orsolya Horvath [1,2] **Katalin Ordog** [1,2] **Kitti Bruszt** [1,2] **Laszlo Deres** [1,2,3] **Ferenc Gallyas** [2,3,4] **Balazs Sumegi**, [2,3,4] **Kalman Toth** [1,2] and **Robert Halmosi** [1,2]

[1]*1st Department of Medicine, University of Pecs, Medical School, Hungary*
[2]*Szentágothai Research Centre, University of Pecs, Hungary*
[3]*HAS-UP Nuclear-Mitochondrial Interactions Research Group, 1245 Budapest, Hungary*
[4]*Department of Biochemistry and Medical Chemistry, University of Pecs, Medical School, Hungary*

Correspondence should be addressed to Robert Halmosi; halmosi.robert@pte.hu

Heart failure (HF) is a complex clinical syndrome with poor clinical outcomes despite the growing number of therapeutic approaches. It is characterized by interstitial fibrosis, cardiomyocyte hypertrophy, activation of various intracellular signalling pathways, and damage of the mitochondrial network. Mitochondria are responsible for supplying the energy demand of cardiomyocytes; therefore, the damage of the mitochondrial network causes cellular dysfunction and finally leads to cell death. BGP-15, a hydroxylamine derivative, is an insulin-sensitizer molecule and has a wide range of cytoprotective effects in animal as well as in human studies. Our recent work was aimed at examining the effects of BGP-15 in a chronic hypertension-induced heart failure model. 15-month-old male SHRs were used in our experiment. The SHR-Baseline group represented the starting point ($n = 7$). Animals received BGP-15 (SHR-B, $n = 7$) or placebo (SHR-C, $n = 7$) for 18 weeks. WKY rats were used as age-matched normotensive controls ($n = 7$). The heart function was monitored by echocardiography. Histological preparations were made from cardiac tissue. The levels of signalling proteins were determined by Western blot. At the end of the study, systolic and diastolic cardiac function was preserved in the BGP-treated animals. BGP-15 decreased the interstitial collagen deposition via decreasing the activity of TGFβ/Smad signalling factors and prevented the cardiomyocyte hypertrophy in hypertensive animals. BGP-15 enhanced the prosurvival signalling pathways (Akt/Gsk3β). The treatment increased the activity of MKP1 and decreased the activity of p38 and JNK signalling routes. The mitochondrial mass of cardiomyocytes was also increased in BGP-15-treated SHR animals due to the activation of mitochondrial biogenesis. The mitigation of remodelling processes and the preserved systolic cardiac function in hypertension-induced heart failure can be a result—at least partly—of the enhanced mitochondrial biogenesis caused by BGP-15.

1. Introduction

Heart failure remained a leading cause of death despite the broadening of therapeutic possibilities [1]. The most important risk factors of heart failure are ischemic heart disease and hypertension [2]. The treatment of hypertension is challenging; there is a high portion of patients who cannot reach the goal blood pressure level having a high risk for the development of heart failure [3]. Sustained elevation of blood pressure induces myocardial remodelling, which is characterized by interstitial fibrosis and cardiomyocyte hypertrophy [4, 5]. These cellular alterations are promoted by oxidative stress [6] and by the activation of various intracellular signal transduction pathways [7, 8]. Numerous

studies have demonstrated that mitochondria which are responsible for the cellular energy supply are also damaged in hypertension-induced cardiac remodelling and heart failure [9, 10]. ROS-induced mtDNA damage can be found in the background of these injuries, and mitochondria themselves become the main sources of endogenous ROS production [11]. The long-term presence of these pathophysiological factors finally can lead to heart failure [12]. Spontaneously hypertensive rat (SHR) has become one of the most intensively studied murine strain in experimental cardiology with pathologies resembling human essential hypertension [13, 14]. Therefore, SHR was used in our work as a hypertension-induced heart failure animal model.

BGP-15 (O-[3-piperidino-2-hydroxy-1-propyl]-nicotinic acid amidoxime dihydrochloride) is an insulin sensitizer molecule, with a protective effect in a wide range of experimental models. BGP-15 protects against oxidative stress in ischemia-reperfusion-induced injury in the Langendorff heart perfusion system [15, 16]. Furthermore, it prevents against atrial fibrillation in a transgenic mouse model of heart failure [17]. BGP-15 has beneficial effects on diastolic dysfunction in diabetic cardiomyopathy on Goto–Kakizaki rats [18]. BGP-15 prevented against the imatinib-induced cardiotoxic effects via decreasing the oxidative damages [19]. BGP-15 protects against the ROS-induced mitochondrial ROS production and preserved the mitochondrial membrane potential in the WRL-68 cell line [20]. Nagy et al. demonstrated that BGP-15 protects against the acetaminophen-provoked hepatocellular injury [21]. Moreover, BGP-15 protects lung structure and activates mitochondrial fusion processes in a model of pulmonary arterial hypertension [22].

Fibrotic remodelling, increased ROS production, activation of MAPK signalling pathways, and mitochondrial damage play a significant role in the abovementioned diseases as well as in the pathomechanism of heart failure. Furthermore, it appears that very little information is available or nothing at all on the effect of BGP-15 in the development of hypertensive cardiomyopathy. Therefore, the aim of our study was to investigate the role of BGP-15 in hypertension-induced heart failure.

We focused predominantly on factors that regulate the remodelling processes, myocardial fibrosis, the pattern of related signalling pathways, and the regulation of mitochondrial biogenesis as well.

2. Materials and Methods

2.1. Ethics Statement. Animals received care according to the Guide for the Care and Use of Laboratory Animals published by the US National Institute of Health (NIH Publication No. 85–23, revised 1996), and the experiment was approved by the Animal Welfare Committee of the University of Pecs, Medical School (permit number: BA02/2000-54/2017).

2.2. Experimental Protocol. 15-month-old male Wistar Kyoto (WKY) and spontaneously hypertensive rats (Charles River Laboratories, Budapest, Hungary) were used in the experiments. One or two animals were housed per cage under standardized conditions throughout the experiment, with

12 h dark-light cycle in solid-bottomed polypropylene cages, and received commercial rat chew and water ad libitum. Seven SHRs were sacrificed at the beginning of the experiment, as a baseline group (SHR-Baseline). SHRs were randomly divided into two groups: SHR-B and SHR-C. The SHR-B group was treated with BGP-15, a water-soluble compound (25 mg/b.w. in kg/day, $n = 7$), while the SHR-C group received only placebo ($n = 7$, SHR-C) per os for 18 weeks. BGP-15 was a gift from N-Gene Inc. (New York, NY, USA). The dosage of BGP-15 administered in the drinking water was based on preliminary data regarding the volume of daily fluid consumption. WKY rats were used as age-matched normotensive controls ($n = 7$). Noninvasive blood pressure measurements were performed on each animal on three occasions at weeks 0, 9, and 18 of the treatment period. Blood pressure measurements were performed by a noninvasive tail-cuff method as described earlier [23, 24]. Blood pressure was measured by the Non-Invasive Blood Pressure System with rat species platform (Panlab, Harvard Apparatus; LE5002). At the beginning and at the end of the 18-week-long period, echocardiographic measurements were performed. At the end of the 18 weeks, the animals were sacrificed, blood was collected to determine the concentration of plasma brain-derived natriuretic peptide (BNP), then hearts were removed. Atria and great vessels were trimmed from the ventricles, and the weight of the ventricles was measured. Hearts were fixed in 10% formalin for histology or freeze-clamped for Western blot analysis. In order to detect the extent of fibrotic areas, histologic samples were stained with Picrosirius red, and collagen type I immunohistochemistry was made. The phosphorylation state of TGFβ, Smad2 and 3, Akt-1, GSK-3β, and MAPK signalling molecules were monitored by Western blotting. In our research, the following group notations were used according to the applied treatment: WKY: age-matched normotensive Wistar-Kyoto rats; SHR-Baseline: 15-month-old spontaneously hypertensive rats before the treatment period; SHR-C: 19-month-old spontaneously hypertensive rats after the 18-week-long placebo treatment; and SHR-B: 19-month-old spontaneously hypertensive rats after the 18-week-long treatment period with BGP-15.

2.3. Echocardiographic Measurements. Transthoracic echocardiography was performed under inhalation anaesthesia at the beginning of the experiment and on the day of sacrifice. The rats were lightly anesthetized with a mixture of 1.5% isoflurane and 98.5% oxygen. The chest of the animals was shaved, and acoustic coupling gel was applied. The animals were imaged in the left lateral position, and a warming pad was used to maintain normothermia. Heart rate did not differ considerably during anaesthesia among the groups. Ventricular dimensions, wall thicknesses, and systolic functions were measured from parasternal short and long-axis views at the midpapillary level. Parameters (E, A, and E') required for the evaluation of diastolic function were measured from the apical 4 chamber view. For the imaging of rats, VEVO 770 high-resolution ultrasound imaging system (VisualSonics, Toronto, Canada) was used, which was equipped with a 25 MHz transducer. The investigators were blinded to the treatment protocol. LV inner dimensions (LVIDd and LVIDs), the thickness

of septum and posterior wall (PW), LV end-diastolic volume (LVEDV), LV end-systolic volume (LVESV), E/A, and E/E' ratio were determined. EF (percentage) was calculated by $100 \times [(LVEDV - LVESV)/LVEDV]$.

2.4. Determination of Plasma B Type Natriuretic Peptide Level.

Blood samples were collected into vacutainer tubes containing EDTA and aprotinin (0.6 IU/ml) and centrifuged at 1600 g for 15 minutes at 4°C to separate plasma, which was collected and kept at −70°C. Plasma B type natriuretic peptide-32 levels (BNP-32) were determined by Enzyme-Linked Immunosorbent Assay method (BNP-32, Rat BNP 32 ELISA Kit, Abcam, ab108815CA, USA) as the datasheet recommends.

2.5. Histology.

For histological examination, hearts were removed at the end of the study after euthanasia was performed by overdosing isoflurane. Ventricles were fixed in 6% formalin and sliced and embedded in paraffin. Five-micrometer-thick sections were cut serially from the base to the apex by a microtome. Seven animals from each group and 3 sections from each animal were used to determine the degree of cardiac fibrosis. Three images (magnification 10x) were randomly taken from the middle region of the LV wall on each section. The fibrotic area was determined on each image, and the mean value of nine images represents each animal. LV sections were stained with Picrosirius red to detect interstitial fibrosis. Slices were also processed for type I collagen (Bios rabbit polyclonal 1:500) immunohistochemistry. The binding was visualized with biotinylated/HRP-conjugated secondary antibody followed by the avidin-biotin-peroxidase detection system (PK-6200 Universal Vectastain ABC Elite Kit, Vector Laboratories, Burlingame, CA) using 3,3'-diaminobenzidine (DAB) as a chromogen. Progress of the immunoreaction was monitored using a light microscope, and the reaction was stopped by the removal of excess DAB with a gentle buffer wash. Animals from each group were used. The degree of fibrosis was quantified by the NIH ImageJ image processing program via its colour deconvolution plug-in.

Picrosirius red staining was performed to measure cardiomyocyte diameter (CD) as a cellular marker of myocardial hypertrophy. Seven animals from each group and 3 sections from each animal were used to determine the cell diameter. Three images (magnification 10x) were randomly taken from the free LV wall on each section. The fitted polygon technique was used to determine the area of the cells. Then, the calculated diameter was used for statistical analysis. In order to evaluate the cardiomyocyte diameter, 250 cardiomyocytes were measured from each animal. The mean value of cell diameter of an animal derived from 250 measurements and each group contained 7 animals.

2.6. Western Blot Analysis.

Fifty milligrams of heart samples were homogenized in ice-cold Tris buffer (50 mmol/l, pH 8.0) containing protease inhibitor (1:100; Sigma-Aldrich Co., #P8340) and phosphatase inhibitor (1:100; Sigma-Aldrich Co., #P5726) as well as 50 mM sodium vanadate. The supernatant was harvested in 2x concentrated SDS-polyacrylamide gel electrophoresis sample buffer. Protein levels were measured with NanoDrop. Glyceraldehyde 3-phosphate dehydrogenase (GAPDH; 1:1000; Cell Signaling #2118) was used as a loading control. Proteins were separated on 12% SDS-polyacrylamide gel and transferred to nitrocellulose membranes. After blocking (2 h with 5% BSA in Tris-buffered saline contained with 1% Tween-20), membranes were probed overnight at 4°C with primary antibodies recognizing the following antigens: transforming growth factor-β (TGF-β; 1:1000; Cell Signaling #3711), Smad2 (1:1000; Invitrogen, 436500), phospho-specific Smad2 Ser465/467 (1:1000; Invitrogen, MA5-15122), Smad3 (1:1000; Cell Signaling #9523), phospho-specific Smad3 Ser423/425 (1:1000; Cell Signaling #9520), protein kinase B (Akt; 1:1000; Cell Signaling #9272), phospho-specific Akt-1/protein kinase B-α Ser473 (1:1000; Cell Signaling #4060), glycogen synthase kinase-3β (GSK-3β; 1:1000; Cell Signaling #9832), phospho-specific glycogen synthase kinase-3β Ser9 (1:1000; Cell Signaling #5558), p38 mitogen-activated protein kinase (p38MAPK; 1:1000; Cell Signaling #8690), phospho-specific p38 mitogen-activated protein kinase Thr180/Tyr182 (1:1000; Cell Signaling #4511), c-Jun N-terminal kinase (JNK; 1:1000; Cell Signaling #9252), phospho-specific c-Jun N-terminal kinase Thr183/Tyr185 (1:1000; Cell Signaling #9255), extracellular signal-regulated kinase (ERK1/2; 1:1000; Cell Signaling #4695), phospho-specific extracellular signal-regulated kinase 1/2 Thr202 (1:1000; Cell Signaling #4370), mitogen-activated protein kinase phosphatase-1 (MKP-1; 1:100; Santa Cruz Biotechnology, sc-373841), peroxisome proliferator-activated receptor gamma coactivator 1-alpha (PGC-1α; 1:1000; Novus Biologicals, NBP1-04676), cAMP response element-binding protein (CREB; 1:1000; Cell Signaling #4820), phospho-specific cAMP response element-binding protein Ser133(1:1000; Cell Signaling #9198), 5' AMP-activated protein kinase (AMPK; 1:1000; Cell Signaling #2532), phospho-specific 5' AMP-activated protein kinase Thr172 (1:1000; Cell Signaling #2535), and voltage-dependent anion channel (VDAC; 1:1000; Cell Signaling #4661). Membranes were washed six times for 5 min in Tris-buffered saline (pH 7.5) containing 1% Tween-20 (TBST) before the addition of horseradish peroxidase-conjugated secondary antibody (goat antirabbit IgG, Sigma Aldrich Co. A0545, 1:3000 dilution; rabbit antimouse IgG, Sigma Aldrich Co., A9044, 1:5000 dilution). Membranes were washed six times for 5 min in TBST, and the antibody-antigen complexes were visualized by means of enhanced chemiluminescence. The results of Western blots were quantified using the NIH ImageJ program.

2.7. Statistical Analysis.

Statistical analysis was performed by SPSS for Windows, version 26.0. All of the data were expressed as the mean ± SEM. The normality of distribution was assessed by the Shapiro-Wilk test. The baseline comparison between the strains was conducted by Student's t-test before randomization. The homogeneity of the groups was tested by Levene's test. Differences between treatment groups were determined by one-way ANOVA. For post hoc comparison, Tukey HSD or Dunnett T3 test was applied. A value of $p < 0.05$ was considered statistically significant.

3. Results

3.1. Effect of BGP-15 Administration on Gravimetric Parameters. At the beginning of the study, the body weight of WKY rats was significantly higher than the SHR rats (WKY: 386.40 ± 4.33 g, SHR-Baseline: 343.21 ± 2.48 g, SHR-C: 346.90 ± 6.65 g, SHR-B: 340.73 ± 6.32 g; $p < 0.01$, WKY vs. SHR groups; Table 1). A similar observation can be made at the end of the study (WKY: 401.45 ± 8.94 g, SHR-C: 358.13 ± 5.08 g, SHR-B: 356.85 ± 4.54 g; $p < 0.05$ WKY vs. SHR groups). At the end of the study, the heart weights (HW) and ventricles weight (VW) were significantly increased in the SHR groups compared to the WKY group (HW: WKY: 1.12 ± 0.04 g, SHR-Baseline: 1.16 ± 0.02, SHR-C: 1.49 ± 0.05 g, SHR-B: 1.23 ± 0.02 g; $p < 0.01$ SHR-B and SHR-C vs. WKY; VW: WKY: 0.95 ± 0.04 g, SHR-Baseline: 1.09 ± 0.02 g , SHR-C: 1.33 ± 0.05 g, SHR-B: 1.23 ± 0.02 g; $p < 0.01$ SHR-C vs. WKY, $p < 0.01$ SHR-B vs. SHR-C). The ratio of ventricular weight to body weight (VW/BW) was increased markedly in the SHR groups compared to WKY animals (VW/BW(mg/g): WKY: 2.28 ± 0.11, SHR-Baseline: 3.19 ± 0.08, SHR-C: 3.73 ± 0.16, SHR-B: 3.21 ± 0.03; $p < 0.01$ SHR groups vs. WKY, $p < 0.05$ SHR-B vs. WKY, $p < 0.01$ WKY vs. SHR-Baseline and SHR-C, $p < 0.01$ SHR-C vs. SHR-Baseline, $p < 0.01$ SHR-B vs. SHR-C). Ventricular weight to the length of right tibia ratio (VW/TL) was also significantly increased (VW/TL (mg/mm): WKY: 21.27 ± 0.79, SHR-Baseline: 24.76 ± 0.82, SHR-C: 29.79 ± 0.94, SHR-B: 25.76 ± 0.46; $p < 0.05$ WKY vs. SHR-Baseline and SHR-B, $p < 0.01$ SHR-C vs. WKY and SHR-Baseline). BGP-15 treatment caused a significant moderation of these ratios ($p < 0.01$ SHR-B vs. SHR-C). The ratio of the lung wet weight-to-dry weight was enhanced in the SHR-C group significantly (lung wet weight/dry weight(g/g): WKY: 4.42 ± 0.26 g/g, SHR-Baseline: 4.51 ± 0.13, SHR-C: 5.68 ± 0.24, SHR-B: 4.68 ± 0.13; $p < 0.01$ SHR-C vs. WKY and SHR-Baseline). BGP-15 caused a significant moderation of this ratio ($p < 0.01$ SHR-B vs. SHR-C).

3.2. Effect of BGP-15 Administration on Systolic Blood Pressure and Echocardiographic Parameters. At the beginning of the study, there was a significant difference between the systolic arterial blood pressure of the WKY and the SHR-Baseline group (WKY: 134.85 ± 1.95 mmHg, SHR-Baseline: 214.28 ± 3.70 mmHg; $p < 0.05$; $n = 7$). Systolic arterial blood pressure values did not differ significantly between the SHR groups at the end of the study (SHR-C: 226.14 ± 3.88 mmHg, SHR-B: 216.85 ± 3.90 mmHg; $p > 0.05$; $n = 7$). Long-term BGP-15 treatment apparently did not exert any significant effect on systolic blood pressure.

At the beginning of the study, the septum and posterior wall thickness was significantly higher in SHR animals compared to WKY animals ($p < 0.01$ SHR-Baseline vs. WKY) (Table 1). By the end of the 18-week treatment period, the severity of left ventricular hypertrophy remained unchanged in SHR-C animals. However, wall thicknesses were significantly reduced as a result of BGP-15 treatment ($p < 0.05$, SHR-B vs. SHR-C). LV end-diastolic (LVEDV) and LV end-systolic volumes (LVESV) were also significantly elevated in SHR-C animals ($p < 0.01$, SHR-C vs. WKY, SHR-Baseline).

BGP-15 treatment was however able to moderate this elevation in SHR-B animals ($p < 0.05$ vs. SHR-C). LV mass was significantly higher in the SHR-Baseline group compared to WKY ($p < 0.05$ SHR-Baseline vs. WKY). In SHR-C animals, this parameter increased further compared to the initial value ($p < 0.01$, SHR-C vs. WKY; $p < 0.05$, SHR-C vs. SHR-Baseline). This parameter was also decreased in the SHR-B group compared to the nontreated animals ($p < 0.05$, SHR-B vs. SHR-C).

The left ventricular systolic function (EF%) reduced in both the SHR groups compared to the initial value; however, this decrease was more pronounced in the SHR-C group than in the treated animals ($p < 0.05$ SHR-B vs. SHR-C). The diastolic function marker E/E' ratio was significantly increased in the SHR-C group ($p < 0.05$ SHR-C vs. SHR-Baseline), indicating a decrease a diastolic dysfunction.

Meanwhile, the BGP-15 treatment decreased significantly the E/E' ratio in the treated group, compared to the SHR-C animals ($p < 0.01$, SHR-B vs. SHR-C).

3.3. Effect of BGP-15 Administration on Plasma BNP Level. By the end of the treatment period, the plasma BNP level increased significantly in the SHR-C group compared to the WKY and SHR-Baseline group ($p < 0.05$, SHR-C vs. WKY and SHR-Baseline group; Table 2). The BGP-15 treatment, however, caused a significant decrease in the level of the biomarker of heart failure in SHR animals ($p < 0.05$, SHR-B vs. SHR-C). The BNP level was only slightly elevated in the SHR-B group.

3.4. Effect of the BGP-15 Administration on Interstitial Collagen Deposition. Histological staining of the left ventricle of the heart was performed with Picrosirius red staining (Figures 1(a) and (b)) and collagen I immunohistochemistry (Figures 1(c) and (d)), which was used to monitor the degree of fibrosis. Only a low amount of interstitial collagen could be seen in the WKY group with Picrosirius red staining (Figure 1(a)). The extent of fibrosis was significantly higher in the SHR groups compared to the WKY group ($p < 0.05$, SHR-Baseline vs. WKY; $p < 0.01$, SHR-C and SHR-B vs. WKY; Figure 1(a)). Chronic high blood pressure-induced heart failure caused a further elevation of collagen deposition in the SHR-C group ($p < 0.01$, vs. SHR-Baseline group). The BGP-15 treatment however resulted in a significant decrease in the amount of interstitial fibrosis in the SHR-B group compared to nontreated hypertensive animals ($p < 0.01$, SHR-B vs. SHR-C; Figure 1(a)) (WKY: $11.78 \pm 1.00\%$; SHR-Baseline: $16.59 \pm 1.03\%$; $SHR-C: 32.42 \pm 1.52\%$; $SHR-B: 22.64 \pm 1.09\%$; Figure 2(b)).

Similar observations were made in the case of type I collagen immunohistochemistry (Figures 1(c) and (d)). Moderate interstitial collagen deposition was observed in the WKY group (WKY: $9.15 \pm 0.54\%$; SHR-Baseline: $15.45 \pm 0.69\%$; SHR-C: $31.24 \pm 0.77\%$; SHR-B: $19.92 \pm 0.72\%$; Figure 1(d)), in the case of hypertensive groups, even the initial value was higher than the in the WKY group ($p < 0.01$ vs. SHR-Baseline). This elevation became more pronounced by the end of the treatment period ($p < 0.01$ SHR-C vs. WKY, SHR-Baseline groups; Figure 1(c)). Due to the treatment, the interstitial collagen deposition was significantly decreased in the

TABLE 1: Effect of BGP-15 administration on gravimetric parameters of SHR animals.

	WKY ($n = 7$)	SHR-baseline ($n = 7$)	SHR-C ($n = 7$)	SHR-B ($n = 7$)
BW^{START} (g)	386.40 ± 4.33	$343.21 \pm 2.48^{**}$	$346.90 \pm 6.65^{**}$	$340.73 \pm 6.32^{**}$
BW^{END} (g)	401.45 ± 8.94	—	$358.13 \pm 5.08^{**}$	$356.85 \pm 4.54^{**}$
HW^{END} (g)	1.12 ± 0.04	1.16 ± 0.02	$1.49 \pm 0.05^{**,\#\#}$	$1.23 \pm 0.02^{\S\S}$
VW^{END} (g)	0.95 ± 0.04	1.09 ± 0.02	$1.33 \pm 0.05^{**,\#\#}$	$1.14 \pm 0.02^{\S\S}$
VW/BW^{END} (mg/g)	2.28 ± 0.11	$3.19 \pm 0.08^{**}$	$3.73 \pm 0.16^{**,\#\#}$	$3.21 \pm 0.03^{*,\S}$
VW/TL^{END} (mg/mm)	21.27 ± 0.79	$24.76 \pm 0.82^{*}$	$29.79 \pm 0.94^{**,\#\#}$	$25.76 \pm 0.46^{*,\S\S}$
Lung wet weight/weight^{END} (g/g)	4.42 ± 0.26	4.51 ± 0.13	$5.68 \pm 0.24^{**,\#\#}$	$4.68 \pm 0.13^{\S\S}$

BW^{START}: body weight at the beginning of the treatment; BW^{END}: body weight at the end of the treatment; HW^{END}: heart weight at the end of the treatment; VW^{END}: ventricles weight at the end of the treatment; TL^{END}: length of the right tibia at the end of the treatment. Values are means + SEM. WKY: age-matched normotensive Wistar-Kyoto rats, $n = 7$; SHR-Baseline: 15-month-old spontaneously hypertensive rats, $n = 7$; SHR-C: nontreated spontaneously hypertensive rats, $n = 7$; SHR-B: spontaneously hypertensive rats receiving BGP-15 for 18 weeks, $n = 7$. $^{*}p < 0.05$ vs. WKY, $^{**}p < 0.01$ vs. WKY, $^{\#\#}p < 0.01$ vs. SHR-Baseline, $^{\S}p < 0.05$ vs. SHR-C, $^{\S\S}p < 0.01$ vs. SHR-C.

TABLE 2: Effect of BGP-15 treatment on echocardiographic parameters.

	WKY ($n = 7$) Mean ± SEM	SHR-Baseline ($n = 7$) Mean ± SEM	SHR-C ($n = 7$) Mean ± SEM	SHR-B ($n = 7$) Mean ± SEM
Septum	1.93 ± 0.03	$2.29 \pm 0.07^{**}$	$2.32 \pm 0.07^{**}$	$2.09 \pm 0.08^{*,\S}$
PW	1.90 ± 0.04	$2.06 \pm 0.06^{*}$	$1.97 \pm 0.08^{*}$	$1.81 \pm 0.07^{\S}$
LVIDd (mm)	7.61 ± 0.14	7.75 ± 0.15	$8.55 \pm 0.23^{**,\#\#}$	$8.31 \pm 0.18^{**}$
LVIDs (mm)	4.54 ± 0.13	4.60 ± 0.21	$5.87 \pm 0.31^{**,\#\#}$	$5.19 \pm 0.32^{\S}$
LVEDV (μl)	310.25 ± 12.85	323.07 ± 14.59	$402.40 \pm 24.76^{**,\#\#}$	$377.19 \pm 17.37^{**}$
LVESV (μl)	96.01 ± 6.85	101.51 ± 12.27	$175.52 \pm 22.46^{**,\#\#}$	$137.23 \pm 16.46^{**,\S}$
LV mass (mg)	1029.81 ± 43.84	$1384.42 \pm 40.69^{**}$	$1587.38 \pm 106.36^{**,\#}$	$1321.44 \pm 75.58^{*,\S}$
EF%	70.48 ± 1.12	69.59 ± 2.41	$57.21 \pm 3.02^{**,\#\#}$	$64.30 \pm 2.88^{*,\S}$
E/A	1.37 ± 0.07	$1.70 \pm 0.09^{**}$	$2.02 \pm 0.06^{**}$	$1.27 \pm 0.08^{\S\S}$
E/E'	30.45 ± 2.00	30.32 ± 2.98	$40.41 \pm 2.94^{**,\#\#}$	$25.71 \pm 3.03^{\S\S}$
BNP (pg/ml)	302.76 ± 13.76	325.19 ± 10.89	$755.14 \pm 33.34^{*,\#}$	$352.04 \pm 22.50^{\S}$

Septum: thickness of the septum; PW: thickness of the posterior wall; LVIDd: left ventricular (LV) inner diameter end-diastolic; LVIDs: LV inner diameter end-systolic; LVEDV: LV end-diastolic volume; LVESV: LV end-systolic volume; LV mass: calculated weight of left ventricle; EF: ejection fraction; E: mitral peak velocity of early filling; A: mitral peak velocity of late filling; E': early diastolic mitral annular velocity; A': late diastolic mitral annular velocity; BNP: B type natriuretic peptide. WKY: age-matched normotensive Wistar-Kyoto rats, $n = 7$; SHR-Baseline: 15-month-old spontaneously hypertensive rats, $n = 7$; SHR-C: 19-month-old spontaneously hypertensive rats received placebo for 18 weeks, $n = 7$; SHR-B: 19-month-old spontaneously hypertensive rats received BGP-15 for 18 weeks, $n = 7$. $^{*}p < 0.05$ vs. WKY, $^{**}p < 0.01$ vs. WKY, $^{\#}p < 0.05$ vs. SHR-Baseline, $^{\#\#}p < 0.01$ SHR-Baseline, $^{\S}p < 0.05$ vs. SHR-C, $^{\S\S}p < 0.01$ vs. SHR-C.

SHR-B group compared to the SHR-C group ($p < 0.01$; Figure 1(c)). It can be concluded that BGP-15 treatment significantly reduced the formation of fibrotic deposits in the myocardium (Figures 1(a)–(d)).

3.5. Effect of BGP-15 Administration on the Diameter of Cardiomyocytes.

Histological sections from the left ventricle of the heart stained with Picrosirius red were also used to study the cell diameters (Figures 1(e) and (f)). The diameter of cardiomyocytes was markedly elevated in SHR groups compared to the WKY group (WKY: $16.02 \pm 0.64\,\mu$m; SHR-Baseline: $22.76 \pm 0.70\,\mu$m; SHR-C: $33.86 \pm 1.82\,\mu$m; SHR-B: $28.57 \pm 0.57\,\mu$m; Figure 1(f)). This difference was the most pronounced in the case of SHR-C ($p < 0.01$, SHR-C vs. WKY). The BGP-15 treatment resulted in significantly lower cell diameters in the SHR-B group compared to the SHR-C group ($p < 0.01$; SHR-B vs. SHR-C; Figure 1(e)).

3.6. Effect of BGP-15 Administration on the TGF-β/SMAD Signalling Pathway.

The level of TGF-β was significantly elevated in all hypertensive groups compared to the WKY group ($p < 0.05$, SHR-B vs. WKY, $p < 0.01$ SHR-Baseline, SHR-C vs. WKY; Figure 2). In the case of the SHR-C group, a further increasing tendency could be seen by the end of the treatment period compared to the baseline values (NS). However, the BGP-15 treatment caused a significant decrease in the TGF-β level compared to the untreated SHR animals ($p < 0.01$, SHR-B vs. SHR-C); moreover, the TGF-β level in this group was even lower than in the SHR-Baseline group ($p < 0.05$, SHR-B vs. SHR-Baseline; Figure 2). In the case of
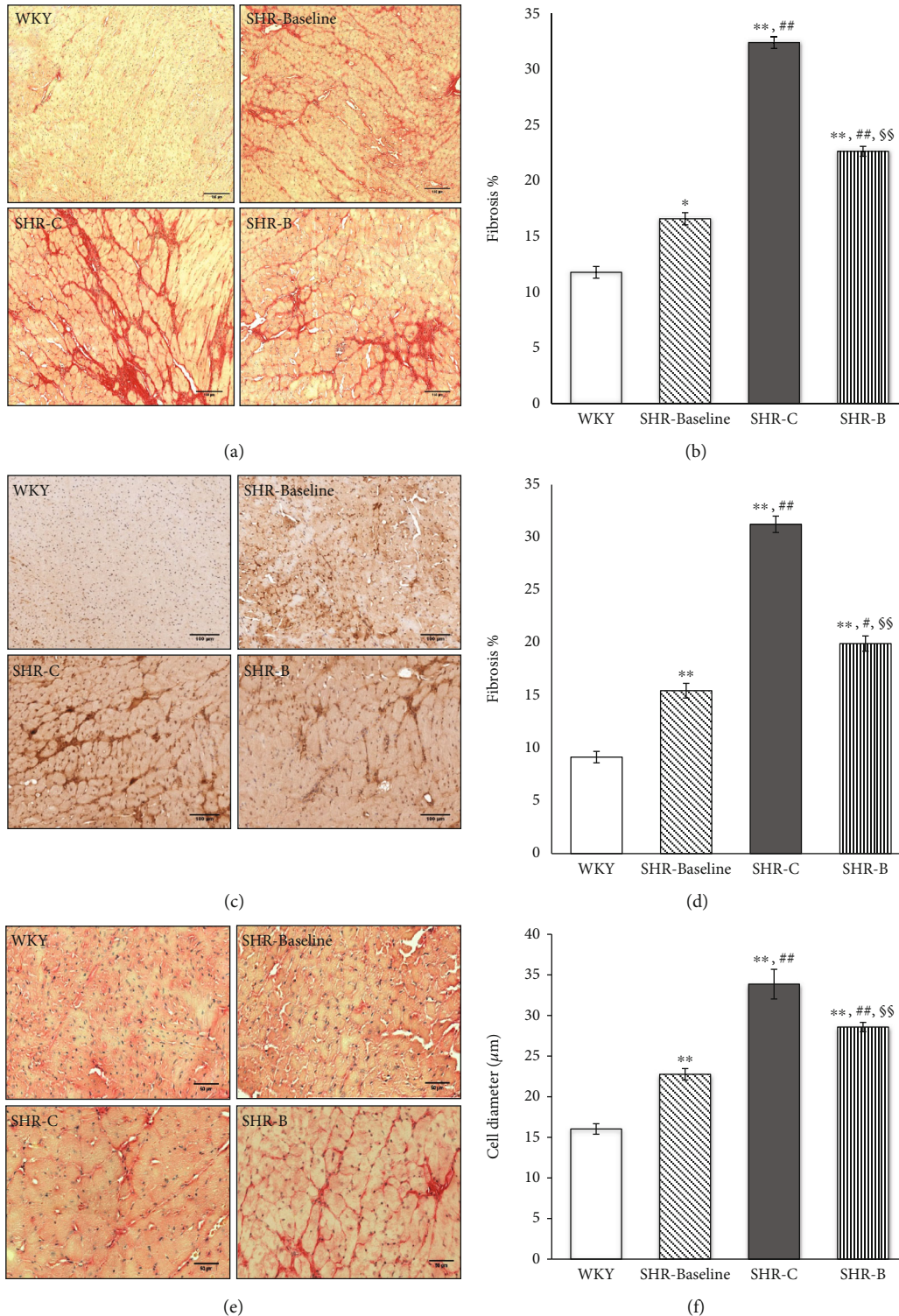
(a)

(b)

(c)

(d)

(e)

(f)

Figure 1: Effect of BGP-15 treatment on the extent of interstitial fibrosis, collagen type I deposition, and on the diameter of cardiomyocytes. Representative histological sections stained with Picrosirius red (a) ($n = 7$). Scale bar: 150 μm, magnification: 10-fold. Densitometric evaluation of the sections is shown (b). $^{*}p < 0.05$ vs. WKY, $^{**}p < 0.01$ vs. WKY, $^{##}p < 0.01$ vs. SHR-Baseline, $^{§§}p < 0.01$ vs. SHR-C. Representative histological sections detected with collagen type I immunohistochemistry (c) ($n = 7$). Scale bar: 100 μm, magnification: 10-fold. Densitometric evaluation of the sections is shown (d). $^{**}p < 0.01$ vs. WKY, $^{##}p < 0.01$ vs. SHR-C, $^{§§}p < 0.01$ vs. SHR-C. Representative histological sections stained with Picrosirius red (e) ($n = 7$). Scale bar: 50 μm, magnification: 10-fold. The average cellular diameter in the different groups is shown (f). $^{**}p < 0.01$ vs. WKY, $^{#}p < 0.05$ vs. SHR-Baseline, $^{§§}p < 0.01$ vs. SHR-C. WKY: age-matched normotensive Wistar-Kyoto rats; SHR-Baseline: 15-month-old spontaneously hypertensive rats; SHR-C: 19-month-old spontaneously hypertensive rats received placebo for 18 weeks; SHR-B: 19-month-old spontaneously hypertensive rats received BGP-15 for 18 weeks.
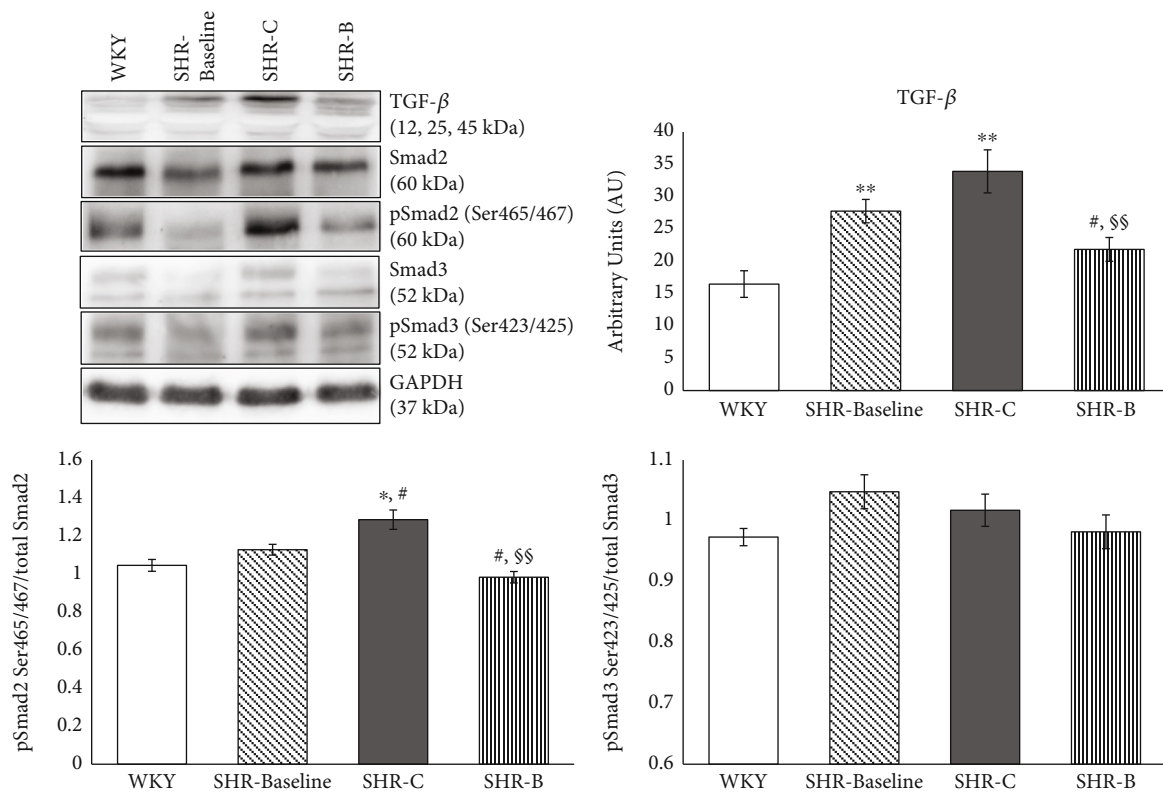
FIGURE 2: Effect of BGP-15 treatment on the TGFβ/Smad signalling pathway. Representative Western blot analysis of TGFβ, Smad2, Smad3, and phosphorylation and densitometric evaluation are shown. GAPDH was used as a loading control. WKY: age-matched normotensive Wistar-Kyoto rats, $n = 7$; SHR-Baseline: 15-month-old spontaneously hypertensive rats, $n = 7$; SHR-C: nontreated spontaneously hypertensive rats, $n = 7$; SHR-B: spontaneously hypertensive rats receiving BGP-15 for 18 weeks, $n = 7$. Values are mean ± SEM. $^*p < 0.05$ vs. WKY, $^{**}p < 0.01$ vs. WKY, $^#p < 0.05$ vs. SHR-Baseline, $^{§§}p < 0.01$ vs. SHR-C.

Smad2 phosphorylation, we observed a mild increase in the SHR-Baseline compared to the WKY; however, this elevation was not significant. The phosphorylation of Smad2$^{Ser465/467}$ was significantly increased in the SHR-C compared to the WKY and Baseline groups ($p < 0.05$). BGP-15 treatment resulted in a significant reduction in the phosphorylation level of Smad2$^{Ser465/467}$ in the treated group ($p < 0.01$ SHR-B vs. SHR-C). There were no significant differences regarding the phosphorylation of Smad3$^{Ser423/425}$ between the groups (Figure 2). GAPDH was used as a loading control.

3.7. Effect of BGP-15 Administration on the Phosphorylation Level of Akt-1 and GSK-3β. The level of Akt-1^{Ser473} phosphorylation was moderate in the WKY group as well as in the SHR-Baseline group (Figure 3.). In the SHR-C group, the phosphorylation of Akt-1^{Ser473} was increased slightly, but significantly ($p < 0.01$ SHR-C vs. WKY and SHR-Baseline groups; Figure 3). However, BGP-15 treatment increased a marked increase in the Akt-1^{Ser473} phosphorylation in SHR-B animals ($p < 0.01$ SHR-B vs. SHR-C group).

The phosphorylation level of GSK-3β^{Ser9} was low in the WKY group similar to the Akt-1^{Ser473} phosphorylation. In the SHR-Baseline and the SHR-C groups, however, slightly but not significantly elevated phosphorylation could be seen. The highest phosphorylation of GSK-3β^{Ser9} was measured in

the SHR-B group. This elevation was highly significant to other SHR groups ($p < 0.05$ SHR-B vs. SHR-C; $p < 0.01$, SHR-B vs. SHR-Baseline group; Figure 3). GAPDH was used as a loading control.

3.8. Effect of BGP-15 Administration on the Activity of MAPKs. The level of MKP-1 protein was low in the WKY and SHR-Baseline groups (Figure 4). A significant increase was however observed in the SHR-C group ($p < 0.01$, SHR-C vs. WKY as well as SHR-Baseline groups). The amount of MKP-1 protein increased further in the SHR-B group as a result of the BGP-15 treatment ($p < 0.01$, SHR-B vs. SHR-C; Figure 4). The level of Erk1/2$^{Thr202/Tyr204}$ phosphorylation was less pronounced in the SHR-C group compared to the WKY group and to baseline level ($p < 0.05$, SHR-C vs. WKY, Figure 4). BGP-15 treatment however caused a significant elevation in the phosphorylation of Erk1/2$^{Thr202/Tyr204}$ compared to the SHR-C group ($p < 0.01$, SHR-B vs. SHR-C; Figure 4). The level of p38-MAPK$^{Thr180/Tyr182}$ and JNK$^{Thr183/Tyr185}$ phosphorylation was low in the WKY and in the SHR-Baseline groups (Figure 4). The highest phosphorylation level of p38-MAPK$^{Thr180/Tyr182}$ and JNK$^{Thr183/Tyr185}$ could be seen in the SHR-C animals ($p < 0.01$, SHR-C vs. WKY and SHR-Baseline). The BGP-15 treatment reduced this phosphorylation of p38-MAPK$^{Thr180/Tyr182}$ and JNK$^{Thr183/Tyr185}$ too, and
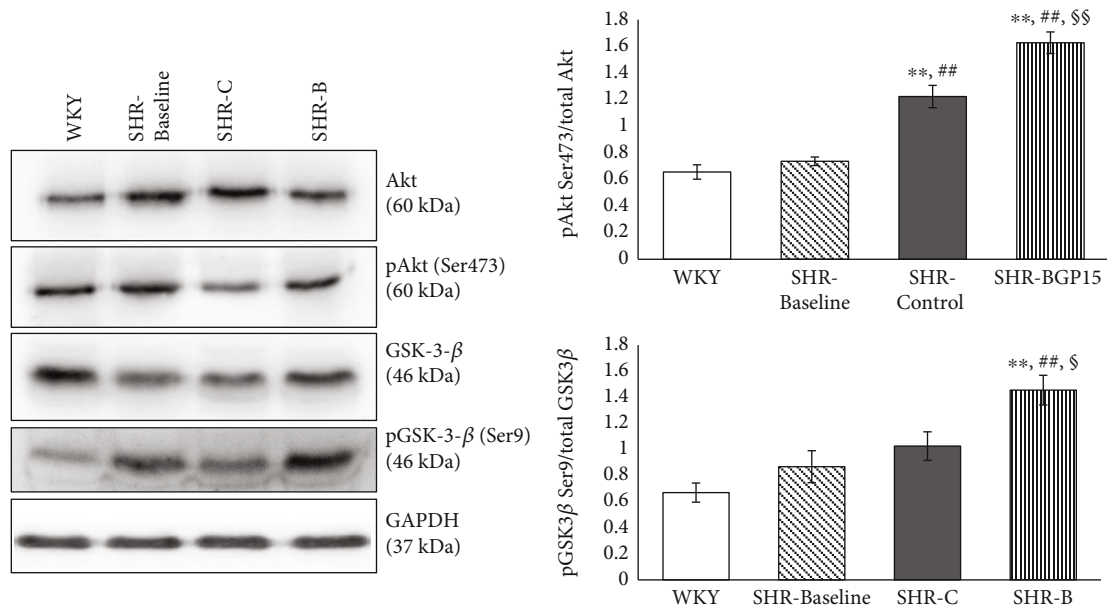
FIGURE 3: Effect of BGP-15 treatment on the phosphorylation of Akt-1^{Ser473} and GSK-3β^{Ser9}. Representative Western blot analysis of Akt-1 and GSK-3β phosphorylation and densitometric evaluation are shown. GAPDH was used as a loading control. WKY: age-matched normotensive Wistar-Kyoto rats, $n = 7$; SHR-Baseline: 15-month-old spontaneously hypertensive rats, $n = 7$; SHR-C: nontreated spontaneously hypertensive rats, $n = 7$; SHR-B: spontaneously hypertensive rats receiving BGP-15 for 18 weeks, $n = 7$. Values are mean ± SEM. $^{**}p < 0.01$ vs. WKY, $^{##}p < 0.01$ vs. SHR-Baseline, $^{\$}p < 0.05$ vs. SHR-C, $^{\$\$}p < 0.01$ vs. SHR-C.

this reduction was significant in the case of JNK$^{Thr183/Tyr185}$ compared to the SHR-C group ($p < 0.01$; Figure 4). GAPDH was used as a loading control.

3.9. Effect of BGP-15 Administration on the Regulation of Mitochondrial Biogenesis.

There were no significant differences between the WKY, SHR-Baseline, and SHR-C groups regarding the PGC-1α level (Figure 5). However, the BGP-15 treatment caused a significant increase in the amount of PGC-1α compared to the nontreated hypertensive animals ($p < 0.01$, SHR-B vs. SHR-Baseline and SHR-C group; Figure 5). In the case of AMPK^{Thr172} phosphorylation, a significant increase was observed in the SHR-C group compared to the SHR-Baseline group ($p < 0.01$, SHR-C vs. SHR-Baseline; Figure 5). The BGP-15 treatment significantly reduced the phosphorylation of AMPK^{Thr172} compared to the SHR-C group ($p < 0.01$ SHR-B vs. SHR-C). The CREB-^{Ser133} phosphorylation was modest in the WKY group similar to the phosphorylation of AMPK^{Thr172} (Figure 5). There was a significant increase in the phosphorylation level of CREB-^{Ser133} in the SHR-C group compared to the baseline value and to the normotensive animals ($p < 0.01$, SHR-C vs. WKY; Figure 5). However, the BGP-15 treatment caused a further increase in the CREB^{Ser133} phosphorylation compared to nontreated SHR animals ($p < 0.05$ SHR-B vs. SHR-C group) and to the baseline value ($p < 0.01$ SHR-B vs. SHR-Baseline). The highest VDAC protein level was observed in the WKY group. This level was significantly lower in the hypertensive groups ($p < 0.01$ WKY vs. SHR-Baseline, SHR-C, and SHR-B). By the end of the treatment period, VDAC became higher compared to the initial value ($p < 0.01$, SHR-

C vs. SHR-Baseline). A further significant increase was seen in the SHR-B group ($p < 0.05$ SHR-B vs. SHR-C). GAPDH was used as a loading control.

4. Discussion

In this work, we aimed to examine the cardioprotective effect of BGP-15 in chronic hypertension-induced heart failure. The major findings of this study are that BGP-15 has a positive effect on cardiac function and on remodelling processes by inhibiting profibrotic signalling factors and by promoting mitochondrial biogenesis in an animal model of hypertension-induced heart failure.

SHR was used to provoke hypertension-induced heart failure. SHR is a widely used animal model in experimental cardiology because it resembles the human essential hypertension [13]. 15-months-old SHRs already showed the unquestionable signs of hypertensive heart disease at the start of the experiments. Left ventricular wall thicknesses and the LV mass were markedly increased in the SHR animals compared to normotensives (Table 2). However systolic left ventricular function was still normal in both normotensive and hypertensive animals. This is in accordance with the results of other workgroups and with our former results [25, 26]. The signs of left ventricular hypertrophy remained marked also by the end of the study in SHR animals. However, systolic (EF%) as well as diastolic left ventricular function (E/E') worsened significantly by that time, and animals showed the signs of heart failure. The worsening of these parameters was considerably lower due to the BGP-15 treatment of hypertensive animals (Table 2). This result
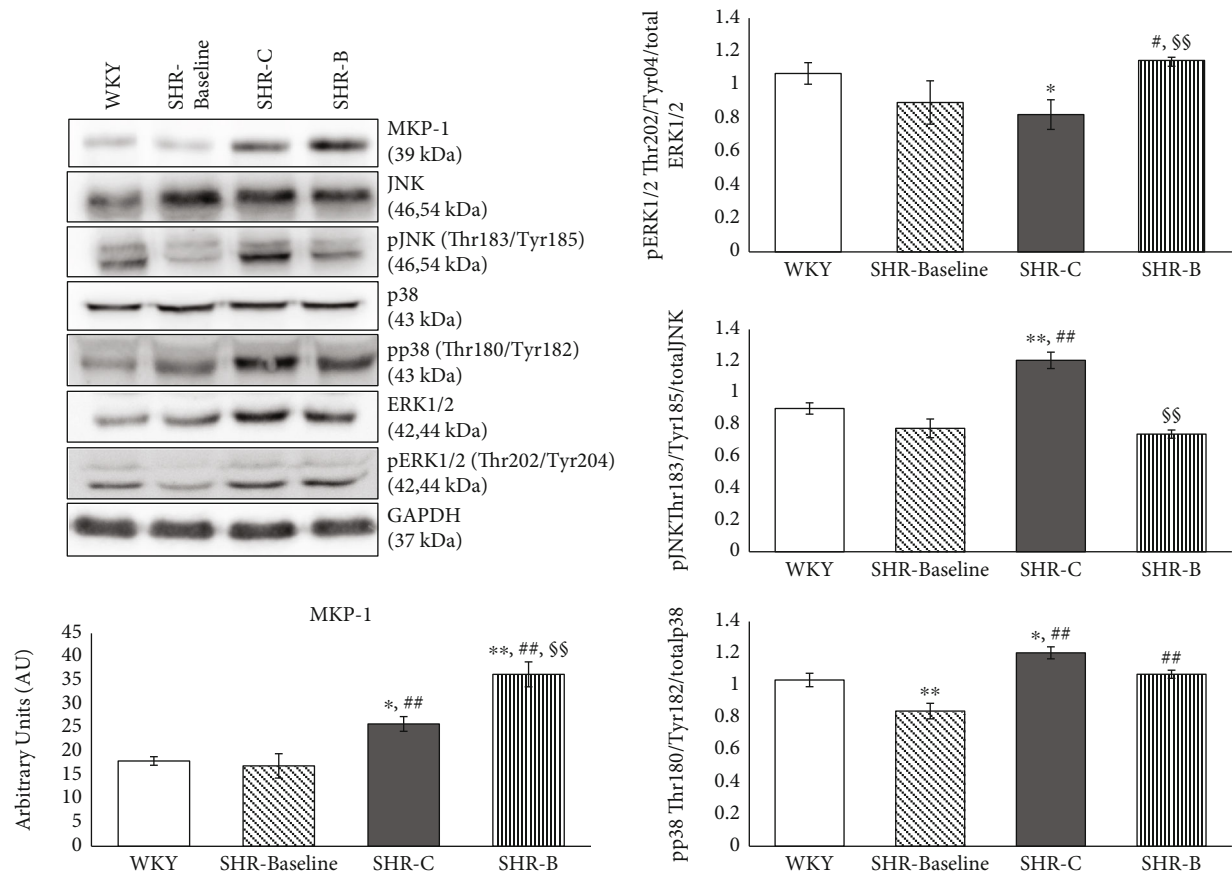
Figure 4: Effect of the BGP-15 treatment on the phosphorylation state of MAP kinases and on MKP-1. Representative Western blot analysis of MKP-1 as well as ERK1/2, p38, and JNK phosphorylation. Densitometric evaluation is also shown. GAPDH was used as a loading control. WKY: age-matched normotensive Wistar-Kyoto rats, $n = 7$; SHR-Baseline: 15-month-old spontaneously hypertensive rats, $n = 7$; SHR-C: nontreated spontaneously hypertensive rats, $n = 7$; SHR-B: spontaneously hypertensive rats receiving BGP-15 for 18 weeks, $n = 7$. Values are mean ± SEM. $^{*}p < 0.05$ vs. WKY, $^{**}p < 0.01$ vs. WKY, $^{##}p < 0.01$ vs. SHR-Baseline, $^{\S\S}p < 0.01$ vs. SHR-C.

supports and complements the results of Sapra et al. that BGP-15 has beneficial effects on cardiac function in murine heart failure [17]. Moreover, left ventricular hypertrophy as well as the severity of left ventricular diastolic dysfunction was not only moderated due to BGP-15 treatment but also improved slightly, showing a so-called reverse remodelling phenomenon.

The BNP plasma level is a biomarker of heart failure. There is a direct proportionality between the severity of heart failure and the BNP level [27]. The marked increase of BNP that was seen in nontreated hypertensive animals (SHR-C) was also positively affected by BGP-15, because it decreased the BNP level to the level of normotensive animals (Table 2).

Hypertensive heart disease including heart failure is characterised by cardiac fibrosis. Extracellular matrix (ECM) remodelling can be observed during cardiac fibrosis, which leads to abnormalities in matrix composition and quality, as well as to decrease heart function [4, 28]. Heart failure is characterized by an increased collagen type I deposition. Thus, collagen type I is a marker of cardiac fibrosis. Collagen type I is one of the major components of the adult human cardiac tissue (approximately 85%) while collagen type III is the other important component (11%) [29]. Ventricular

remodelling was characterized by cardiomyocyte hypertrophy and an extensive myocardial collagen deposition [30]. Both phenomena could be seen in hypertensive animals. BGP-15, however, prevented against hypertension-induced cardiac interstitial fibrosis and cardiomyocyte hypertrophy (Figure 1). The transforming growth factor-β (TGFβ)/Smad signalling route has a major role in the regulation of cardiac fibrosis [31, 32]. Activation of TGF-β/Smad signalling promotes myofibroblast formation and extracellular matrix (ECM) production that are leading to cardiac fibrosis [33]. In our recent work, hypertension induced a marked cardiac fibrosis by the activation of the TGF-β/Smad pathway (Figure 2). Both the level of TGF-β and the phosphorylation of Smad2$^{Ser465/467}$ were significantly reduced due to BGP-15 treatment; therefore, it can be a mechanism in the background of decreased fibrosis, observed in the SHR-B group. The BGP-15-induced inhibition of fibrosis and cardiomyocyte hypertrophy are on the other hand the main causes of the improved cardiac function and structure compared to nontreated SHRs (Tables 1 and 2).

It is well known that the MAPK signalling pathway also plays an important role in the pathogenesis of hypertension-induced cardiac remodelling and heart failure [7, 34, 35].
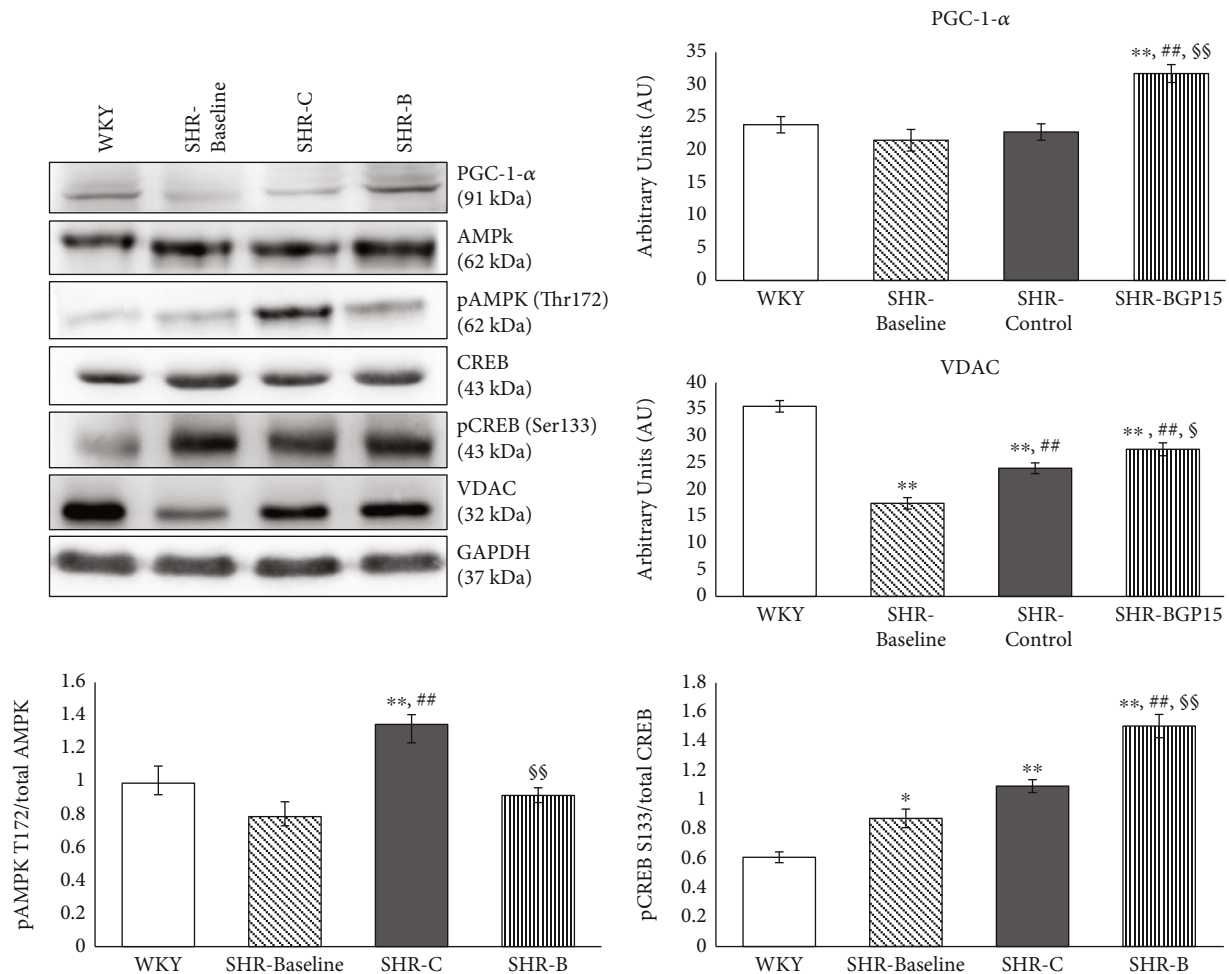
Figure 5: Effect of the BGP-15 treatment on the regulation of mitochondrial biogenesis. Representative Western blot analysis of PGC-1α, VDAC, CREB, AMPK, and phosphorylation of CREB and AMPK. Densitometric evaluation is also shown. GAPDH was used as a loading control. WKY: age-matched normotensive Wistar-Kyoto rats, $n = 7$; SHR-Baseline: 15-month-old spontaneously hypertensive rats, $n = 7$; SHR-C: nontreated spontaneously hypertensive rats, $n = 7$; SHR-B: spontaneously hypertensive rats receiving BGP-15 for 18 weeks, $n = 7$. Values are mean ± SEM. $^*p < 0.05$ vs. WKY, $^{**}p < 0.01$ vs. WKY, $^{##}p < 0.01$ vs. SHR-Baseline, $^{\$}p < 0.05$ vs. SHR-C, $^{\$\$}p < 0.01$ vs. SHR-C.

MAP kinases, predominantly p38 MAPK and JNK, are other important regulators of myocardial fibrosis [24, 36, 37]. The activity of MAP kinases are regulated by dual-specificity phosphatases (DUSPs) or MAPK phosphatases (MKPs) that can dephosphorylate MAPKs and in this way regulate—actually inhibit—their activity [34, 38]. In our recent work, the expression of MKP-1 increased significantly due to BGP-15 treatment in comparison with the SHR-C animals (Figure 4) As a consequence of the increased amount of MKP-1, the p38 MAPK and JNK phosphorylation decreased in the treated animals, in accordance with several previous studies that also confirmed the beneficial effect of BGP-15 on the phosphorylation state of p38 MAPK and JNK (Figure 4) [19, 22]. In the case of ERK phosphorylation, an opposite change could be seen in our work, because BGP-15 increased the ERK1/2 phosphorylation (Figure 4). Regarding BGP-15, there are studies that are in accordance with our results. Szabo et al. demonstrated that BGP-15 treatment increased the phosphorylation of ERK1/2 in WRL-68 cells [22]. However, in another work, BGP-15 decreased the phosphorylation of ERK1/2 in

imatinib-induced cardiotoxicity [19]. Because ERK1/2 is a member of prosurvival signalling factors, its activation is beneficial in the failed myocardium [25, 39].

Akt-1 also belongs to prosurvival signalling factors, and it can promote "physiological" hypertrophy; however, it inhibits the pathological hypertrophy that is mainly characterised by cardiac collagen accumulation [40–42]. GSK-3β is a downstream target of Akt-1 and Akt-1 which via the phosphorylation of GSK-3β can promote the survival of chronically stressed cardiomyocytes in heart failure as demonstrated by previous works [25]. The cytoprotective effect due to increased phosphorylation of Akt-1 and GSK-3β is mediated via their protective effect on the structure and function of mitochondria [43]. In our recent study, BGP-15 increased significantly the phosphorylation of Akt-1 and GSK-3β compared to the nontreated SHR animals (Figure 3); therefore, the BGP-15 treatment activates the prosurvival signalling pathways.

The contractile function of cardiomyocytes is in strong correlation with the energy-producing capacity of the mitochondrial network [44]. Numerous studies have demonstrated
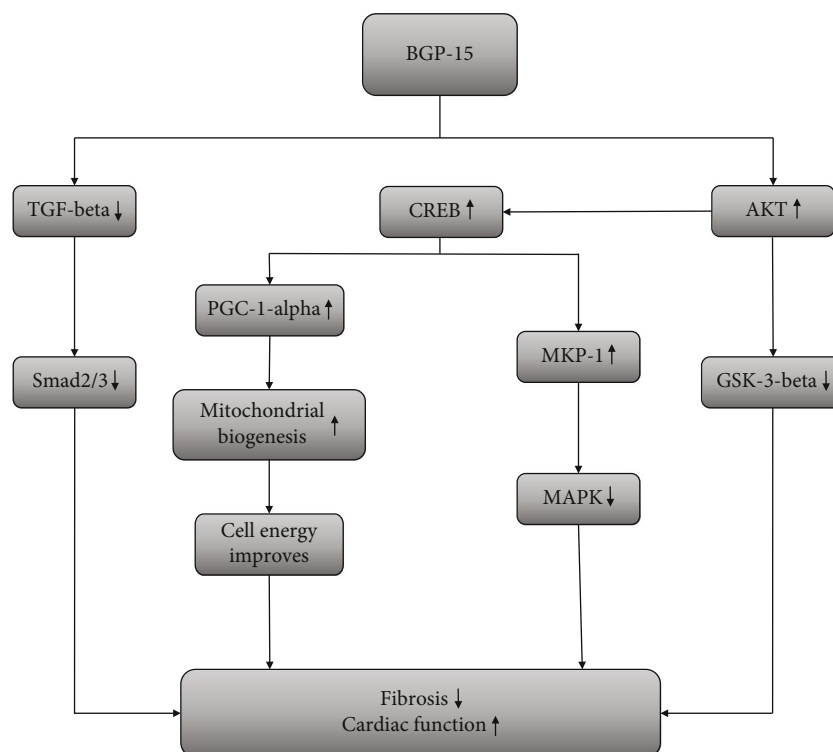
FIGURE 6: The suspected mechanism of BGP-15 treatment in a hypertension-induced heart failure model. BGP-15 has a beneficial effect against hypertension-induced cardiac remodelling and cardiac fibrosis. The BGP-15 treatment decreases the activity of TGFβ/Smad and MAPK signalling factors and in this way prevents against hypertension-induced interstitial collagen deposition. BGP-15 favourably influences the prosurvival signalling pathways. Moreover, the mitochondrial biogenesis is activated due to BGP-15 administration, thereby resulting in an increase in mitochondrial mass.

that mitochondrial biogenesis is an essential step in mitochondrial quality control and is a highly vulnerable process in heart failure [45, 46]. PGC-1α is the master signalling factor of biogenesis, and it is regulated in different ways, among others by AMPK and CREB [47–49]. We found that the expression level of PCG-1α increased due to BGP-15 treatment compared to SHR-C animals (Figure 5). Phosphorylation of AMPK was however reduced as a result of the treatment (Figure 5). AMPK activation is a consequence of increased AMP to ATP ratio, which is a sign of energy depletion. Therefore, this reduction of AMPK phosphorylation indicates a favourable change in the energy production of cardiomyocytes [50, 51]. Phosphorylation of CREB was on the other hand increased in BGP-15-treated SHR animals compared to nontreated ones (Figure 5). BGP-15 via the activation of CREB increased the expression level of PGC-1α, which in turn can yield in enhanced mitochondrial biogenesis and in increased high energy phosphate production. CREB transcription factor can also increase the production of MKP-1 and thereby can decrease the activity of the MAPK signal pathway, too [52, 53], which could be seen in our study. We determined the amount of VDAC, an outer mitochondrial membrane protein to characterize the number of mitochondria in cardiomyocytes. The elevation of VDAC in BGP-15-treated animals proved that there is an increased mitochondrial biogenesis and mitochondrial mass in cardiomyocytes.

In conclusion, BGP-15 treatment exerted a marked protective effect against the development of hypertension-induced heart failure via the inhibition of the fibrotic remodelling of the heart. This effect could be explained by its beneficial effect on signal transduction factors and by the increased mitochondrial biogenesis (Figure 6).

Data Availability

The authors confirm that all data is fully available without restriction. All relevant data is described within the paper.

Ethical Approval

Animals received care according to the Guide for the Care and Use of Laboratory Animals published by the US National Institute of Health, and the experiment was approved by the Animal Research Review Committee of the University of Pecs, Medical School (permit number: BA02/2000-54/2017). The manuscript does not contain clinical studies or patient data.

Conflicts of Interest

On behalf of all authors, the corresponding author states that there is no conflict of interest.

Authors' Contributions

All authors contributed to the study conception and design. Material preparation, data collection, and analysis were performed by Orsolya Horvath, Katalin Ordog, Kitti Bruszt, Laszlo Deres, Ferenc Gallyas, Balazs Sumegi, Kalman Toth, and Robert Halmosi. The first draft of the manuscript was written by Orsolya Horvath, and all authors commented on the previous versions of the manuscript. All authors read and approved the final manuscript. Prof. Balazs Sumegi has unexpectedly passed away during the course of this study. This paper is dedicated to his memory.

Acknowledgments

References

[1] E. J. Benjamin, P. Muntner, A. Alonso et al., "Heart Disease and Stroke Statistics—2019 update: a report from the American Heart Association," *Circulation*, vol. 139, pp. e56–e528, 2019.

[2] C. D. Kemp and J. V. Conte, "The pathophysiology of heart failure," *Cardiovascular Pathology*, vol. 21, no. 5, pp. 365–371, 2012.

[3] F. Jarraya, "Treatment of hypertension: which goal for which patient?," *Advances in Experimental Medicine and Biology*, vol. 956, pp. 117–127, 2016.

[4] P. Kong, P. Christia, and N. G. Frangogiannis, "The pathogenesis of cardiac fibrosis," *Cellular and Molecular Life Sciences*, vol. 71, no. 4, pp. 549–574, 2014.

[5] J. G. Travers, F. A. Kamal, J. Robbins, K. E. Yutzey, and B. C. Blaxall, "Cardiac fibrosis: the fibroblast awakens," *Circulation Research*, vol. 118, no. 6, pp. 1021–1040, 2016.

[6] A. M. Rababa'h, A. N. Guillory, R. Mustafa, and T. Hijjawi, "Oxidative stress and cardiac remodeling: an updated edge," *Current Cardiology Reviews*, vol. 14, no. 1, pp. 53–59, 2018.

[7] A. J. Muslin, "MAPK signalling in cardiovascular health and disease: molecular mechanisms and therapeutic targets," *Clinical Science*, vol. 115, no. 7, pp. 203–218, 2008.

[8] W. Zhang, V. Elimban, M. S. Nijjar, S. K. Gupta, and N. S. Dhalla, "Role of mitogen-activated protein kinase in cardiac hypertrophy and heart failure," *Experimental and Clinical Cardiology*, vol. 8, no. 4, pp. 173–183, 2003.

[9] G. W. Dorn, R. B. Vega, and D. P. Kelly, "Mitochondrial biogenesis and dynamics in the developing and diseased heart," *Genes & Development*, vol. 29, no. 19, pp. 1981–1991, 2015.

[10] B. Zhou and R. Tian, "Mitochondrial dysfunction in pathophysiology of heart failure," *The Journal of Clinical Investigation*, vol. 128, no. 9, pp. 3716–3726, 2018.

[11] D. B. Zorov, M. Juhaszova, and S. J. Sollott, "Mitochondrial ROS-induced ROS release: an update and review," *Biochimica et Biophysica Acta*, vol. 1757, no. 5-6, pp. 509–517, 2006.

[12] Y. K. Tham, B. C. Bernardo, J. Y. Y. Ooi, K. L. Weeks, and J. R. McMullen, "Pathophysiology of cardiac hypertrophy and heart failure: signaling pathways and novel therapeutic targets," *Archives of Toxicology*, vol. 89, no. 9, pp. 1401–1438, 2015.

[13] G. Itter, W. Jung, P. Juretschke, B. A. Schoelkens, and W. Linz, "A model of chronic heart failure in spontaneous hypertensive rats (SHR)," *Laboratory Animals*, vol. 38, no. 2, pp. 138–148, 2016.

[14] M. Kokubo, A. Uemura, T. Matsubara, and T. Murohara, "Noninvasive evaluation of the time course of change in cardiac function in spontaneously hypertensive rats by echocardiography," *Hypertension Research*, vol. 28, no. 7, pp. 601–609, 2005.

[15] R. Halmosi, Z. Berente, E. Osz, K. Toth, P. Literati-Nagy, and B. Sumegi, "Effect of poly(ADP-ribose) polymerase inhibitors on the ischemia-reperfusion-induced oxidative cell damage and mitochondrial metabolism in Langendorff heart perfusion system," *Molecular Pharmacology*, vol. 59, no. 6, pp. 1497–1505, 2001.

[16] E. Szabados, P. Literati-Nagy, B. Farkas, and B. Sumegi, "BGP-15, a nicotinic amidoxime derivate protecting heart from ischemia reperfusion injury through modulation of poly(-ADP-ribose) polymerase," *Biochemical Pharmacology*, vol. 59, no. 8, pp. 937–945, 2000.

[17] G. Sapra, Y. K. Tham, N. Cemerlang et al., "The small-molecule BGP-15 protects against heart failure and atrial fibrillation in mice," *Nature Communications*, vol. 5, no. 1, p. 5705, 2014.

[18] M. Bombicz, D. Priksz, R. Gesztelyi et al., "The drug candidate BGP-15 delays the onset of diastolic dysfunction in the Goto-Kakizaki rat model of diabetic cardiomyopathy," *Molecules*, vol. 24, no. 3, p. 586, 2019.

[19] Z. Sarszegi, E. Bognar, B. Gaszner et al., "BGP-15, a PARP-inhibitor, prevents imatinib-induced cardiotoxicity by activating Akt and suppressing JNK and p38 MAP kinases," *Molecular and Cellular Biochemistry*, vol. 365, no. 1-2, pp. 129–137, 2012.

[20] K. Sumegi, K. Fekete, C. Antus et al., "BGP-15 protects against oxidative stress- or lipopolysaccharide-induced mitochondrial destabilization and reduces mitochondrial production of reactive oxygen species," *PLoS One*, vol. 12, no. 1, p. e0169372, 2017.

[21] G. Nagy, A. Szarka, G. Lotz et al., "BGP-15 inhibits caspase-independent programmed cell death in acetaminophen-induced liver injury," *Toxicology and Applied Pharmacology*, vol. 243, no. 1, pp. 96–103, 2010.

[22] A. Szabo, K. Sumegi, K. Fekete et al., "Activation of mitochondrial fusion provides a new treatment for mitochondria-related diseases," *Biochemical Pharmacology*, vol. 150, pp. 86–96, 2018.

[23] Y. Kubota, K. Umegaki, S. Kagota et al., "Evaluation of blood pressure measured by tail-cuff methods (without heating) in spontaneously hypertensive rats," *Biological & Pharmaceutical Bulletin*, vol. 29, no. 8, pp. 1756–1758, 2006.

[24] L. Deres, K. Eros, O. Horvath et al., "The effects of bradykinin B1 receptor antagonism on the myocardial and vascular consequences of hypertension in SHR rats," *Front Physiol*, vol. 10, 2019.

[25] E. Bartha, I. Solti, L. Kereskai et al., "PARP inhibition delays transition of hypertensive cardiopathy to heart failure in spontaneously hypertensive rats," *Cardiovascular Research*, vol. 83, no. 3, pp. 501–510, 2009.

[26] D. Loch, V. Chan, A. Hoey, and L. Brown, "Rosuvastatin attenuates heart failure and cardiac remodelling in the ageing spontaneously hypertensive rat," *Basic & Clinical Pharmacology & Toxicology*, vol. 105, no. 4, pp. 262–270, 2009.

[27] C. Magnussen and S. Blankenberg, "Biomarkers for heart failure: small molecules with high clinical relevance," *Journal of Internal Medicine*, vol. 283, no. 6, pp. 530–543, 2018.

[28] N. G. Frangogiannis, "Cardiac fibrosis: cell biological mechanisms, molecular pathways and therapeutic opportunities," *Molecular Aspects of Medicine*, vol. 65, pp. 70–99, 2019.

[29] S. Hinderer and K. Schenke-Layland, "Cardiac fibrosis - a short review of causes and therapeutic strategies," *Advanced Drug Delivery Reviews*, vol. 146, pp. 77–82, 2019.

[30] R. T. Cowling, D. Kupsky, A. M. Kahn, L. B. Daniels, and B. H. Greenberg, "Mechanisms of cardiac collagen deposition in experimental models and human disease," *Translational Research*, vol. 209, pp. 138–155, 2019.

[31] Z. Zi, D. A. Chapnick, and X. Liu, "Dynamics of TGF-β/Smad signaling," *FEBS Letters*, vol. 586, no. 14, pp. 1921–1928, 2012.

[32] H. Khalil, O. Kanisicak, V. Prasad et al., "Fibroblast-specific TGF-β-Smad2/3 signaling underlies cardiac fibrosis," *The Journal of Clinical Investigation*, vol. 127, no. 10, pp. 3770–3783, 2017.

[33] A. Biernacka, M. Dobaczewski, and N. G. Frangogiannis, "TGF-β signaling in fibrosis," *Growth Factors*, vol. 29, no. 5, pp. 196–202, 2011.

[34] R. Liu and J. D. Molkentin, "Regulation of cardiac hypertrophy and remodeling through the dual-specificity MAPK phosphatases (DUSPs)," *Journal of Molecular and Cellular Cardiology*, vol. 101, pp. 44–49, 2016.

[35] B. A. Rose, T. Force, and Y. Wang, "Mitogen-activated protein kinase signaling in the heart: angels versus demons in a heart-breaking tale," *Physiological Reviews*, vol. 90, no. 4, pp. 1507–1546, 2010.

[36] N. A. Turner and N. M. Blythe, "Cardiac fibroblast p38 MAPK: a critical regulator of myocardial remodeling," *Journal of Cardiovascular Development and Disease*, vol. 6, no. 3, p. 27, 2019.

[37] S. M. Craige, K. Chen, R. M. Blanton, J. F. Keaney Jr., and S. Kant, "JNK and cardiometabolic dysfunction," *Bioscience Reports*, vol. 39, no. 7, 2019.

[38] K. Magyar, L. Deres, K. Eros et al., "A quinazoline-derivative compound with PARP inhibitory effect suppresses hypertension-induced vascular alterations in spontaneously hypertensive rats," *Biochimica et Biophysica Acta*, vol. 1842, no. 7, pp. 935–944, 2014.

[39] L. Zhu, N. Fang, P. Gao, X. Jin, H. Wang, and Z. Liu, "Differential ERK1/2 signaling and hypertrophic response to endothelin-1 in cardiomyocytes from SHR and Wistar-Kyoto rats: a potential target for combination therapy of hypertension," *Current Vascular Pharmacology*, vol. 13, no. 4, pp. 467–474, 2015.

[40] X. Rossello and D. M. Yellon, "The RISK pathway and beyond," *Basic Research in Cardiology*, vol. 113, no. 1, 2018.

[41] A. H. Chaanine and R. J. Hajjar, "AKT signalling in the failing heart," *European Journal of Heart Failure*, vol. 13, no. 8, pp. 825–829, 2011.

[42] J. Heineke and J. D. Molkentin, "Regulation of cardiac hypertrophy by intracellular signalling pathways," *Nature Reviews. Molecular Cell Biology*, vol. 7, no. 8, pp. 589–600, 2006.

[43] S. Miyamoto, A. N. Murphy, and J. H. Brown, "Akt mediated mitochondrial protection in the heart: metabolic and survival pathways to the rescue," *Journal of Bioenergetics and Biomembranes*, vol. 41, no. 2, pp. 169–180, 2009.

[44] M. S. Martínez, A. García, E. Luzardo et al., "Energetic metabolism in cardiomyocytes: molecular basis of heart ischemia and arrhythmogenesis," *Vessel Plus*, vol. 1, pp. 130–141, 2017.

[45] A. Pisano, B. Cerbelli, E. Perli et al., "Impaired mitochondrial biogenesis is a common feature to myocardial hypertrophy and end-stage ischemic heart failure," *Cardiovascular Pathology*, vol. 25, no. 2, pp. 103–112, 2016.

[46] A. Garnier, D. Fortin, C. Deloménie, I. Momken, V. Veksler, and R. Ventura-Clapier, "Depressed mitochondrial transcription factors and oxidative capacity in rat failing cardiac and skeletal muscles," *The Journal of Physiology*, vol. 551, no. 2, pp. 491–501, 2003.

[47] P. J. Fernandez-Marcos and J. Auwerx, "Regulation of PGC-1α, a nodal regulator of mitochondrial biogenesis," *The American Journal of Clinical Nutrition*, vol. 93, no. 4, pp. 884S–890S, 2011.

[48] C. Cantó and J. Auwerx, "PGC-1alpha, SIRT1 and AMPK, an energy sensing network that controls energy expenditure," *Current Opinion in Lipidology*, vol. 20, no. 2, pp. 98–105, 2009.

[49] F. R. Jornayvaz and G. I. Shulman, "Regulation of mitochondrial biogenesis," *Essays Biochem*, vol. 47, pp. 69–84, 2010.

[50] C. Beauloye, L. Bertrand, S. Horman, and L. Hue, "AMPK activation, a preventive therapeutic target in the transition from cardiac injury to heart failure," *Cardiovascular Research*, vol. 90, no. 2, pp. 224–233, 2011.

[51] X. Li, J. Liu, Q. Lu et al., "AMPK: a therapeutic target of heart failure—not only metabolism regulation," *Bioscience Reports*, vol. 39, no. 1, 2019.

[52] C.-Y. Huang and T.-H. Tan, "DUSPs, to MAP kinases and beyond," *Cell & Bioscience*, vol. 2, no. 1, p. 24, 2012.

[53] C. Casals-Casas, E. Álvarez, M. Serra et al., "CREB and AP-1 activation regulates MKP-1 induction by LPS or M-CSF and their kinetics correlate with macrophage activation versus proliferation," *European Journal of Immunology*, vol. 39, no. 7, pp. 1902–1913, 2009.

Research Article

Pentoxifylline Attenuates Arsenic Trioxide-Induced Cardiac Oxidative Damage in Mice

Atefeh Gholami [1,2] **Sara Ataei** [3] **Davoud Ahmadimoghaddam** [1,2] **Navid Omidifar** [4] **and Amir Nili-Ahmadabadi** [1,2]

[1]*Medicinal Plants and Natural Products Research Center, Hamadan University of Medical Sciences, Hamadan, Iran*
[2]*Department of Pharmacology and Toxicology, School of Pharmacy, Hamadan University of Medical Sciences, P.O. Box 8678-3-65178, Hamadan, Iran*
[3]*Department of Clinical Pharmacy, School of Pharmacy, Hamadan University of Medical Sciences, Hamadan, Iran*
[4]*Clinical Education Research Center, Department of Pathology, School of Medicine, and Biotechnology Research Center, Shiraz University of Medical Sciences, Shiraz, Iran*

Correspondence should be addressed to Amir Nili-Ahmadabadi; amirnili54@gmail.com

This study was undertaken to evaluate the therapeutic potential effect of pentoxifylline (PTX) against arsenic trioxide (ATO)-induced cardiac oxidative damage in mice. Thirty-six male albino mice were divided into six groups and treated intraperitoneally with normal saline (group 1), ATO (5 mg/kg; group 2), PTX (100 mg/kg; group 3), and different doses of PTX (25, 50, and 100 mg/kg; groups 4, 5, and 6, respectively) with ATO. After four weeks, the blood sample was collected for biochemical experiments. In addition, cardiac tissue was removed for assessment of oxidative stress markers and histopathological changes (such as hemorrhage, necrosis, infiltration of inflammatory cells, and myocardial degeneration). The findings showed that ATO caused a significant raise in serum biochemical markers such as lactate dehydrogenase (LDH), creatine phosphokinase (CPK) and troponin-I (cTnI), glucose, total cholesterol (TC), and triglyceride (TG) levels. In addition to histopathological changes in cardiac tissue, ATO led to the significant increase in cardiac lipid peroxidation (LPO) and nitric oxide (NO); remarkable decrease in the activity of cardiac antioxidant enzymes such as catalase (CAT), superoxide dismutase (SOD), and glutathione peroxidase (GPx); and the depletion of the total antioxidant capacity (TAC) and total thiol groups (TTGs). PTX was able to reduce the increased levels of serum cardiac markers (LDH, CPK, cTnI, TC, and TG), cardiac LPO, and improve antioxidant markers (TAC, TTGs, CAT, SOD, and GPx) alongside histopathologic changes. However, no significant changes were observed in elevated serum glucose and cardiac NO levels. In conclusion, the current study showed the potential therapeutic effect of PTX in the prevention of ATO-induced cardiotoxicity via reversing the oxidative stress.

1. Introduction

Arsenic is an environmental contaminant that is widely widespread in water, soil, and air due to its industrial and agricultural applications [1]. The epidemiologic evidence showed that high-chronic arsenic exposure has been associated with hepatorenal failure and cardiovascular disorders [2–4]. However, arsenic compounds have been used to treat various diseases from the past to the present [5].

Arsenic trioxide (ATO) is an effective chemotherapeutic drug used in the treatment of acute promyelocytic leukemia (APL), but its usage has been limited because of cardiovascular side effects, such as ventricular tachycardia, QT prolongation, torsade de pointes, and sudden cardiac death [6, 7]. These side effects can be caused through mitochondrial dysfunction and excess generation of reactive oxygen species (ROS) [8], functional changes of ion channels, and disrupted balance of intracellular and extracellular ions [9].

Phosphodiesterase inhibitors block one or more subtypes of the phosphodiesterase enzymes (PDEs), thereby preventing the inactivation of the cAMP and/or cGMP in various cells. In recent years, the antioxidant and anti-inflammatory

properties of phosphodiesterase inhibitors have been considered in several studies [10–12]. For instance, Mohammadi et al. (2011) showed that selective phosphodiesterase inhibitors could increase survival of Langerhans islets by preventing free radical formation [13]. Moreover, sildenafil, as phosphodiesterase 5-selective inhibitor, can have beneficial role in improvement of toxicities caused via cadmium [14] and lead acetate [15].

Pentoxifylline (PTX), as a methyl xanthine derivative and nonselective PDE, is commonly used to treat intermittent claudication and peripheral vascular diseases, reducing platelet aggregation and improving red blood cell deformability [16]. Recent evidence showed that PTX inhibits ROS generation and improves capillary circulation and tissue oxygenation in various organs. For instance, Yao et al. (2016) showed that PTX could prevent intermittent hypobaric hypoxia induced-oxidative stress in testicular tissue by maintaining redox homeostasis [17]. Zhang et al. (2005) reported that PTX might be beneficial in reducing hydrogen peroxide induced embryo injury and improve in vitro fertilization (IVF) outcome [18]. Additionally, the findings of Egin et al. (2016) indicate the effective effects of PTX on oxidative stress reduction in the abdominal compartment syndrome animal model [19].

Despite the antioxidant properties of PTX, there is no evidence of the therapeutic potential of this drug on ATO-induced cardiotoxicity. Therefore, the current study was designed to assess the PTX effects on the oxidative damage induced by ATO in the heart tissue of mice.

2. Materials and Methods

Pentoxifylline, 2,4,6-tripyridyl-s-triazine (TPTZ), 1,1,3,3-tetramethoxypropane, bovine serum albumin (BSA), sulfanilamide, 5,5′dithiobis-2-nitro benzoic acid (DTNB), 2-thiobarbituric acid (TBA), and N-(1-naphthyl) ethylenediamine dihydrochloride were obtained from Sigma-Aldrich Chemical Company (St. Louis, MO, USA). Arsenic trioxide powder was purchased from Merck (Darmstadt, Germany).

2.1. Animals and Experimental Protocol. Thirty-six male albino mice (25 ± 2.5 g) ranging from 1 to 2 months in age were obtained from the animal house of Hamadan University of Medical Sciences (HUMS). The animals were kept in standard cages at suitable temperature ($23 \pm 2°C$), 12/12 h light/-dark cycle, and relative humidity 50% and received a standard diet and water *ad libitum*. The ethical concerns of animals' experiments were considered carefully, and its protocol was approved by the HUMS ethics review board (Ethical code number: IR.UMSHA.REC.1397.463).

In this study, the toxic dose of ATO 5 mg/kg/day was used based on the animal model proposed by Li et al. (2002) [20]. In addition, based on pilot studies, the dosage range of PTX was considered 25-100 mg/kg/day.

Accordingly, the mice were divided randomly into six groups of six each and treated for four consecutive weeks by intraperitoneal (i.p.) injection as follows:

Group 1: the mice received normal saline (control group)
Group 2: the mice received ATO (5 mg/kg/day)
Group 3: the mice received PTX (100 mg/kg/day)
Group 4: the mice received ATO (5 mg/kg/day) + PTX (25 mg/kg/day)
Group 5: the mice received ATO (5 mg/kg/day) + PTX (50 mg/kg/day)
Group 6: the mice received ATO (5 mg/kg/day) + PTX (100 mg/kg/day)

It should be noted that groups 4-6 were treated with different doses of PTX 1 h before ATO administration. In addition, the highest dose of PTX (100 mg/kg) was considered to show its safety in group 3. Twenty-four hours after the completion of treatment, each animal was weighed and anesthetized by ketamine (50 mg/kg) and xylazine (10 mg/kg), and its blood sample was taken through cardiac puncture. Then, blood sample was centrifuged (at 3000 g, 10 min), and its serum was kept at -20°C for the biochemical analysis. Furthermore, the heart was removed for preparation of tissue homogenate (10%, w/v). Briefly, half of the heart tissue was homogenized with phosphate-buffered saline (50 mM, pH 7.3) and centrifuged at 3000 g, 10 min at 4°C. Finally, its supernatant was removed for the biochemical experiments. Another part of tissue was fixed in 10% formaldehyde solution for histopathological analysis.

2.2. Determination of Glucose and Total Triglyceride and Cholesterol. Glucose, total cholesterol, and triglyceride serum levels were determined using commercial kits (Pars Azmoon, Tehran kit, Iran).

2.3. Lactate Dehydrogenase Assay. Lactate dehydrogenase (LDH) activity in serum sample was measured by determining the rate of oxidation of NADH by an enzymatic colorimetric kit (Pars Azmoon Co., Tehran, Iran). The absorbance change per minute was detected at 340 nm using spectrophotometric instrument (Analytik Jena Specord 50 Plus), and its results were expressed as U/L.

2.4. Creatine Phosphokinase Assay. The activity of serum creatine phosphokinase (CPK) was assayed by an enzymatic colorimetric kit (Pars Azmoon Co., Tehran, Iran). Based on the kit's procedure, creatine kinase converts creatine into ADP and phosphocreatine. The absorbance change per minute was detected at 340 nm, and its data were expressed as U/L.

2.5. Troponin-I Assay. Cardiac troponin-I (cTnI) levels in serum samples were assayed by Enzyme Linked-Immuno-Sorbent Assay (ELISA) kit, according to the manufacturer's instructions (Shanghai Crystal Day Biotech Co., LTD, China).

2.6. Lipid Peroxidation Assay. Cardiac lipid peroxidation was measured via the reaction of TBA with active-aldehyde intermediates such as MDA. Briefly, heart homogenate supernatant (100 μl) was mixed with 500 μl reagent containing TBA (0.2%) in H_2SO_4 (0.05 M) and subsequently heated for 30 min at 100°C in boiling water bath [21, 22]. The peak absorbance was detected at 532 nm against different concentration of MDA as the standard, and its results reported as nmol/mg protein.

2.7. Total Antioxidant Capacity Assay. The total antioxidant capacity (TAC) was determined in the heart homogenate supernatant by measuring the reduction of Fe^{3+}-TPTZ complex to the Fe^{2+}-TPTZ by a reductant at low pH [22, 23]. Briefly, a reagent was prepared by mixing 20 mM $FeCl_3$, acetate buffer (300 mM, pH 3.6), and TPTZ (10 mM) in 40 mM HCL, in the ratio 1 : 10 : 1. In the next stage, 20 μl of sample and 200 μl reagent were mixed and incubated for 15 min. The maximum absorbance of Fe^{2+}-TPTZ complex was detected at 593 nm against standard curve. Results were reported as nmol/mg protein.

2.8. Determination of Total Thiol Group (TTGs). Total thiol groups (TTGs) were assayed in heart homogenate supernatant using DTNB reagent [24]. Briefly, 200 μl of Tris-EDTA buffer solution (0.25 M Tris base, 20 mM EDTA, pH 8.2) and 10 μl of sample were mixed together in microplate well, and its initial absorbance was detected at 412 nm. Then, 10 μl of DTNB reagent (10 mmol/l in methanol) was added and incubated at 37°C for 15 min. The final absorbance of each samples (A2) and also DTNB blank (B) was detected again at 412 nm. The thiol contents were calculated by reduced glutathione as standard and presented as nmol/mg protein.

2.9. Nitric Oxide Assay. Nitric oxide (NO) was determined in heart homogenate supernatant by Griess reagent (1% sulfanilamide, 0.1% NED, and 2.5% phosphoric acid) as described by Nili-Ahmadabadi et al. [21]. Briefly, 100 μl of sample and 100 μl reagent were mixed in microplate well and incubated for 15 min at 37°C. The optimum absorbance was detected at 520 nm against different concentration of sodium nitrate solution as the standard. The results reported as nmol/mg protein.

2.10. Catalase Assay. The cardiac catalase (CAT) activity was determined by detecting the rate of decomposition of hydrogen peroxide (H_2O_2) by a UV-Vis spectrophotometric system at 240 nm. CAT activity unit (U/mg protein) was defined as 1 μmol of H_2O_2 disappearance/min/mg protein [25].

2.11. Superoxide Dismutase Assay. The cardiac superoxide dismutase (SOD) activity was determined according to the kit brochure from ZellBio GmbH Company, Germany. In this experiment, SOD activity unit (U/mg protein) was defined as the amount of enzyme that catalyzes decomposition of 1 $\mu mole$ of superoxide radical anions to H_2O_2 and oxygen molecules in one minute.

2.12. Glutathione Peroxidase Assay. The cardiac glutathione peroxidase (GPx) activity was assayed according to the kit brochure from ZellBio GmbH Company, Germany. In this experimentation, GPx activity unit (U/mg protein) was defined as the amount of enzyme that catalyzes the oxidation of 1 $\mu mole$ NADPH per minute.

2.13. Protein Assay. At the end of each experiment, protein level of heart homogenate supernatant was measured by Bradford method that is based on an absorbance shift of the dye Coomassie Brilliant Blue G-250 at 595 nm.

2.14. Histopathological Analysis. The cardiac tissue was fixed in 10% formaldehyde solution at least 24 h before histopathological examination. The paraffin-embedded block was prepared using automatic tissue processor, and then, samples cut into 4-6 μm thick sections by a rotating microtome [26]. After staining cardiac tissue by hematoxylin and eosin (H&E) dye, stained samples were evaluated under light microscope (Olympus CX31 microscope). After examination under screening power (40x), we examined at least 20 LPF (low power field, 100x) of each slide searching for any area of necrosis, hemorrhage, inflammation, and myocardial degeneration. Percent of abnormal findings in each LPF was roughly estimated with eye examination and the final number considered by taking average of results of different fields. The abnormal results were confirmed by HPF (high power field, 400x) examination just in case. It should be noted that the microscopic observations were scored as 0 (0%), 1 (1–25%), 2 (26–50%), 3 (51–75%), and 4 (76–100%) according to the percentage of histopathological changes.

2.15. Statistical Analysis. The data were analyzed by the GraphPad Prism software, version 6.0, and presented as mean ± standard error of the mean (SEM). The statistical differences between values were compared by one-way analysis of variance (ANOVA) followed by Tukey's post hoc test for quantitative variables. The significance degree was set at $P < 0.05$.

3. Results

3.1. Animal Body and Tissue Weight. As shown in Table 1, a significant decrease was observed in weight gain in the ATO group compared to the control group ($P < 0.05$). No significant changes were found in heart weight/body weight index in different groups.

3.2. Serum Levels of Glucose, Total Triglyceride, and Cholesterol. As shown in Figure 1, administration of ATO significantly raised total cholesterol and triglyceride serum levels in comparison to the control group ($P < 0.001$ and $P < 0.001$, respectively). PTX was able to reduce the increased levels of triglyceride at the employed doses of 50 and 100 mg/kg ($P < 0.05$) and total cholesterol serum levels at the doses of 25, 50, and 100 mg/kg ($P < 0.05$, $P < 0.001$, and $P < 0.01$, respectively). No significant changes were observed in the glucose serum level in the treatment groups.

3.3. Serum Levels of Cardiac Markers. As shown in Figure 2, the administration of ATO could remarkably increase cTnI ($P < 0.001$), CPK ($P < 0.001$), and LDH ($P < 0.001$) serum levels in comparison with the control group. PTX administration could decrease the serum levels of LDH and CPK, at the doses of 50 and 100 mg/kg, in mice exposed to ATO. In addition, a significant decrease was found in cTnI levels following treatment with all doses of PTX compared to ATO group.

TABLE 1: Body and heart weight changes in studied groups.

Groups	Initial body weight (g)	Final body weight (g)	Weight gain (g)	Heart weight (g)	Heart weight/final body weight x 100
Control	25.7 ± 1.6	38.1 ± 1.7	12.4 ± 1.2	0.17 ± 0.01	0.45 ± 0.02
ATO (5 mg/kg)	26.1 ± 1.4	31.6 ± 2.1	5.5 ± 1.8[#]	0.15 ± 0.02	0.47 ± 0.05
PTX (100 mg/kg)	24.8 ± 2.1	35.6 ± 2.5	10.8 ± 1.4	0.17 ± 0.01	0.46 ± 0.03
ATO + PTX (25 mg/kg)	26.7 ± 1.6	32.5 ± 1.9	5.8 ± 1.2	0.15 ± 0.02	0.47 ± 0.07
ATO + PTX (50 mg/kg)	24.6 ± 1.3	30.9 ± 1.9	6.3 ± 1.6	0.15 ± 0.01	0.51 ± 0.05
ATO + PTX (100 mg/kg)	27.1 ± 1.7	33.6 ± 2.1	6.5 ± 2.2	0.16 ± 0.01	0.47 ± 0.05

The results are expressed as means ± SEM, $n = 6$ for each group. [#]$P < 0.05$ vs. control group. ATO: arsenic trioxide (equal 5 mg/kg); PTX: pentoxifylline.
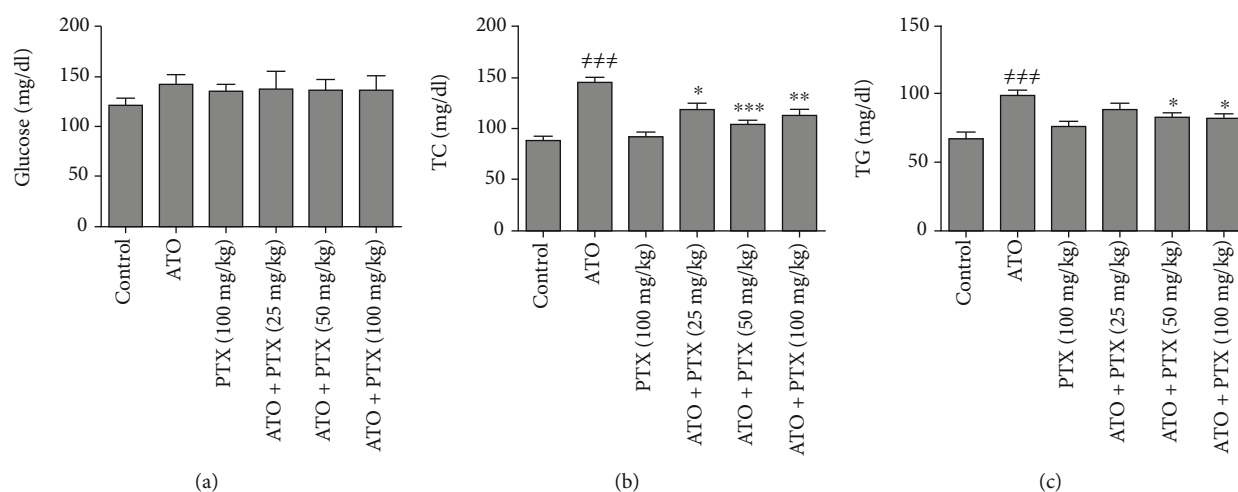

FIGURE 1: Effect of PTX on glucose and lipid serum levels in ATO-exposed mice. Statistical analysis used one-way ANOVA with Tukey's test. The results are expressed as means ± SEM, $n = 6$ for each group. [###]$P < 0.001$ vs. control group; *$P < 0.05$, **$P < 0.01$, and ***$P < 0.001$ vs. ATO group. Glucose (a); TC: total cholesterol (b); TG: total triglyceride (c); ATO: arsenic trioxide (equal 5 mg/kg); PTX: pentoxifylline.

3.4. Cardiac Oxidative Stress Biomarkers. Following ATO administration, the levels of LPO ($P < 0.001$) and NO ($P < 0.01$) were increased, and TAC ($P < 0.001$) as well as TTG ($P < 0.01$) levels were decreased in heart tissues compared to the control group. PTX at dose 100 mg/kg significantly improved TTGs and TAC of heart tissue compared to the ATO group ($P < 0.05$). In addition, PTX could decrease cardiac lipid peroxidation at doses 50 and 100 mg/kg ($P < 0.05$ and $P < 0.01$, respectively). No significant changes were observed in the cardiac NO level in the treatment groups compared to the ATO group (Figure 3).

3.5. Cardiac Antioxidant Enzymes. As shown in Figure 4, the administration of ATO significantly decreased cardiac antioxidant enzymes activity including CAT ($P < 0.01$), SOD ($P < 0.001$), and GPx ($P < 0.01$) in comparison with the control group. PTX at dose 100 mg/kg significantly increased CAT activity of heart tissue compared to the ATO group ($P < 0.05$). In addition, PTX could improve cardiac SOD and GPx activity at doses 50 and 100 mg/kg.

3.6. Histopathological Changes. As summarized in Table 2, coagulative necrosis, infiltration of inflammatory cells, focal hemorrhage, and myocardial degeneration were observed in cardiac tissue of ATO-treated mice. PTX reduced some pathologic changes, such as necrosis and inflammation, in a dose-dependent manner (Figure 5).

4. Discussion

The present study suggests more evidence to support the involvement of oxidative stress in the pathogenesis of ATO-induced cardiotoxicity. Additionally, the results revealed the link between the antioxidant effects of PTX and its therapeutic potential against cardiac oxidative damage induced by the ATO.

Dyslipidemia is one of the most important risk factors in cardiovascular disease that can be characterized by increased triglyceride and/or cholesterol [27]. In this study, ATO-induced hypercholesterolemia may be due to increased β-hydroxy β-methylglutaryl-CoA (HMG-CoA) reductase
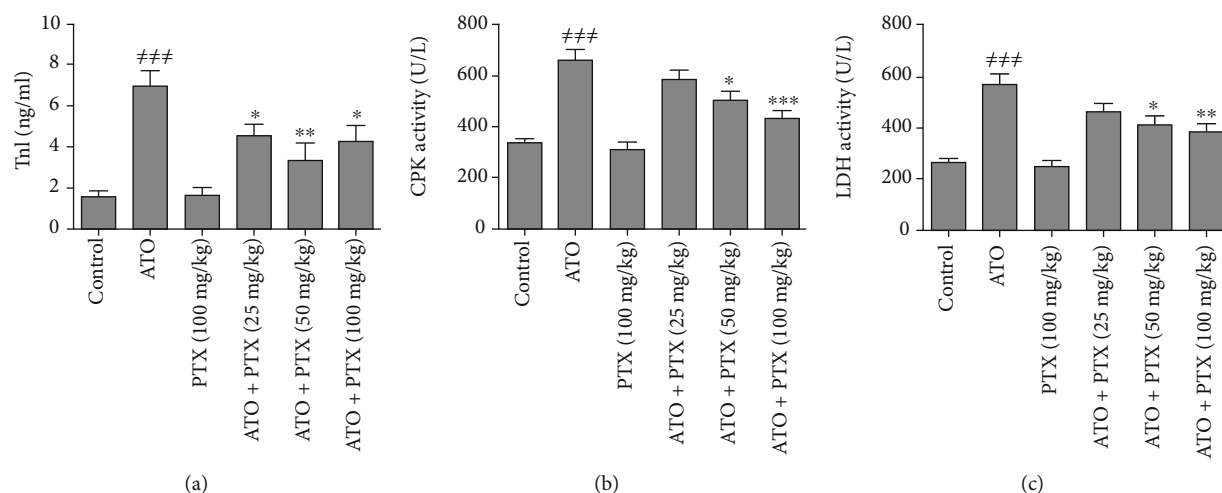
Figure 2: Effect of PTX on serum cardiac markers in ATO-exposed mice. Statistical analysis used one-way ANOVA with Tukey's test. The results are expressed as means ± SEM, $n = 6$ for each group. $^{###}P < 0.001$ vs. control group; $^{*}P < 0.05$, $^{**}P < 0.01$, and $^{***}P < 0.001$ vs. ATO group. TnI: troponin-I (a); CPK: creatine phosphokinase (b); LDH: lactate dehydrogenase (c); ATO: arsenic trioxide (equal 5 mg/kg); PTX: pentoxifylline.

activity, as reported by Afolabi et al. (2015) [28]. In addition, arsenic can inhibit the elimination of cholesterol from the body by inhibiting enzyme of cholesterol 7α-hydroxylase and preventing the biosynthesis of bile acids [28, 29]. There is little evidence regarding the influence of PTX on lipid profile. Previously, Tani et al. have shown that cilostazol, a selective type 3 phosphodiesterase inhibitor, may decrease serum triglycerides and increase HDL cholesterol in diabetic rats by increasing LPL activity. Their findings suggested that raised cAMP stimulates hydrolyzes triglycerides in lipoproteins by the release of lipoprotein lipase (LPL) from adipocytes, which may explain the reduction of serum triglyceride levels [30].

It is documented that increased levels of LDH, CPK, and cTnI in blood serum are considered as reliable diagnostic markers of myocardial toxicity [5, 31]. cTnI is cardiac regulatory protein that controls the calcium-mediated interaction between myosin and actin [32]. This protein is known as the specific and sensitive marker for the diagnosis of myocardial dysfunction [31]. LDH is a cytosolic enzyme, which is existent in various tissues involved in glycolytic pathway [33].

In the current findings, ATO intoxication caused a significant increase in the cTnI, LDH, and CPK serum levels that might due to changes in the plasma membrane integrity of cardiac myocytes and subsequently their leakage into the blood serum [34, 35]. In addition, the previous studies showed that the release of cTnI from myocardial tissue was proportional to the size and extent of tissue damage and systolic dysfunction [36, 37]. Administration of PTX significantly decreased the cTnI, LDH, and CPK serum levels as well as necrosis and inflammation in cardiac tissue towards normal in ATO-treated experimental mice. In agreement with our pathological observations, the decrease in the LDH and CPK serum levels showed a dose-dependent protection. This may be due to the membrane stabilizing effect of PTX on the myocardium, improving the cardiac damage and thereby limiting the leakage of these enzymes from the

myocardial tissue. Improvements of capillary circulation and tissue oxygenation are well-known mechanisms of PTX that may be involved in preventing cardiac oxidative damage caused by ATO.

Oxidative stress (OS) is the consequence of an imbalance between antioxidant systems and reactive oxygen/nitrogen species (ROS/RNS) involved in cellular damage [38]. Manna et al. (2008) and Sun et al. (2016) studies showed that ROS/RNS are generated during inorganic arsenic metabolism in various cells [25, 39]. In this regard, our data revealed heart LPO and NO production were raised in response to ATO while cardiac TTG and TAC levels were reduced, which is in line with Hemmati et al. (2008) and Binu et al. (2017) studies [5, 40]. Overall, LPO is one of the characteristic features of OS related to arsenic toxicity, which is due to oxidative degradation of polyunsaturated acids in the cell membrane [41]. Arsenic increases the amount of free iron by releasing iron from ferritin molecule. Free iron through the Fenton reaction causes excessive production of ROS and subsequent increase in lipid peroxidation [42]. PTX was able to reduce the level of LPO in the heart tissue, which may be related to decrease the ROS generation in cardiac tissue. The part of the antioxidant effects of PTX can be attributed to its effects on reducing the activation of neutrophils, because activated neutrophils can produce superoxide radicals through NADPH oxidase [16]. In addition, PTX, an effective inhibitor of superoxide anion generation, is likely to affect the initiation and/or propagation of LPO [43]. This medicine can reduce the production of hydroxyl and superoxide radicals by inhibiting xanthine oxidase [19].

NO is an important mediator which plays a key role in the regulation of various cells. However, actions of NO are multifaceted, and its excessive production can lead to nitrosative stress [44]. Following administration of ATO, increased NO may be associated with the induction of nitric oxide synthase, which is in agreement with the findings of Kesavan et al. (2014) [45]. The reaction of NO and
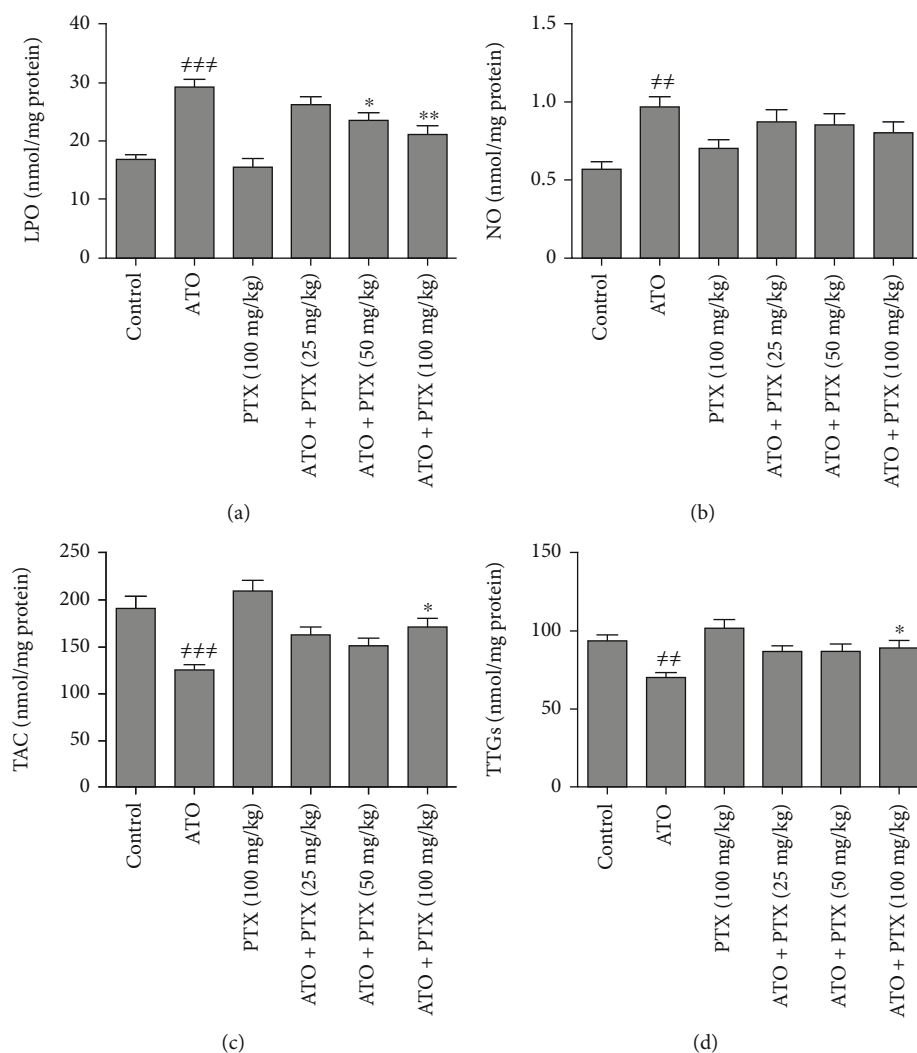
(a)

(b)

(c)

(d)

FIGURE 3: Effect of PTX on cardiac oxidative stress markers in ATO-exposed mice. Statistical analysis used one-way ANOVA with Tukey's test. The results are expressed as means ± SEM, $n = 6$ for each group. $^{\#\#}P < 0.01$ and $^{\#\#\#}P < 0.001$ vs. control group; $^{*}P < 0.05$ and $^{**}P < 0.01$ vs. ATO group. LPO: lipid peroxidation (a); NO: nitric oxide (b); TAC: total antioxidant capacity (c); TTGs: total thiol groups (d); ATO: arsenic trioxide (equal 5 mg/kg); PTX: pentoxifylline.

superoxide anion creates peroxynitrite radicals. These radicals aggravate the cellular damage through lipid peroxidation, necrosis, and apoptosis by nitration of tyrosine residues on tissue proteins [46]. There is different evidence regarding the effects of PTX on NO production. Some of these studies have suggested the inducible effects of PTX, and some have indicated its inhibitory effects on NO production. For instance, Beshay et al. showed that PTX suppress nitric oxide synthase in macrophages and its changes correlated with cellular cAMP levels [47]. In this study, PTX did not show any inhibitory effects on ATO-induced nitrosative stress when the cardiac NO levels were evaluated.

Thiol-based antioxidant system plays the main role of cellular defense against ROS/RNS-mediated oxidative injury [25, 38]. Thiol groups, as a catalyst in disulfide exchange reaction, scavenge the free radicals and detoxifying different xenobiotics and subsequently convert to oxidized form [25]. Our findings showed depletion of thiol-based antioxidant system in myocardium due to ATO toxicity, which is

consistent with other reports [48, 49]. Previously, it has been described that ATO can be bound to the thiol groups and attenuates the cell antioxidant defense [50, 51]. In addition, there has been evidence of the arsenic destructive effects on enzymes affecting the level of the thiol groups, such as glutathione reductase and glutathione-S-transferase [25, 52].

Antioxidant enzymes, such as SOD, CAT, and GPx, are considered to be the first line of cellular defense against the destructive effects of free radicals [53]. Among these, the enzyme of SOD catalytically converts the superoxide radical anions into hydrogen peroxide (H_2O_2) and oxygen molecules while CAT catalyzes the decomposition of H_2O_2 to oxygen and water molecules. GPx can also minimize the destructive effects of H_2O_2 by using thiol molecules such as glutathione, as a reductant [54]. As our findings shown, reduced activity of SOD, CAT, and GPx enzymes can be related to cardiac oxidative damage induced by ATO which is in line with the other reports [25, 55]. Inhibition of SOD activity in ATO-intoxicated mice might be due to the increased generation
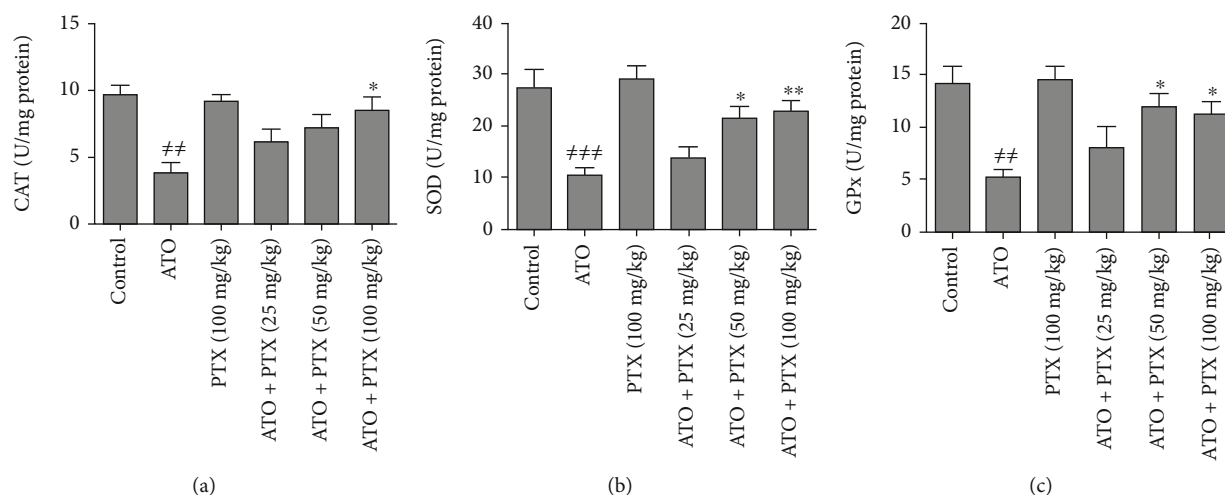
(a)

(b)

(c)

FIGURE 4: Effect of PTX on cardiac antioxidant enzymes in ATO-exposed mice. Statistical analysis used one-way ANOVA with Tukey's test. The results are expressed as means ± SEM, $n = 6$ for each group. $^{##}P < 0.01$ and $^{###}P < 0.001$ vs. control group; $^{*}P < 0.05$ and $^{**}P < 0.01$ vs. ATO group. CAT: catalase (a); SOD: superoxide dismutase (b); GPx: glutathione peroxidase (c); ATO: arsenic trioxide (equal 5 mg/kg); PTX: pentoxifylline.

TABLE 2: Histopathological alterations of cardiac tissue in experimental groups.

Groups	Coagulative necrosis	Infiltration of inflammatory cells	Focal hemorrhage	Myocardial degeneration
Control	0 ± 0	0 ± 0	0 ± 0	0 ± 0
ATO (5 mg/kg)	$1.78 \pm 0.21^{###}$	$2.96 \pm 0.33^{###}$	$2.53 \pm 0.27^{###}$	$2.21 \pm 0.14^{###}$
PTX (100 mg/kg)	0 ± 0	0 ± 0	0 ± 0	0 ± 0
ATO + PTX (25 mg/kg)	1.63 ± 0.18	2.91 ± 0.46	2.1 ± 0.37	1.70 ± 0.36
ATO + PTX (50 mg/kg)	$1.01 \pm 0.14^{*}$	1.94 ± 0.29	$1.20 \pm 0.42^{*}$	1.29 ± 0.40
ATO + PTX (100 mg/kg)	$0.81 \pm 0.31^{**}$	$1.42 \pm 0.18^{**}$	$1.41 \pm 0.12^{*}$	1.47 ± 0.23

The results are expressed as means ± SEM, $n = 6$ for each group. $^{###}P < 0.001$ vs. control group; $^{*}P < 0.05$ and $^{**}P < 0.01$ vs. ATO group. Statistical analysis used one-way ANOVA with Tukey's test. The microscopic observations were scored as 0 (0%), 1 (1–25%), 2 (26–50%), 3 (51–75%), and 4 (76–100%) according to the percentage of histopathological changes. ATO: arsenic trioxide (equal 5 mg/kg); PTX: pentoxifylline.
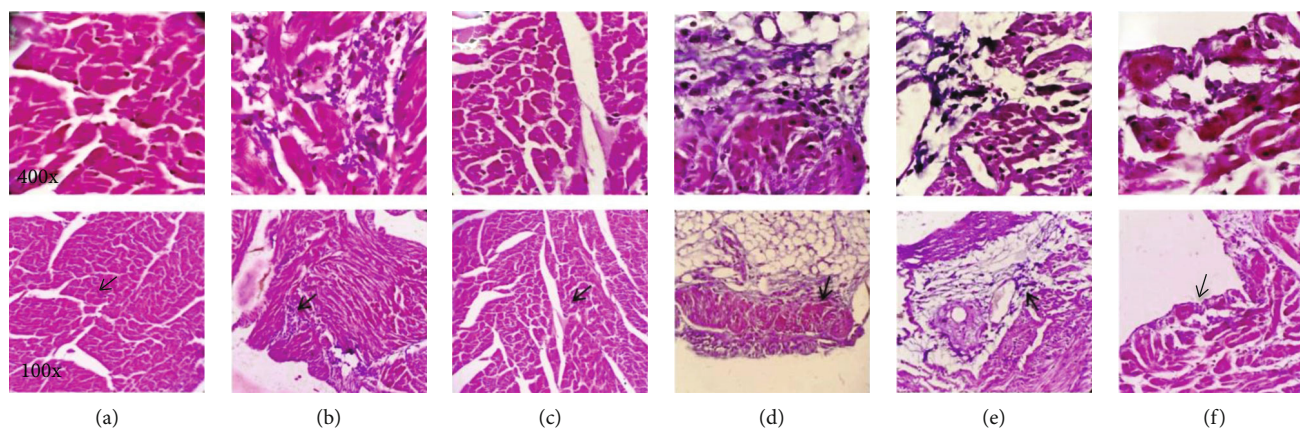

(a)

(b)

(c)

(d)

(e)

(f)

FIGURE 5: Photomicrographs of cardiac tissue in different groups: (a) control group; (b) ATO; (c) PTX (100 mg/kg); (d) ATO + PTX (25 mg/kg); (e) ATO + PTX (50 mg/kg); (f) ATO + PTX (100 mg/kg). The samples were dyed by hematoxylin and eosin. Original magnification of upper row photomicrographs is 400x and lower row photomicrographs 100x. Cardiac tissue samples of the control and PTX groups (a, c) did not show pathologic alterations, and normal myocytes with clear nuclei were observed. Coagulative necrosis and inflammation were detected in the cardiac samples of the ATO-exposed mice (b). In the treatment groups (d–f), some pathologic alterations, such as coagulative necrosis and inflammation, were decreased in a dose-dependent manner. ATO: arsenic trioxide (equal 5 mg/kg); PTX: pentoxifylline.

of superoxide anions [56]. In addition, NADH coenzyme is vital to activate CAT from its inactivated form; inadequate supply of this coenzyme during ATO metabolism may be due to reason for decrease of CAT activity [57].

PTX noticeably increased SOD, CAT, and GPx activity, which may be associated with inhibition of superoxide anion generation and subsequently improvement of oxidant/antioxidant status in cardiac tissue of ATO-intoxicated mice.

Our findings show that PTX is able to increase the level of TTGs in cardiac tissue, which may be associated with increased production of active thiols such as glutathione. In this regard, Duranti et al. suggest that some of the phosphodiesterase inhibitors, such as tadalafil, may increase glutathione levels by increasing the activity of the enzyme glutathione peroxidase [58]. In addition, PTX-induced cAMP levels may induce glutathione-S-transferase expression and activity via the protein kinase A pathway, which may regulate detoxification of arsenic [59].

In conclusion, our findings indicated that PTX, especially at the dose of 100 mg/kg, was effective in improving ATO-induced dyslipidemia and cardiotoxicity. PTX could increase endogenous antioxidant defense, especially thiol-based antioxidant system, against oxidative destruction to protect heart tissue. In addition, improving oxidative/antioxidant balance in heart tissue following PTX administration could be an important cause of reducing ATO-induced pathogenic changes such as coagulative necrosis and inflammation. Therefore, this drug might be a suitable candidate to prevent cardiac complications caused by ATO in APL patients. However, these evidences need further studies.

Data Availability

The authors confirm that the data supporting the findings of this study are available within the article.

Conflicts of Interest

The authors declare that there is no conflict of interest.

Acknowledgments

References

[1] Y. Zhou, L. Niu, K. Liu, S. Yin, and W. Liu, "Arsenic in agricultural soils across China: distribution pattern, accumulation trend, influencing factors, and risk assessment," *Science of The Total Environment*, vol. 616-617, pp. 156–163, 2018.

[2] N. Das, S. Paul, D. Chatterjee et al., "Arsenic exposure through drinking water increases the risk of liver and cardiovascular diseases in the population of West Bengal, India," *BMC Public Health*, vol. 12, no. 1, 2012.

[3] L. Y. Zheng, J. G. Umans, F. Yeh et al., "The association of urine arsenic with prevalent and incident chronic kidney disease: evidence from the Strong Heart Study," *Epidemiology*, vol. 26, no. 4, pp. 601–612, 2015.

[4] C. L. Tsinovoi, P. Xun, L. A. McClure et al., "Arsenic exposure in relation to ischemic stroke: the Reasons for Geographic and Racial Differences in Stroke study," *Stroke*, vol. 49, no. 1, pp. 19–26, 2018.

[5] A. Hemmati, S. Olapour, H. N. Varzi et al., "Ellagic acid protects against arsenic trioxide–induced cardiotoxicity in rat," *Human & Experimental Toxicolog*, vol. 37, no. 4, pp. 412–419, 2018.

[6] Y. Sun, L. Wang, Y. Que, H. Zhu, X. Yang, and D. Li, "Ventricular repolarization dynamics in arsenic trioxide treatment of acute promyelocytic leukemia," *International Journal of Cardiology*, vol. 306, pp. 163–167, 2020.

[7] V. P. Vineetha and K. G. Raghu, "An overview on arsenic trioxide-induced cardiotoxicity," *Cardiovascular Toxicology*, vol. 19, no. 2, pp. 105–119, 2019.

[8] R. C. Vineetha, P. Binu, P. Arathi, and R. H. Nair, "L-ascorbic acid and α-tocopherol attenuate arsenic trioxide-induced toxicity in H9c2 cardiomyocytes by the activation of Nrf2 and Bcl2 transcription factors," *Toxicology Mechanisms and Methods*, vol. 28, no. 5, pp. 353–360, 2018.

[9] H. Haybar, S. Shahrabi, H. Rezaeeyan, H. Jodat, and N. Saki, "Strategies to inhibit arsenic trioxide-induced cardiotoxicity in acute promyelocytic leukemia," *Journal of Cellular Physiology*, vol. 234, no. 9, pp. 14500–14506, 2019.

[10] G. Hepgül, S. Tanrıkulu, H. R. Ünalp et al., "Preventive effect of pentoxifylline on acute radiation damage via antioxidant and anti-inflammatory pathways," *Digestive Diseases and Sciences*, vol. 55, no. 3, pp. 617–625, 2010.

[11] R. Khakhariya, S. Rathod, H. Gandhi et al., "Carboplatin-induced Fanconi-like syndrome in rats: amelioration by pentoxifylline," *Environmental Toxicology and Pharmacology*, vol. 37, no. 1, pp. 185–194, 2014.

[12] F. Mayyas, K. H. Alzoubi, and Z. Al-Taleb, "An evaluation of the effect of pentoxifylline on blood pressure and myocardial oxidative status following intake of western diet," *Clinical and Experimental Hypertension*, vol. 37, no. 8, pp. 666–673, 2015.

[13] M. Mohammadi, S. Atashpour, N. Pourkhalil et al., "Comparative improvement in function of isolated rat Langerhans islets by various phosphodiesterase 3, 4 and 5 inhibitors," *Asian Journal of Animal and Veterinary*, vol. 6, no. 12, pp. 1233–1240, 2011.

[14] A. H. BARAN, A. BERK, M. B. KAYMAZ, and G. AKTAY, "Antioxidant effect of sildenafil on cadmium-induced liver, lung and kidney injury," *The FABAD Journal of Pharmaceutical Sciences*, vol. 45, no. 1, pp. 37–44, 2020.

[15] R. Aghababaeian, M. Ghazi-Khansari, K. Abdi, F. Taghadosinejad, and M. Abdollahi, "Protective effects of sildenafil and dipyridamol from lead-induced lipid peroxidation in perfused rat liver," *International Journal of Pharmacology*, vol. 1, no. 2, pp. 157–160, 2005.

[16] M. F. McCarty, J. H. O'Keefe, and J. J. DiNicolantonio, "Pentoxifylline for vascular health: a brief review of the literature," *Open Heart*, vol. 3, no. 1, p. e000365, 2016.

[17] C. Yao, G. Li, Y. Qian et al., "Protection of pentoxifylline against testis injury induced by intermittent hypobaric hypoxia," *Oxidative Medicine and Cellular Longevityv*, vol. 2016, pp. 1–9, 2016.

[18] X. Zhang, R. K. Sharma, A. Agarwal, and T. Falcone, "Effect of pentoxifylline in reducing oxidative stress-induced embryotoxicity," *Journal of Assisted Reproduction and Genetic*, vol. 22, no. 11-12, pp. 415–417, 2005.

[19] S. Eğin, K. Açıksarı, G. Ercan et al., "Effects of pentoxifylline on oxidative stress in rats with abdominal compartment syndrome model," *International Journal of Surgery Open*, vol. 5, pp. 5–10, 2016.

[20] Y. Li, X. Sun, L. Wang, Z. Zhou, and Y. J. Kang, "Myocardial toxicity of arsenic trioxide in a mouse model," *Cardiovascular toxicology.*, vol. 2, no. 1, pp. 63–74, 2002.

[21] A. Nili-Ahmadabadi, F. Ali-Heidar, A. Ranjbar et al., "Protective effect of amlodipine on diazinon-induced changes on oxidative/antioxidant balance in rat hippocampus," *Research in Pharmaceutical Sciences*, vol. 13, no. 4, pp. 368–376, 2018.

[22] M. Alvandi, D. Dastan, and A. S. Soleimani, "The role of Allium saralicum extract on prevention of acetaminophen-induced hepatic failure: an experimental study," *Research Journal of Pharmacognosy.*, vol. 7, no. 2, pp. 43–51, 2020.

[23] N. Omidifar, A. Nili-Ahmadabadi, A. Gholami, D. Dastan, D. Ahmadimoghaddam, and H. Nili-Ahmadabadi, "Biochemical and histological evidence on the protective effects of Allium hirtifolium Boiss (Persian shallot) as an herbal supplement in cadmium-induced hepatotoxicity," *Evidence-Based Complementary and Alternative Medicine*, vol. 2020, 8 pages, 2020.

[24] M.-L. Hu, "[41] Measurement of protein thiol groups and glutathione in plasma," in *Methods in Enzymology*, vol. 233, pp. 380–385, Academic Press, 1994.

[25] P. Manna, M. Sinha, and P. C. Sil, "Arsenic-induced oxidative myocardial injury: protective role of arjunolic acid," *Archives of Toxicology*, vol. 82, no. 3, pp. 137–149, 2008.

[26] R. D. Cardiff, C. H. Miller, and R. J. Munn, "Manual hematoxylin and eosin staining of mouse tissue sections," *Cold Spring Harbor Protocols*, vol. 2014, no. 6, 2014.

[27] A. Nili-Ahmadabadi, Z. Akbari, D. Ahmadimoghaddam, and A. Larki-Harchegani, "The role of ghrelin and tumor necrosis factor alpha in diazinon-induced dyslipidemia: insights into energy balance regulation," *Pesticide Biochemistry and Physiology*, vol. 157, pp. 138–142, 2019.

[28] O. K. Afolabi, A. D. Wusu, O. O. Ogunrinola et al., "Arsenic-induced dyslipidemia in male albino rats: comparison between trivalent and pentavalent inorganic arsenic in drinking water," *BMC Pharmacology and Toxicology*, vol. 16, no. 1, p. 15, 2015.

[29] T. Li, M. Matozel, S. Boehme et al., "Overexpression of cholesterol 7α-hydroxylase promotes hepatic bile acid synthesis and secretion and maintains cholesterol homeostasis," *Hepatology*, vol. 53, no. 3, pp. 996–1006, 2011.

[30] T. Tani, K. Uehara, T. Sudo, K. Marukawa, Y. Yasuda, and Y. Kimura, "Cilostazol, a selective type III phosphodiesterase inhibitor, decreases triglyceride and increases HDL cholesterol levels by increasing lipoprotein lipase activity in rats," *Atherosclerosis*, vol. 152, no. 2, pp. 299–305, 2000.

[31] A. Qureshi, Y. Gurbuz, and J. H. Niazi, "Biosensors for cardiac biomarkers detection: a review," *Sensors and Actuators B: Chemical*, vol. 171, pp. 62–76, 2012.

[32] S. Sharma, P. G. Jackson, and J. Makan, "Cardiac troponins," *Journal of clinical pathology*, vol. 57, no. 10, pp. 1025-1026, 2004.

[33] D. H. Priscilla and P. S. M. Prince, "Cardioprotective effect of gallic acid on cardiac troponin-T, cardiac marker enzymes, lipid peroxidation products and antioxidants in experimentally induced myocardial infarction in Wistar rats," *Chemico-Biological Interactions*, vol. 179, no. 2-3, pp. 118–124, 2009.

[34] R. Afroz, E. Tanvir, N. Karim et al., "Sundarban honey confers protection against isoproterenol-induced myocardial infarction in Wistar rats," *BioMed Research International*, vol. 2016, 10 pages, 2016.

[35] Y. Sato, T. Kita, Y. Takatsu, and T. Kimura, "Biochemical markers of myocyte injury in heart failure," *Heart*, vol. 90, no. 10, pp. 1110–1113, 2004.

[36] S. K. Engle, W. H. Jordan, M. L. Pritt et al., "Qualification of cardiac troponin I concentration in mouse serum using isoproterenol and implementation in pharmacology studies to accelerate drug development," *Toxicologic Pathology*, vol. 37, no. 5, pp. 617–628, 2009.

[37] M. Adamcová, T. Šimůnek, H. Kaiserová et al., "In vitro and in vivo examination of cardiac troponins as biochemical markers of drug-induced cardiotoxicity," *Toxicology*, vol. 237, no. 1-3, pp. 218–228, 2007.

[38] H. Zeinvand-Lorestani, A. Nili-Ahmadabadi, F. Balak, G. Hasanzadeh, and O. Sabzevari, "Protective role of thymoquinone against paraquat-induced hepatotoxicity in mice," *Pesticide Biochemistry and Physiology*, vol. 148, pp. 16–21, 2018.

[39] T.-L. Sun, Z. Liu, Z.-J. Qi, Y.-P. Huang, X.-Q. Gao, and Y.-Y. Zhang, "(-)-Epigallocatechin-3-gallate (EGCG) attenuates arsenic-induced cardiotoxicity in rats," *Food and Chemical Toxicology*, vol. 93, pp. 102–110, 2016.

[40] P. Binu, N. Priya, S. Abhilash, R. C. Vineetha, and R. H. Nair, "Studies on curative efficacy of monoterpene eugenol on anti-leukemic drug arsenic trioxide induced cardiotoxicity," *Biomedicine & Pharmacotherapy*, vol. 91, pp. 559–566, 2017.

[41] I. Kucukkurt, S. Ince, H. H. Demirel, R. Turkmen, E. Akbel, and Y. Celik, "The effects of boron on arsenic-induced lipid peroxidation and antioxidant status in male and female rats," *Journal of Biochemical and Molecular Toxicology*, vol. 29, no. 12, pp. 564–571, 2015.

[42] V. Mathews, M. Paul, M. Abhilash, A. Manju, S. Abhilash, and R. H. Nair, "Myocardial toxicity of acute promyelocytic leukaemia drug-arsenic trioxide," *European Review for Medical and Pharmacological Sciences*, vol. 17, Supplement 1, pp. S34–SS8, 2013.

[43] M. Gavella and V. Lipovac, "Effect of pentoxifylline on experimentally induced lipid peroxidation in human spermatozoa," *International Journal of Andrology*, vol. 17, no. 6, pp. 308–313, 1994.

[44] M. Neri, I. Riezzo, C. Pomara, S. Schiavone, and E. Turillazzi, "Oxidative-nitrosative stress and myocardial dysfunctions in sepsis: evidence from the literature and postmortem observations," *Mediators of Inflammation*, vol. 2016, 12 pages, 2016.

[45] M. Kesavan, T. S. Sarath, K. Kannan et al., "Atorvastatin restores arsenic-induced vascular dysfunction in rats: modulation of nitric oxide signaling and inflammatory mediators," *Toxicology and Applied Pharmacology*, vol. 280, no. 1, pp. 107–116, 2014.

[46] S. Bektas, K. Karakaya, M. Can et al., "The effects of tadalafil and pentoxifylline on apoptosis and nitric oxide synthase in liver ischemia/reperfusion injury," *The Kaohsiung Journal of Medical Sciences*, vol. 32, no. 7, pp. 339–347, 2016.

[47] E. Beshay, F. Croze, and G. J. Prud'homme, "The Phosphodiesterase Inhibitors Pentoxifylline and Rolipram Suppress Macrophage Activation and Nitric Oxide Production _in Vitro_ and _in Vivo_," *Clinical Immunology*, vol. 98, no. 2, pp. 272–279, 2001.

[48] M. V. Varghese, M. Abhilash, M. Alex et al., "Attenuation of arsenic trioxide induced cardiotoxicity through flaxseed oil in experimental rats," *Redox Report*, vol. 22, no. 6, pp. 346–352, 2017.

[49] W. Zhang, C. Guo, R. Gao, M. Ge, Y. Zhu, and Z. Zhang, "The protective role of resveratrol against arsenic trioxide-induced cardiotoxicity," *Evidence-Based Complementary and Alternative Medicine*, vol. 2013, 8 pages, 2013.

[50] Y. Shiobara, Y. Ogra, and K. T. Suzuki, "Animal species difference in the uptake of dimethylarsinous acid (DMAIII) by red blood cells," *Chemical Research in Toxicology*, vol. 14, no. 10, pp. 1446–1452, 2001.

[51] S. Hirano, Y. Kobayashi, X. Cui, S. Kanno, T. Hayakawa, and A. Shraim, "The accumulation and toxicity of methylated arsenicals in endothelial cells: important roles of thiol compounds," *Toxicology and Applied Pharmacology*, vol. 198, no. 3, pp. 458–467, 2004.

[52] V. M. Rodríguez, L. del Razo, J. Limón-Pacheco et al., "Glutathione reductase inhibition and methylated arsenic distribution in Cd1 mice brain and liver," *Toxicological Sciences*, vol. 84, no. 1, pp. 157–166, 2005.

[53] O. Ighodaro and O. Akinloye, "First line defence antioxidants-superoxide dismutase (SOD), catalase (CAT) and glutathione peroxidase (GPX): their fundamental role in the entire antioxidant defence grid," *Alexandria Journal of Medicine*, vol. 54, no. 4, pp. 287–293, 2018.

[54] F. Firozian, S. Karami, A. Ranjbar, M. T. Azandaryani, and A. Nili-Ahmadabadi, "Improvement of therapeutic potential _N_ -acetylcysteine in acetaminophen hepatotoxicity by encapsulation in PEGylated nano-niosomes," *Life Sciences*, vol. 255, p. 117832, 2020.

[55] A. K. Das, R. Sahu, T. K. Dua et al., "Arsenic-induced myocardial injury: Protective role of _Corchorus olitorius_ leaves," *Food and Chemical Toxicology*, vol. 48, no. 5, pp. 1210–1217, 2010.

[56] Y. Hu, J. Li, B. Lou et al., "The role of reactive oxygen species in arsenic toxicity," *Biomolecules*, vol. 10, no. 2, p. 240, 2020.

[57] A. K. Das, S. Bag, R. Sahu et al., "Protective effect of Corchorus olitorius leaves on sodium arsenite-induced toxicity in experimental rats," *Food and Chemical Toxicology*, vol. 48, no. 1, pp. 326–335, 2010.

[58] G. Duranti, R. Ceci, P. Sgrò, S. Sabatini, and L. Di Luigi, "Influence of the PDE5 inhibitor tadalafil on redox status and antioxidant defense system in C2C12 skeletal muscle cells," *Cell Stress and Chaperones*, vol. 22, no. 3, pp. 389–396, 2017.

[59] S. Dasari, M. Ganjayi, L. Oruganti, H. Balaji, and B. Meriga, "Glutathione S-transferases detoxify endogenous and exogenous toxic agents-minireview," *Journal of Dairy, Veterinary & Animal Research*, vol. 5, no. 5, p. 00154, 2017.

Research Article

Novel PGC-1α/ATF5 Axis Partly Activates UPRmt and Mediates Cardioprotective Role of Tetrahydrocurcumin in Pathological Cardiac Hypertrophy

Bing Zhang,[1] Yanzhen Tan,[1] Zhengbin Zhang,[2] Pan Feng,[3] Wenyuan Ding,[1] Qian Wang,[4] Hongliang Liang,[1] Weixun Duan,[1] Xiaowu Wang,[1] Shiqiang Yu,[1] Jincheng Liu,[1] Dinghua Yi [ID],[1] Yang Sun [ID],[5] and Wei Yi [ID][1]

[1]Department of Cardiovascular Surgery, Xijing Hospital, The Fourth Military Medical University, 127 Changle West Road, Xi'an, 710032, China
[2]The 309 Hospital of PLA, 17 Heishanhu Street, Beijing 100091, China
[3]Department of Cardiothoracic Surgery, 305 Hospital of PLA, A13 Wenjin Road, Beijing 100017, China
[4]Department of Nutrition, The Fourth Military Medical University, 169 Changle West Road, Xi'an, 710032, China
[5]Department of Geriatrics, Xijing Hospital, The Fourth Military Medical University, 127 Changle West Road, Xi'an, 710032, China

Correspondence should be addressed to Dinghua Yi; yidh@fmmu.edu.cn, Yang Sun; dr_yangsun@163.com, and Wei Yi; yiwei@fmmu.edu.cn

Mitochondrial unfolding protein response (UPRmt) effectively resists the pathological cardiac hypertrophy and improves the mitochondrial function. However, the specific activation mechanism and drugs that can effectively activate UPRmt in the cardiac muscle are yet to be elucidated. The aim of this study was to determine the regulation role of UPRmt on preventing pathological cardiac hypertrophy by tetrahydrocurcumin (THC) and explore its underlying molecular mechanism. Male C57BL/6J wild-type (WT) mice were divided into a control group and subjected to sham treatment for 4 weeks, and a test group which was subjected to transverse aortic constriction (TAC) surgery. Animals in the control and test group were orally administered THC (50 mg/kg) for 4 weeks after TAC procedure; an equivalent amount of saline was orally administered in the control sham-treated group and the TAC group. Subsequently, oxidative stress and UPRmt markers were assessed in these mice, and cardiac hypertrophy, fibrosis, and cardiac function were tested. Small interfering RNA (siRNA) targeting proliferator-activated receptor-gamma coactivator (PGC)-1α and activating transcription factor 5 (ATF5) were used to determine the UPRmt activation mechanism. THC supplement partly upregulated UPRmt effectors and inhibited TAC-induced oxidative stress compared with TAC-operated WT mice, thereby substantially attenuating contractile dysfunction, cardiac hypertrophy, and fibrosis. Furthermore, PGC-1α knockdown blunted the UPRmt activation and the cardioprotective role of THC. The interaction between PGC-1α and ATF5 was tested in neonatal rat cardiac myocytes under normal conditions. The results showed that PGC-1α was an upstream effector of ATF5 and partly activated UPRmt. In vitro, phenylephrine- (PE-) induced cardiomyocyte hypertrophy caused ATF5 upregulating rather than downregulating corresponding to the downregulation of PGC-1α. The PGC-1α/ATF5 axis mediated the UPRmt activation and stress-resistance role of THC in vitro. Collectively, the present study provides the first evidence that PGC-1 and ATF5 can form a signaling axis to partly activate UPRmt that mediates the cardioprotective role of THC in pathological cardiac hypertrophy.

1. Introduction

Pathological cardiac hypertrophy involves a series of gene expression changes, epidermal morphology, and cardiac function produced by hypertrophic factors such as stress load, inflammation, and oxidative stress [1]. Increase of cardiac afterload leads to abnormal expression of cardiac fetal genes, fibrotic reconstruction of extracellular matrix, and contractile dysfunction, ineluctably progressing to the terminal stage-heart failure [2, 3]. Although at present there are many drugs for preventing and treating cardiac hypertrophy, various side effects resulting from different drug reactions, mechanisms, and sources warrant the need for novel safe and effective drugs for prevention and treatment of cardiac hypertrophy [4]. In recent years, some natural substances have gained a lot of attention as potential candidates for anticardiac hypertrophic drugs since they are safe and nontoxic, reduce oxidative stress, and possess strong anti-inflammatory and antiapoptotic properties [5].

Oxidative stress is the result of an imbalance between the production of the reactive oxygen species (ROS) and the body's antioxidant systems. It has been identified as one of the significant contributing factors in the development of cardiac hypertrophy [11]. UPR^{mt} is activated under various conditions of mitochondrial dysfunction such as ROS overproduction and unfolded protein accumulation in mitochondria [12]. UPR^{mt} mainly increases transcription of numerous mitochondrial protective genes including molecular chaperones, proteases, and antioxidant enzymes located primarily in the mitochondrial matrix via a mitochondrial-to-nuclear signal transduction pathway [13]. Recently, a research confirmed that myocardial UPR^{mt} was significantly activated in mice with cardiac pressure overload and in patients with aortic stenosis and that the enhanced UPR^{mt} significantly improved mitochondrial function and myocardial contractility [14]. UPR^{mt} is therefore considered to be an important therapeutic target in the treatment of myocardial injury caused by pressure overload. However, the specific activation mechanism and the drugs that can effectively activate UPR^{mt} in the heart still need to be explored.

Studies have shown that THC, the major metabolite of curcumin, exhibits stronger antioxidant activity than curcumin [6]. THC was also found to exert similar cardiac-protective effects as curcumin, including anti-ischemic injury, antihypertensive injury, and antivascular injury, exerting effects against oxidative stress by enhancing activities of key endogenous antioxidant enzymes [7–9]. Moreover, a recent study reported that in rats with chronic kidney disease, THC protects against concurrent cardiac hypertrophy [10]. However, the role and mechanism of action of THC in pressure-overload cardiac hypertrophy remains unclear.

This study showed that PGC-1α acts as the upstream activating molecule of ATF5 and partly upregulates downstream UPR^{mt} effectors. PGC-1α/ATF5/UPR^{mt} also mediates the protective role of THC against pathological cardiac hypertrophy and oxidative stress induced by pressure overload in vivo and by PE treatment in vitro. This study established a new regulatory mechanism of UPR^{mt} activation via the PGC-1α/ATF5 axis and confirmed its role in mediating the pharmacological function of THC.

2. Methods

2.1. Experimental Animals.
The subjects in this study were mice which were raised and used in experiments in accordance with the Guide for the Care and Use of Laboratory Animals of the Chinese Animal Welfare Committee, and the protocol has been approved by the Fourth Military Medical University Committee on Animal Care. WT male C57BL/6 mice (20–25 g, 8–10-week-old) were obtained from the Experimental Animal Center of the Fourth Military Medical University, Xi'an, Shaanxi, China, and were housed in cages (10-12 animals/cage) under a 12 : 12-h light/dark cycle (lights on 06 : 00) at 22–24°C, and had access to a regular ad libitum pellet diet.

2.2. Reagents.
THC was purchased from Maya reagent co., ltd, Jiaxing, Zhejiang, China. The fluorescent probe $2',7'$-dichlorofluorescein diacetate (DCFH-DA) for assessing intracellular ROS production was purchased from the Beyotime Institute of Biotechnology (Shanghai, China). Dihydroethidium (DHE, for assessing ROS production in cardiac tissues) and the Lipofectamine® 3000 transfection reagent were purchased from Invitrogen (Carlsbad, CA, USA). Kits for detecting superoxide dismutase (SOD) activities and malondialdehyde (MDA) content were purchased from the Institute of Nanjing Jiancheng Bio-Engineering Institute (Nanjing, Jiangsu, China). While primary antibodies against transforming growth factor beta-1 (TGF)-β1, alpha-smooth muscle actin (α-SMA), atrial natriuretic peptide (ANP), NADPH oxidase 4 (NOX 4), and ATF5 were obtained from Abcam (Cambridge, MA, USA), primary antibody against α-actinin was obtained from Sigma (St. Louis, MO, USA), and those against myosin heavy chain beta (β-MHC), gp91 phox, and PGC-1α were purchased from Santa Cruz Biotechnology (Santa Cruz, CA, China). Primary antibodies against C/EBP homologous protein (CHOP) and ATF4 were purchased from Cell Signaling Technology (Boston, MA, USA) and that against glyceraldehyde 3-phosphate dehydrogenase (GAPDH) was obtained from cmcTAG (Milwaukee, WI, USA). The rabbit anti-goat, goat anti-rabbit, and goat anti-mouse secondary antibodies were purchased from the Zhongshan Company (Beijing, China). PGC-1α siRNA and ATF5 siRNA were purchased from the GenePharma Company (Shanghai, China). Trizol reagent and RNA extraction kit was purchased from TIANGEN (Beijing, China). The primers used in this study were synthesized by GenScript Biotech Corp. (Nanjing, China). Bicinchoninic acid assay was purchased from Solarbio co, LTD (Shanghai, China). ECL reagent was purchased from Millipore (Billerica, MA, USA).

2.3. In Vivo Experimental Design and Treatment.
Experiment 1 was designed to investigate the influence of THC administration in alleviating the development of cardiac remodeling and oxidative stress induced by TAC. This experiment comprised of mice randomly selected and categorized into four

groups as follows: 15 WT mice formed the sham+vehicle group, which underwent a sham operation and were intragastrically administered with the vehicle (polyethylene glycol) for 4 weeks; 15 WT mice formed the SHAM+THC group, which underwent a sham operation and were intragastrically administered with THC (50 mg/kg/d) for 4 weeks; 15 WT mice formed the TAC+vehicle group, which underwent the TAC operation and were intragastrically administered with the vehicle (polyethylene glycol) for 4 weeks; and 15 WT mice formed the TAC+THC group, which underwent the TAC operation and were intragastrically administered with a previously tried dose of THC (50 mg/kg/d) [15] for 4 weeks.

Experiment 2 was designed to determine the effect PGC-1α exerted in the cardioprotective role of THC. Thirty WT mice were selected for intramyocardial injection of lentivirus (LV)-scrambled siRNA, while thirty WT mice were given intramyocardial injection of LV-PGC-1α siRNA. Two weeks later, all the 60 mice belonging to the two groups underwent TAC surgery, following which 15 mice from each group were randomly selected to receive intragastric administration of the vehicle, while the remaining mice were intragastrically administered with THC (50 mg/kg/d) for 4 weeks.

2.3.1. Preparation and Intramyocardial Injection of the LV-PGC-1α siRNA. Thirty mice were subjected to an intramyocardial injection of 1×10^9 lentiviral genome particles carrying siRNA against PGC-1α (GenePharma Company, Shanghai, China) as mentioned in Section 2.3. Intramyocardial injection of the LV-PGC-1α siRNA was administered to the mice as follows [16]: the mice were anesthetized, and the heart was exposed through an oblique incision approximately 0.5 cm long between the fourth and fifth costal margin on the left side of the sternum. The lentivirus injection (injection volume of 25 μl) was administered in the front, side, and back of the left ventricle. Sham and TAC surgeries were performed 2 weeks later.

2.3.2. TAC. TAC surgery was performed to establish cardiac hypertrophy in the murine model as previously described [17]. Briefly, mice were anesthetized in an induction chamber with 2% isoflurane mixed with pure oxygen (0.5–1.0 l/min), following which mice were intubated endotracheally and put on ventilator (Minivent Type 845, Hugo Sachs Electronic, March, Germany, 100–120/min 0.15-ml tidal volume). Median thoracotomy was performed to expose the aortic arch, which was then constricted using a 7-0 silk suture ligature tied firmly with a 27-gauge needle between the carotid arteries. The needle was immediately removed, and the chest was closed and sutured. Sham-operated mice underwent the same surgical procedure except for the ligation of the aortic arch. After TAC, the mice were kept warm at a constant temperature on a 38°C and carefully observed until free to move.

2.4. Neonatal Rat Cardiomyocytes (NRCMs) Culture and Treatment. Newborn Sprague Dawley (SD) rats were obtained from the Experimental Animal Center of the Fourth Military Medical University, Xi'an, Shaanxi, China. Isolation and culture of NRCMs were performed as described previously [18]. The heart was harvested from newborn SD rats and cut up into small fragments. The tissue fragments were digested in phosphate-buffered saline (PBS) solution containing 1% collagenase-I (Sigma V900891; Sigma-Aldrich, St. Louis, MO, USA). NRCMs were plated at a density of 5 $\times 10^5$ cells per ml and were cultured in the serum-containing culture medium [DME/F-12 (Gibco, Carlsbad, CA, USA), 10% new bovine serum (Gibco, Carlsbad, CA, USA), penicillin (100 U/ml), streptomycin (100 U/ml), and bromodeoxyuridine (BrdU) (0.1 mM; to inhibit fibroblast proliferation)] for 48 hours at 37°C with 5% CO2. Next, the NRCMs were incubated with PE at a concentration of 50 μM for 24 h to induce cardiomyocyte hypertrophy [19]. Successful induction of hypertrophy was determined by the increased cell surface area (as seen by α-actinin staining) and expression levels of hypertrophic markers (β-MHC and ANP). NRCMs were infected by adenovirus (Ad)- PGC-1α or Ad-Gfp for 4 h to assess PGC-1α overexpression at a multiplicity of infection (MOI) of 60 (virus dose was 3×10^7 pfu/ml). NRCMs were transfected with PGC-1α siRNA or ATF5 siRNA using Lipofectamine 3000 (Thermo Fisher Scientific, San Jose, California, USA) to assess the effect of PGC-1α or ATF5 knockdown [18]. Twenty-four hours later, the cells were treated with PE in the presence or absence of THC (5 μM) for 24 hours [20]. The efficiency of knockdown was confirmed by western blot.

2.5. Echocardiography. The ultrasound technicians were not informed of the protocol of the study and the details of the animal groups to ensure unbiased reporting. Transthoracic ultrasonography was performed using a VisualSonics 770 echocardiograph (VisualSonics 770, Toronto, ON, Canada), and a 30-MHz transducer was used to record the views in both parasternal long-axis and short-axis of the left ventricle. The indexes that can be detected through echocardiography include ejection fractions (EF)% and fraction shortening (FS)% (indicating the cardiac function), interventricular septal thickness at end diastole (IVSd), and left ventricular posterior wall thickness at end diastole (LVPWd) (indicating the thickness of ventricular wall). The above parameters were calculated by the Vevo Lab 3.1.0 software (FUJIFILM VisualSonics, Inc. Toronto, ON, Canada).

2.6. ROS Detection. Four weeks after the sham or TAC surgery, seven mice from each group were weighed and anesthetized as mentioned in Section 2.3.2. The mice were then euthanized via carotid artery bleeding. The sternum was cut open, and the heart was exposed, following which the inferior vena cava was cut off and the aorta was occluded. The heart was perfused with PBS to flush the blood out of the heart through aortic root twice and then perfusion-fixed with 4% paraformaldehyde, 5% sucrose, and 20 mM EDTA (pH 7.4) for 10 min. The heart was then harvested, embedded in optimal-cutting-temperature (OCT) compound, immediately frozen in liquid nitrogen, and then stored at -80°C. 5-μm-thick sections were cut and then stained with the oxidative fluorescent dye dihydroethidium (DHE; Sigma-Aldrich, MO, USA) according to the manufacturer's instructions.

Cellular ROS production was detected by a staining process involving washing a confocal dish containing NRCMs with serum-free DME/F-12 culture medium 3 times after treatment. The confocal dish was then stained with dichloro-dihydro-fluorescein diacetate (DCFH-DA) which is deesterified intracellularly and is converted to the highly fluorescent molecule $2',7'$-dichlorofluorescein (DCF) in the presence of ROS. Cellular ROS production was detected by determining the fluorescence intensity at an excitation wavelength of 488 nm and an emission wavelength of 525 nm [21].

2.7. Histological Analysis. The other sections of each heart tissue were stained with hematoxylin-eosin (HE) or Masson trichrome to evaluate the cross-sectional area of cardiomyocytes and collagen deposition, respectively, as described previously [18]. The sections were visualized using a digital scanning imaging system Olympus FV1000 (Olympus, Tokyo, Japan), and the cross-sectional area of the cardiomyocytes and the degree of fibrosis were quantified using the Image J software (NIH, Bethesda, MD, USA).

2.8. Determination of MDA Content and SOD Activity. The oxidative stress markers, MDA content, and SOD activity in the heart tissues were detected using purchased MDA and SOD kits using the detection steps based on the manufacturer's instructions. The data were analyzed using spectrophotometry via a SpectraMax M5 device (Molecular Devices, Washington D.C., USA).

2.9. Immunofluorescence Staining. Immunofluorescence staining was performed to detect the surface area and PGC-1α expression of cardiac myocytes. A NRCMs covered confocal dish was washed with PBS after treatment and then fixed with 4% paraformaldehyde at 4°C for 30 min. The cells were then treated with 0.05% Triton X-100 for permeabilization, and NRCMs were incubated with 1% bovine serum albumin. The NRCMs were then incubated with α-actinin or PGC-1α at 4°C for 12 h followed by incubation with a Cy3-conjugated goat anti-mouse or F488-conjugated goat anti-rabbit secondary antibody at 37°C for 2 h resulting in $4',6$-diamidino-2-phenylindole (DAPI) stained nuclei. The cells were then observed under a confocal microscope. At least 40 cells in the confocal dishes from each group stained with α-actinin and 5 fields of confocal dishes stained with PGC-1α were visualized randomly using an Olympus FV10C-W3 laser confocal microscope (Olympus, Japan). The Image J software (NIH) was used to calculate the cardiomyocyte surface area and immunofluorescence intensity.

2.10. Quantitative Real-Time PCR. Four weeks after the sham or TAC surgery, eight mice from each group were weighed and euthanized via carotid artery bleeding as described in Section 2.6. The heart tissues were harvested and flushed with PBS; heart weight was then recorded, and the heart weight/body weight (HW/BW) ratio was then calculated. A small piece of tissue was cut from the left ventricle and placed into a tube containing Trizol reagent. The total RNA was extracted from the specimen (or the cultured NRCMs after treatment) following the instructions of the RNA extraction kit. The RNA was then reverse-transcribed into complementary DNA using a SuperScript first-strand synthesis system (Invitrogen, CA, USA). Reverse transcriptase (RT-PCR) was performed with the CFX96 real-time PCR system-C1000 Thermal Cycler (Bio-Rad Laboratories, Hercules, CA, USA). *GAPDH* served as the standard gene for the normalization of transcription levels of target genes. The sequences of primers used in this study are listed in supplementary materials Table S1.

2.11. Western Blotting. Total proteins were extracted from the left ventricle of the heart and cultured NRCMs after treatment using RIPA lysis buffer. Concentration of the protein sample was detected by using bicinchoninic acid assay (BCA). The extracted and quantified proteins were separated by 10% sodium dodecyl sulfate-polyacrylamide gel electrophoresis (SDS-PAGE) and transferred to the polyvinylidene difluoride (PVDF) membranes (Millipore, Billerica, MA, USA). The membranes were blocked with 5% skimmed milk powder dissolved in Tris-buffered saline (TBST) buffer [150 mM NaCl, 50 mM Tris (pH 7.5), and 0.1% Tween-20) for 2–3 h at 20–25°C. Subsequently, the membranes were incubated with the appropriate primary antibodies at 4°C for 12 h. The membranes were proved with the corresponding horseradish peroxidase- (HRP-) conjugated secondary antibodies at 20-25°C for 2 h. The enhanced chemiluminescence (ECL) reagent was added, and the blots were scanned using ChemiDoc™ XRS (Bio-Rad Laboratories, Hercules, CA, USA). The gray value of protein bands was visualized and analyzed using Image Lab 2.0 (Genmall Biotechnology Co., Ltd, Wuhan, China). GAPDH was used as the internal control to normalize the protein expression.

2.12. Statistical Analysis. All data were expressed as the mean ± SEM and processed and analyzed in GraphPad Prism 7.0 (GraphPad Software, In., San Diego, CA, USA). The statistical significance of differences between multiple groups was processed using one-way ANOVA followed by Bonferroni's multiple comparison. In this study, p value less than 0.05 ($p < 0.05$) was considered to be a statistically significant difference.

3. Results

3.1. UPR^{mt} Induced by TAC Was Further Enhanced in THC Treated Mice. The effect of THC on TAC-induced oxidative stress and on UPR^{mt} regulation was evaluated. Four weeks after TAC surgery, the systemic inflammation was obvious, but THC was seen to alleviate this effect, as shown in Figure S1. The protein expressions of NADPH oxidases 2 (gp91 phox) and 4 (NOX 4) were tested, and the results are shown in Figures 1(a)–1(c). TAC operation increased the expression of gp91 phox and NOX 4, while THC treatment significantly attenuated these responses. Furthermore, it was found that THC treatment enhanced the expression of PGC-1α in TAC-operated mice, as shown in Figure 1(d). As classical markers of UPR^{mt}, the expression of ATF5, CHOP, and ATF4 was also seen to be significantly increased after TAC, while THC treatment only further
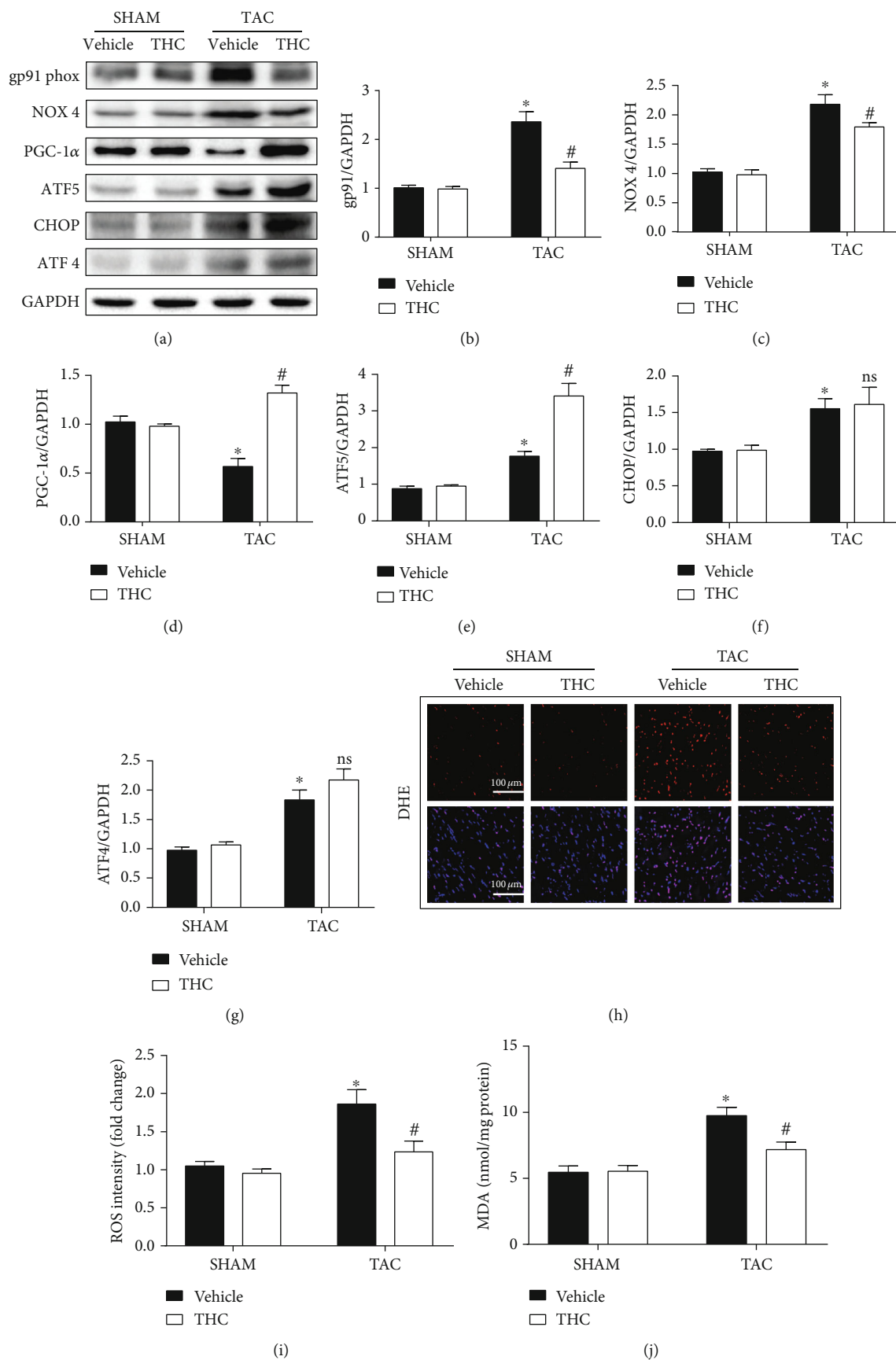
(a)

(b)

(c)

(d)

(e)

(f)

(g)

(h)

(i)
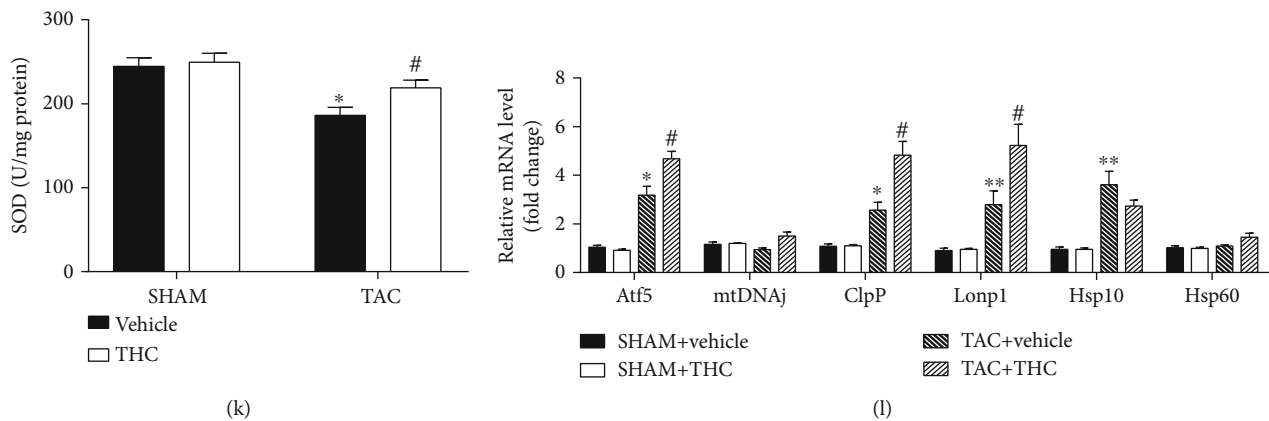
(j)

Figure 1: Continued.

(k)

(l)

FIGURE 1: UPR^{mt} induced by TAC was further enhanced in THC-treated mice. (a) Representative western blot of gp91 phox, NOX 4, PGC-1α, ATF5, CHOP, and ATF4 in murine hearts from indicated groups. (b–g) Quantification of gp91 phox, NOX 4, PGC-1α, ATF5, CHOP, and ATF4 protein expression ($n = 6$ mice per group). (h) Representative images of DHE staining (red) and DAPI (blue). (bar = 100 μm). (i) Statistical diagram of ROS intensity ($n = 6$ mice per group). (j) Statistical diagram of MDA content ($n = 6$ mice per group). (k) Statistical diagram of SOD activity ($n = 6$ mice per group). (l) Real-time PCR analysis of the expression of genes encoding UPR^{mt} markers Atf5, mtDNAj, ClpP, Lonp1, Hsp10, and Hsp60 in each group ($n = 6$ mice per group). The data were analyzed by one-way ANOVA. $^{*}p < 0.05$, $^{**}p < 0.01$ vs. SHAM, $^{#}p < 0.05$ vs. TAC. In the bar graphs, the data are presented as the mean ± SEM.

upregulated ATF5 expression, as shown in Figures 1(a) and 1(e)–1(g). The results of the oxidative stress production caused by ROS and MDA and the antioxidant factor, SOD are shown in Figures 1(h)–1(k). THC treatment alleviated the TAC-induced oxidative stress production (ROS and MDA) and enhanced the antioxidant activity (SOD). The expression of several classic UPR^{mt} effector genes was examined by q-RT-PCR, and the results are shown in Figure 1(l). TAC-induced upregulation of ATF5, Clp proteolytic protein subunit (ClpP), and mitochondrial lon protease homolog (Lonp1) was further enhanced by THC treatment.

3.2. THC Protected against Pathological Cardiac Hypertrophy in Mice after TAC. Four weeks following Sham or TAC surgery, the cardiac hypertrophy model was confirmed by echocardiographic data and histological staining. As shown in Figure 2(a), the heart weight to body weight ratio (HW/BW) was higher in TAC-operated mice than in sham-operated mice, while treatment with THC for 4 weeks decreased the HW/BW. Representative M-mode echocardiographic graphs are shown in Figure 2(b). As shown in Figure 2(c)–2(e), the EF% were seen to decrease, the IVSd and the LVPWd were seen to increase 4 weeks after TAC surgery, while treatment with THC improved the cardiac function and decreased the IVSd and LVPWd. The gross heart and HE stained heart section graphs are shown in Figure 2(f); THC treatment alleviated cardiac hypertrophy and ventricular wall thickening caused by TAC surgery. As shown in Figure 2(g), THC-treated mice showed a decrease of average cross-sectional area after TAC. Further, after 4 weeks of TAC, the gene expression levels for myosin heavy chain α (α-MHC) were significantly downregulated, while that for β-MHC was significantly upregulated in the heart, as shown in Figures 2(h) and 2(i). THC treatment reversed this trend, suggesting a good prognosis. In Figures 2(j) and 2(k), the results showed

that expression of other classic cardiac hypertrophic genes encoding ANP and brain natriuretic peptide (BNP) was also upregulated by TAC, while treatment with THC decreased this response.

Cardiac fibrosis is an important hallmark in myocardial remodeling [22]. This study demonstrated the effect THC exerted on TAC-induced cardiac fibrosis. Masson stained heart section graphs (interstitial and perivascular) are shown in Figure S2(a). As shown in Figure S2(b), the collagen volume in the left ventricle was increased in TAC-operated mice, while THC treatment attenuated the collagen deposition. The protein expression of transforming growth factor-beta 1 (TGF-β1) and α-SMA was seen to increase 4 weeks after TAC, while THC treatment decreased the expression of TGF-β1 and α-SMA, as shown in Figure S2(c)-(e). Expression levels of several other fibrotic genes were evaluated by QT-PCR, and the results were shown in Figure S2(f)-(h). TAC-induced upregulation of connective tissue growth factor (CTGF), collagen-1 (Col-1), and collagen-3 (Col-3) was alleviated by THC treatment.

3.3. The Protective Effect of THC in Cardiac Remodeling Was Blunted by PGC-1α Knockdown. The role of PGC-1α in mediating the anticardiac hypertrophic role of THC was confirmed in this study. LV carrying siRNA against PGC-1α was administrated in the hearts of the mice. The EF% was decreased, the HW/BW ratio, thickness of left ventricular wall, hypertrophy degree of cardiomyocytes, left ventricular collagen volume, and the expression of hypertrophic and fibrotic markers were increased after TAC, in PGC-1α knockdown mice as shown in Figures 3(a)–3(f). These observations therefore confirmed that the protective role of THC against cardiac remodeling was blunted by knockdown PGC-1α.

3.4. The Antioxidant and UPR^{mt} Activating Effects of THC Were Blunted by PGC-1α Knockdown In Vivo. The protein

(a)

(b)

(c)

(d)

(e)
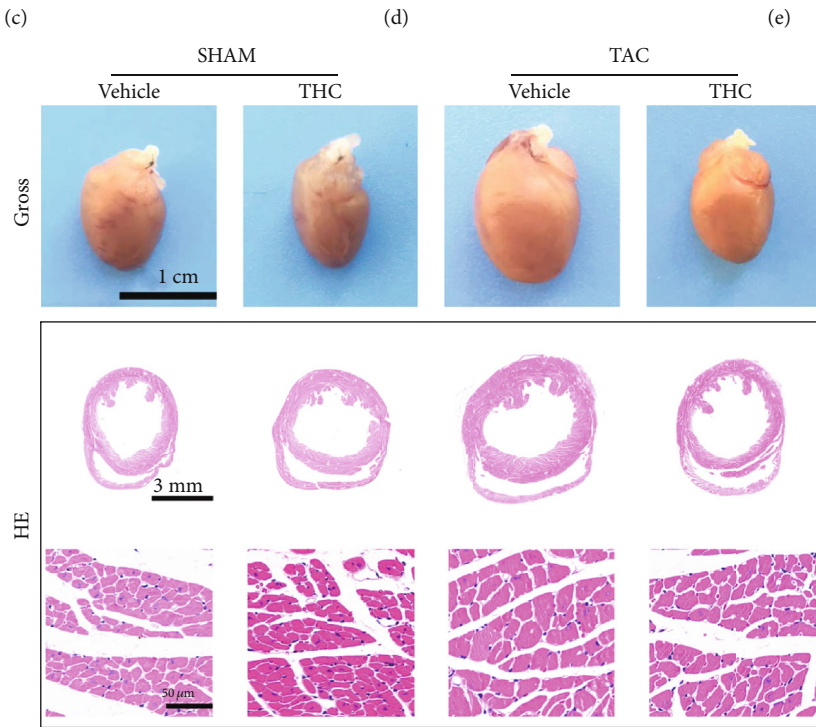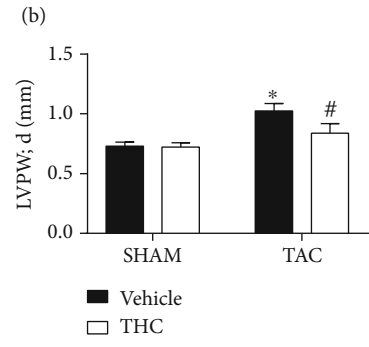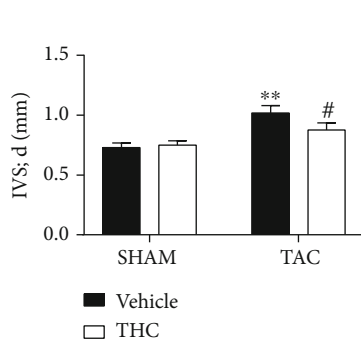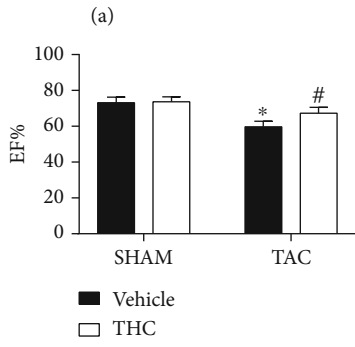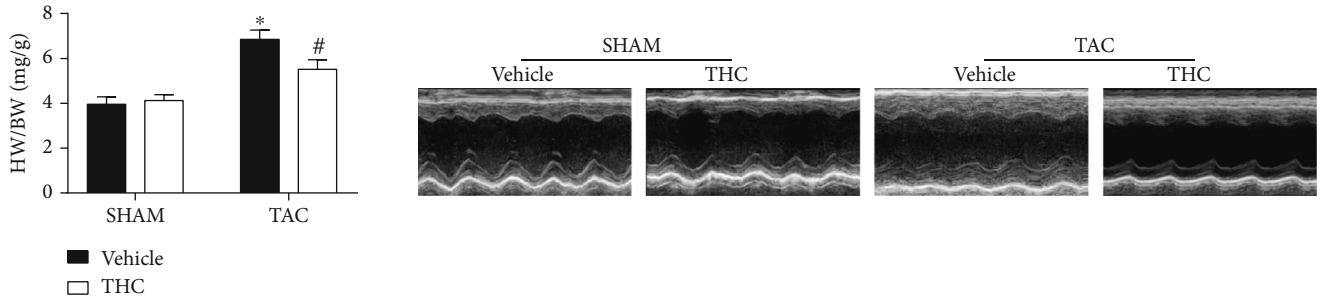
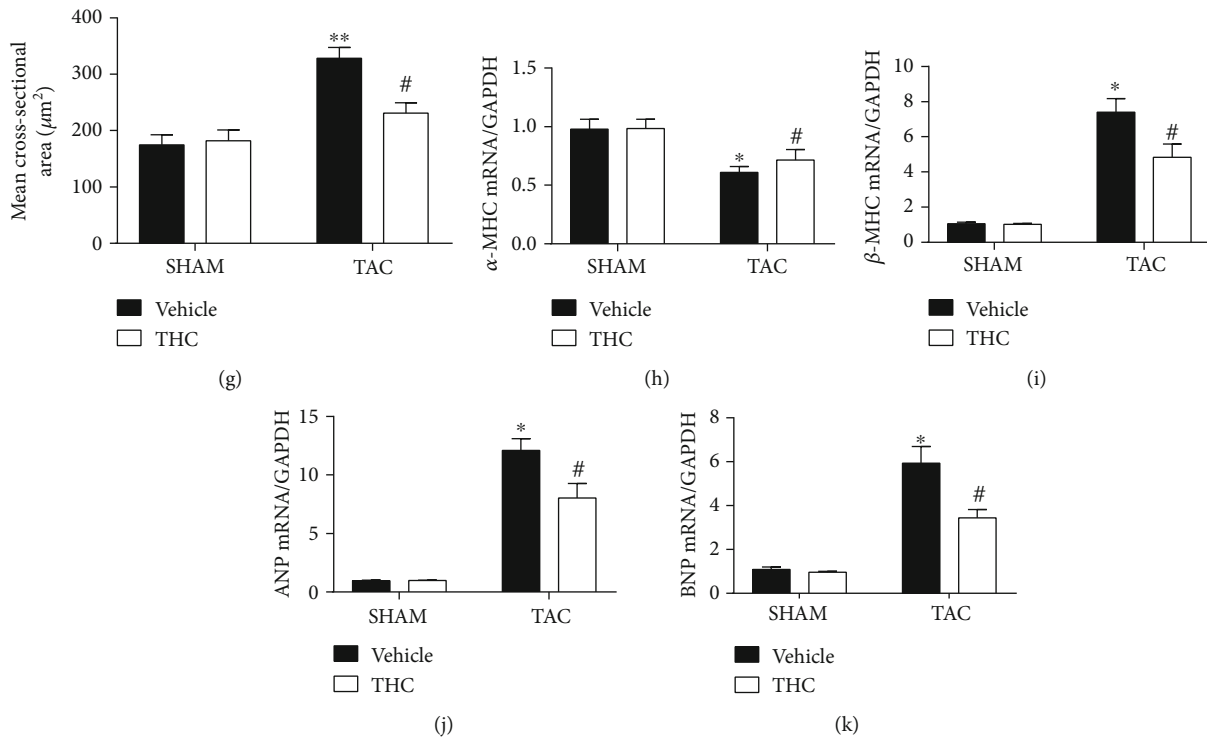(f)

FIGURE 2: Continued.

(g)

(h)

(i)

(j)

(k)

Figure 2: THC protected cardiac dysfunction and hypertrophy in mice after TAC. (a) The HW/BW ratio in mice after 4 weeks of TAC ($n = 6$ mice per group). (b) Representative M-mode echocardiographic images of the indicated groups ($n = 10$ mice per group). (c–e) The EF%, IVSd, and LVPWd, accordingly, determined by analyzing the echocardiographic images ($n = 10$ mice per group). (f) Representative images of the gross murine heart and sections stained with hematoxylin and eosin (HE) ($n = 6$ mice per group). (g) Mean cross-sectional area of cardiomyocytes from the indicated groups ($n = 6$ mice per group). (h–k) Real-time polymerase chain reaction (real-time PCR) analysis of the expression of genes encoding hypertrophic markers α-MHC, β-MHC, ANP, and BNP in each group ($n = 6$ mice per group). The data were analyzed by one-way ANOVA. $^*p < 0.05$, $^{**}p < 0.01$ vs. SHAM, $^\#p < 0.05$ vs. TAC. In the bar graphs, the data are presented as the mean ± SEM.

expression of PGC-1α in PGC-1α knockdown mice was markedly decreased, and the expression of ATF5 was decreased correspondingly, as shown in Figures 4(a), 4(d), and 4(e). The TAC-induced oxidative stress was aggravated by PGC-1α knockdown, as evidenced by the upregulation of gp91 phox and NOX 4 (Figures 4(a)–4(c)), increased production of ROS and MDA, and decreased content of SOD (Figure 4(f)–4(i)). There was no significant difference in the above oxidation indices between TAC+PGC-1α siRNA group and TAC+THC+PGC-1α siRNA group. This shows that the upregulation of Atf5, ClpP, and Lonp1 mRNA expression was also blunted by PGC-1α knockdown, as shown in Figure 4(j). These results suggest that THC protects against TAC-induced cardiac hypertrophy at least partially through alleviating oxidative stress and activating UPR^{mt} via activating PGC-1α.

3.5. THC Alleviated PE-Induced Cardiomyocyte Hypertrophy and Partly Activated UPR^{mt} In Vitro.

The antihypertrophic effect of THC was further tested by using PE to induce hypertrophy in NRCMs. The representative immunostaining graphs are shown in Figure 5(a). As shown in Figure 5(b), the growth of PE-induced cardiomyocytes was significantly attenuated by THC supplement. The protein expression of the two hypertrophic marker molecules, ANP and β-MHC,

was upregulated after PE administration, while THC supplement decreased ANP and β-MHC expression, as shown in Figures 5(c)–5(e). Furthermore, PE administration also triggered oxidative stress in NRCMs as evidenced by ROS production and upregulation of gp91 phox and NOX 4, as shown in Figures 5(f)–5(h) and Figures 5(k)–5(l). THC supplement alleviated the oxidative stress caused by PE and also upregulated PGC-1α and ATF5, as shown in Figures 5(i)–5(j). The expression of classic UPR^{mt} effector genes was examined by qRT-PCR, and the results are shown in Figure 5(m). TAC-induced upregulation of ATF5, mtDNAj, ClpP, and Lonp1 was further enhanced by THC treatment, while the expression of CHOP and ATF4 was not affected significantly by THC treatment.

3.6. PGC-1α Knockdown Abolished the Antioxidative and UPR^{mt} Activating Effect of THC in PE-Induced Hypertrophy of Cardiomyocytes.

PGC-1α siRNA was transfected in NRCMs to confirm the role exerted by PGC-1α. As shown in Figures 6(a)–6(e), PE-induced hypertrophy of cardiomyocytes and upregulation of ANP and β-MHC were exaggerated by PGC-1α knockdown, while the protective role of THC against hypertrophy was also blunted by PGC-1α knockdown. This condition remained consistent for oxidative stress. As shown in Figures 6(f)–6(j), PGC-1α was
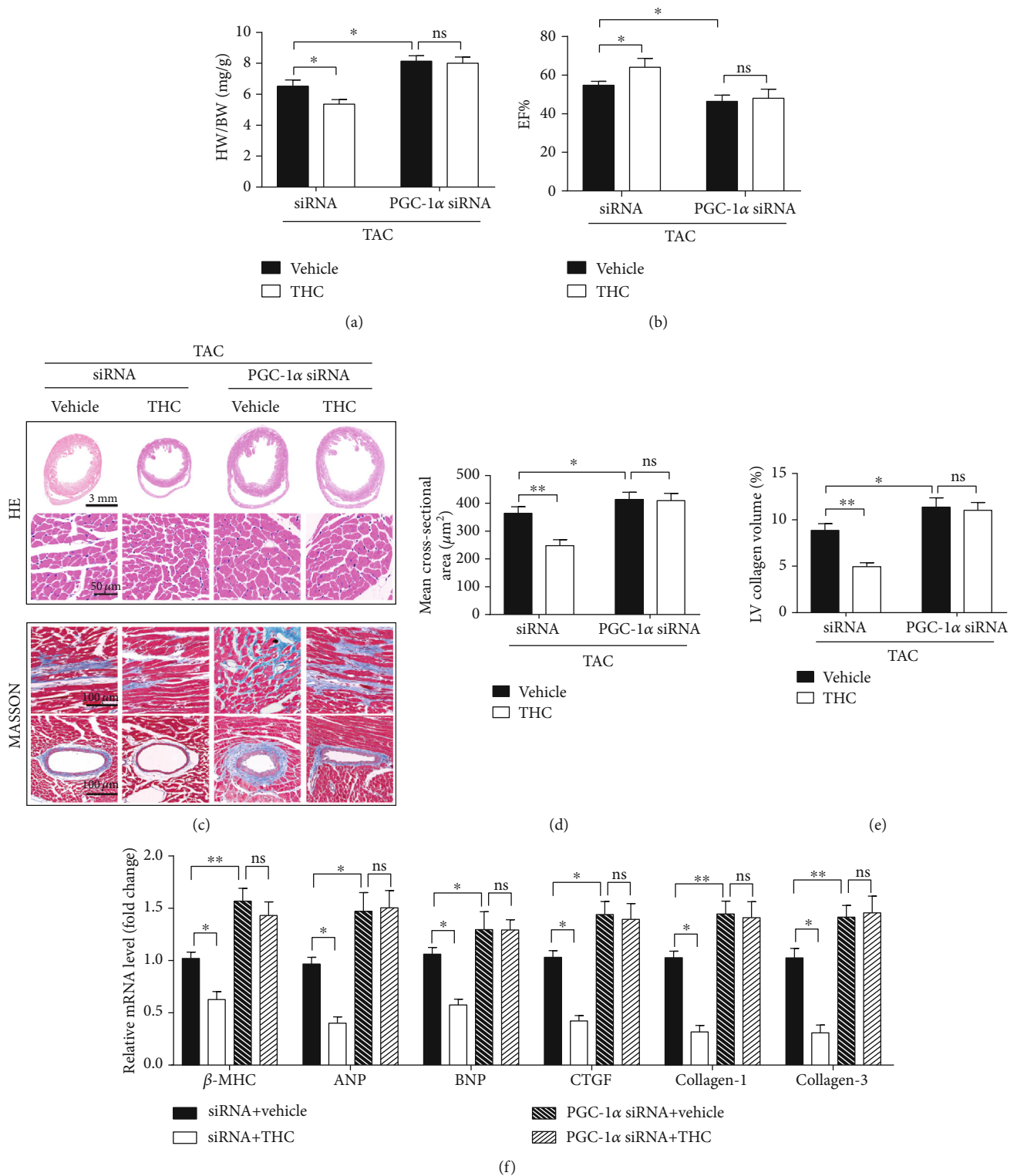
Figure 3: The protective effect of THC in cardiac remodeling was blunted by PGC-1α knockdown. (a) The HW/BW ratio in mice from indicated groups ($n = 6$ mice per group). (b) The EF% was determined by analyzing the echocardiographic images ($n = 10$ mice per group). (c) Representative images of the heart sections stained with HE and Masson stain ($n = 6$ mice per group). (d) The mean cross-sectional area of cardiomyocytes from the indicated groups ($n = 6$ mice per group). (e) The LV collagen volume in different groups ($n = 6$ mice per group). (f) Real-time PCR analysis of the expression of genes encoding the hypertrophic markers β-MHC, ANP, and BNP, and the fibrotic markers CTGF, collagen-1, and collagen-3 in each group ($n = 5 - 6$ mice per group). The data were analyzed by one-way ANOVA. $^*p < 0.05$, $^{**}p < 0.01$ between the two indicated groups; ns, not significant. In the bar graphs, the data are presented as the mean ± SEM.
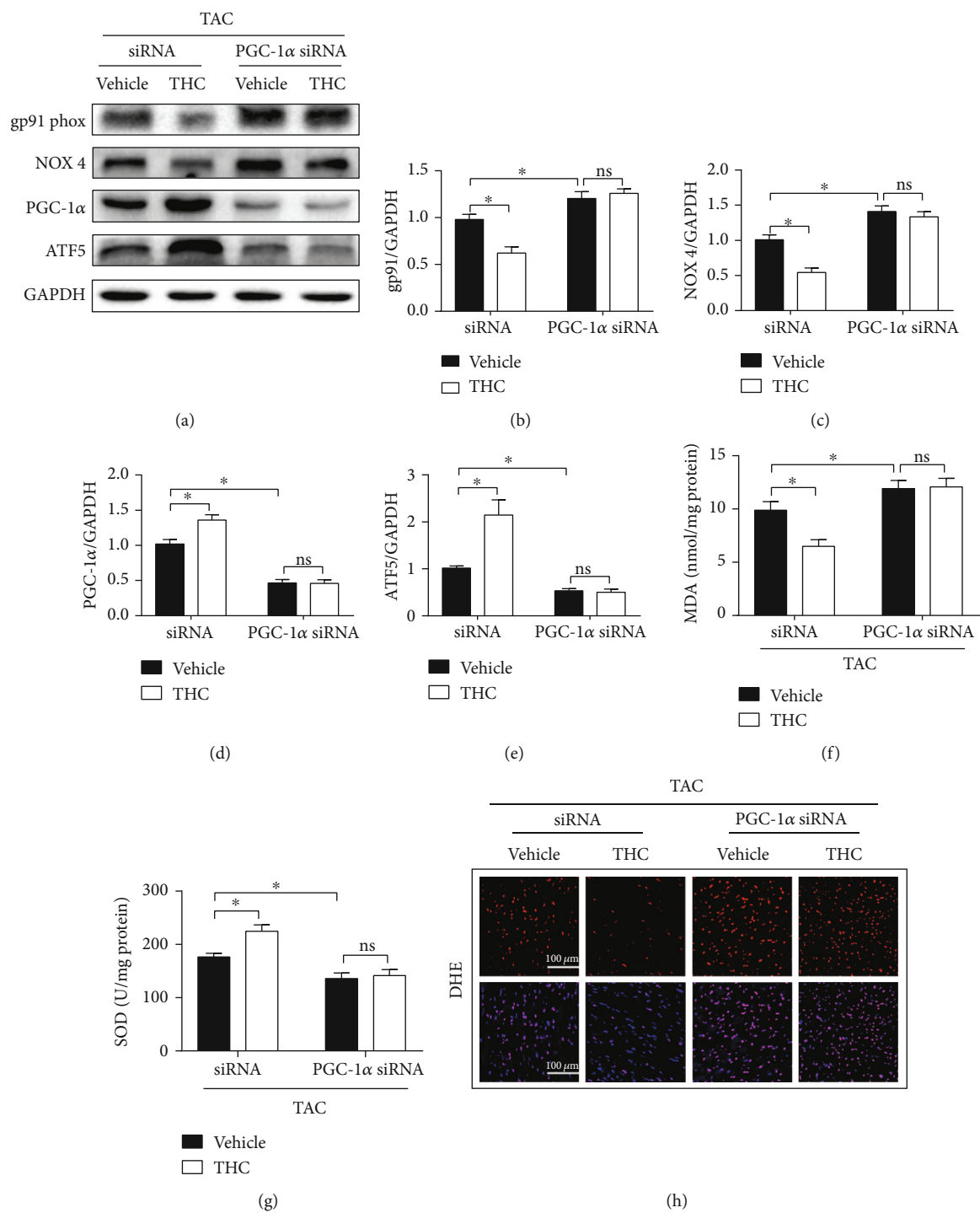
(a)

(b)

(c)

(d)

(e)
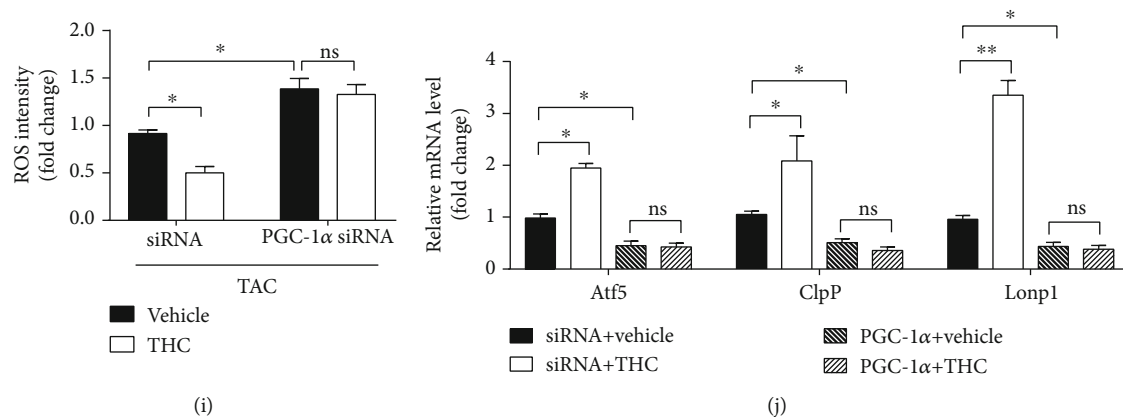
(f)

(g)

(h)

Figure 4: Continued.

(i)

(j)

FIGURE 4: The antioxidant and UPR^{mt} activating effects of THC were blunted by PGC-1α knockdown in vivo. (a) Representative western blot of gp91 phox, NOX 4, PGC-1α, and ATF5 in murine hearts from indicated groups. (b–e) Quantification of gp91 phox, NOX 4, PGC-1α, and ATF5 protein expression ($n = 6$ mice per group). (f) Statistical diagram of MDA content ($n = 6$ mice per group). (g) Statistical diagram of SOD activity ($n = 6$ mice per group). (h) Representative images of DHE staining (red) and DAPI (blue). (bar = 100 μm). (i) Statistical diagram of ROS intensity ($n = 6$ mice per group). (j) RT-PCR analysis of the expression of genes encoding Atf5, ClpP, and Lonp1 in each group ($n = 6$ mice per group). The data were analyzed by one-way ANOVA. $^*p < 0.05$, $^{**}p < 0.01$ between the two indicated groups; ns: not significant. In the bar graphs, the data are presented as the mean ± SEM.

markedly downregulated after knockdown, and ATF5 was also decreased, but the protein expressions of gp91 phox and NOX 4 were enhanced. Furthermore, the upregulation of UPR^{mt} effector genes (Atf5, mtDNAj, ClpP, and Lonp1) induced by THC was also abolished by PGC-1α siRNA, as shown in Figure 6(k). However, no significant difference was seen in the above oxidation indices between PE+PGC-1α siRNA group and PE+THC+PGC-1α siRNA group.

3.7. PGC-1α/ATF5 Formed a Signaling Axis to Partly Activate UPR^mt. The interaction of PGC-1α and ATF5 that played a role in the regulation of UPR^{mt} activation was further elucidated by transfecting NRCMs with adenovirus overexpressing PGC-1α. As shown in Figures 7(a)–7(c), under normal conditions, the ATF5 expression was upregulated in line with the overexpression of PGC-1α. Under PE treatment, although ATF5 expression increased and PGC-1α expression decreased, overexpression of PGC-1α further significantly upregulated ATF5. Meanwhile, the mRNA expression of ClpP and Lonp1 also synchronized with the changes of ATF5 expression, as shown in Figure 7(d). In turn, ATF5 expression was downregulated in line with the knockdown of PGC-1α under normal conditions, while PE treatment downregulated PGC-1α but upregulated the expression of ATF5 and UPR^{mt} effectors, as shown in Figures 7(e)–7(h). This suggests that there are other signaling pathways capable of activating ATF5 and UPR^{mt} in PE-treated NRCMs.

3.8. PGC-1α/ATF5 Axis Mediated the Cardioprotective and UPR^mt Activating Effect of THC. NRCMs were treated with ATF5 siRNA, and the knockdown effect of ATF5 siRNA was confirmed as there was no significant change in PGC-1α protein expression, as shown in Figures 8(a)–8(c). PE-induced upregulation of ANP and β-MHC mRNA were exaggerated by ATF5 knockdown, while the protective role of THC against hypertrophy was also blunted by ATF5

knockdown, as shown in Figure 8(d). PE-treated NRCMs with THC supplement showed downregulation of gp91 phox and NOX4, while ATF5 siRNA abolished this effect. However, ATF5 siRNA did not inhibit the expression of PGC-1α, as shown in Figures 8(e) and 8(f). Furthermore, ATF5 siRNA also blunted the upregulation of mtDNAj, ClpP, and Lonp1 by THC treatment, as shown in Figure 8(g). Notably, it was determined that PGC-1α enhanced the cardioprotective effect of THC, further activating ATF5 and downstream UPR^{mt}, as shown in Figure 8(h).

4. Discussion

Hypertension is a major global health problem in present times with no significant improvement seen in managing or controlling its effects and incidence [23]. Hypertension increases the pressure load on the left ventricle of the heart resulting in cardiomyocyte compensatory hypertrophy thereby enhancing contractility. However, long-term pressure overload leads to decompensatory changes in cardiomyocytes resulting in a decompensated stage in which the cardiac function is weakened, eventually causing heart failure [24]. Previous studies have demonstrated that inhibition of pathological cardiac hypertrophy can significantly alleviate pressure overload-induced cardiac function injury and heart failure [25]. Therefore, it is important to explore new safe and effective drugs to inhibit and treat cardiac hypertrophy. This study determined that PGC-1α and ATF5 can form a signaling axis to partly activate UPR^{mt}. Furthermore, PGC-1α/ATF5/UPR^{mt} mediates the protective role of THC in TAC-induced cardiac hypertrophy and oxidative stress. The UPR^{mt} activating effect of the PGC-1α/ATF5 axis and the cardioprotective effect of THC was also verified in PE-induced hypertrophic NRCMs. This study found a new mechanism for the regulation of UPR^{mt} activation and
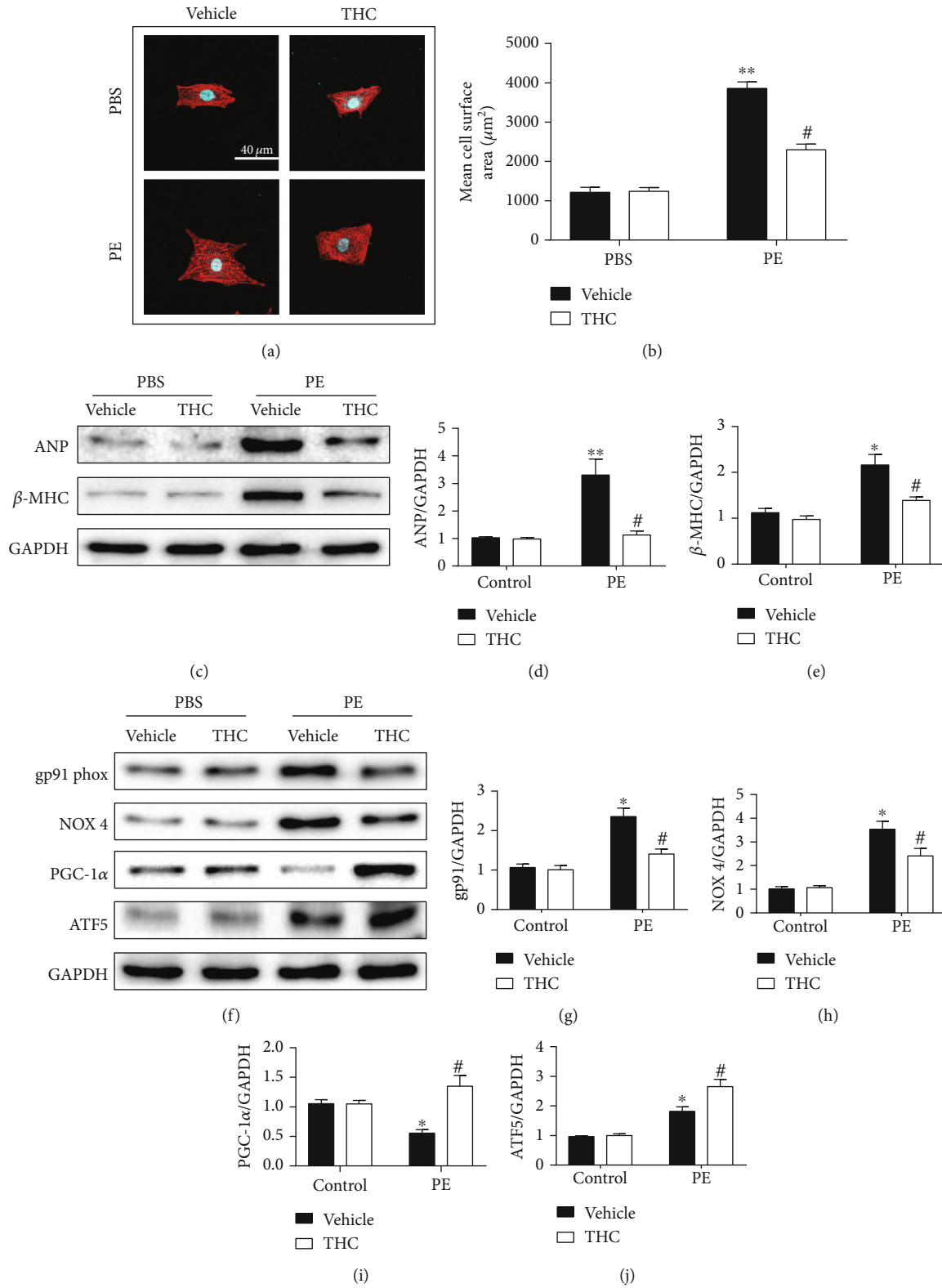
(a)

(b)

(c)

(d)

(e)

(f)

(g)

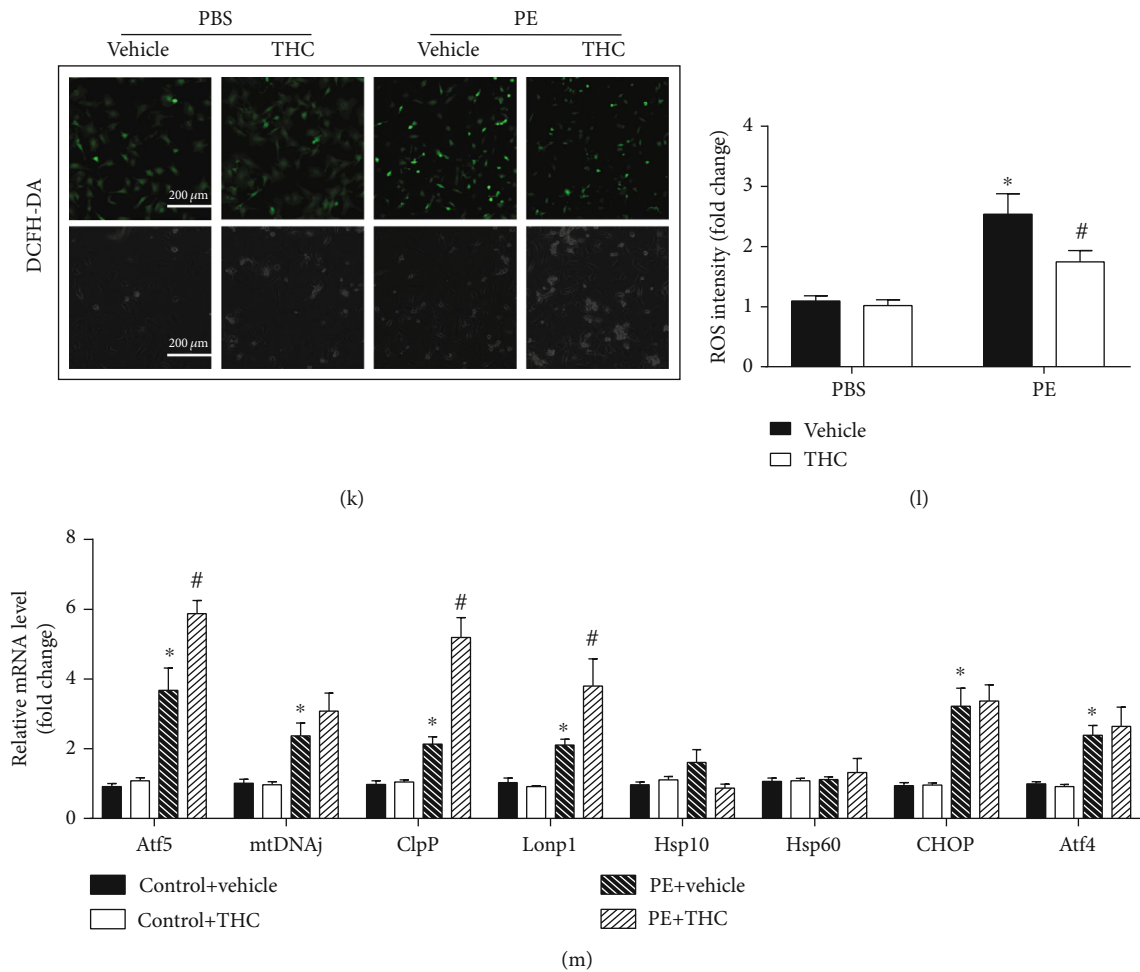(h)

(i)

(j)

FIGURE 5: Continued.

(k)

(l)

(m)

FIGURE 5: THC alleviated PE-induced cardiomyocyte hypertrophy and partly activated UPR^{mt} in vitro. (a) Representative immunofluorescence images of the NRCMs stained by α-actinin (red) and DAPI (blue) observed under a confocal microscope. (bar = 40 μm) (b) The mean cell surface area of NRCMs from the indicated groups ($n = 5$ samples per group, ≥ 30 cells per sample were randomly measured). (c) Representative western blot of ANP and β-MHC in NRCMs from indicated groups. (d–e) Quantification of ANP and β-MHC protein expression ($n = 5$ samples per group). (f) Representative western blot of gp91 phox, NOX 4, PGC-1α, and ATF5 in NRCMs from indicated groups. (g–j) Quantification of gp91 phox, NOX 4, PGC-1α, and ATF5 protein expression ($n = 5$ samples per group). (k) Representative images of DCFH-DA staining (green) (bar = 100 μm). (l) Statistical diagram of ROS intensity ($n = 5$ samples per group). (m) RT-PCR analysis of the expression of genes encoding Atf5, mtDNAj, ClpP, Lonp1, Hsp10, Hsp60, CHOP, and Atf4 in each group ($n = 5$ samples per group). The data were analyzed by one-way ANOVA. $^{*}p < 0.05$, $^{**}p < 0.01$ vs. control, $^{#}p < 0.05$ vs. PE. In the bar graphs, the data are presented as the mean $\pm$ SEM.

proved THC to be a new drug activating UPR^{mt} to inhibit mitochondrial dysfunction.

Under the stimulation of different neurohumoral or mitochondrial stress, the protein-folding machinery in mitochondria is damaged, thereby leading to the production of misfolded and dysfunctional proteins. Dysfunction of the mitochondrial respiratory chain is accompanied by an increase in ROS and oxidative stress, which interferes with the protein integrity and folding process, leading to a vicious cycle of mitochondrial damage and cardiac dysfunction [36]. The mitochondrial damage and cardiac dysfunction activates UPR^{mt} response. Activation of UPR^{mt} involves a signal transduction pathway from mitochondria to nucleus, activating specific nuclear transcription factors. As a result, the expression of several genes protecting the mitochondria, especially

those coding for molecular chaperones (like hsp10 and hsp60), antioxidant enzymes, and proteases located in the mitochondrial matrix (ClpP and Lonp1), is upregulated and helps in cell survival [12]. Recent research has elucidated the classical pathways of UPR active in mammalian mitochondria. Increased phosphorylation of eukaryotic initiation factor 2 alpha (eIF2α) activates the expression of *CHOP*, *ATF4*, and *ATF5*, thereby enhancing the mitochondrial protective action, although the relationship between CHOP, ATF4, and ATF5 is not entirely clear [12]. Furthermore, Smyrnias et al. confirmed that enhanced UPR^{mt} activation significantly improved mitochondrial function and myocardial contractility, reduced myocardial cell mortality, and alleviated pathological myocardial fibrosis and remodeling. The positive regulation by myocardial cell UPR^{mt} is expected to
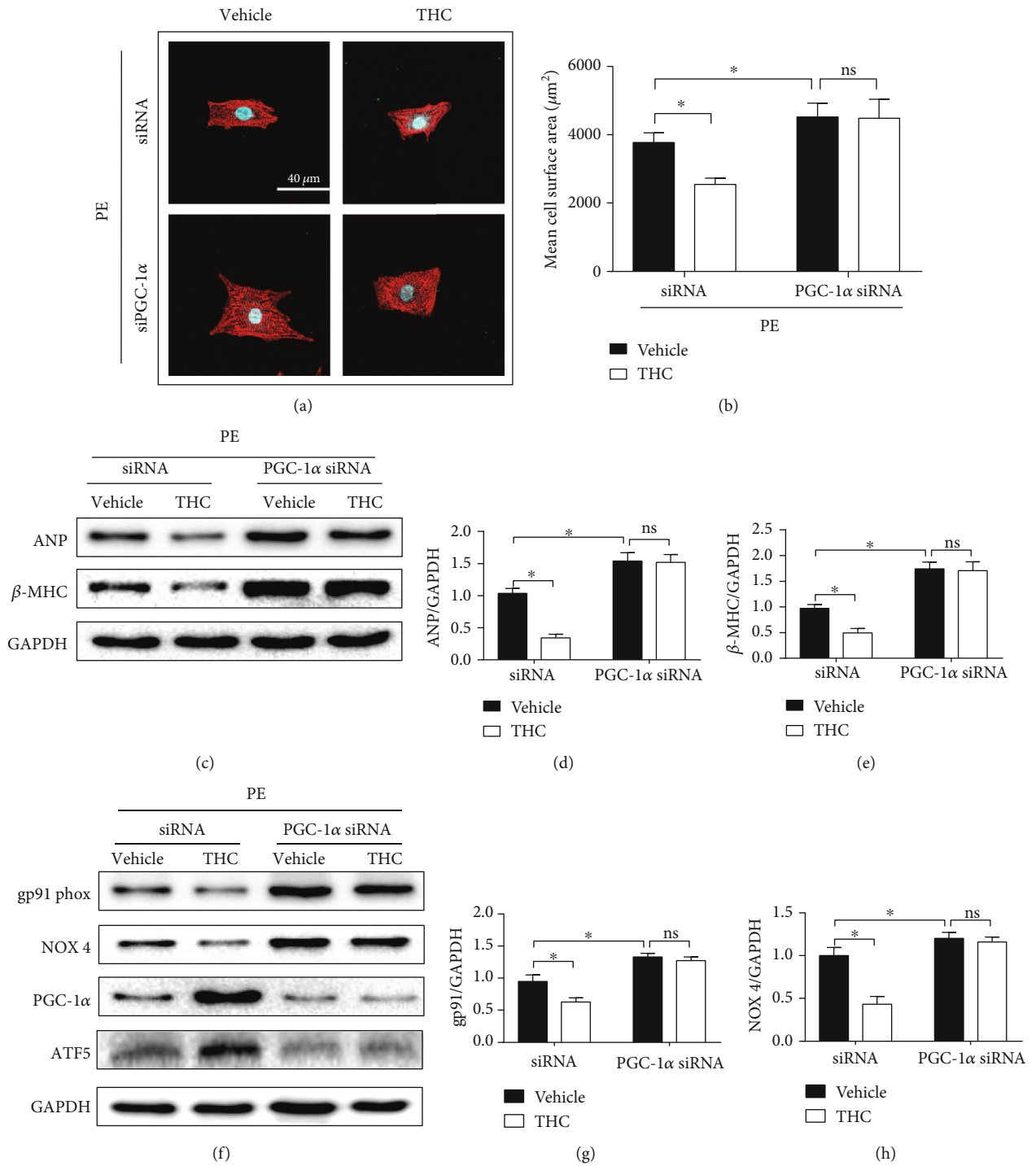
(a)

(b)

(c)

(d)

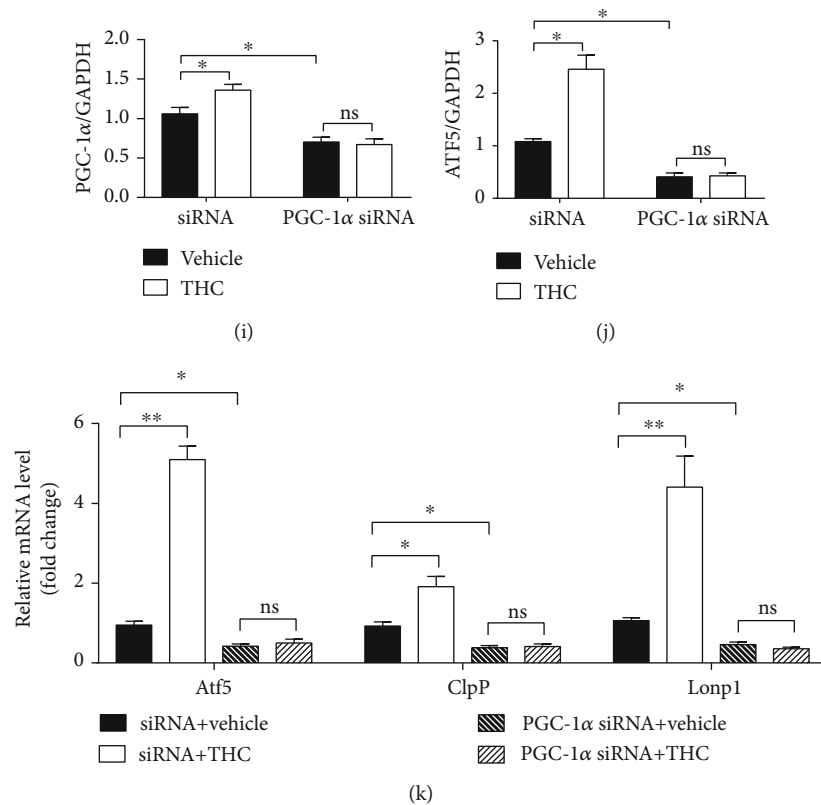(e)

(f)

(g)

(h)

Figure 6: Continued.

(i)

(j)

(k)

FIGURE 6: PGC-1α knockdown abolished the antioxidative and UPR^{mt} activating effect of THC in PE-induced cardiomyocytes hypertrophy. (a) Representative immunofluorescence images of the NRCMs stained by α-actinin (red) and DAPI (blue) observed under a confocal microscope. (bar = 40 μm). (b) The mean cell surface area of NRCMs from the indicated groups ($n = 5$ samples per group, ≥30 cells per sample were randomly measured). (c) Representative western blot of ANP and β-MHC in NRCMs from indicated groups. (d–e) Quantification of ANP and β-MHC protein expression ($n = 5$ samples per group). (f) Representative western blot of gp91 phox, NOX 4, PGC-1α, and ATF5 in NRCMs from indicated groups. (g–j) Quantification of gp91 phox, NOX 4, PGC-1α, and ATF5 protein expression ($n = 5$ samples per group). (k) RT-PCR analysis of the expression of genes encoding Atf5, ClpP, and Lonp1 ($n = 5$ samples per group). The data were analyzed by one-way ANOVA. $^*p < 0.05$ between the two indicated groups; ns: not significant. In the bar graphs, the data are presented as the mean ± SEM.

be an important target for the treatment of stress-induced myocardial injury [14]. However, the specific activation mechanism and the drugs that can effectively activate UPR^{mt} in the heart needs further detailed evaluation.

THC, a major metabolite of curcumin, exhibits a stronger antioxidant activity than curcumin [6]. Previous studies have confirmed the protective role of THC in multiple animal models of hypertension induced by cadmium, iron, and L-arginine methyl ester (L-NAME) for its strong antioxidant properties [9, 15, 26]. THC has been shown to exert protective roles in diabetic cardiomyopathy and myocardial infarction via the antioxidant stress pathway [8, 27]. The possibility of activation of UPR^{mt} by THC for protection against pressure overload-induced cardiac hypertrophy has been investigated in this study. ROS production and accumulation has previously been confirmed to be involved in the promotion of pathological cardiac hypertrophy and HF in humans and animal models [32, 33]. Moreover, activation of key mediators by excessive ROS production can also modulate the extracellular matrix function, promoting cardiac fibrotic remodeling [34]. Hypertrophic stimuli induce abnormal

ROS production and further promote oxidative stress. Thus, effective regulation of mitochondrial redox homeostasis in cardiomyocytes is a promising strategy for the treatment of pathological cardiac hypertrophy and heart failure [18]. THC exerts an obvious protective role via inhibition of free radical and ROS production and promotion of antioxidant mechanism in several pathological models [27, 35]. In this study, THC treatment was found to significantly attenuate TAC-induced oxidative stress. Notably, THC treatment was found to further upregulate PGC-1α, ATF5, and several UPR^{mt} effectors. This led to the possibility of the existence of any potential THC facilitated UPR^{mt} activation modes which may exert a protective effect against pathological cardiac hypertrophy.

Therefore, the effect that THC exerts in pathological cardiac hypertrophy was investigated. The pathological cardiac remodeling including cardiomyocyte apoptosis and abnormal fibrosis formation with reduced cardiac function results in heart failure [1]. This study considered impaired heart function as one important indicator of transition from the compensated period of cardiac hypertrophy to the
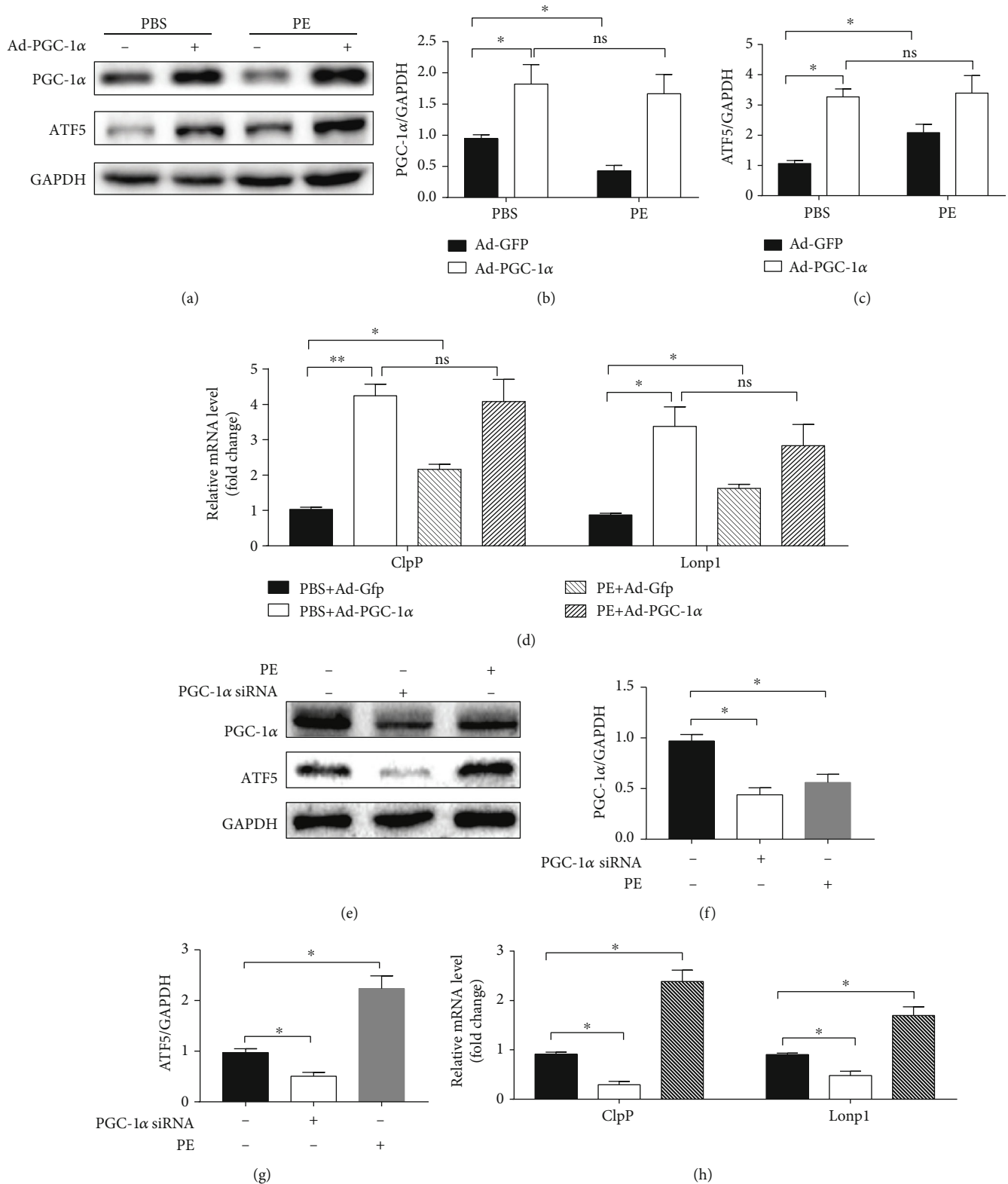
(a)

(b)

(c)

(d)

(e)

(f)

(g)

(h)

Figure 7: PGC-1α/ATF5 formed an signaling axis to partly activate UPR^{mt}. (a) Representative western blot of PGC-1α and ATF5 in NRCMs from indicated groups. (b–c) Quantification of PGC-1α and ATF5 protein expression ($n = 5$ samples per group). (d) RT-PCR analysis of the expression of genes encoding ClpP and Lonp1 ($n = 5$ samples per group). (e) Representative western blot of PGC-1α and ATF5 in NRCMs from indicated groups. (f–g) Quantification of PGC-1α and ATF5 protein expression ($n = 5$ samples per group). (h) RT-PCR analysis of the expression of genes encoding ClpP and Lonp1 ($n = 5$ samples per group). The data were analyzed by one-way ANOVA. $^{*}p < 0.05$, $^{**}p < 0.01$ between the two indicated groups; ns: not significant. In the bar graphs, the data are presented as the mean ± SEM.

(a)

(b)

(c)

(d)

(e)

(f)

(g)

Figure 8: Continued.

(h)
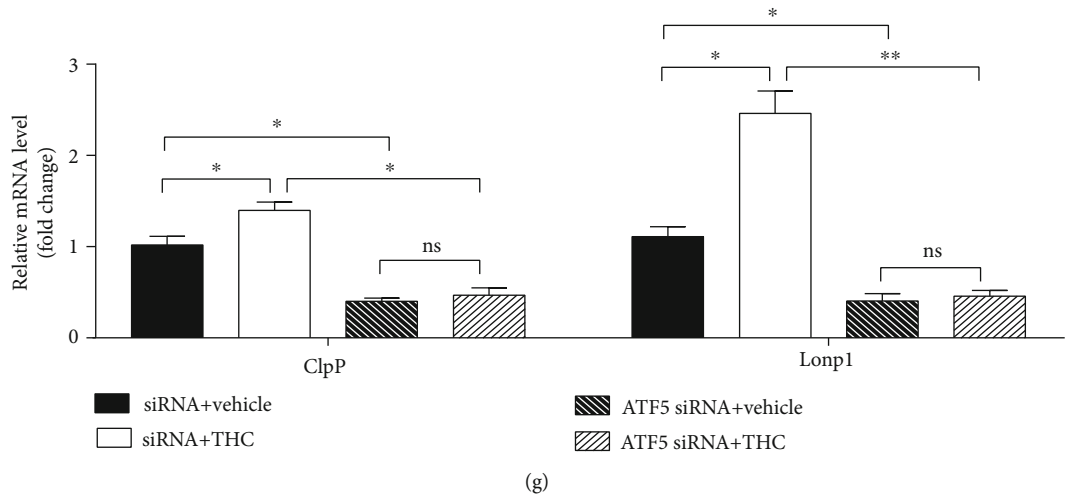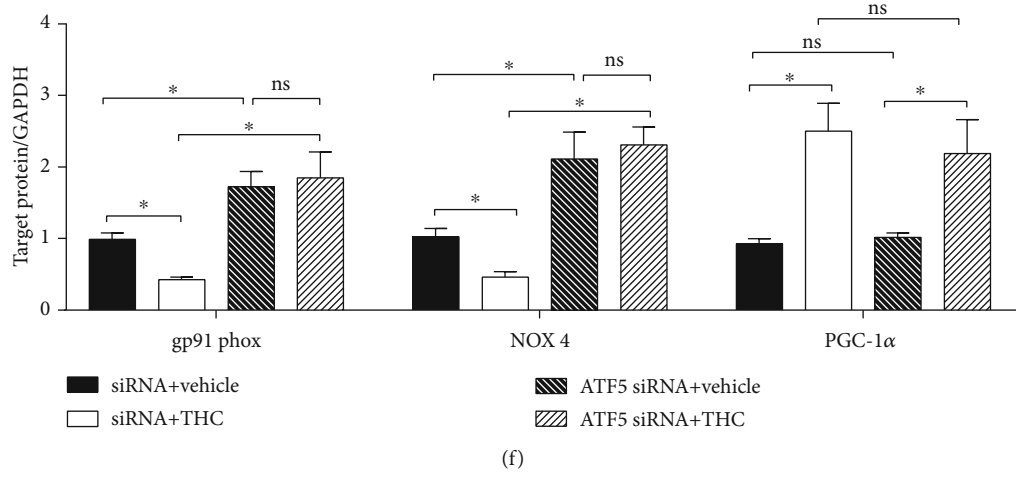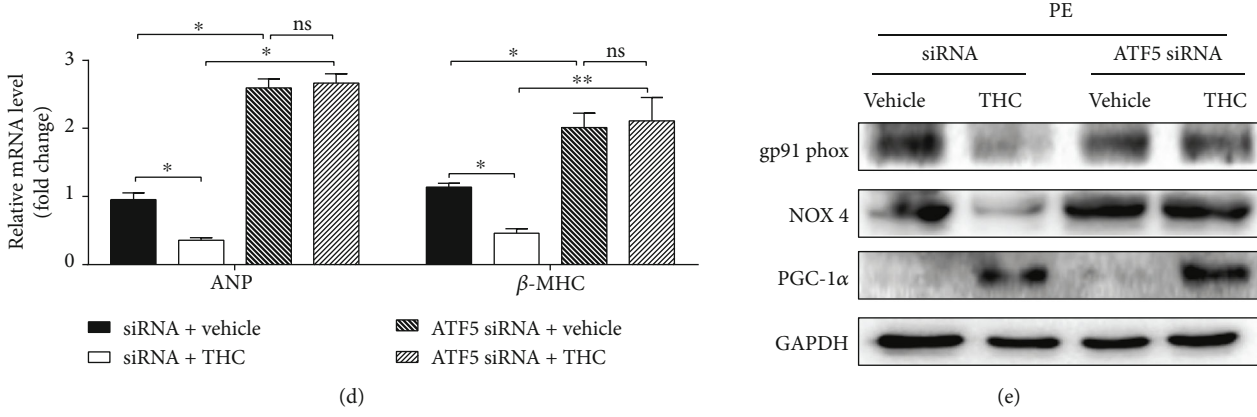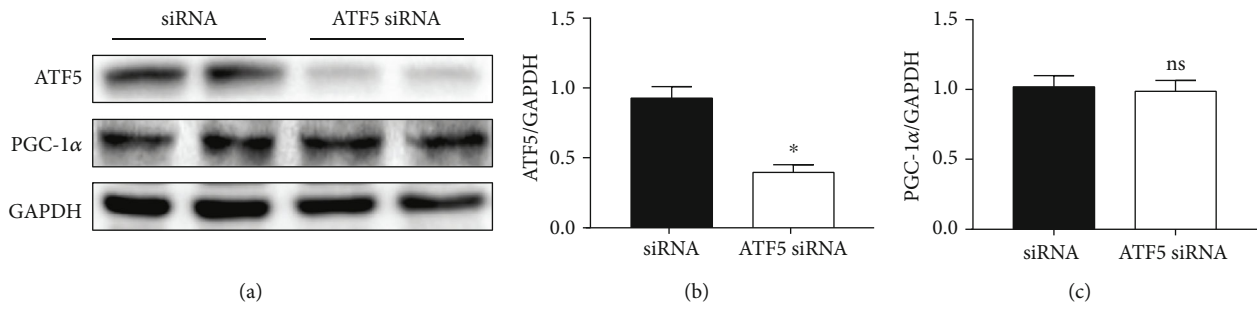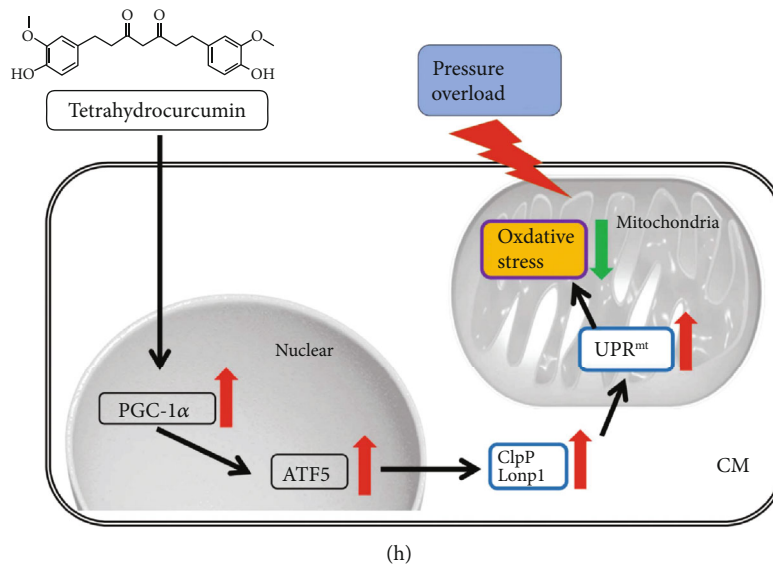
FIGURE 8: PGC-1α/ATF5 mediated the cardioprotective and UPR^{mt} activating effect of THC. (a) Representative western blot of ATF5 and PGC-1α in NRCMs from indicated groups. (b–c) Quantification of ATF5 and PGC-1α protein expression ($n = 5$ samples per group). (d) RT-PCR analysis of the expression of genes encoding ANP and β-MHC ($n = 5$ samples per group). (e) Representative western blot of gp91 phox, NOX 4, and PGC-1α in NRCMs from indicated groups. (f) Quantification of gp91 phox, NOX 4, and PGC-1α protein expression ($n = 5$ samples per group). (g) RT-PCR analysis of the expression of genes encoding ClpP and Lonp1 ($n = 5$ samples per group). (h) THC activates PGC-1α/ATF5 axis and downstream UPR^{mt} to alleviate oxidative stress and pathological cardiac hypertrophy induced by pressure overload. The data were analyzed by one-way ANOVA. $^{*}p < 0.05$, $^{**}p < 0.01$ between the two indicated groups; ns: not significant. In the bar graphs, the data are presented as the mean ± SEM.

decompensated period. Four weeks after TAC, mice cardiac function was significantly decreased, as evidenced by EF%. Intragastric THC administration (50 mg/kg/d) for 4 weeks markedly improved cardiac function, delaying the transition to the decompensated period of cardiac injury. Cardiac fibrosis is another important hallmark of pathological cardiac remodeling [22]. There is convincing evidence that excessive collagen deposition adversely affects heart function by increasing diastolic stiffness, impairing systolic function, worsening ventricular tachyarrhythmia, and ultimately leading to heart failure [28]. A recent study reported that THC attenuates renal fibrosis by inhibiting the expression of α-SMA and oxidative stress in rats with chronic kidney disease (CKD) [10]. This study primarily determined that THC treatment significantly decreased the collagen deposition in the left ventricle 4 weeks after TAC surgery. Confirmation of the antifibrotic role of THC and its potential mechanism warrants the need for more detailed studies. Previous studies have confirmed that increased expression of α-MHC can enhance the supply of energy to the heart by improving the myocardial contractile velocity, while the increased expression of β-MHC can reduce the energy consumption of cardiomyocytes [29]. When hypertrophic stimuli to the heart is prolonged or severe, expression of α-MHC decreases while expression of β-MHC increases in cardiomyocytes [30]. A previous study confirmed that sustained hyperexpression of α-MHC in cardiomyocytes exerts a certain important role in improving cardiac function [31]. Following TAC, the expression of α-MHC decreased, and the expression of β-MHC increased; however, THC treatment blunted this

expression trend, indicating a good prognosis in pathological cardiac hypertrophy. This led to the inference that THC treatment effectively inhibits the progression of pathological cardiac hypertrophy.

In the present study, THC treatment activated ATF5 expression, besides CHOP and ATF4. THC can therefore activate UPR^{mt} via a novel ATF5-dependent way, supported by the fact that the effect of enhanced UPR^{mt} activation on the mitochondrial dysfunction of stressed cardiomyocytes depends on the enhanced expression of ATF5 [14]. Since PGC-1α was also upregulated by THC, the interactions between PGC-1α and UPR^{mt} were further investigated. PGC-1α mediates the anticardiac hypertrophic role of several medicines [37, 38]. It also exerts a cardioprotective role in ischemia and reperfusion-induced and exhaustive exercise-induced heart injury due to its antioxidant activity [39, 40]. However, whether PGC-1α exerts an effect in the activation of UPR^{mt} remains unclear. PGC-1α siRNA was used to inhibit the cardioprotective role of THC both in vivo and in vitro. Meanwhile, the ATF5 and UPR^{mt} effectors activated by THC were also downregulated by PGC-1α knockdown. The interaction between PGC-1α and ATF5 was confirmed by transfecting NRCMs with PGC-1α siRNA or Ad- PGC-1α under normal conditions. The results showed that ATF5 protein expression was significantly regulated in line with PGC-1α expression. However, when NRCMs were treated with ATF5 siRNA, PGC-1α expression did not change significantly under normal conditions. This confirmed that PGC-1α functions as the upstream regulator of ATF5 in the cardioprotective effect of THC treatment, and that the effect on

UPR^{mt} activation is blunted by PGC-1α siRNA and ATF5 siRNA. Based on our results, we conclude that the novel PGC-1α/ATF5 axis can activate UPR^{mt} in cardiomyocytes, and it can be activated by THC treatment. Interestingly, when NRCMs were treated with PE, PGC-1α was downregulated, but ATF5 was upregulated. Therefore, it can be concluded that there exist other modes of PE-mediated upregulation of UPR^{mt} which warrant further in-depth research.

Smyrnias et al. also studied the expression levels of UPR^{mt} effectors in cardiomyocytes under different stimuli such as pressure overload, isoproterenol, nicotinamide riboside, G-TPP, and Paraquat and concluded that different stimuli activates UPR^{mt} in different modes. For example, pressure overload mainly upregulates ATF5, ClpP, and Lonp1, while G-TPP (10 μmol/l for 8 hrs) treatment upregulates CHOP, Lonp1, Hsp60, and Hsp10 [14]. In this study, mRNA expression of ATF5, ClpP, Lonp1, and Hsp10 and protein expression of ATF5, CHOP, and ATF4 were seen to be upregulated by pressure overload in mice hearts. On the other hand, mRNA expression of ATF5, CHOP, ATF4, mtDNAj, ClpP, and Lonp1 was upregulated by PE administration in isolated NRCMs. Although different UPR^{mt} effectors were upregulated under pressure overload in vivo or with PE treatment in vitro, THC treatment further upregulated Lonp1 and ClpP mRNA expression via the PGC-1α/ATF5 axis. However, it is indicated that some mechanisms by which THC and PGC-1α/ATF5 axis regulate gene expression mode of UPR^{mt} effectors, remains unknown and needs more in-depth research.

5. Conclusion

This study primarily verified that the newfound PGC-1α/ATF5 axis can partly activate UPR^{mt} and mediate the protective role of THC against pathological cardiac hypertrophy and oxidative stress induced by pressure overload. In vitro experiments elucidated the upstream and downstream relationship of this signal axis and the role of media in stress-resistance of THC in PE-induced hypertrophy of cardiomyocytes. This study also confirms a new mode of UPR^{mt} regulation in cardiomyocytes, by which THC exerts its well-known antioxidant role. These results provide the possibility to treat pressure overload caused by cardiac hypertrophy and heart failure by therapeutic THC supplement and also provides a new possibility of treating oxidative stress. However, further studies are needed to explore the mechanism and mode of UPR^{mt} activation under different conditions.

Data Availability

The data used to support the findings of this study are available from the corresponding author upon request.

Conflicts of Interest

The authors declare that there are no conflicts of interest.

Authors' Contributions

Bing Zhang, Yanzhen Tan, Zhengbin Zhang, and Pan Feng contributed equally to this work.

Acknowledgments

Supplementary Materials

Supplementary Table 1 (Table S1): a list of the primers used in the RT-PCR. Supplementary Figure 1 (Figure S1): verified the anti-inflammatory effect of THC during pressure overload-induced cardiac injury. Supplementary Figure 2 (Figure S2): verified that THC ameliorated cardiac fibrosis induced by TAC in vivo. Figure S1 and S2 further confirmed the cardioprotective role of THC in pathological cardiac hypertrophy. (Supplementary Materials)

References

[1] I. Shimizu and T. Minamino, "Physiological and pathological cardiac hypertrophy," Journal of Molecular and Cellular Cardiology, vol. 97, pp. 245–262, 2016.

[2] J. A. Hill and E. N. Olson, "Cardiac plasticity," The New England Journal of Medicine, vol. 358, no. 13, pp. 1370–1380, 2008.

[3] K. Q. Deng, J. Li, Z. G. She et al., "Restoration of circulating MFGE8 (milk fat globule-EGF factor 8) attenuates cardiac hypertrophy through inhibition of Akt pathway," Hypertension, vol. 70, no. 4, pp. 770–779, 2017.

[4] A. J. Marian and E. Braunwald, "Hypertrophic cardiomyopathy: genetics, pathogenesis, clinical manifestations, diagnosis, and therapy," Circulation Research, vol. 121, no. 7, pp. 749–770, 2017.

[5] A. Ray, S. Rana, D. Banerjee et al., "Improved bioavailability of targeted Curcumin delivery efficiently regressed cardiac hypertrophy by modulating apoptotic load within cardiac microenvironment," Toxicology and Applied Pharmacology, vol. 290, pp. 54–65, 2016.

[6] B. Aggarwal, L. Deb, and S. Prasad, "Curcumin differs from tetrahydrocurcumin for molecular targets, signaling pathways and cellular responses," Molecules, vol. 20, no. 1, pp. 185–205, 2015.

[7] U. Kukongviriyapan, K. Apaijit, and V. Kukongviriyapan, "Oxidative stress and cardiovascular dysfunction associated with cadmium exposure: beneficial effects of curcumin and tetrahydrocurcumin," The Tohoku Journal of Experimental Medicine, vol. 239, no. 1, pp. 25–38, 2016.

[8] M. S. Ali, M. P. Mudagal, and D. Goli, "Cardioprotective effect of tetrahydrocurcumin and rutin on lipid peroxides and antioxidants in experimentally induced myocardial infarction in rats," Die Pharmazie, vol. 64, no. 2, pp. 132–136, 2009.

[9] S. Nakmareong, U. Kukongviriyapan, P. Pakdeechote et al., "Antioxidant and vascular protective effects of curcumin and tetrahydrocurcumin in rats with L-NAME-induced hypertension," *Naunyn-Schmiedeberg's Archives of Pharmacology*, vol. 383, no. 5, pp. 519–529, 2011.

[10] W. L. Lau, M. Khazaeli, J. Savoj et al., "Dietary tetrahydrocurcumin reduces renal fibrosis and cardiac hypertrophy in 5/6 nephrectomized rats," *Pharmacology Research & Perspectives*, vol. 6, no. 2, article e00385, 2018.

[11] S. K. Maulik and S. Kumar, "Oxidative stress and cardiac hypertrophy: a review," *Toxicology Mechanisms and Methods*, vol. 22, no. 5, pp. 359–366, 2012.

[12] T. Shpilka and C. M. Haynes, "The mitochondrial UPR: mechanisms, physiological functions and implications in ageing," *Nature Reviews. Molecular Cell Biology*, vol. 19, no. 2, pp. 109–120, 2018.

[13] N. U. Naresh and C. M. Haynes, "Signaling and regulation of the mitochondrial unfolded protein response," *Cold Spring Harbor Perspectives in Biology*, vol. 11, no. 6, 2019.

[14] I. Smyrnias, S. P. Gray, D. O. Okonko et al., "Cardioprotective effect of the mitochondrial unfolded protein response during chronic pressure overload," *Journal of the American College of Cardiology*, vol. 73, no. 14, pp. 1795–1806, 2019.

[15] W. Sangartit, P. Pakdeechote, V. Kukongviriyapan, W. Donpunha, S. Shibahara, and U. Kukongviriyapan, "Tetrahydrocurcumin in combination with deferiprone attenuates hypertension, vascular dysfunction, baroreflex dysfunction, and oxidative stress in iron-overloaded mice," *Vascular Pharmacology*, vol. 87, pp. 199–208, 2016.

[16] H. Pei, Q. Yu, Q. Xue et al., "Notch1 cardioprotection in myocardial ischemia/reperfusion involves reduction of oxidative-/nitrative stress," *Basic Research in Cardiology*, vol. 108, no. 5, p. 373, 2013.

[17] J. Wang, E. Gao, T. O. Chan et al., "Induced overexpression of Na$^+$/Ca2$^+$ exchanger does not aggravate myocardial dysfunction induced by transverse aortic constriction," *Journal of Cardiac Failure*, vol. 19, no. 1, pp. 60–70, 2013.

[18] M. Zhai, Z. Liu, B. Zhang et al., "Melatonin protects against the pathological cardiac hypertrophy induced by transverse aortic constriction through activating PGC-1β: in vivo and in vitro studies," *Journal of Pineal Research*, vol. 63, no. 3, 2017.

[19] Z. W. Pan, Y. Zhang, D. H. Mei et al., "Scutellarin exerts its anti-hypertrophic effects via suppressing the Ca2$^+$-mediated calcineurin and CaMKII signaling pathways," *Naunyn-Schmiedeberg's Archives of Pharmacology*, vol. 381, no. 2, pp. 137–145, 2010.

[20] S. Mishra, M. Mishra, P. Seth, and S. K. Sharma, "Tetrahydrocurcumin confers protection against amyloid β-induced toxicity," *Neuroreport*, vol. 22, no. 1, pp. 23–27, 2011.

[21] B. Zhang, M. Zhai, B. Li et al., "Honokiol ameliorates myocardial ischemia/reperfusion injury in type 1 diabetic rats by reducing oxidative stress and apoptosis through activating the SIRT1-Nrf2 signaling pathway," *Oxidative Medicine and Cellular Longevity*, vol. 2018, Article ID 3159801, 16 pages, 2018.

[22] A. L. Moens, E. Takimoto, C. G. Tocchetti et al., "Reversal of cardiac hypertrophy and fibrosis from pressure overload by tetrahydrobiopterin: efficacy of recoupling nitric oxide synthase as a therapeutic strategy," *Circulation*, vol. 117, no. 20, pp. 2626–2636, 2008.

[23] J. D. Melgarejo, G. E. Maestre, L. Thijs et al., "Prevalence, treatment, and control rates of conventional and ambulatory hypertension across 10 populations in 3 continents," *Hypertension*, vol. 70, no. 1, pp. 50–58, 2017.

[24] X. Tang, X. F. Chen, N. Y. Wang et al., "SIRT2 acts as a cardioprotective deacetylase in pathological cardiac hypertrophy," *Circulation*, vol. 136, no. 21, pp. 2051–2067, 2017.

[25] G. G. Schiattarella and J. A. Hill, "Inhibition of hypertrophy is a good therapeutic strategy in ventricular pressure overload," *Circulation*, vol. 131, no. 16, pp. 1435–1447, 2015.

[26] W. Sangartit, U. Kukongviriyapan, W. Donpunha et al., "Tetrahydrocurcumin protects against cadmium-induced hypertension, raised arterial stiffness and vascular remodeling in mice," *PLoS One*, vol. 9, no. 12, article e114908, 2014.

[27] K. Li, M. Zhai, L. Jiang et al., "Tetrahydrocurcumin Ameliorates Diabetic Cardiomyopathy by Attenuating High Glucose-Induced Oxidative Stress and Fibrosis via Activating the SIRT1 Pathway," *Oxidative Medicine and Cellular Longevity*, vol. 2019, Article ID 6746907, pp. 1–15, 2019.

[28] D. C. Rockey, P. D. Bell, and J. A. Hill, "Fibrosis–a common pathway to organ injury and failure," *The New England Journal of Medicine*, vol. 372, no. 12, pp. 1138–1149, 2015.

[29] P. VanBuren, D. E. Harris, N. R. Alpert, and D. M. Warshaw, "Cardiac V1 and V3 myosins differ in their hydrolytic and mechanical activities in vitro," *Circulation Research*, vol. 77, no. 2, pp. 439–444, 1995.

[30] K. Nakao, W. Minobe, R. Roden, M. R. Bristow, and L. A. Leinwand, "Myosin heavy chain gene expression in human heart failure," *The Journal of Clinical Investigation*, vol. 100, no. 9, pp. 2362–2370, 1997.

[31] J. James, L. Martin, M. Krenz et al., "Forced expression of alpha-myosin heavy chain in the rabbit ventricle results in cardioprotection under cardiomyopathic conditions," *Circulation*, vol. 111, no. 18, pp. 2339–2346, 2005.

[32] K. Huynh, B. C. Bernardo, J. R. McMullen, and R. H. Ritchie, "Diabetic cardiomyopathy: mechanisms and new treatment strategies targeting antioxidant signaling pathways," *Pharmacology & Therapeutics*, vol. 142, no. 3, pp. 375–415, 2014.

[33] C. Murdoch, M. Zhang, A. Cave, and A. Shah, "NADPH oxidase-dependent redox signalling in cardiac hypertrophy, remodelling and failure," *Cardiovascular Research*, vol. 71, no. 2, pp. 208–215, 2006.

[34] D. A. Siwik and W. S. Colucci, "Regulation of matrix metalloproteinases by cytokines and reactive oxygen/nitrogen species in the myocardium," *Heart Failure Reviews*, vol. 9, no. 1, pp. 43–51, 2004.

[35] M. Naito, X. Wu, H. Nomura et al., "The protective effects of tetrahydrocurcumin on oxidative stress in cholesterol-fed rabbits," *Journal of Atherosclerosis and Thrombosis*, vol. 9, no. 5, pp. 243–250, 2002.

[36] N. Diguet, S. A. J. Trammell, C. Tannous et al., "Nicotinamide riboside preserves cardiac function in a mouse model of dilated cardiomyopathy," *Circulation*, vol. 137, no. 21, pp. 2256–2273, 2018.

[37] R. R. Gao, X. D. Wu, H. M. Jiang et al., "Traditional Chinese medicine Qiliqiangxin attenuates phenylephrine-induced cardiac hypertrophy via upregulating PPARγ and PGC-1α," *Annals of Translational Medicine*, vol. 6, no. 8, p. 153, 2018.

[38] Y. Chen, Y. Chang, N. Zhang, X. Guo, G. Sun, and Y. Sun, "Atorvastatin attenuates myocardial hypertrophy in spontaneously hypertensive rats via the C/EBPβ/PGC-1α/UCP3

pathway," *Cellular Physiology and Biochemistry : International Journal of Experimental Cellular Physiology, Biochemistry, and Pharmacology*, vol. 46, no. 3, pp. 1009–1018, 2018.

[39] X. Zhang, H. Hu, J. Luo et al., "A novel danshensu-tetramethylpyrazine conjugate DT-010 provides cardioprotection through the PGC-1α/Nrf2/HO-1 pathway," *Biological & Pharmaceutical Bulletin*, vol. 40, no. 9, pp. 1490–1498, 2017.

[40] Z. Ping, L.-f. Zhang, Y.-j. Cui et al., "The protective effects of salidroside from exhaustive exercise-induced heart injury by enhancing the PGC-1 α-NRF1/NRF2 pathway and mitochondrial respiratory function in rats," *Oxidative Medicine and Cellular Longevity*, vol. 2015, Article ID 876825, 9 pages, 2015.

Research Article

Peptidomics Analysis Reveals Peptide PDCryab1 Inhibits Doxorubicin-Induced Cardiotoxicity

Li Zhang ⓘ,[1] **Xuejun Wang** ⓘ,[1] **Mengwen Feng** ⓘ,[1] **Hao Zhang** ⓘ,[1] **Jia Xu** ⓘ,[1]
Jingjing Ding ⓘ,[2] **Zijie Cheng** ⓘ,[1] **and Lingmei Qian** ⓘ[1,3]

[1]*Department of Cardiology, The First Affiliated Hospital of Nanjing Medical University, Nanjing 210029, China*
[2]*Department of General Practice, Tongren Hospital, Shanghai Jiao Tong University School of Medicine, 1111 Xianxia Road,*
 Shanghai 200336, China
[3]*Department of Cardiology, Tongren Hospital, Shanghai Jiao Tong University School of Medicine, 1111 Xianxia Road,*
 Shanghai 200336, China

Correspondence should be addressed to Zijie Cheng; zjcheng@njmu.edu.cn and Lingmei Qian; lmqian@njmu.edu.cn

Doxorubicin (DOX) is limited due to dose-dependent cardiotoxicity. Peptidomics is an emerging field of proteomics that has attracted much attention because it can be used to study the composition and content of endogenous peptides in various organisms. Endogenous peptides participate in various biological processes and are important sources of candidates for drug development. To explore peptide changes related to DOX-induced cardiotoxicity and to find peptides with cardioprotective function, we compared the expression profiles of peptides in the hearts of DOX-treated and control mice by mass spectrometry. The results showed that 236 differential peptides were identified upon DOX treatment, of which 22 were upregulated and 214 were downregulated. Next, we predicted that 31 peptides may have cardioprotective function by conducting bioinformatics analysis on the domains of each precursor protein, the predicted score of peptide biological activity, and the correlation of each peptide with cardiac events. Finally, we verified that a peptide (SPFYLRPPSF) from Cryab can inhibit cardiomyocyte apoptosis, reduce the production of reactive oxygen species, improve cardiac function, and ameliorate myocardial fibrosis in vitro and vivo. In conclusion, our results showed that the expression profiles of peptides in cardiac tissue change significantly upon DOX treatment and that these differentially expressed peptides have potential cardioprotective functions. Our study suggests a new direction for the treatment of DOX-induced cardiotoxicity.

1. Introduction

Doxorubicin (DOX), a typical broad-spectrum and highly effective antitumor drug, is widely used in the clinical treatment of various malignant tumors, such as breast cancer, lymphoma, and leukemia [1]. However, its widespread clinical application is limited by cumulative dose-dependent toxicity in multiple organs, especially cardiotoxicity [2]. Research has shown that DOX can induce chronic heart failure when the cumulative clinical dose exceeds 400-700 mg/m^2 (adult) or 300 mg/m^2 (child), which greatly limits the dose of DOX for clinical treatment [3]. It is currently recognized that the main mechanism of DOX-induced cardiotoxicity is oxidative stress and the apoptosis of cardiomyo-

cytes [4, 5]. DOX can induce cardiomyocyte apoptosis, which can develop into chronic heart failure, through the generation of a large amount of reactive oxygen species and cell calcium overload because of its high affinity for myocardial tissue and tendency for accumulation in cardiomyocytes [6, 7]. Currently, no drugs except dexrazoxane can be utilized clinically to prevent or cure DOX-induced cardiotoxicity. Therefore, to find an intervention strategy, it is necessary to explore the mechanism of cardiotoxicity caused by DOX from a new perspective.

Peptidomics, an emerging field of proteomics [8], is a method for comprehensively analyzing peptides in various biological samples by mass spectrometry [9, 10]. It can be used for systematically, qualitatively, and quantitatively

studying the composition and content of endogenous peptides in organisms under physiological or pathological conditions. With the development of peptidomics, a class of small-molecule peptides composed of 3-50 amino acids has been found to be important participants in a variety of life activities, including apoptosis [11], immune regulation [12], cell differentiation [13], nervous system regulation [14], and reproduction regulation [15], and because of their advantages, such as easy synthesis, small molecular weight, nontoxic metabolites, and easy access to cells, they have become a new favorite in the field of drug research and development [16]. Humanin, a 24 amino acid peptide, is encoded by the open reading frame in the mitochondrial 16S rRNA region and has shown cardiomyocyte protection and antioxidant and antiapoptosis properties [17, 18]. Humanin can enhance the cardioprotective effect of dexrazoxane on DOX-induced cardiotoxicity, which may indicate its use as an adjuvant for dexrazoxane to reduce DOX-induced cardiotoxicity [19]. Exenatide pretreatment inhibits DOX-induced production of reactive oxygen species and apoptosis in cardiomyocytes and improves cardiac dysfunction through the upregulation of autophagy, indicating its therapeutic potential for preventing DOX-induced cardiotoxicity [20]. Apelin is an endogenous peptide ligand of the APJ receptor that can prevent the activation of cardiac fibroblasts and the production of collagen by inhibiting sphingosine kinase 1. In addition, the use of apelin in the stage of reactive fibrosis can prevent myocardial structural remodeling and ventricular dysfunction [21]. Therefore, considering peptides, we may find new clues for the protection of DOX-induced cardiotoxicity.

In this study, we established a cardiotoxicity model by continuous doxorubicin injection. Nano-LC-MS/MS mass spectrometry was utilized to explore the dynamic changes in the composition of the endogenous peptides in mouse heart tissue and screen for potentially functional peptides related to DOX-induced cardiotoxicity. Subsequently, we analyzed the differentially expressed peptides using a bioinformatics approach and predicted 31 peptides that may have cardioprotective functions. Finally, a peptide derived from Cryab was verified to antagonize cardiomyocyte apoptosis and reduce ROS production. This study used peptidomics as an entry point to explore the means of preventing or ameliorating the cardiotoxicity caused by doxorubicin, providing new ideas for the study of DOX-induced cardiotoxicity.

2. Materials and Methods

2.1. Mice. Six-week-old male C57BL/6 mice weighing 16-20 g were purchased from the Shanghai Slake Experimental Animal Co., Ltd., and raised at the SPF Laboratory Animal Center of Nanjing Medical University. The experiment was started one week after the animals were purchased. The experimental animals were randomly allocated to two groups: the control group and the DOX group, with 12 mice in each group. In the DOX group, the mice were injected intraperitoneally with 5 mg/kg DOX a week for a total of 4 injections with a cumulative dose of 20 mg/kg [22], while the control group was injected intraperitoneally with an equal volume of saline. All animal experiments were carried out in accordance with the Guide for the Care and Use of Laboratory Animals published by the National Institutes of Health (NIH Publications No. 85-23, revised 1996) and reviewed by the Animal Experiment Ethics Committee of Nanjing Medical University (Nanjing, China).

2.2. Echocardiography and Histological Determination. After DOX or saline administration, the animals were maintained for 2 weeks; mice were lightly anesthetized with 1.5% isoflurane and allowed to breathe spontaneously, and then echocardiography was performed to detect mouse cardiac function. High-resolution small animal ultrasound imaging system (Vevo 3100) was used to obtain M-mode ultrasound measurements for the DOX injection group and normal group mice. The main measurement indicators included ejection fraction (EF) and fractional shortening (FS). Other echocardiographic parameters including left ventricular end-systolic diameter (LVEDs), left ventricular end-diastolic diameter (LVEDd), left ventricular end-systolic anterior wall thickness (LVAWs), and left ventricular end-diastolic anterior wall thickness (LVAWd). Further, left ventricular fractional shortening (FS%) was calculated as $[(LVEDd - LVEDs)/LVEDd] \times 100$; left ventricular ejection fraction (EF%) was calculated as $[(LVEDV - LVESV)/LVEDV] \times 100$, $LVEDV = [7 LVEDd^3/(2.4 + LVEDd)]$, and $LVESV = [7 LVEDs^3/(2.4 + LVEDs)]$. After the mice were euthanized by carbon dioxide asphyxiation, the ventricular tissue was collected and immediately fixed in 4% paraformaldehyde for 48 hours. Samples were dehydrated, paraffin embedded, and sectioned into 5 μm thick slices on a sliding microtome (Leica, Nussloch, Germany). Then, the myocardial sections were dewaxed, rehydrated, and stained with Masson's trichrome, and the degree of myocardial fibrosis was observed under the microscope. Blue collagen staining was quantified using ImageJ software (version 1.52t, National Institutes of Health, Bethesda, MD, USA).

2.3. Peptide Extraction. The heart tissue samples were added with Tris-HCl according to the volume ratio of 1 : 3, heated and boiled for 10 min, then cooled in an ice water bath, and then broken by ultrasonic wave at 100 Hz for more than 5 s, with an interval of 5 s and ultrasonication for 2 min. Then, the final concentration of 1 M glacial acetic acid was added into the sample tube, and vortex oscillation was performed for 2 min. Then, acetonitrile with final concentration of about 50% was added. The sample tube was centrifuged at $12000 \times g$ at 4°C for 10 min; after that, the supernatant was transferred to a clean EP tube for freeze-drying. Next, add 80% acetone solution, vortex, vibrate, ultrasonicate in a water bath for 2 min and 4°C, centrifugate at high speed at $20000 \times g$ for 30 min, and then take the supernatant and transfer to a clean EP tube for freeze-drying. Finally, add 200 μl of 0.1% TFA solution for redissolution and remove salt with C18 with sample loading of 80 μg, freeze-dry, and set aside.

2.4. LC/MS and Peptide Identification. We considered that the heart of mice was small. In order to make the sample quality detected by mass spectrometry more sufficient, we

used the hearts of four mice to mix into one sample. Four mouse heart tissues of DOX treatment were mixed as one DOX sample and four normal mouse heart tissues were mixed as one control sample, a total of three groups of DOX and three groups of control. The peptides were identified by nano-LC-MS/MS on a Q Exactive Plus mass spectrometer (Thermo) couple with LC1000. Solvent A (Milli-Q [Millipore, Billerica, MA] water with 0.1% formic acid and 2% acetonitrile) and solvent B (90% acetonitrile with 0.1% formic acid) were used for chromatographic separation. The peptides were eluted with 5% solvent B for 5 minutes at a rate of 300 nl/min, 5-40% solvent B for 65 minutes, 40-80% solvent B for 1 minute, 80% solvent B for 4 minutes, and then 5% solvent B over 20 minutes. Q Exactive Plus (Thermo Fisher) was performed in an information-dependent data acquisition mode to enable automatically switching between MS and MS/MS acquisition. MS spectra were obtained in the mass range of 350-2000 m/z. Xcalibur software (Thermo Scientific, version 3.1.66.10) was used for automatic peak identification, 10 s dynamic exclusion, and tandem mass spectrometry analysis of the top 20 precursor protein ions at 30% normalized collision energy. The intensities of identified peptides were calculated by MaxQuant software (version 1.6.6.0) and used label-free quantification.

All MS/MS data were analyzed by MaxQuant software, and the UniProt_mouse database (UniProt release 2019_11) was searched based on nonspecific digestion technology. The mass tolerance of the fragment ion in MaxQuant was 0.050 Da and that of the parent ion was 10.0 PPM. Oxidation of methionine was designated as a variable modification. The selection criterion for the differentially expressed peptides was a fold change larger than 2 with a P value < 0.05 (Student's t-test).

2.5. Bioinformatics Analysis. The peptide isoelectric point (PI) and molecular weight (MW) information were obtained online (https://web.expasy.org/protparam/). First, the UniProt database (http://www.uniport.org/) was used to find the source of differential peptides. Functional Annotation Tool DAVID Bioinformatics Resources 6.8 (https://david.ncifcrf.gov/) was used to elucidate the potential functions of the precursor proteins of the identified peptides according to the biological process, molecular function, and cellular component categories of Gene Ontology (GO) annotations and KEGG pathways. Second, the relationship of the differential peptides' precursor proteins with various cardiovascular diseases and apoptosis was analyzed using the GeneAnalytics website (http://geneanalytics.genecards.org/) and Cytoscape 3.5.1 software. Third, the biological activity of peptides was predicted through Peptide Ranker [23, 24] (http://bioware.ucd.ie/~compass/biowareweb/, ranker scores greater than 0.5 indicate possible activity) in order to find potential peptides. The protein interactions were analyzed using the STRING website (https://string-db.org/, version: 11.0) and Cytoscape 3.5.1 software. The amino acid sequences of the different species were analyzed using the protein database on the NCBI website (https://www.ncbi.nlm.nih.gov/homologene/), and the results were compared with DNAMAN (version 9.0) software.

2.6. Peptide Synthesis and Administration. The following peptide sequences were synthesized in this experiment: PDCryab1: RKKRRQRRR-SPFYLRPPSF, PDCryab2: RKKRRQRRR-SPFYLRPPSFLR, PDCryab3: RKKRRQRRR-SPFYLRPPSFLRAPS, PDCryab4: RKKRRQRRR-TSLSPFYLRPPSFL, and scramble peptide of PDCryab1: RKKRRQRRR-LSFRFPSPYP. We used scramble peptide to serve as the control peptide, which shares same amino acids with Cryab but sequenced as a scramble peptide.

The RKKRRQRRR sequence is a cell-penetrating peptide composed of nine amino acids in HIV-1 Tat (49-57). The purity of all peptides was more than 95%. The peptides were synthesized by the Shanghai Science Peptide Biological Technology Co., Ltd. (Shanghai, China). The peptide crystal was dissolved in sterile water to obtain a storage solution of 10 mM and diluted to the final concentration corresponding to the experiment. For the cell experiments, peptides were added to the culture supernatant 2 hours before DOX treatment.

2.7. Cell Culture and Experimental Design. The H9c2 cell line of rat cardiomyocytes was purchased from the Cell Bank of the Shanghai Academy of Biosciences. H9c2 cells were cultured in a sterile incubator (37°C, 5% CO_2) with high-glucose DMEM supplemented with 10% fetal bovine serum and 1% penicillin and streptomycin. The H9c2 cells were subcultured every 2 days and were in good condition for use in the experiments.

For the initial cell experiments, the cells were allocated to 6 groups: (I) control group, (II) DOX (1 μM) treatment group (DOX), (III) DOX and PDCryab1 (50 μM) [25, 26] cotreatment group (DOX+P1), (IV) DOX and PDCryab2 (50 μM) cotreatment group (DOX+P2), (V) DOX and PDCryab3 (50 μM) cotreatment group (DOX+P3), and (VI) DOX and PDCryab4 (50 μM) cotreatment group (DOX+P4). In addition, for the subsequent cell experiments, the cells were allocated to the following groups: (I) control group, (II) PDCryab1 (50 μM) treatment group, (III) DOX (1 μM) treatment group (DOX), (IV) DOX and PDCryab1 (10 μM) cotreatment group (10), (V) DOX and PDCryab1 (20 μM) cotreatment group (20), and (VI) DOX and PDCryab1 (50 μM) cotreatment group (50). After 24 hours of these treatments, the cells were collected for the appropriate analysis.

2.8. Analysis of Cell Viability. Cell viability was determined with a cell counting kit-8 (CCK-8) kit (Dojindo Molecular Technologies, Inc., Kumamoto, Japan) according to the following steps. The subcultured H9c2 cells were seeded in 96-well plates at a density of 1×10^4 cells/well, and upon reaching the adherence stage, the cells were treated with drugs as described above. Ten microliters of the CCK-8 reagent was added to each well and maintained away from light in 37°C incubators. After incubation for 2 hours, the intensity of the light absorption at 450 nm wavelength was measured by a microplate reader.

2.9. Western Blot Analysis. The protein in the H9c2 cells was extracted with lysis buffer (including RIPA and 1% PMSF)

and quantified by a BCA assay kit (23229; Thermo Fisher Scientific). The protein samples were mixed with 1x SDS loading buffer and denatured by boiling at 95°C for 5 minutes. After cooling on ice for 4 minutes, the protein samples were separated by 10% SDS-PAGE gel and then transferred to nitrocellulose membranes (Millipore, USA). After being blocked with 5% skimmed milk at room temperature for 1.5 hours, specific antibodies, namely, anti-PARP (1 : 1000, #9542, CST), anti-caspase3 (1 : 1000, #9665, CST), β-actin (1 : 2000, #4970, CST), and antitubulin α/β (1 : 2000, #2148, CST), were incubated with the membrane overnight at 4°C. The membrane was washed once with TBST buffer 5 times for 5 minutes each time. Protein expression was quantitatively analyzed by Image Lab software (Bio-Rad, Hercules, CA, USA). Western blot results were normalized by tubulin or β-actin.

2.10. Detection of ROS, SOD, and MDA. Reactive oxygen species (ROS) were detected by an ROS assay kit (Beyotime, China) according to standard procedures. H9c2 cells were passaged to a 6-well plate at a density of 2×10^5 cells/well. After the cells reached 80% confluence, the cells were treated with drugs for a specified time. The DCFH-DA fluorescence probe was diluted to $10 \mu M$ in DMEM without serum. The 6-well plate medium was transferred to a clean centrifuge tube for preservation, and 1 ml of diluted DCFH-DA fluorescence probe was added to each well and incubated at 37 °C in the dark for 20 minutes. After incubation, the supernatant was discarded, and the cells were washed twice with serum-free DMEM medium and then washed twice with PBS. The ROS fluorescence intensity in the cells was observed by inverted fluorescence microscopy and quantified by ImageJ software. SOD and MDA assay kits (Nanjing Jiancheng Biocompany) are used to detect SOD and MDA levels in the cell supernatant that has been retained according to the protocol.

2.11. Mitochondrial Membrane Potential. JC-1 Mitochondrial Membrane Potential Assay Kit (Beyotime, China) was used to analyze mitochondrial injury according to the manufacturer's instructions. In short, the cells were washed with PBS and incubated with JC solution for 10 min at 37°C. And then, the cells were washed with dilution buffer again and analyzed on a laser scanning confocal microscope.

2.12. TUNEL Assay. Cells were seeded (1×10^5 cells per well) in 6-well plates. After DOX treatment, the cells were washed twice with PBS and fixed with 4% paraformaldehyde. Apoptotic cells were visualized with TUNEL staining according to the manufacturer's protocol (Promega). TUNEL fluorescence intensity/DAPI fluorescence density was used to calculate the percentage of positive cells, and the density was evaluated using ImageJ software 1.26 (Wayne Rasband, National Institutes of Health, Bethesda, MD, USA).

2.13. LDH Release. The level of LDH was detected by LDH Release Assay Kit (Beyotime, China). The reaction solution was prepared according to the manufacturer's instructions. The cell supernatant or serum ($120 \mu l$/well) was collected and mixed with reaction solution ($60 \mu l$/well), and then the mixtures were added into 96-well plates. The cells were

wrapped in tin foil and incubated for 30 min at RT on the shaker. Finally, the absorbance was detected with a microplate reader at 490 nm wavelength.

2.14. Histological Staining. Hearts were harvested and immediately fixed in 4% paraformaldehyde for 48 hours. Samples were dehydrated, paraffin embedded, sectioned into $5 \mu m$ thick slices on a sliding microtome (Leica, Nussloch, Germany), and stained with Sirius red and hematoxylin and eosin (H&E). The yocyte cross-sectional areas were measured via fluorescein isothiocyanate-conjugated WGA (L4895; Sigma, St. Louis, MO, USA) staining. A quantitative digital image analysis system (Image-Pro Plus 6.0) was used to measure the cross-sectional area of the cardiomyocyte from images that had been captured from fluorescein isothiocyanate- (FITC-) conjugated wheat germ agglutinin- (WGA-) (Invitrogen, Thermo Fisher Scientific) stained sections.

2.15. Real-Time PCR. Total RNA was extracted from cells using TRIzol reagent (Thermo Fisher Scientific). The concentration of RNA was determined by measuring the absorbance ratio of 260/280 nm using a NanoDrop ND-1000 spectrophotometer (Thermo Scientific). Reverse transcription of RNA was performed using a PrimeScript™ RT Reagent Kit with gDNA eraser (RR047A; Takara, Tokyo, Japan), and cDNA was analyzed by qRT-PCR using SYBR® Premix Ex Taq™ (RR420A; Takara, Tokyo, Japan). The data were normalized to the levels of GAPDH and further analyzed using the $2^{-\Delta\Delta CT}$ method.

2.16. Statistical Analysis. The experimental data and statistical graphs were analyzed by GraphPad Prism 8 software. All data are presented as the means ± standard deviation (SD). Statistical differences were measured with an unpaired 2-sided Student t-test or 2-way ANOVA with Bonferroni correction for multiple comparisons. When the P value < 0.05, the difference was considered significant.

3. Results

3.1. Peptidomics Research Process Using Mouse Heart Tissue. We used male C57BL/6 mice to construct an animal model of cardiotoxicity by intraperitoneally injecting DOX and then collecting heart tissues to extract peptides for mass spectrometry analysis. The schematic process is shown in Figure 1(a). Dox-induced cardiac dysfunction was remarkably decreased in the Dox injection group, which was indicated by a decrease in EF and FS (Figures 1(b) and 1(c)). Masson's staining results showed the cardiac fibrosis alterations, as evidenced by cardiac fiber rupture and decreased cardiomyocyte area (Figures 1(d) and 1(e)). Thus, we established a cardiotoxicity model induced by DOX injection.

3.2. Identification of Differential Peptide Expression Profiles Related to DOX-Induced Cardiotoxicity. Mass spectrometry results revealed 2945 detected peptides, 236 of which were differentially expressed (P value < 0.05 and fold change ≥2) (Supple. Table 1). In the DOX-induced cardiotoxicity group, 22 peptides were upregulated and 214 peptides were downregulated (Figure 2(a)). The heat map shows the
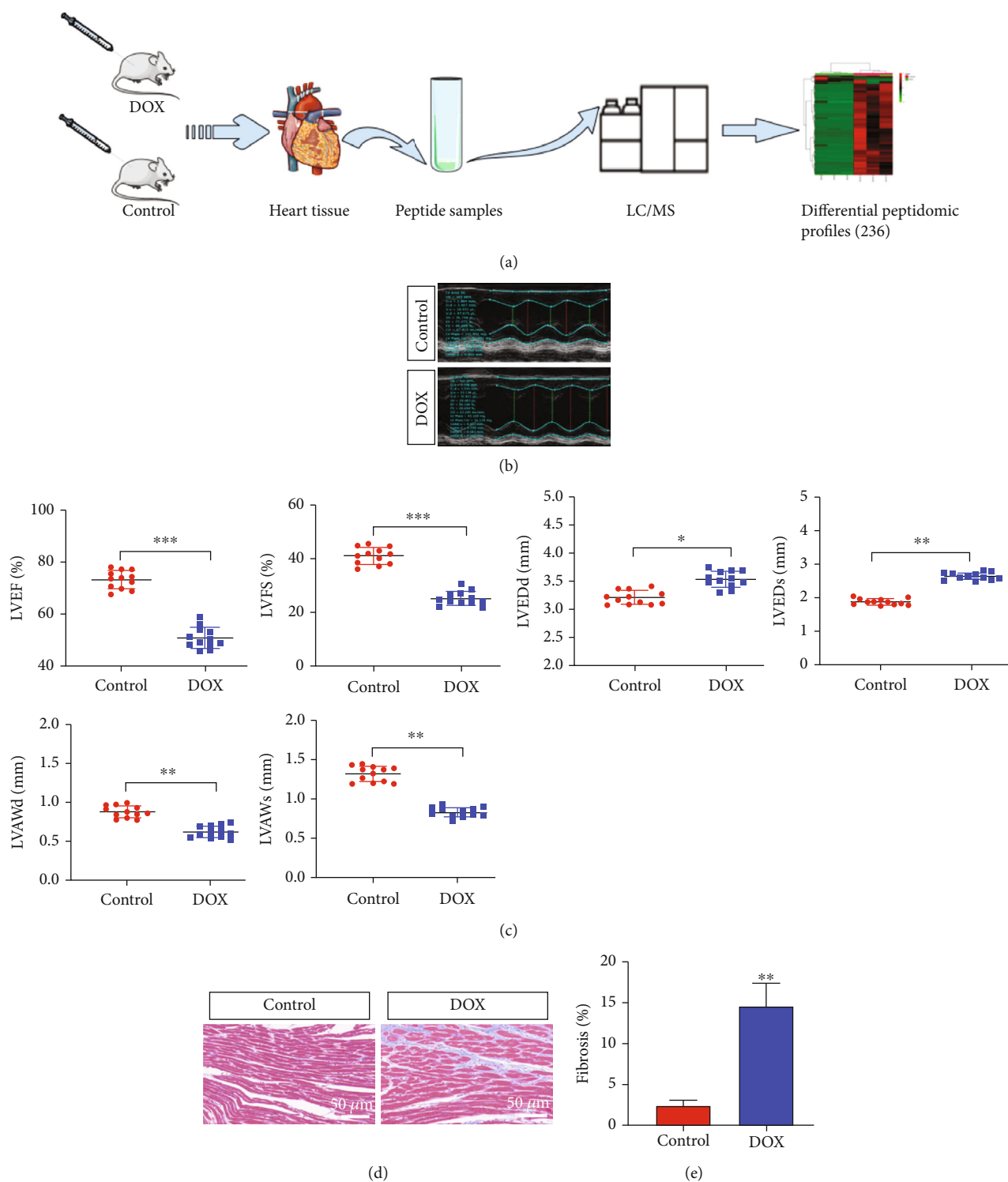
(a)

(b)

(c)

(d)

(e)

FIGURE 1: Peptidomics research process and the successful construction of a mouse model. (a) The process of peptide identification in the mouse heart tissues by LC/MS mass spectrometry. (b) Representative M-mode echocardiography-derived graphs of the DOX group and control group. (c) Quantitative data echocardiography analysis ($N = 12$ mice per group). (d, e) Representative photographs of Masson's trichrome staining show cardiac fiber rupture and decreased cardiomyocyte area in the DOX group. Quantification data of Masson's trichrome staining. Magnified 400x. The data represent the means ± SD. ***$P < 0.001$.

significant differences in the peptide profiles of cardiotoxic tissues treated with doxorubicin and normal heart tissues (Figure 2(b)). 47 peptides were expressed exclusively in the control group and 5 peptides were expressed in the DOX group (Supple. Table 2). Three peptides possessing 7 different precursor proteins are listed in Supple. Table 3.

(a)

(b)

(c)

(d)

(e)

(f)
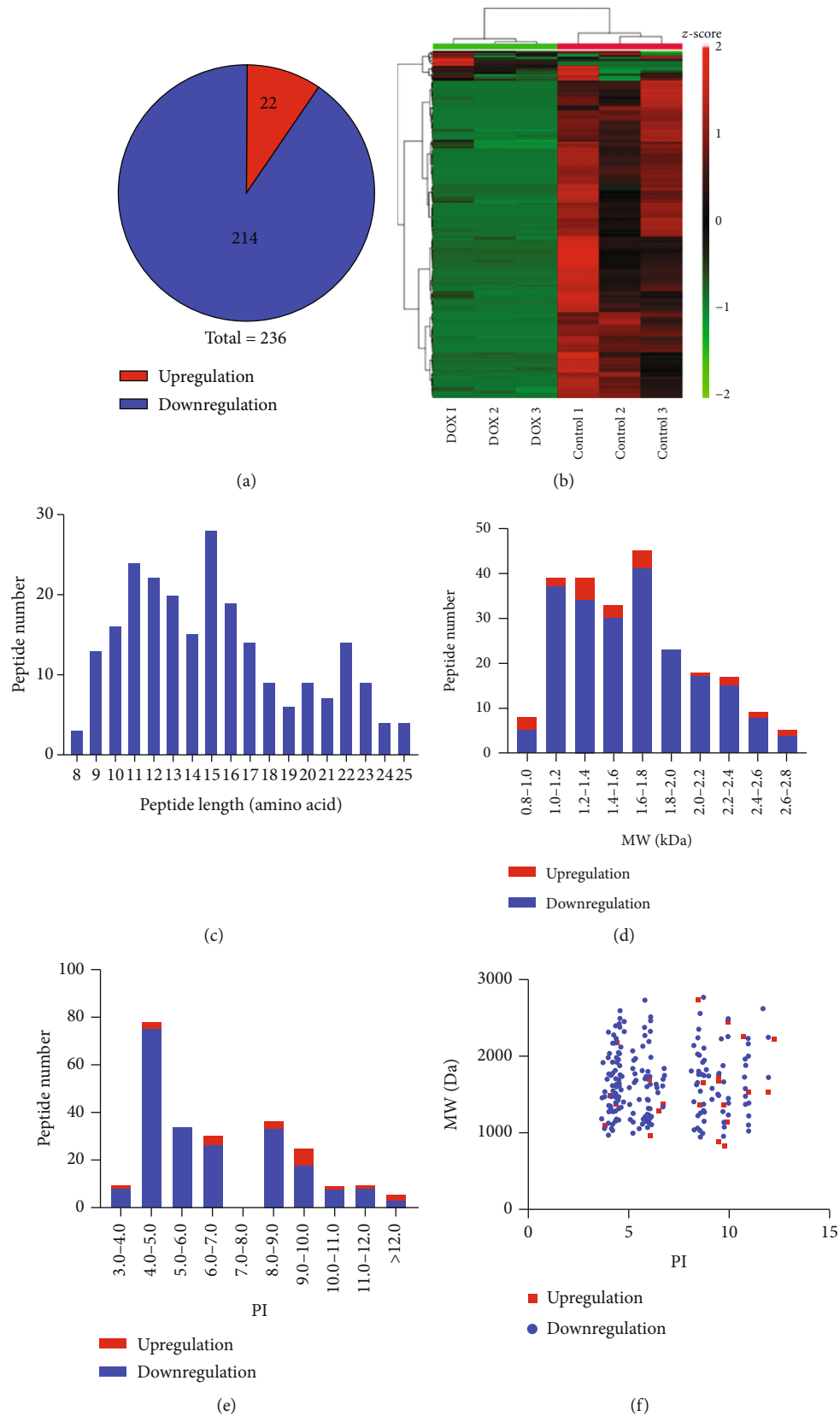
FIGURE 2: Identification and features of differentially expressed peptides. (a) Identification of the number of differentially expressed peptides. (b) Heat map of the differentially expressed peptides. Red indicates upregulation, and green indicates downregulation. (c) Distribution of the differentially expressed peptides by length. (d) Molecular weight (MW) of the differentially expressed peptides. (e) Isoelectric point (PI) of the differentially expressed peptides. (f) The correlation between the distribution of differentially expressed peptides by MW and PI.

FIGURE 3: Analysis of four cleavage sites of the differentially expressed peptides. (a) The distribution of the four cleavage sites in the upregulated peptides. (b) The distribution of four cleavage sites in the downregulated peptides.

We found that the distribution of different peptide lengths was relatively large and mainly concentrated in two ranges: 9-17 and 22-23 amino acids (Figure 2(c)). We also explored the molecular weight (MW) and isoelectr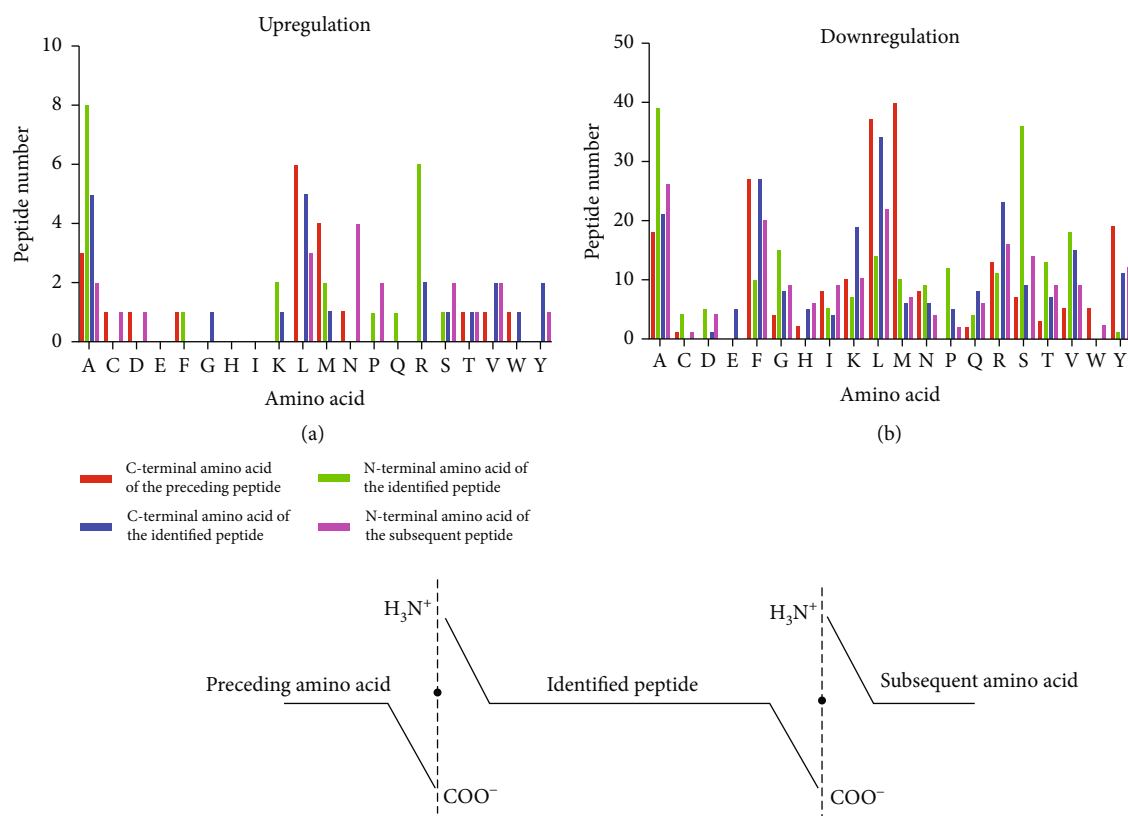ic point (PI) of differentially expressed peptides and found that the MW of the differentially expressed peptides was distributed between 0.8 and 2.8 kDa, with the downregulated peptides mainly concentrated in the 1.0-2.0 kDa range and the upregulated peptides concentrated in the 0.8-1.0 kDa and 1.2-1.8 kDa ranges (Figure 2(d)). The isoelectric point analysis showed that, overall, the differentially expressed peptides were mainly in the PI 4-7 and PI 8-10 ranges (Figure 2(e)). The distribution of upregulated and downregulated peptides was consistent with that of all peptides, and there was no significant difference in the distribution between the upregulated and downregulated groups. In addition, we analyzed the correlation between the distribution of differential peptide MW and PIs. The peptides were mainly clustered into four groups: near PI 4, PI 6, PI 8, and PI 10 (Figure 2(f)).

3.3. Analysis of Four Cleavage Sites in the Differentially Expressed Peptides.
Based on the peptide described data, we analyzed the C-terminal and N-terminal cleavage sites of the differentially expressed peptides, which mainly included the following four cleavage sites: the C-terminal amino acid of the preceding peptide, the N-terminal amino acid of the identified peptide, the C-terminal amino acid of the identi-

fied peptide, and the N-terminal amino acid of the subsequent peptide. In the upregulated peptide group, leucine (L) was the most abundant amino acid at the C-terminus of the preceding peptide, alanine (A) was the most abundant amino acid at the N-terminus of the identified peptide, alanine (A) and leucine (L) were the most abundant amino acids at the C-terminus of the identified peptide, and asparagine (N) was the most abundant amino acid at the N-terminus of the subsequent peptide (Figure 3(a)). In the downregulated group, the most abundant amino acids in the above four cleavage sites were methionine (M), alanine (A), leucine (L), and alanine (A), as shown in Figure 3(b). The four cleavage sites of 236 peptides were different in the upregulated and downregulated groups.

3.4. Bioinformatics Analysis.
To predict the potential function of 236 differentially expressed peptides, we performed GO and pathway analysis on their precursor proteins. GO analysis results showed the molecular function, biological process, and cellular component in the downregulation proteins (Figures 4(a)–4(c)). Interestingly, we found that downregulated proteins were mainly associated with Poly(A) RNA binding, transport, and mitochondrial function. Downregulated protein analysis showed transmembrane transporter activity, ATP synthesis, mitochondrial respiratory chain (Figures 4(d)–4(f)). The KEGG pathway analysis showed that the precursor proteins of the differential peptides were mainly involved in oxidative phosphorylation

Molecular function

(a)

Biological process

(b)

Cellular component

(c)

FIGURE 4: Continued.

(d)

(e)

(f)
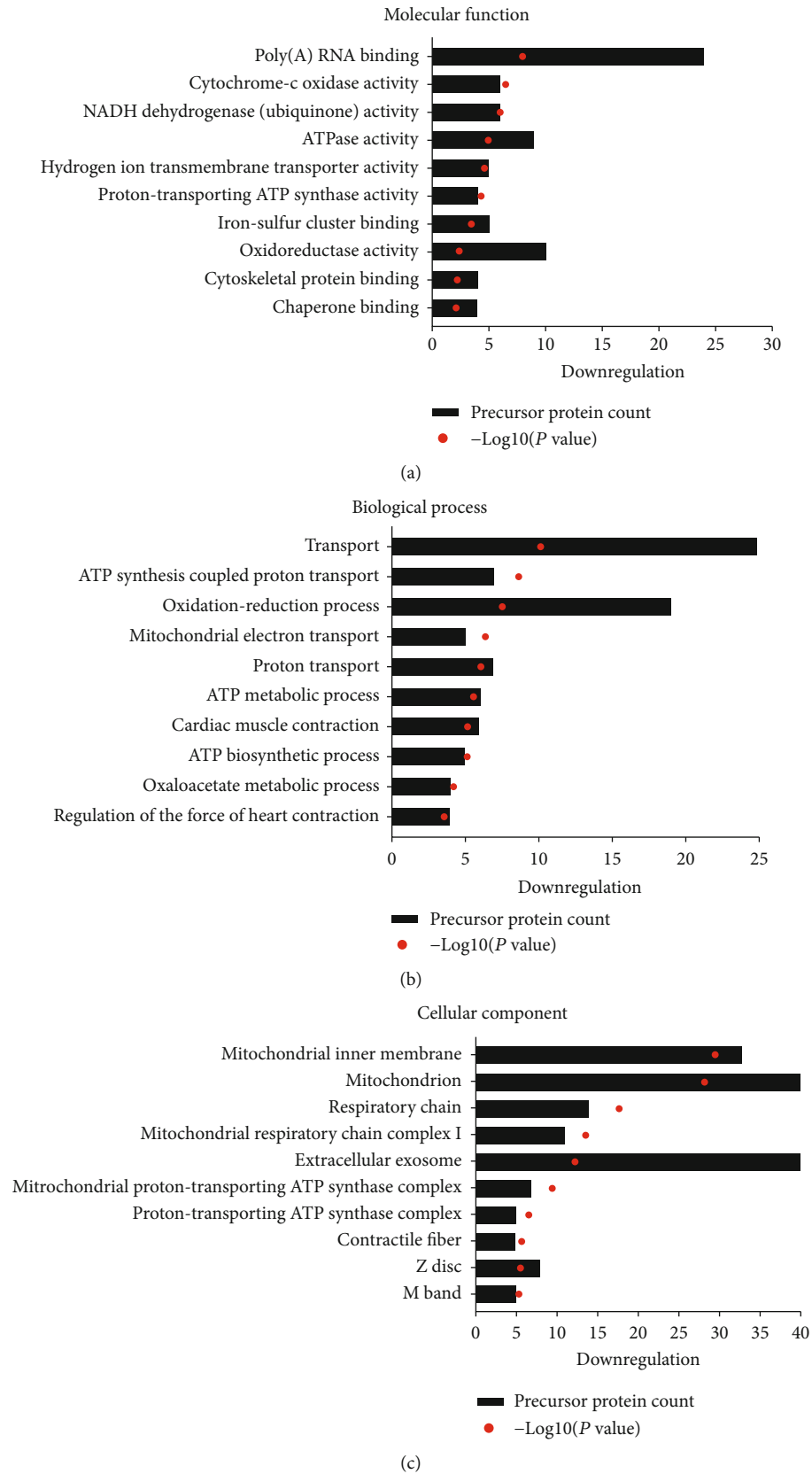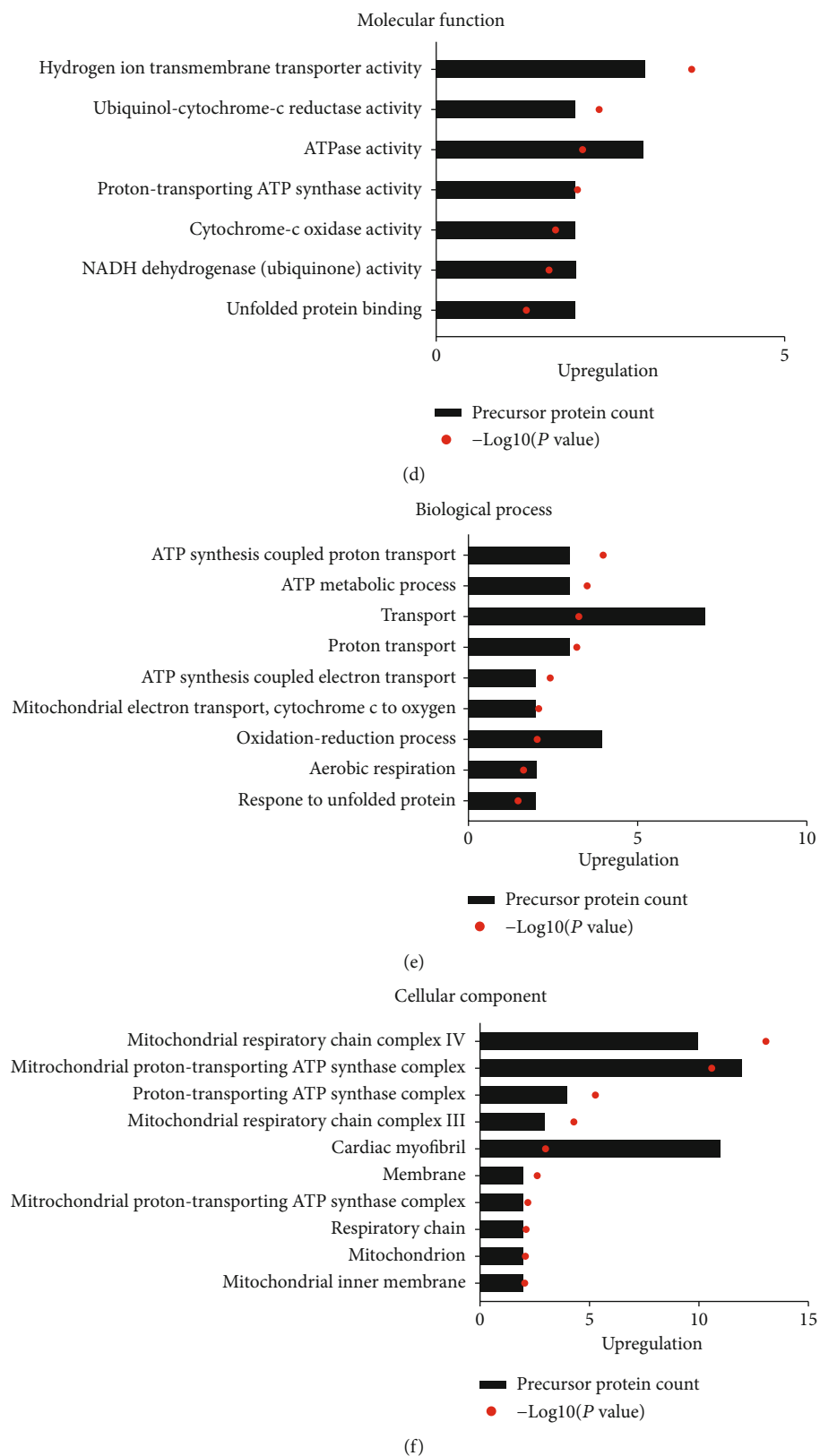
FIGURE 4: Gene Ontology (GO) and pathway analysis. (a) Molecular function of downregulated peptides' precursor proteins. (b) Biological processes of downregulated peptides' precursor proteins. (c) Cellular components of downregulated peptides' precursor proteins. (d) Molecular function of upregulated peptides' precursor proteins. (e) Biological processes of upregulated peptides' precursor proteins. (f) Cellular components of upregulated peptides' precursor proteins.

(a)

(b)

FIGURE 5: Analysis of the protein interaction network. (a) Pathway analysis of the precursor proteins of the differentially expressed peptides. (b) Interaction network of precursor proteins of these differentially expressed peptides as determined with STRING (https://string-db.org/, version: 11.0). The confidence level: medium confidence 0.400. Red: the main proteins associated with oxidative phosphorylation.

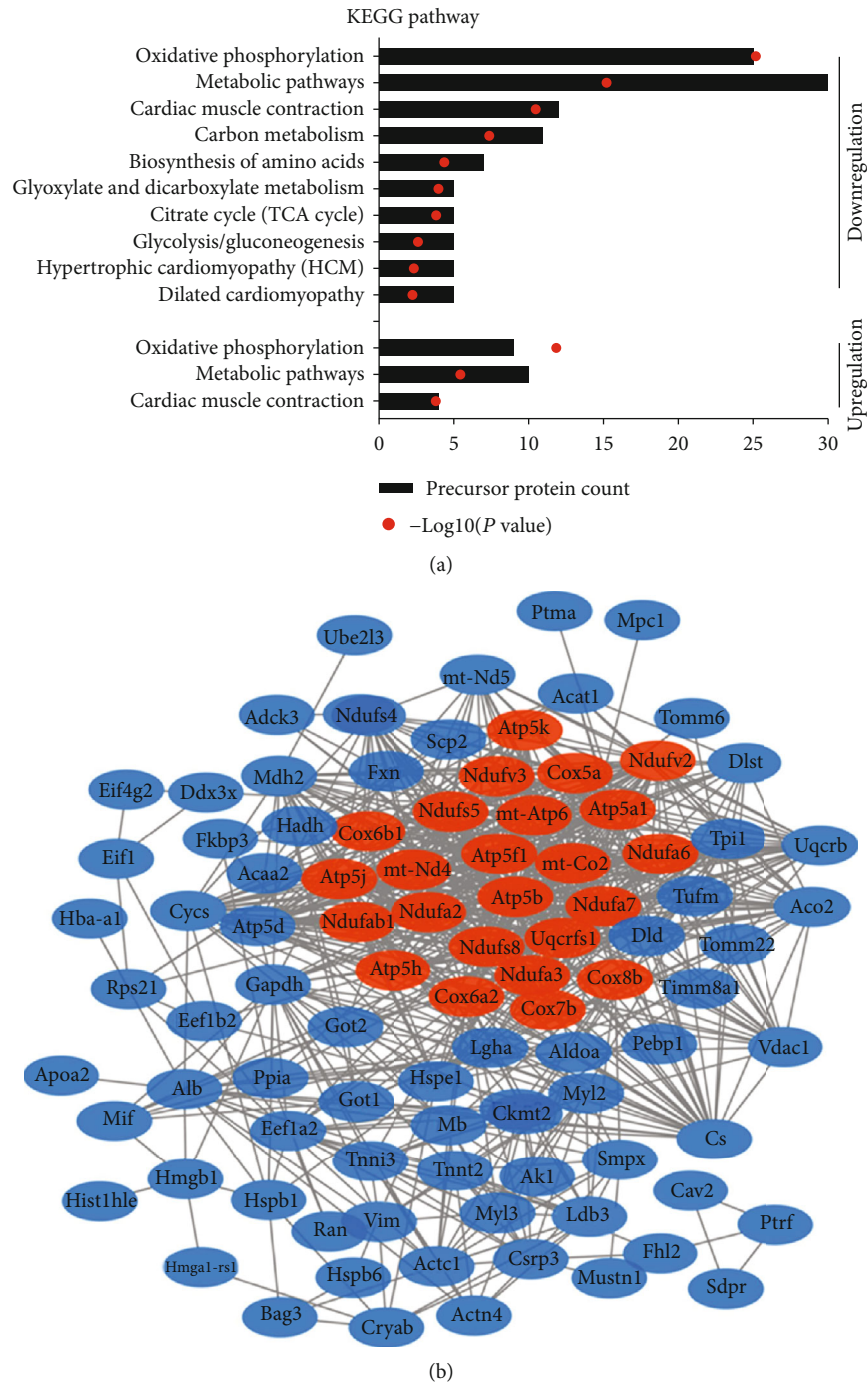and metabolism signaling pathways, which are closely related to the occurrence and development of myocardial injury (Figure 5(a)). Next, we analyzed the interaction network of the precursor proteins of these differential peptides using the STRING website (https://string-db.org/, version: 11.0). We found multiple interaction networks, with the main protein interaction network related to oxidative phosphorylation in mitochondria (Figure 5(b)).

3.5. Prediction of Myocardial Protective Peptides. First, we sought to determine the precursor proteins of the differentially expressed peptides related to cardiovascular diseases, oxidative phosphorylation, and cardiomyocyte apoptosis through the GeneAnalytics website (http://geneanalytics .genecards.org/) and Cytoscape 3.5.1 software. The correlations between the precursor proteins and various cardiovascular diseases are shown in Figure 6(a). The correlation
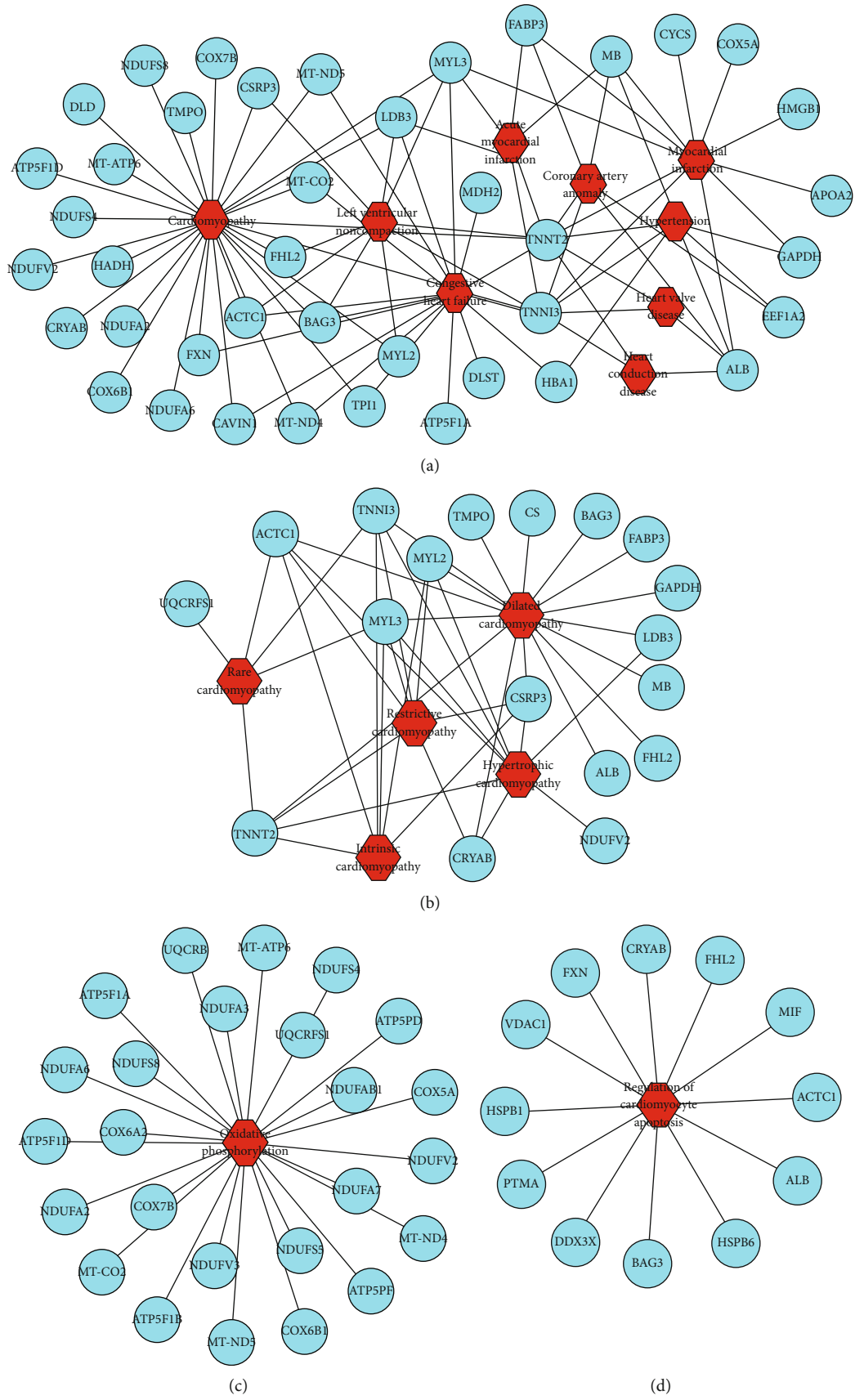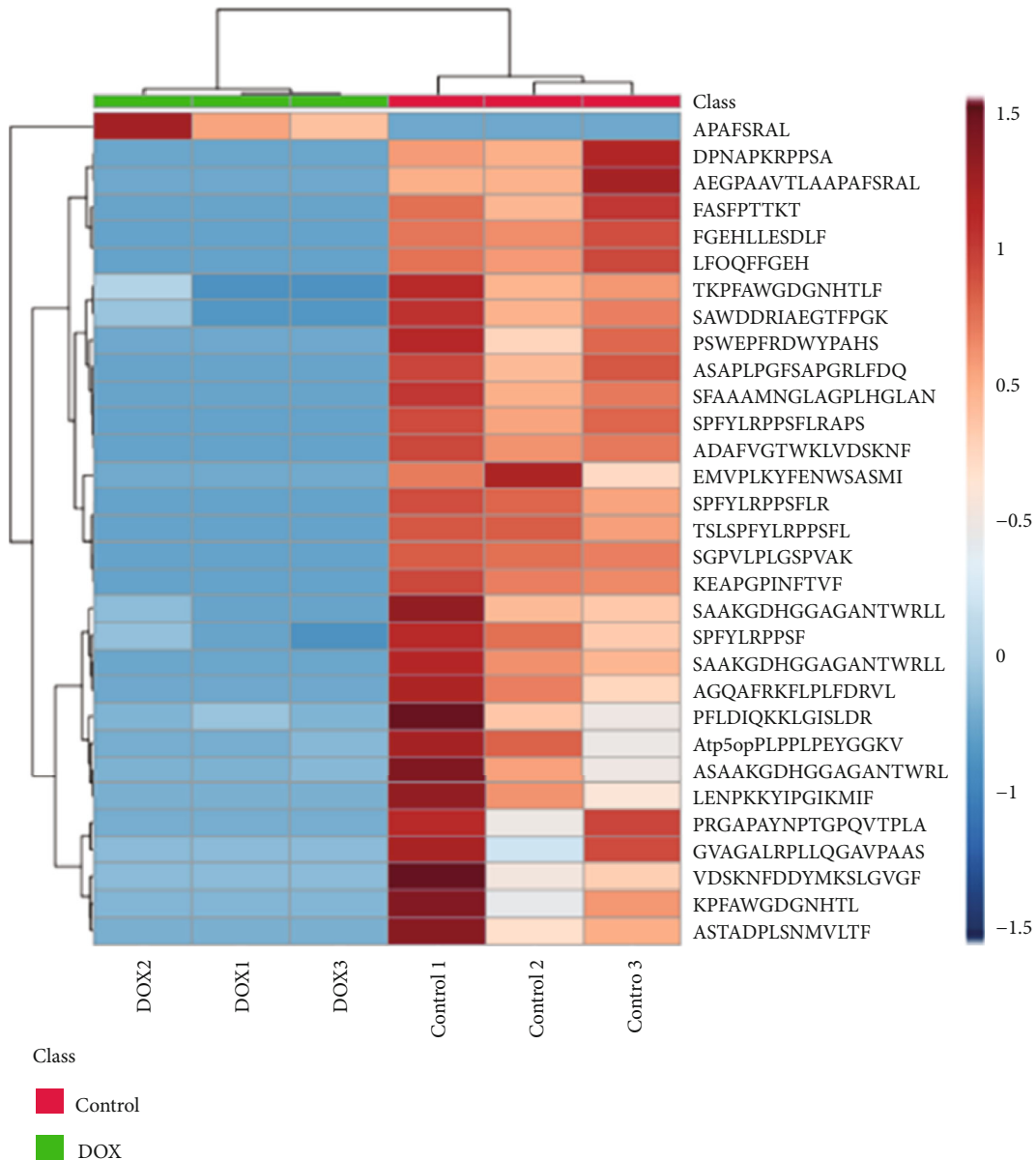
Figure 6: Continued.

(e)

FIGURE 6: Analysis of the precursor proteins of differentially expressed peptides related to potential myocardial protection. (a) Analysis of these precursor proteins related to cardiovascular diseases. (b) Analysis of these precursor proteins related to various cardiomyopathies. (c, d) Analysis of these precursor proteins related to oxidative phosphorylation and cardiomyocyte apoptosis. (e) Heat map analysis of 31 peptides that may confer myocardial protection.

between the precursor proteins and cardiomyopathy is shown in Figure 6(b). The precursor proteins associated with oxidative phosphorylation and cardiomyocyte apoptosis are shown in Figures 6(c) and 6(d). Next, we used the UniProt database (https://www.UniProt.org/) to study the function of the differentially expressed peptides and their precursor proteins and used Peptide Ranker (http://bioware.ucd.ie/~compass/biowareweb/, ranker scores greater than 0.5 indicate possible activity) to predict the probability that a differentially expressed peptide is involved in a biological activity. Finally, we screened 31 differentially expressed peptides that may have myocardial protective function

(Table 1). The heat map shows small differences within the group of 31 peptides and large differences between the behavior activity groups (Figure 6(e)).

3.6. Preliminary Functional Exploration of Peptides Derived from Cryab. Research has shown that Cryab protein plays an important role in myocardial protection. First of all, we verified the protein level of Cryab before and after DOX treatment. Our results showed that the protein level of Cryab was significantly reduced after DOX treatment (Figure 7(a)). Thus, we wondered if it might have a cardioprotective effect by cracking down key peptides. Among the 31 predicted

TABLE 1: The details of 31 predicted peptides which may have cardioprotective function.

Protein	UniProt accession	Peptide sequence	Peptide location	PTM description (positions)	Domain/region description	Peptide ranker score	Fold change
Atp5pb	Q9CQQ7	PLPPLPEYGGKVRLGLIPEEF	43-63			0.64	-13.77
Cox2	P00405	EMVPLKYFENWSASMI	212-227			0.61	-40.55
Cox6b	P56391	SAWDDRIAEGTFPGK	71-85		CHCH	0.84	-20.82
Cox6a2	P43023	ASAAKGDHGGAGANTWRLLT	13-32		Topological domain	0.84	-20.82
Cox6a2	P43023	KPFAWGDGNHTL	70-81		Topological domain	0.69	-12.77
Cox6a2	P43023	SAAKGDHGGAGANTWRLLTF	14-33			0.85	-5.96
Cox6a2	P43023	SAAKGDHGGAGANTWRLLTFVL	14-35			0.64	-47.59
Cox6a2	P43023	TKPFAWGDGNHTLF	69-82		Topological domain	0.71	-3.70
Cryab	P23927	FGEHLLESDLF	28-38			0.53	-24.10
Cryab	P23927	LFDQFFGEH	23-31			0.62	-9.15
Cryab	P23927	SPFYLRPPSF	45-54	Phosphoserine (45), omega-N-methylated arginine (50)		0.92	-2.69
Cryab	P23927	SPFYLRPPSFLR	45-56	Phosphoserine (45), omega-N-methylated arginine (50)		0.92	-9.66
Cryab	P23927	SPFYLRPPSFLRAPS	45-59	Phosphoserine (45, 59), omega-N-methylated arginine (50)	sHSP	0.81	-9.10
Cryab	P23927	TSLSPFYLRPPSFL	42-55	Phosphoserine (45), omega-N-methylated arginine (50)		0.76	-6.90
Cs	Q9CZU6	SFAAAMNGLAGPLHGLANQEV	288-308			0.61	-3.87
Cycs	P62897	LENPKKYIPGTKMIF	69-83	N6-Acetyllysine (73), N6-succinyllysine (73)	Iron (heme axial ligand)	0.66	-20.24
Fabp3	P11404	VDSKNFDDYMKSLGVGF	12-28	Phosphotyrosine; by Tyr-kinases (20), phosphoserine (23)		0.51	-12.80
Fabp3	P11404	ADAFVGTWKLVDSKNF	2-17	N-Acetylalanine (2), phosphothreonine (8)		0.58	-8.14
Hba	P01942	FASFPTTKT	34-42			0.53	-9.31
Hmgb1	P63158	DPNAPKRPPSA	91-101	Phosphoserine (100)	HMG box 2, LPS binding (lipid A), cytokine-stimulating activity	0.53	-8.52
Hspe1	Q64433	AGQAFRKFLPLFDRVL	2-17	N-Acetylalanine (2), N6-acetyllysine (8)		0.87	-51.60
Hspb1	P14602	AEGPAAVTLAAPAFSRALNRQL	64-85		sHSP, interaction with TGFB1I1	0.59	-7.88
Hspb1	P14602	APAFSRAL	74-81		Interaction with TGFB1I1	0.77	293.23
Hspb1	P14602	PSWEPFRDWYPAHS	14-27	Phosphoserine; by MAPKAPK2, MAPKAPK3, PKA, and PKC (15, 27)		0.75	-4.05
Hspb6	Q5EBG6	ASAPLPGFSAPGRLFDQ	15-31	Phosphoserine (16)	Involved in stabilization of the HSPB1:HSBP6 heterodimer	0.82	-13.42
Ldb3	Q9JKS4	PRGAPAYNPTGPQVTPLARGTFQRA	511-535	Omega-N-methylarginine (512, 529)		0.53	-12.84
Ldb3	Q9JKS4	SGPVLPLGSPVAK	156-168			0.61	-7.08
Myl2	P51667	KEAPGPINFTVF	71-82			0.77	-14.90

TABLE 1: Continued.

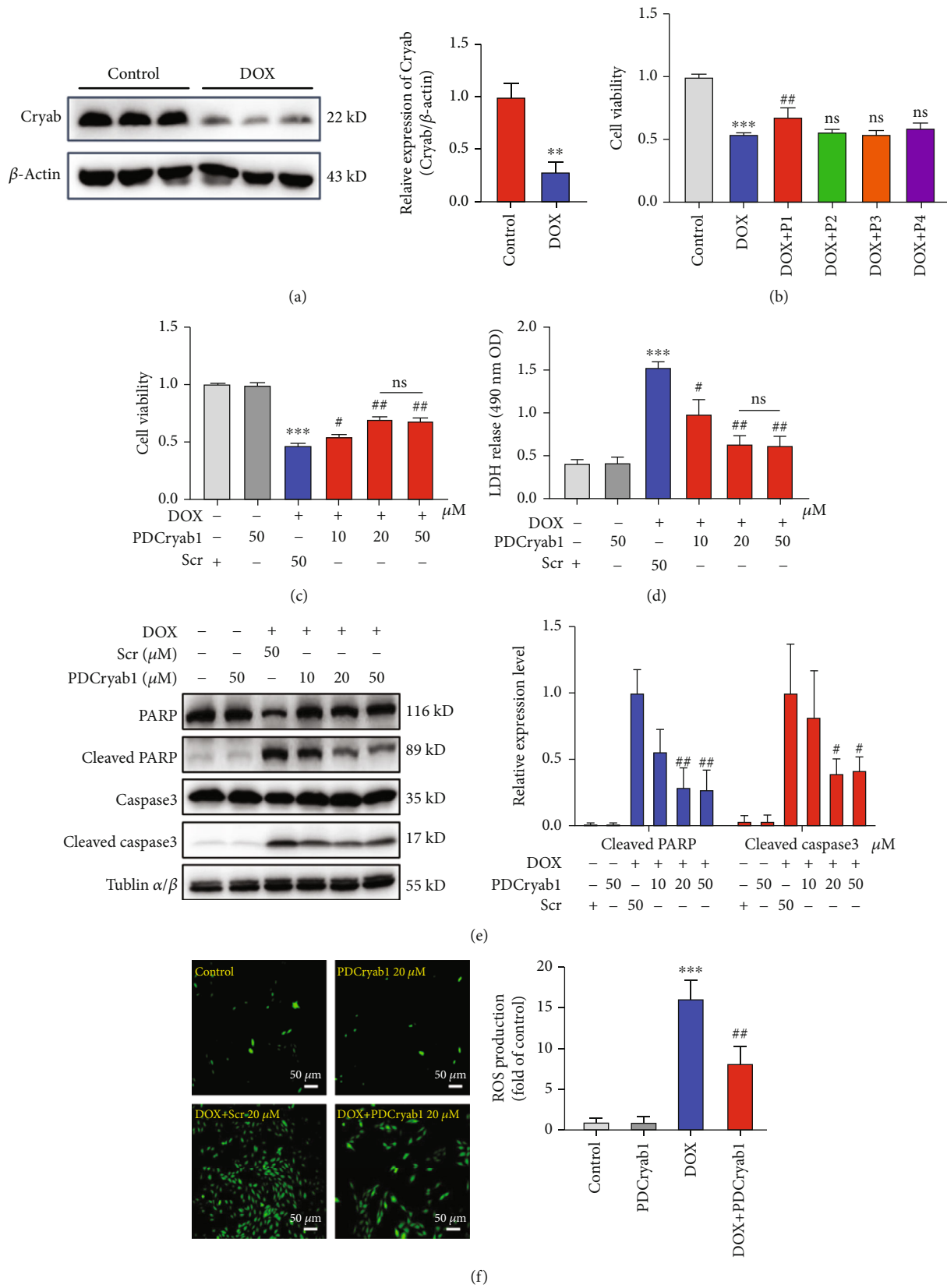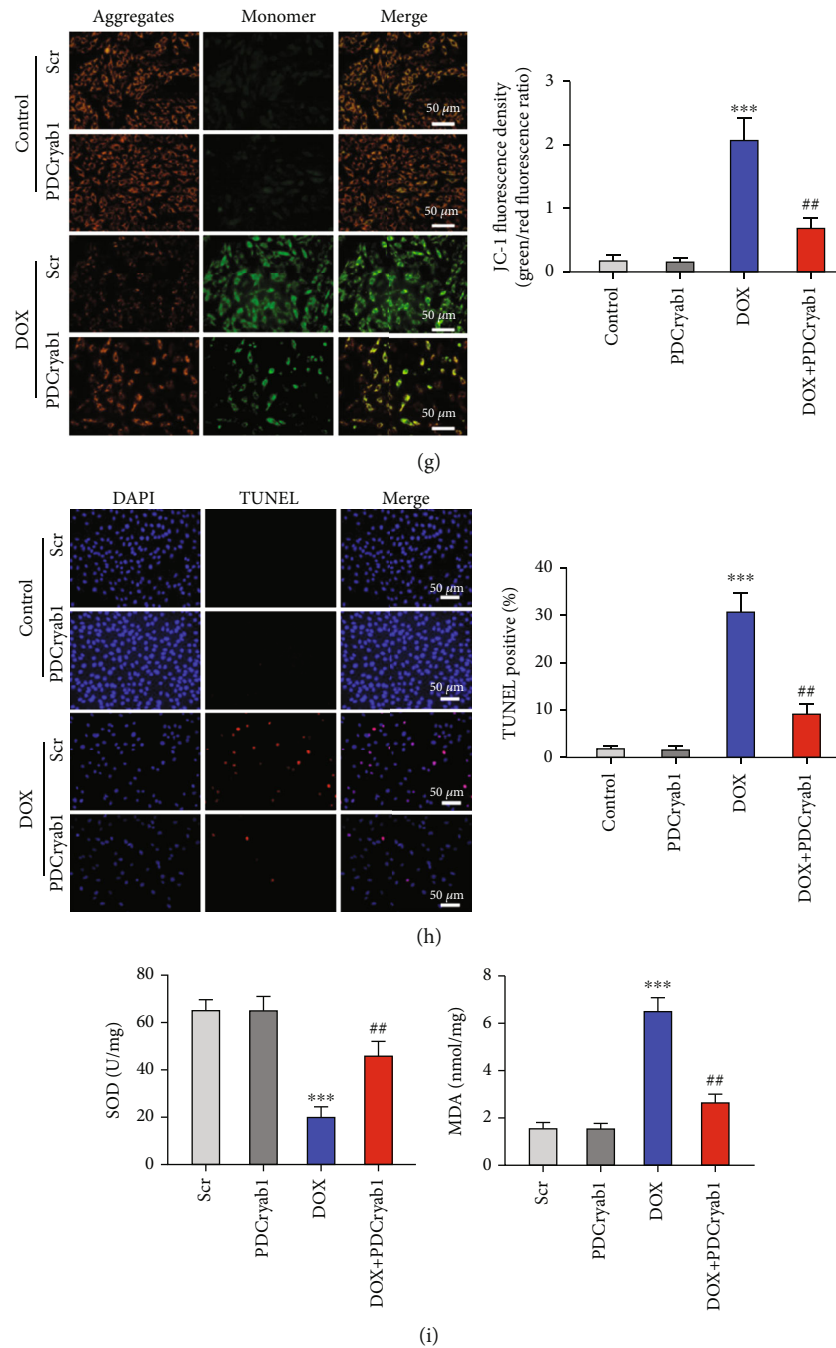| Protein	UniProt accession	Peptide sequence	Peptide location	PTM description (positions)	Domain/region description	Peptide ranker score	Fold change
Ndufs4	Q9CXZ1	ASTADPLSNMVLTF	115-128			0.63	-45.08
Ndufs5	Q99LY9	PFLDIQKKLGISLDR	2-16			0.58	-7.48
Uqcrfs1	Q9CR68	GVAGALRPLLQGAVPAASEPPVLDV	21-45			0.81	-12.83

(a)

(b)

(c)

(d)

(e)

(f)

Figure 7: Continued.

(g)

(h)

(i)

FIGURE 7: PDCryab1 attenuates DOX-induced cardiomyocyte apoptosis and the generation of reactive oxygen species (ROS). (a) The protein level of Cryab was significantly decreased after DOX treatment. (b) The effect of four peptides derived from Cryab on the viability of cells after DOX treatment, as determined by CCK-8 assay (one-way ANOVA analysis with Bonferroni's multiple comparison test). (c) The effect of PDCryab1 at different concentrations on the viability of cells after DOX treatment, as determined by CCK-8 assay (two-way ANOVA analysis with Bonferroni's multiple comparison test). (d) Treatment of PDCryab1 significantly reduced LDH release (two-way ANOVA analysis with Bonferroni's multiple comparison test). (e) Western blot analysis of cleaved PARP and cleaved caspase3. The quantification data for cleaved PARP and cleaved caspase3 (two-way ANOVA analysis with Bonferroni's multiple comparison test). (f) Representative photographs of ROS stained in the H9c2 cells. A DCFH-DA probe was used to detect intracellular ROS. Magnification 100x. The peptide concentration was $20\,\mu$M. Green: ROS. Quantification data for the ROS (two-way ANOVA analysis with Bonferroni's multiple comparison test). (g) Representative photographs of mitochondrial membrane potential in H9c2 cells (two-way ANOVA analysis with Bonferroni's multiple comparison test). Magnification 200x. (h) Representative photographs of TUNEL in H9c2 cells (two-way ANOVA analysis with Bonferroni's multiple comparison test). Magnification 100x. (i) SOD and MDA were detected (two-way ANOVA analysis with Bonferroni's multiple comparison test). The data represent the means ± SD. $^{**}P < 0.01$ and $^{***}P < 0.001$ versus the control group. $^{\#}P < 0.05$ and $^{\#\#}P < 0.01$ versus the DOX/DOX+Scr group. ns: not statistically significant.

peptides, six peptides were derived from Cryab and downregulated in the DOX group. Therefore, we selected four peptides that have a relatively high ranker score for the preliminary functional experiments with H9c2 cells: SPFYLRPPSF (45-54), SPFYLRPPSFLR (45-56), SPFYLRPPSFLRAPS (45-59), and TSLSPFYLRPPSFL (42-55). We named these peptides PDCryab1-4 (peptides derived from Cryab). Subsequently, we preliminarily verified the functions of these four peptides in H9c2 cells. We confirmed the PDCryab1 (SPFYLRPPSF) peptide to significantly enhance the viability of DOX-treated cardiomyocytes (Figure 7(b)). The analysis of PDCryab1 (SPFYLRPPSF) conservation in various species is shown in Supple. Fig. 1A. PDCryab1 has a high degree of homology among various species, especially *Homo sapiens*, mouse, and Rattus. HCD MS/MS annotation of the PDCryab1 peptide (SPFYLRPPSF) derived from the Cryab sequence spanning amino acids 45-54 is shown in Supple. Fig. 1B. PDCryab1 protect cells against DOX-induced cell damage, as evidenced by increased cell viability and decreased LDH release (Figures 7(c) and 7(d)). To study the function of PDCryab1 in DOX-induced cardiotoxicity, the apoptosis and ROS production levels were evaluated. The results showed that PDCryab1 could reduce the activation of PARP and caspase3 (Figure 7(e)). Simultaneously, $20\,\mu M$ PDCryab1 also decreased the generation of reactive oxygen species (Figure 7(f)). Besides, we also provided data about early apoptosis and PDCryab1 could reduce cell apoptosis rates, as indicated by mitochondrial membrane potential and TUNEL assay (Figures 7(g) and 7(h)). Last, we verified the SOD and MDA content in the supernatant. Our results showed that PDCryab1 significantly alleviated oxidative stress, as evidenced by increased SOD and decreased MDA content (Figure 7(i)).

3.7. Functional Analysis of PDCryab1 In Vivo. To further investigate the function of PDCryab1, we established a DOX-induced cardiotoxicity model. A cumulative dose of 20 mg/kg of doxorubicin (DOX) was administered via 4 weekly i.p. injections (Figure 8(a)). Body weight was significantly decreased in the DOX injection group, whereas PDCryab1 abolished this effect during DOX injection (Figure 8(b)). Treatment of PDCryab1 significantly improved the cardiac function, as evidenced by echocardiography analysis (Figures 8(c) and 8(d)). We also performed Sirius red staining, and our results showed that treatment of PDCryab1 alleviated DOX-induced cardiac fibrosis (Figures 8(e) and 8(f)). Besides, we verified the cardiomyocyte area via HE staining and WGA staining. Our results demonstrated that intervention of PDCryab1 improved the DOX-induced cardiac damage, as evidenced by increased cardiomyocyte area and decreased LDH release (Figures 8(g)–8(j)). Lastly, heart tissues were harvested to verify the cardiac marker, ANF and BNP. Our results revealed that treatment of PDCryab1 significantly reduced the mRNA level of ANF and BNP, suggesting a beneficial effect of PDCryab1 (Figures 8(k) and 8(l)).

4. Discussion

As we all know, DOX is widely used in the treatment of various tumors as a basic chemotherapy drug. However, the cardiotoxicity induced by DOX has become an increasingly serious problem and has been challenging many experts in the cardiovascular field [27]. Although there have been many studies on DOX-induced cardiotoxicity in recent years, the problem has not been resolved. To date, we used peptidomics to comprehensively analyze the changes in peptide profiles related to DOX-induced cardiotoxicity and successfully identified differentially expressed peptides in heart tissues. By analyzing the physicochemical properties and bioinformatics of these differentially expressed peptides, we provide new insights into the clinical problem of DOX-induced cardiotoxicity.

In this study, we identified a total of 236 peptides expressed at a difference that exceeds 2-fold changes. These peptides comprised fewer than 25 amino acids, and the molecular weight was less than 3.0 kDa, which suggested that the peptides identified in this study were valid. Many of these peptides originated from the same precursor protein, which attracted our attention. It is known that most peptides are produced by protein cleavage, and proteases play a key role in the cleavage process by specifically identifying cleavage sites [28]. In addition, the different cleavage sites recognized by the protease will have a great influence on the biological function of the cleaved peptides [29]. Our finding also indicated that the protease follows specific rules in the process of protein cleavage. Physicochemical properties, including peptide length, molecular weight, isoelectric point, and cleavage sites, are helpful for us to select the potential peptides. First, the liposoluble peptides are easily entered cells. Second, the peptides that have a long half-life are stable in cells. Third, relative lower length peptides are easily entered cells.

Through a bioinformatics analysis of these differential peptides, the cellular components enriched with these peptides were the mitochondrial inner membrane and mitochondrial respiratory chain, and the biological functions enriched with these peptides were related to the synthesis and metabolism of ATP. Mitochondria are considered the main target organelles of DOX in cardiomyocytes [30]. Some studies have shown that DOX preferentially accumulates in the mitochondria of cardiomyocytes, causing mitochondrial swelling and mitochondrial dysfunction [31, 32]. The pathway analysis results show that these peptides are mainly involved in oxidative phosphorylation and metabolic pathways. In energy metabolism, ATP is the main energy supplying compound in the body, and the main mechanism of its formation is oxidative phosphorylation. The decrease in mitochondrial energy supply caused by DOX can lead to a change in cardiac metabolism. The levels of ATP and creatine phosphate in the hearts of DOX-treated rats were decreased, indicating a decrease in mitochondrial energy metabolism [33]. In addition, DOX can inhibit the use of glucose by the myocardium while reducing the beta-oxidation of long-chain fatty acids, which may eventually lead to the development of myocardial energy metabolism disorders [34]. Therefore, attenuating the myocardial metabolic changes caused by DOX is one of the strategies to alleviate DOX-induced cardiotoxicity and in which these peptides may play key roles.

Cardiomyocyte apoptosis is a vital biological event of DOX-induced cardiotoxicity [4]. Studies have found that
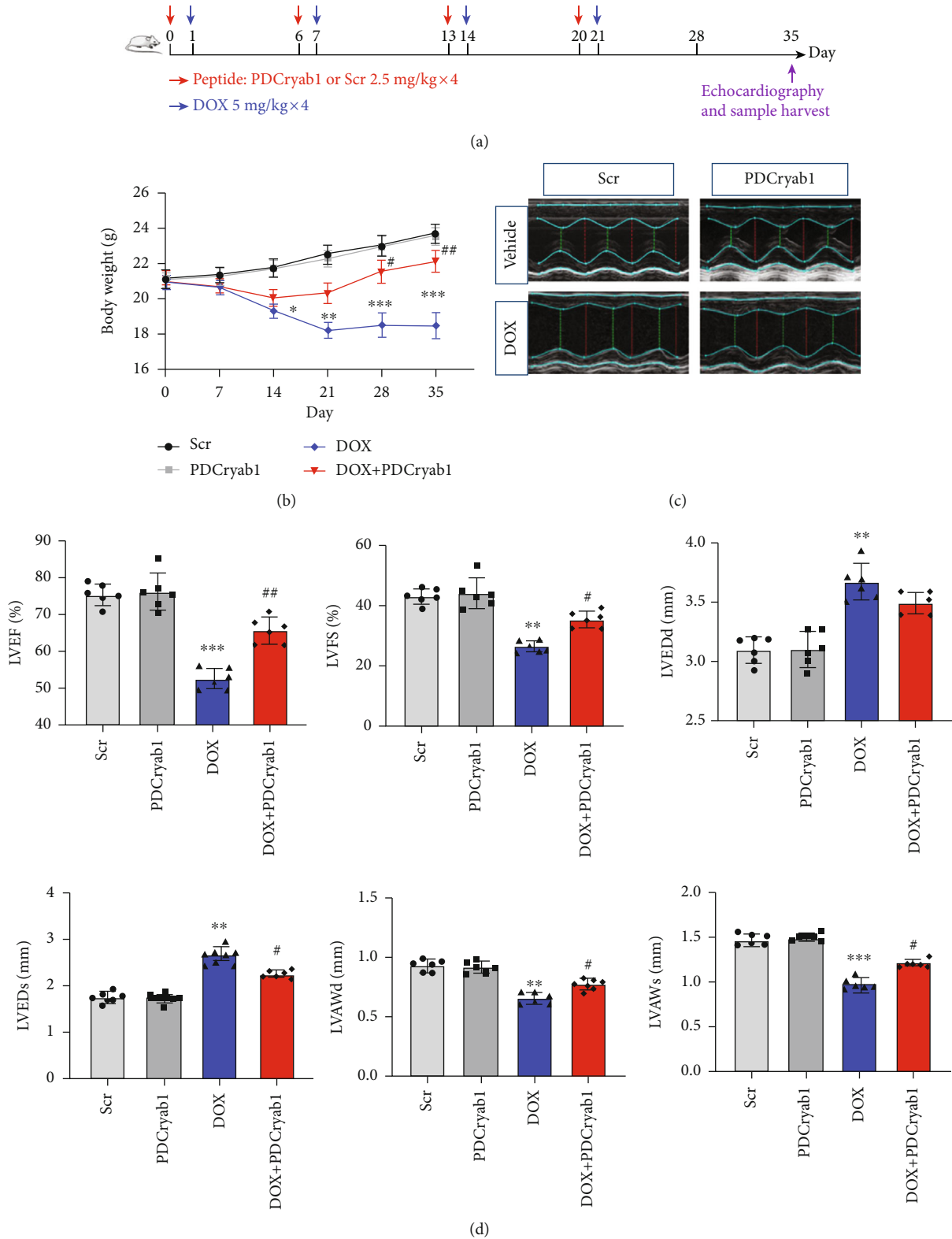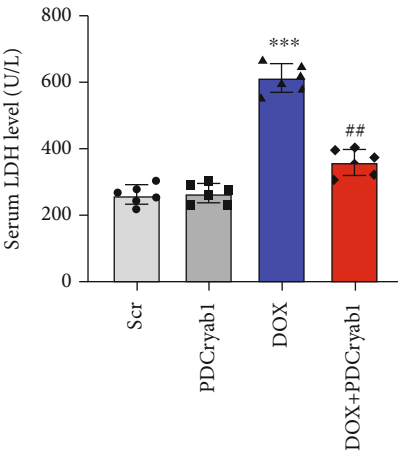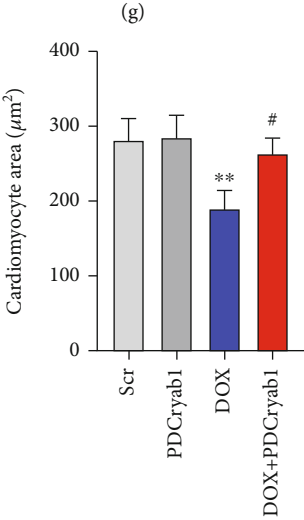
(a)

(b)

(c)

(d)

FIGURE 8: Continued.

(e)

(f)

(g)

(h)

(i)

(j)

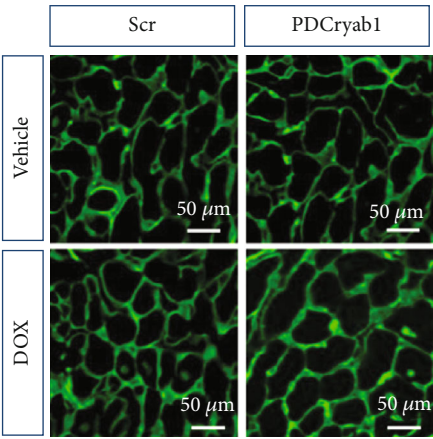FIGURE 8: Continued.
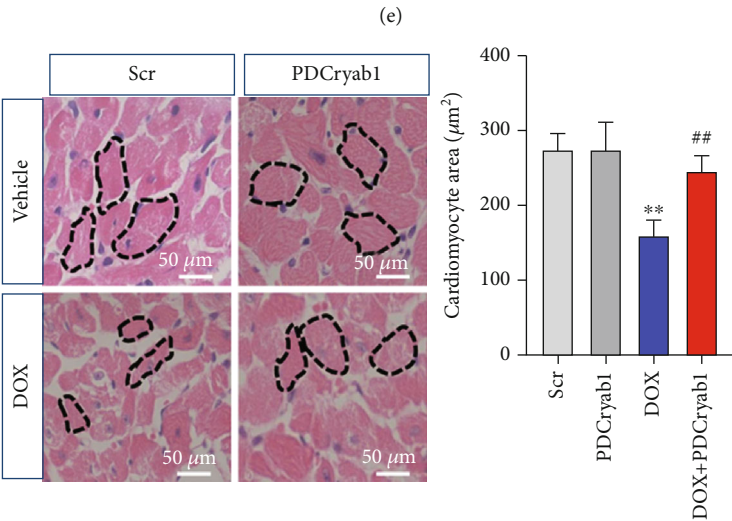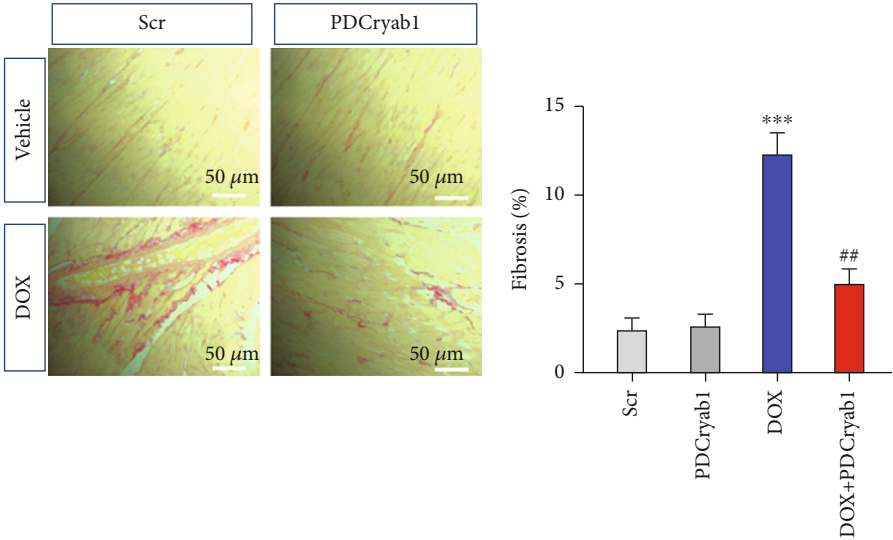
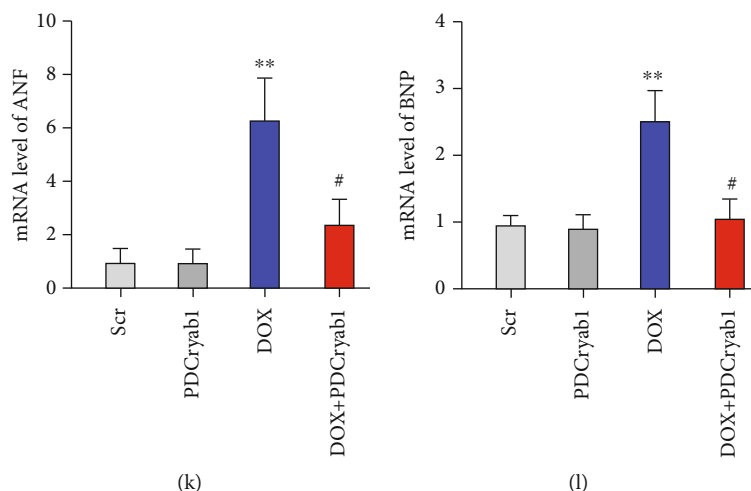(k)   (l)

FIGURE 8: Functional analysis of PDCryab1 in vivo. (a) Schematic map of DOX-induced cardiotoxicity. (b) Body weight was detected (two-way ANOVA analysis with Bonferroni's multiple comparison test). (c) Representative photographs of echocardiography analysis were recorded. (d) Quantification data of echocardiography analysis (two-way ANOVA analysis with Bonferroni's multiple comparison test). (e) Representative photographs of Sirius red staining. (f) Quantification data of Sirius red staining (two-way ANOVA analysis with Bonferroni's multiple comparison test). (g) Representative photographs of HE staining and quantification data of HE staining (two-way ANOVA analysis with Bonferroni's multiple comparison test). (h) Representative photographs of WGA staining. (i) Quantification data of WGA staining (two-way ANOVA analysis with Bonferroni's multiple comparison test). (j) LDH release was detected (two-way ANOVA analysis with Bonferroni's multiple comparison test). (k, l) mRNA levels of ANF and BNP were detected (two-way ANOVA analysis with Bonferroni's multiple comparison test). $**P < 0.01$ and $***P < 0.001$ versus the control group. $^{\#}P < 0.05$ and $^{\#\#}P < 0.01$ versus the DOX/DOX+Scr group. ns: not statistically significant.

some biologically active peptides, such as ICL1-9 [35] and pNaKtide [4, 26], play a protective role in the process of cardiomyocyte apoptosis. In this study, many precursor proteins of differentially expressed peptides are involved in the regulation of cardiomyocyte apoptosis, including heat shock protein beta-1 (Hspb1) [36], alpha-crystallin B chain (Cryab) [37], heat shock protein beta-6 (Hspb6) [38], and actin, alpha cardiac muscle 1 (Actc1) [39]. Cryab is the most abundant small heat shock protein (sHSP) in cardiomyocytes, and it can antagonize myocardial ischemia/reperfusion injury and is essential for normal cardiac function [40]. In addition, Cryab can inhibit the apoptosis of neonatal mouse cardiomyocytes treated with H_2O_2 [37]. Some studies have shown that peptides often play a biological role similar to that of their precursor proteins [41]. As shown in Table 1, of the 31 peptides that we predicted to be active, 6 were from Cryab, and all of them were downregulated in the DOX treatment group, findings consistent with the theory stated above. Therefore, we speculate that these six peptides may be involved in the regulation of Cryab in cardiomyocytes and may have the same function as Cryab. Interestingly, the peptides derived from Hspb1 are both upregulated and downregulated, while Hspb1 is recognized as a protein with a cardioprotective effect. The function of these peptides is worthy of further verification. If the upregulated peptides also have cardioprotective effects, whether the peptide has the same function as its precursor protein needs to be further clarified.

In this study, PDCryab1 (SPFYLRPPSF) was a downregulated peptide in the DOX treatment group that was derived from the Cryab protein, has high homology among various

species, and had not been previously reported. Our previous experiments demonstrated that PDCryab1 can inhibit cardiomyocyte apoptosis, reduce the production of reactive oxygen species, improve cardiac function, and ameliorate myocardial fibrosis. Although we have confirmed that PDCryab1 has a myocardial protective effect in vitro and in vivo, there were still some limitations to our study. For example, whether the type of cleavage or modification affects the function of PDCryab1 remains to be verified. In addition, the specific mechanism by which PDCryab1 exerts its biological function is also particularly important and will be the focus of our future research.

The peptide AEGPAAVTLAAPAFSRALNRQL was downregulated in the DOX treatment group. It was in the sHSP domain and interaction with the TGFB1I1 region of the Hspb1 protein. Hspb1 can inhibit the apoptosis caused by oxidative stress and protect the myocardium [36]. The domain is a region in a protein that has an independent structure and function, and this function often does not depend on the other regions of a protein molecule. Therefore, a peptide located in a domain region is more likely to have independent biological activity [42]. AEGPAAVTLAAPAFSRALNRQL was in the domain of Hspb1, and its predicted biological activity score was 0.59 (more than 0.5), which suggested that it may have an antiapoptotic effect and may be another therapeutic target of DOX-induced cardiotoxicity. In addition, Hspb1 can interact with VEGF and transforming growth factor (TGFB1I1) to regulate angiogenesis [43], and this peptide is in the region that interacts with TGFB1I1. We speculate that this peptide may also play a previously unidentified role in angiogenesis.

A peptide derived from Hmgb1 also attracted our attention. Its sequence was DPNAPKRPPSA (91-101). High mobility group box 1 (Hmgb1) is a DNA-binding nuclear nonhistone protein that plays an important role in the occurrence and development of cardiovascular diseases [44]. In general, Hmgb1 is passively released from necrotic cells, and living cells can actively secrete it under certain pathological conditions [45]. Studies have shown that DOX can significantly increase the expression level of Hmgb1 in cardiomyocytes, resulting in cardiomyocyte apoptosis and cardiac dysfunction, and that silencing Hmgb1 can protect the myocardium from DOX-induced cardiotoxicity [45, 46]. In addition, Hmgb1 has also been proven to be involved in DOX-induced autophagy-related cardiotoxicity and is predicted to be a biomarker of DOX-induced cardiotoxicity [47]. However, a recent study showed that Hmgb1 can upregulate the expression of Hspb1 and attenuate the cardiomyocyte apoptosis associated with DOX-induced cardiomyopathy [48]. Therefore, Hmgb1 undoubtedly plays an important role in DOX-induced cardiomyocyte apoptosis, but the specific effect of Hmgb1 on cardiomyocyte apoptosis remains to be clarified. Here, we found a peptide derived from Hmgb1 that was downregulated in the DOX treatment group and had a high prediction score for biological activity. This peptide was located in the region with cytokine-stimulating activity and a phosphorylation site (100). The elucidation of the function of this peptide will help to not only clarify the specific effect of Hmgb1 on cardiomyocyte apoptosis but also provide a new intervention strategy for DOX-induced cardiotoxicity.

In summary, we used peptidomics to elucidate the mechanism of DOX-induced cardiotoxicity and explore cardiotoxicity protection strategies; 236 differentially expressed peptides were successfully screened in this study. Through bioinformatics analysis and experimental verification, PDCryab1 became a candidate for protecting the myocardium against DOX-induced cell apoptosis. Our study provides a new approach for the treatment of DOX-induced cardiotoxicity.

Data Availability

The data that support the findings of this study are available from the corresponding author upon reasonable request.

Conflicts of Interest

The authors declare no conflicts of interest.

Authors' Contributions

Li Zhang, Xuejun Wang, and Mengwen Feng performed the experiments, analyzed the data, and wrote the manuscript. Hao Zhang and Jia Xu performed some animal experiments and bioinformatics analysis. Jingjing Ding participated in some in vitro experiments. Zijie Cheng and Lingmei Qian contributed to the study design and concept and supervised the project. Li Zhang, Xuejun Wang, and Mengwen Feng contributed equally to this work.

Supplementary Materials

Supplemental Fig. 1: conservation analysis and HCD MS/MS annotation of the peptide PDCryab1. (A) Conservation analysis of PDCryab1 (SPFYLRPPSF) in various species. (B) HCD MS/MS annotation of the peptide PDCryab1 (SPFYLRPPSF) derived from Cryab spanning amino acids 45-54. All fragment ions are annotated to within 20 ppm. Supple. Table 1: 236 differentially expressed peptides and precursor proteins (DOX vs. control). Supple. Table 2: identification of unique peptides. Supple. Table 3: the same peptides derived from several precursor proteins. (*Supplementary Materials*)

References

[1] R. M. Damiani, D. J. Moura, C. M. Viau, R. A. Caceres, J. A. P. Henriques, and J. Saffi, "Pathways of cardiac toxicity: comparison between chemotherapeutic drugs doxorubicin and mitoxantrone," *Archives of Toxicology*, vol. 90, no. 9, pp. 2063–2076, 2016.

[2] M. Cagel, E. Grotz, E. Bernabeu, M. A. Moretton, and D. A. Chiappetta, "Doxorubicin: nanotechnological overviews from bench to bedside," *Drug Discovery Today*, vol. 22, no. 2, pp. 270–281, 2017.

[3] D. L. Li and J. A. Hill, "Cardiomyocyte autophagy and cancer chemotherapy," *Journal of Molecular and Cellular Cardiology*, vol. 71, pp. 54–61, 2014.

[4] J. Shi, E. Abdelwahid, and L. Wei, "Apoptosis in anthracycline cardiomyopathy," *Current Pediatric Reviews*, vol. 7, no. 4, pp. 329–336, 2011.

[5] L. Rochette, C. Guenancia, A. Gudjoncik et al., "Anthracyclines/trastuzumab: new aspects of cardiotoxicity and molecular mechanisms," *Trends in Pharmacological Sciences*, vol. 36, no. 6, pp. 326–348, 2015.

[6] K. B. Wallace, "Adriamycin-induced interference with cardiac mitochondrial calcium homeostasis," *Cardiovascular Toxicology*, vol. 7, no. 2, pp. 101–107, 2007.

[7] C. Chen, L. Jiang, M. Zhang et al., "Isodunnianol alleviates doxorubicin-induced myocardial injury by activating protective autophagy," *Food & Function*, vol. 10, no. 5, pp. 2651–2657, 2019.

[8] D. C. Dallas, A. Guerrero, E. A. Parker et al., "Current peptidomics: applications, purification, identification, quantification, and functional analysis," *Proteomics*, vol. 15, no. 5-6, pp. 1026–1038, 2015.

[9] S. A. Slavoff, A. J. Mitchell, A. G. Schwaid et al., "Peptidomic discovery of short open reading frame–encoded peptides in human cells," *Nature Chemical Biology*, vol. 9, no. 1, pp. 59–64, 2013.

[10] S. S. Rubakhin, J. D. Churchill, W. T. Greenough, and J. V. Sweedler, "Profiling signaling peptides in single mammalian

cells using mass spectrometry," *Analytical Chemistry*, vol. 78, no. 20, pp. 7267–7272, 2006.

[11] L. T. Dang, N. T. Feric, C. Laschinger et al., "Inhibition of apoptosis in human induced pluripotent stem cells during expansion in a defined culture using angiopoietin-1 derived peptide QHREDGS," *Biomaterials*, vol. 35, no. 27, pp. 7786–7799, 2014.

[12] M. Chimen, H. M. McGettrick, B. Apta et al., "Homeostatic regulation of T cell trafficking by a B cell-derived peptide is impaired in autoimmune and chronic inflammatory disease," *Nature Medicine*, vol. 21, no. 5, pp. 467–475, 2015.

[13] L. S. Chaturvedi and M. D. Basson, "Glucagonlike peptide 2 analogue teduglutide: stimulation of proliferation but reduction of differentiation in human Caco-2 intestinal epithelial cells," *JAMA Surgery*, vol. 148, no. 11, pp. 1037–1042, 2013.

[14] H. Zhu, X. Wang, M. Wallack et al., "Intraperitoneal injection of the pancreatic peptide amylin potently reduces behavioral impairment and brain amyloid pathology in murine models of Alzheimer's disease," *Molecular Psychiatry*, vol. 20, no. 2, pp. 252–262, 2015.

[15] R. Ivell and R. Anand-Ivell, "Insulin-like peptide 3 (INSL3) is a major regulator of female reproductive physiology," *Human Reproduction Update*, vol. 24, no. 6, pp. 639–651, 2018.

[16] K. Fosgerau and T. Hoffmann, "Peptide therapeutics: current status and future directions," *Drug Discovery Today*, vol. 20, no. 1, pp. 122–128, 2015.

[17] A. Voigt and H. F. Jelinek, "Humanin: a mitochondrial signaling peptide as a biomarker for impaired fasting glucose-related oxidative stress," *Physiological Reports*, vol. 4, no. 9, article e12796, 2016.

[18] S. Thummasorn, K. Shinlapawittayatorn, S. C. Chattipakorn, and N. Chattipakorn, "High-dose humanin analogue applied during ischemia exerts cardioprotection against ischemia/reperfusion injury by reducing mitochondrial dysfunction," *Cardiovascular Therapeutics*, vol. 35, no. 5, Article ID e12289, 2017.

[19] Y. Lue, C. Gao, R. Swerdloff et al., "Humanin analog enhances the protective effect of dexrazoxane against doxorubicin-induced cardiotoxicity," *American Journal of Physiology-Heart and Circulatory Physiology*, vol. 315, no. 3, pp. H634–H643, 2018.

[20] K. H. Lee, H. Cho, S. Lee et al., "Enhanced-autophagy by exenatide mitigates doxorubicin-induced cardiotoxicity," *International Journal of Cardiology*, vol. 232, pp. 40–47, 2017.

[21] D. Pchejetski, C. Foussal, C. Alfarano et al., "Apelin prevents cardiac fibroblast activation and collagen production through inhibition of sphingosine kinase 1," *European Heart Journal*, vol. 33, no. 18, pp. 2360–2369, 2012.

[22] J. Oh, B. S. Lee, G. Lim et al., "Atorvastatin protects cardiomyocyte from doxorubicin toxicity by modulating survivin expression through FOXO1 inhibition," *Journal of Molecular and Cellular Cardiology*, vol. 138, pp. 244–255, 2020.

[23] C. Mooney, N. J. Haslam, G. Pollastri, and D. C. Shields, "Towards the improved discovery and design of functional peptides: common features of diverse classes permit generalized prediction of bioactivity," *PLoS One*, vol. 7, no. 10, article e45012, 2012.

[24] C. M. Montone, A. L. Capriotti, C. Cavaliere et al., "Peptidomic strategy for purification and identification of potential ACE-inhibitory and antioxidant peptides in Tetradesmus obliquus microalgae," *Analytical and Bioanalytical Chemistry*, vol. 410, no. 15, pp. 3573–3586, 2018.

[25] F. Y. Lee, P. L. Shao, C. G. Wallace et al., "Combined therapy with SS31 and mitochondria mitigates myocardial ischemia-reperfusion injury in rats," *International Journal of Molecular Sciences*, vol. 19, no. 9, 2018.

[26] H. Li, A. Yin, Z. Cheng et al., "Attenuation of Na/K-ATPase/Src/ROS amplification signal pathway with pNaktide ameliorates myocardial ischemia-reperfusion injury," *International Journal of Biological Macromolecules*, vol. 118, Part A, pp. 1142–1148, 2018.

[27] D. Liu, Z. Ma, S. Di et al., "AMPK/PGC1α activation by melatonin attenuates acute doxorubicin cardiotoxicity via alleviating mitochondrial oxidative damage and apoptosis," *Free Radical Biology and Medicine*, vol. 129, pp. 59–72, 2018.

[28] F. Li, Y. Wang, C. Li et al., "Twenty years of bioinformatics research for protease-specific substrate and cleavage site prediction: a comprehensive revisit and benchmarking of existing methods," *Briefings in Bioinformatics*, vol. 20, no. 6, pp. 2150–2166, 2019.

[29] B. H. J. van den Berg and A. Tholey, "Mass spectrometry-based proteomics strategies for protease cleavage site identification," *Proteomics*, vol. 12, no. 4-5, pp. 516–529, 2012.

[30] Y. Ichikawa, M. Ghanefar, M. Bayeva et al., "Cardiotoxicity of doxorubicin is mediated through mitochondrial iron accumulation," *Journal of Clinical Investigation*, vol. 124, no. 2, pp. 617–630, 2014.

[31] P. Wang, L. Wang, J. Lu et al., "SESN2 protects against doxorubicin-induced cardiomyopathy via rescuing mitophagy and improving mitochondrial function," *Journal of Molecular and Cellular Cardiology*, vol. 133, pp. 125–137, 2019.

[32] V. A. Sardão, P. J. Oliveira, J. Holy, C. R. Oliveira, and K. B. Wallace, "Morphological alterations induced by doxorubicin on H9c2 myoblasts: nuclear, mitochondrial, and cytoskeletal targets," *Cell Biology and Toxicology*, vol. 25, no. 3, pp. 227–243, 2009.

[33] M. Tokarska-Schlattner, M. Zaugg, C. Zuppinger, T. Wallimann, and U. Schlattner, "New insights into doxorubicin-induced cardiotoxicity: the critical role of cellular energetics," *Journal of Molecular and Cellular Cardiology*, vol. 41, no. 3, pp. 389–405, 2006.

[34] R. A. Carvalho, R. P. Sousa, V. J. Cadete et al., "Metabolic remodeling associated with subchronic doxorubicin cardiomyopathy," *Toxicology*, vol. 270, no. 2-3, pp. 92–98, 2010.

[35] L. A. Grisanti, T. P. Thomas, R. L. Carter et al., "Pepducin-mediated cardioprotection via beta-arrestin-biased beta2-adrenergic receptor-specific signaling," *Theranostics*, vol. 8, no. 17, pp. 4664–4678, 2018.

[36] X. Liu, K. Liu, C. Li et al., "Heat-shock protein B1 upholds the cytoplasm reduced state to inhibit activation of the Hippo pathway in H9c2 cells," *Journal of Cellular Physiology*, vol. 234, no. 4, pp. 5117–5133, 2019.

[37] R. Chis, P. Sharma, N. Bousette et al., "α-Crystallin B prevents apoptosis after H_2O_2 exposure in mouse neonatal cardiomyocytes," *American Journal of Physiology-Heart and Circulatory Physiology*, vol. 303, no. 8, pp. H967–H978, 2012.

[38] G. S. Liu, H. Zhu, W. F. Cai et al., "Regulation of BECN1-mediated autophagy by HSPB6: insights from a human HSPB6(S10F) mutant," *Autophagy*, vol. 14, no. 1, pp. 80–97, 2018.

[39] H. K. Jiang, G. R. Qiu, J. Li-Ling, N. Xin, and K. L. Sun, "Reduced ACTC1 expression might play a role in the onset

of congenital heart disease by inducing cardiomyocyte apoptosis," *Circulation Journal*, vol. 74, no. 11, pp. 2410–2418, 2010.

[40] J. L. Martin, R. Mestril, R. Hilal-Dandan, L. L. Brunton, and W. H. Dillmann, "Small heat shock proteins and protection against ischemic injury in cardiac myocytes," *Circulation*, vol. 96, no. 12, pp. 4343–4348, 1997.

[41] X. Gao, H. Zhang, W. Zhuang et al., "PEDF and PEDF-derived peptide 44mer protect cardiomyocytes against hypoxia-induced apoptosis and necroptosis via anti-oxidative effect," *Scientific Reports*, vol. 4, article 5637, 2014.

[42] J. Pereira and A. N. Lupas, "The ancestral KH peptide at the root of a domain family with three different folds," *Bioinformatics*, vol. 34, no. 23, pp. 3961–3965, 2018.

[43] S. H. Choi, H. J. Lee, Y. B. Jin et al., "MMP9 processing of HSPB1 regulates tumor progression," *PLoS One*, vol. 9, no. 1, article e85509, 2014.

[44] A. Funayama, T. Shishido, S. Netsu et al., "Cardiac nuclear high mobility group box 1 prevents the development of cardiac hypertrophy and heart failure," *Cardiovascular Research*, vol. 99, no. 4, pp. 657–664, 2013.

[45] Y. Yao, X. Xu, G. Zhang, Y. Zhang, W. Qian, and T. Rui, "Role of HMGB1 in doxorubicin-induced myocardial apoptosis and its regulation pathway," *Basic Research in Cardiology*, vol. 107, no. 3, p. 267, 2012.

[46] E. Taskin, C. Guven, K. S. Tunc et al., "Silencing HMGB1 expression inhibits adriamycin's heart toxicity via TLR4 dependent manner through MAPK signal transduction," *Journal of B.U.O.N.*, vol. 25, no. 1, pp. 554–565, 2020.

[47] P. Luo, Y. Zhu, M. Chen et al., "HMGB1 contributes to adriamycin-induced cardiotoxicity via up-regulating autophagy," *Toxicology Letters*, vol. 292, pp. 115–122, 2018.

[48] T. Narumi, T. Shishido, Y. Otaki et al., "High-mobility group box 1-mediated heat shock protein beta 1 expression attenuates mitochondrial dysfunction and apoptosis," *Journal of Molecular and Cellular Cardiology*, vol. 82, pp. 1–12, 2015.

Research Article

LCZ696 Ameliorates Oxidative Stress and Pressure Overload-Induced Pathological Cardiac Remodeling by Regulating the Sirt3/MnSOD Pathway

Shi Peng [iD],[1] **Xiao-feng Lu,**[1] **Yi-ding Qi,**[2] **Jing Li,**[3] **Juan Xu,**[1] **Tian-you Yuan,**[1] **Xiao-yu Wu,**[1] **Yu Ding,**[1] **Wen-hua Li,**[4] **Gen-qing Zhou,**[1] **Yong Wei,**[1] **Jun Li,**[1] **Song-wen Chen** [iD],[1] **and Shao-wen Liu** [iD][1]

[1]Department of Cardiology, Shanghai General Hospital, School of Medicine, Shanghai Jiao Tong University, Shanghai, China
[2]Department of Cardiology, Shanghai Chest Hospital, Shanghai Jiao Tong University, China
[3]Department of Ultrasound, The Second Affiliated Hospital of Soochow University, Suzhou, China
[4]Department of Cardiology, Affiliated Wujin Hospital of Jiangsu University, China

Correspondence should be addressed to Song-wen Chen; chensongwen@hotmail.com
and Shao-wen Liu; shaowen.liu@hotmail.com

Aims. We aimed to investigate whether LCZ696 protects against pathological cardiac hypertrophy by regulating the Sirt3/MnSOD pathway. *Methods.* *In vivo*, we established a transverse aortic constriction animal model to establish pressure overload-induced heart failure. Subsequently, the mice were given LCZ696 by oral gavage for 4 weeks. After that, the mice underwent transthoracic echocardiography before they were sacrificed. *In vitro*, we introduced phenylephrine to prime neonatal rat cardiomyocytes and small-interfering RNA to knock down Sirt3 expression. *Results.* Pathological hypertrophic stimuli caused cardiac hypertrophy and fibrosis and reduced the expression levels of Sirt3 and MnSOD. LCZ696 alleviated the accumulation of oxidative reactive oxygen species (ROS) and cardiomyocyte apoptosis. Furthermore, Sirt3 deficiency abolished the protective effect of LCZ696 on cardiomyocyte hypertrophy, indicating that LCZ696 induced the upregulation of MnSOD and phosphorylation of AMPK through a Sirt3-dependent pathway. *Conclusions.* LCZ696 may mitigate myocardium oxidative stress and apoptosis in pressure overload-induced heart failure by regulating the Sirt3/MnSOD pathway.

1. Introduction

Cardiac hypertrophy is a pathological remodeling process of the heart characterized by hypertrophied cardiomyocytes, interstitial fibrosis, perivascular fibrosis, and decreased cardiac compliance. The process can eventually lead to malignant arrhythmias, heart failure, and even sudden cardiac death [1, 2]. Heart failure is the final stage of all the cardiovascular diseases and is currently a heavy burden for national medical and health services. Although several treatment options, such as CRT (Cardiac Resynchronization Therapy), exist, heart failure-associated morbidity and mortality are still on the rise. Thus, there is a need to identify novel therapeutic targets against the condition [3].

LCZ696 is an angiotensin-receptor-neprilysin inhibitor (ARNI) consisting of the neprilysin inhibitor sacubitril (AHU377) and angiotensin-receptor blocker (ARB) valsartan [4]. Recent clinical trials have revealed that LCZ696 is superior to enalapril in reducing mortality and rehospitalization rate in patients with chronic heart failure [5, 6]. Moreover, LCZ696 can reduce both sudden cardiac death and deaths from progressive heart failure compared to angiotensin-converting enzyme inhibitors (ACEI), such as enalapril [5]. Although LCZ696 is effective in the treatment

of heart failure [7, 8], the specific mechanism underlying its role in long-term pressure overload-induced cardiac hypertrophy and sequential heart failure remains unknown.

The intracellular generation and scavenging of reactive oxygen species (ROS) are usually in a homeostasis state under normal physiological conditions. However, under various pathogenic stimuli, such as irradiation, anticancer agents, and aromatic hydrocarbons, the accumulation of ROS far exceeds the clearance capacity of cells. Consequently, various macromolecules suffer from oxidative stress damage, including lipid peroxidation, oxidative damage to DNA, protein oxidation, and monosaccharide oxidation [9]. Reactive oxygen species can enhance the progression of cardiac hypertrophy and heart failure [10–13]. Cardiac hypertrophy causes elevated mitochondrial ROS levels, which in turn induces myocardium apoptosis and further aggravates hypertrophy, ending up in a vicious circle [14]. ROS can activate multiple signaling cascades during cardiac hypertrophy. As such, impeding ROS and breaking the vicious cycle may hold promise for improving cardiac hypertrophy [15].

Sirtuins are a family of nicotinamide adenine nucleotide-(NAD$^+$-) dependent class III histone deacetylases (HDACs) consisting of seven homologues. Among the homologues, sirtuin 3 (Sirt3) is the most extensively studied because of the decisive role it plays in a variety of diseases. Sirt3 is highly expressed in tissues requiring high energy metabolisms, especially in the heart tissues. The role of Sirt3 in mitochondrial dysfunction and redox homeostasis has been extensively demonstrated [16, 17]. Recent studies have shown that Sirt3 plays a crucial role in defending mitochondria from oxidative damage [18]. Also, it has been elaborated that Sirt3 deficiency exacerbates cardiac hypertrophy and heart failure in transverse aortic constriction mice, whereas Sirt3 overexpression protects against maladaptive ventricular remodeling [19, 20]. Given this, we hypothesized that the potential mechanisms underlying the beneficial effects of LCZ696 on pathological cardiac remodeling could be mediated by the Sirt3-dependent pathway.

The results of the present study showed that LCZ696 upregulated Sirt3 expression levels both in hypertrophied cardiac myocytes with transverse aortic constriction and cardiomyocytes induced with phenylephrine (PE). Also, we observed that the cardioprotective effects of LCZ696 were partly mediated by the Sirt3-dependent pathway.

2. Materials and Methods

2.1. Reagents.
The following antibodies were purchased from Cell Signaling Technology: anti glyceraldehyde-3-phosphate dehydrogenase (GAPDH, anti-Sirt3 rabbit monoclonal antibody, anti-MnSOD rabbit monoclonal antibody, anti-COX IV rabbit monoclonal antibody, anti-AMPK rabbit monoclonal antibody, and anti phospho-AMPK rabbit monoclonal antibody. Mouse monoclonal anti sarcomeric alpha-actinin, rabbit monoclonal anti-Bcl-2 antibody, rabbit monoclonal anti-Bax antibody, mouse monoclonal anti-3-nitrotyrosine, and rabbit polyclonal anti-4 hydroxynonenal were purchased from Abcam (Cambridge, MA, United States). LCZ696 was

purchased from MedChemExpress (Monmouth Junction, NJ, USA) and dissolved in corn oil.

2.2. Animals and Treatments.
Eight-week-old male C57BL/6 mice and neonatal Sprague-Dawley (SD) rats were obtained from GemPharmatech Co. Ltd. (Nanjing, China). The animals had free access to food and drinking water. All the animal experiments were conducted as per the guidelines of the care and use of laboratory animals of the Shanghai Jiao Tong University School of Medicine.

Transverse aortic constriction surgery was performed as previously described [21]. In brief, mice were anaesthetized with a mixture of ketamine (100 mg/kg) and xylazine (5 mg/kg) through intraperitoneal injection. The lack of toe pinching reflex indicated successful anaesthesia. The chest cavity was opened to the second intercostal space, and the adipose and connective tissue around the aortic arch was gently separated. The constriction was applied between the left common carotid artery and the innominate artery, by tying a 6-0 nylon suture ligature against a 27-gauge needle. The thorax was closed using a 6-0 suture, and mice were left to rest on a warming pad until they were fully awake. The sham-operated mice underwent the same operation procedure devoid of aortic ligation. After the ligation, the mice were randomly divided into four groups: sham+vehicle group, sham+LCZ696 group, TAC+vehicle group, and TAC+LCZ696 group. To determine the role of LCZ696 in pathological cardiac remodeling, mice were administered with LCZ696 at a dose of 20 mg/kg/d through gavage. The dosage of LCZ696 was selected according to previous studies [22, 23]. The vehicle group was given the same volume of corn oil. After 4 weeks, hearts were snap-frozen in liquid nitrogen, then kept at -80°C for subsequent analyses.

2.3. Hemodynamic and Echocardiographic Measurements.
The VEVO 2100 echocardiography system (Visual Sonics Inc., Toronto, Canada) was used to perform transthoracic echocardiography as per the methods described previously. Briefly, 4 weeks after TAC surgery, the mice were anaesthetized with 2.5% isoflurane. Subsequently, M-mode echocardiography was used to obtain left ventricular internal diameter at end-systole (LVIDs), left ventricular internal diameter at end-diastole (LVIDd), left ventricular end-diastolic volume (LVEDV), and end-systolic volume (LVESV). After taking the measurements, the following calculations were made:

$$\text{Left ventricle ejection fraction (LVEF)} = \frac{\text{LVEDV} - \text{LDESV}}{\text{LVEDV}} \times 100\%,$$

(1)

$$\text{LV fractional shortening (FS)} = \frac{\text{LVEDD} - \text{LVESD}}{\text{LVEDD}}.$$

(2)

2.4. Morphology and Immunohistochemistry.
The removed hearts were immersed in 10% KCl, leaving the hearts arrested during diastole. Hearts were fixed with paraformaldehyde (4%), embedded in paraffin, and sectioned serially (5-6 μm). The slides were stained with hematoxylin-eosin (HE) and wheat germ agglutinin (WGA, Invitrogen, Carlsbad, CA,

USA) to observe the morphology of cardiomyocytes. Picric Sirius red (PSR) staining and Masson trichrome staining were performed to detect collagen deposition and fibrosis. The cross-sectional area of myocytes was calculated using Image-Pro Plus 6.0 (Media Cybernetics, Rockville, MD, United States). Immunohistochemical staining of α-SMA (Abcam, Cambridge, UK) was performed to evaluate the transformation of fibroblasts to myofibroblasts. The 3-nitrotyrosine (NT) staining and 4 hydroxynonenal (4-HNE) staining (Abcam, Cambridge, UK) were performed to assess the levels of oxidative stress in the myocardium.

2.5. Dihydroethidium Staining. Production of intracellular superoxide in the myocardium was detected using in situ dihydroethidium (DHE, Invitrogen Molecular Probes, Eugene, OR, USA) fluorescence. Hearts from different groups were embedded in an optimal cutting temperature compound (OCT Compound, Sakura Finetek USA, Inc., Torrance, CA, United States) and cut into $5 \mu m$ sections. Frozen sections were washed with PBS and incubated with $10 \mu mol/L$ DHE working solution for 30 min. The images were captured using a fluorescence microscope (DM2500, Leica).

2.6. Western Blot Analysis. Hearts and primary cardiomyocyte lysate homogenates were prepared as previously described [24]. Briefly, proteins of whole heart homogenates or cell lysates from different treatments were separated using SDS-polyacrylamide gel electrophoresis (SDS-PAGE) and transferred onto polyvinylidene difluoride membranes (PVDF membranes, Millipore, Billerica, MA, USA). After blocking with 5% nonfat powder milk for 1 h, the membranes were incubated with primary antibodies overnight at 4°C. The primary and secondary antibodies used in our experiments were listed in the Supplementary materials Table S4. The next day, the membranes were washed with the TBST buffer, then incubated with horseradish peroxidase-conjugated secondary antibodies for 1 h at room temperature. The bands were detected using an ImageQuant LAS 4000 Imager (General Electric Co.), and gray-scale value analysis was performed using the Gel-Pro analyzer.

2.7. Real-Time Polymerase Chain Reaction Analysis. Total RNA from the frozen heart tissues or primary cardiomyocytes was extracted using the TRIzol Reagent (Invitrogen Life Technologies, USA). Subsequently, the RNA was reverse transcribed to cDNA using a PrimeScript™ RT Master Mix Kit (Takara). Quantitative real-time PCR was performed using a SYBR Green Fast qPCR mix (Takara) with the ABI 7500 Real-Time PCR System (ABI, Carlsbad, CA, USA). The expression levels of the target genes were normalized to that of GAPDH. The primer sequences used in this procedure are listed in Supplementary Table S1 and S2.

2.8. Cell Culture and Treatment. Primary neonatal rat cardiomyocytes (NRCMs) were isolated via enzymatic digestion, as described previously. Briefly, hearts from 1- to 3-day-old SD rat pups were minced into tiny pieces and transferred to a centrifuge tube. Ventricles were digested in PBS supplemented with 0.1% trypsin-EDTA and 1 mg/mL collagenase

IV (Life Technologies, Darmstadt, Germany) until the digestive enzyme solution was clear. After differential preplating for 2 hours in the incubator, cardiac fibroblasts were attached to the bottom of the petri dish and discarded. Cardiomyocytes were collected and seeded onto different culture plates. The NRCMs were cultured in DMEM supplemented with 10% fetal bovine serum (FBS, GIBCO) and $100 \mu M$ Brdu (Sigma-Aldrich) at 37°C and 5% CO_2 for 24 h. After that, the culture medium was replaced with Dulbecco's modified Eagle medium (DMEM, Life Technologies) containing 2% FBS and $100 \mu M$ Brdu. To induce cardiomyocyte hypertrophy, the NRCMs were treated with phenylephrine (PE, Sigma-Aldrich, $50 \mu mol/L$) for 24 h. The LCZ696 dosage was $20 \mu M$. After different treatments, the cells were collected for further analysis.

2.9. Cell Surface Area Analysis. Primary neonatal rat cardiomyocytes were seeded onto a confocal dish (D35-20-1.5P, Cellvis, Mountain View, CA) according to the instructions of the manufacturer. Then, the cells were stained with α-actinin immunofluorescence. Cell surface area was calculated using Image-Pro Plus 6.0 (Media Cybernetics, Rockville, MD, United States).

2.10. Quantification of ROS Generation. Intracellular levels of ROS were assessed using a fluorescence probe, $2'7'$-dichlorofluorescein diacetate (DCFH-DA, Abcam, Cambridge, MA, United States) as per the manufacturer's instructions. Briefly, NRCMs were stimulated with different treatments for a specific period. After that, the cells were washed with wash buffer and incubated with $25 \mu M$ DCFDA at 37°C in the dark for 45 min, then washed again with wash buffer. Mitochondrial ROS deposition was evaluated using MitoSOX red staining (Invitrogen, Carlsbad, CA, USA). The pictures were captured using a fluorescence microscope (DM3000, Leica).

2.11. Cell Apoptosis Assay. Myocardial apoptosis was detected through terminal deoxynucleotidyl transferase-mediated dUTP nick-end labeling (TUNEL) staining using an In Situ Cell Death Detection Kit (Roche Applied Science, Mannheim, Germany) following the manufacturer's instructions. In brief, sections or primary NRCMs were fixed in 4% paraformaldehyde and washed in PBS. After they were permeabilized with 0.3% Triton X-100 and 0.1% sodium citrate, the cells were incubated with the TUNEL reaction mixture for 1 h at 37°C. Then, slides or coverslips were mounted with DAPI (Invitrogen, Carlsbad, CA, USA). Pictures were taken using a fluorescence microscope (Leica DM3000, Germany).

2.12. Transfection. Small interference RNA (siRNA) for Sirt3 (si-Sirt3) and negative control siRNA (si-NC) were purchased from RiboBio Co. Ltd. (Shanghai, China). The interference sequences are listed in the Supplementary Table S3. NRCMs were transfected with the siRNAs using Lipofectamine RNAiMAX (Invitrogen) according to the manufacturer's instructions. Knockdown efficiency was assessed using Western blot assay (Supplementary Figure S1). Cells transfected with Sirt3 siRNA were then treated with or without PE ($50 \mu M$) for 24 h.

2.13. Statistical Analysis. Data analysis was performed using GraphPad Prism 8.0 (GraphPad Software, San Diego, CA, United States). All values are presented as mean ± standard error of the mean (SEM). All the data acquired from our experiments are in accordance with normal distribution. Differences between two groups were analyzed using unpaired Student's t-test. One-way ANOVA followed by Bonferroni post hoc test was used for multiple-group comparisons. p value < 0.05 was considered statistically significant.

3. Results

3.1. LCZ696 Improves Cardiac Function and Alleviates Cardiac Hypertrophy in Pressure Overload-Induced Cardiac Remodeling. To determine the effect of LCZ696 on pathological cardiac hypertrophy, wild type mice were administered with LCZ696 via oral gavage at a dose of 20 mg/kg/d for 4 weeks. After 4 weeks of aortic constriction, the mice were anaesthetized, and echocardiography was performed. Administration of LCZ696 increased ejection fraction and fractional shortening (Figures 1(a) and 1(b)), which were both dramatically decreased following TAC surgery. Similarly, TAC caused marked pathological cardiac hypertrophy as indicated by increased ratios of heart weight (HW) to body weight (BW), lung weight (LW) to BW, and HW to tibia length (TL). LCZ696 treatment reduced these ratios, suggesting improved cardiac hypertrophy contractile dysfunction. General view under the microscope and HE staining of the cardiac cross-section also confirmed that TAC-induced cardiac dilation was significantly inhibited by LCZ696 (Figure 1(d)). Furthermore, HE and WGA staining showed that LCZ696 substantially reduced the cross-sectional area of cardiomyocytes (Figures 2(a) and 2(b)). Also, the mRNA markers of cardiac hypertrophy, including atrial natriuretic peptide (ANP), brain natriuretic peptide (BNP), and β-myosin heavy chain (β-MHC), also referred to as fetal genes, were overtly surged in TAC-primed hearts compared with the sham group. Expectedly, LCZ696 treatment significantly decreased the expression levels of these fetal genes (Figure 2(c)).

3.2. LCZ696 Attenuates TAC-Induced Cardiac Fibrosis. Myocardial fibrosis is a crucial feature in pathological cardiac remodeling, which results in impaired cardiac compliance and a decline in the pumping function of the heart. These together promote the progression of hypertrophy to heart failure. Herein, we estimated the effect of LCZ696 in TAC-induced cardiac fibrosis, a classic feature of pathological cardiac hypertrophy, to further elucidate the role of LCZ696 in maladaptive cardiac hypertrophy. Picric Sirius red (PSR) staining and Masson's trichrome staining showed that no significant collagen deposition occurred in the sham group. However, the hearts of TAC mice exhibited severe collagen deposition both in interstitial and in perivascular areas (Figures 3(a) and 3(b)). As expected, LZC696 treatment significantly attenuated TAC-induced cardiac fibrosis (Figure 3(d)). Furthermore, immunohistochemistry staining revealed that LCZ696 treatment markedly alleviated α-SMA deposition, which is the hallmark of the transformation of fibroblasts to myofibroblasts. Moreover, we detected the transcription levels of fibrotic markers, including collagen I, collagen III, TGF-β, and CTGF. TAC-induced upregulation of these genes was overtly reversed by LCZ696 treatment (Figure 3(e)).

3.3. LCZ696 Mitigates TAC-Induced Myocardium Oxidative Stress and Cellular Apoptosis. Given that oxidative stress can deteriorate cardiac hypertrophy and heart failure [11–13], we examined the effect of LCZ696 on TAC-induced hearts for oxidative stress damage. Pathological hypertrophic stimuli remarkably triggered the production of peroxide byproducts, such as nitrotyrosine (NT) and 4 hydroxynonenal (4-HNE) and superoxide accumulation, as indicated by DHE staining (Figures 4(a)–4(c)). Consistent with our speculations, LCZ696 reduced the deposition of ROS in the myocardium as a result of pressure overload. Furthermore, we assessed myocardial apoptosis using terminal deoxynucleotidyl transferase-mediated dUTP nick-end labeling (TUNEL) assay. LCZ696 attenuated cardiomyocyte apoptosis, as revealed by TUNEL staining (Figure 5(a)). In addition, we examined Bax and Bcl-2 protein levels in different groups, which are both protein markers for apoptosis detection. As expected, LCZ696 remarkably decreased the level of Bax and Bcl-2 expression induced by TAC (Figures 5(b) and 5(c)).

Given that LCZ696 can exert antihypertrophic and antifibrosis effects and attenuate oxidative stress, we further explored the antioxidant reagents in the TAC-induced mice. Pathological hypertrophic stimuli overtly reduced the expression level of MnSOD and Sirt3, whereas LCZ696 treatment distinctly reversed the downregulation of MnSOD and Sirt3 (Figures 5(d)–5(g)). Moreover, we found that LCZ696 upregulated the phosphorylation of AMPK, which was inhibited by pressure overload (Figures 5(h) and 5(i)). Given this, we hypothesized that LCZ696 might exert an antihypertrophic effect by modulating Sirt3 in an AMPK-dependent manner. Thus, we conducted *in vitro* experiments to confirm our speculations.

3.4. LCZ696 Blocks the Hypertrophic Response and Alleviates Oxidative Stress and Apoptosis in NRCMs Stimulated with Phenylephrine. Here, we verified the effect of LCZ696 on NRCMs. Firstly, we conducted a cell viability assay to evaluate effect of different concentrations of LCZ696 on cardiomyocyte viability (Supplementary Figure S2), and we used 20 μM LCZ696 to incubate with NRCMs in the following *in vitro* experiments. Then, phenylephrine (PE, 50 μmol/L) was used to stimulate NRCMs for 24 h to imitate the process of cardiac hypertrophy *in vitro*. As expected, LCZ696 reduced the surface area of hypertrophied cardiomyocytes, as demonstrated by α-actinin staining (Figures 6(a) and 6(b)). Likewise, transcription levels of other hypertrophic markers, such as atrial natriuretic peptide (ANP), brain natriuretic peptide (BNP), and β-myosin heavy chain (β-MHC), were significantly increased in the PE-treated cardiomyocytes compared with the control group. LCZ696 overtly reduced the expression of these fetal genes (Figure 6(c)).
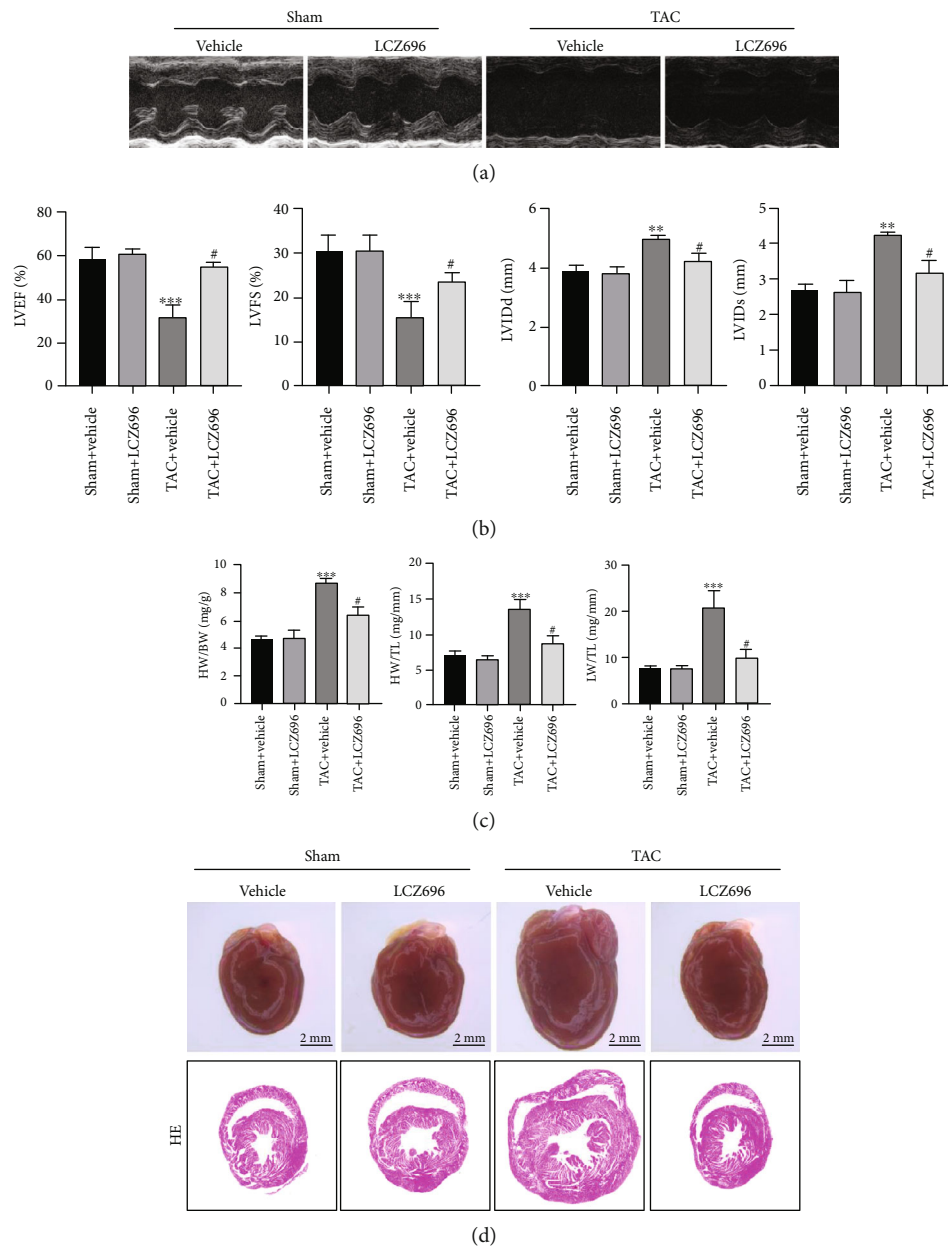
(a)

(b)

(c)

(d)

Figure 1: LCZ696 improved cardiac function in pressure overload-induced cardiac hypertrophy. (a) Representative images of echocardiography for sham or TAC mice treated with vehicle or LCZ696 for 4 weeks. (b) Cardiac function as determined by echocardiography ($n = 6$ mice per group). (c) Statistics analysis of HW/BW, HW/TL, and LW/TL for different groups ($n = 6$ mice per group). (d) Anatomical view of the whole heart in different groups under a dissecting microscope and representative images of cross-sectional HE staining. Data are presented as mean $\pm$ SEM. $^{***}p < 0.001$ vs. sham+vehicle group, $^{#}p < 0.05$ vs. TAC+vehicle group. BW: body weight; HW: heart weight; LW: lung weight; TL: tibia length; HE: hematoxylin-eosin; LVEF: left ventricular ejection fraction; LVFS: left ventricular fractional shortening; LVIDd: left ventricular end-diastolic diameter; LVIDs: left ventricular end-systolic diameter; TAC: transverse aortic constriction.

We also monitored the oxidative damage induced by phenylephrine in NRCMs. LCZ696 reduced the intensity of DCFH fluorescence in NRCMs following PE treatment. Furthermore, we detected the levels of superoxide in the mitochondria via MitoSOX staining (Life Technologies, Darmstadt, Germany). As anticipated, LCZ696 significantly reduced the oxidative stress in the mitochondria

(Figure 6(e)). Besides, LCZ696 reduced cardiomyocyte apoptosis, as witnessed by TUNEL staining (Figure 6(f)).

3.5. LCZ696 Represses Cardiac Hypertrophy by Upregulating Sirt3. Here, we explored the underlying mechanisms of the antihypertrophic effect of LCZ696 in a PE-induced cardiomyocyte hypertrophy model. First, we tested the expression

(a)

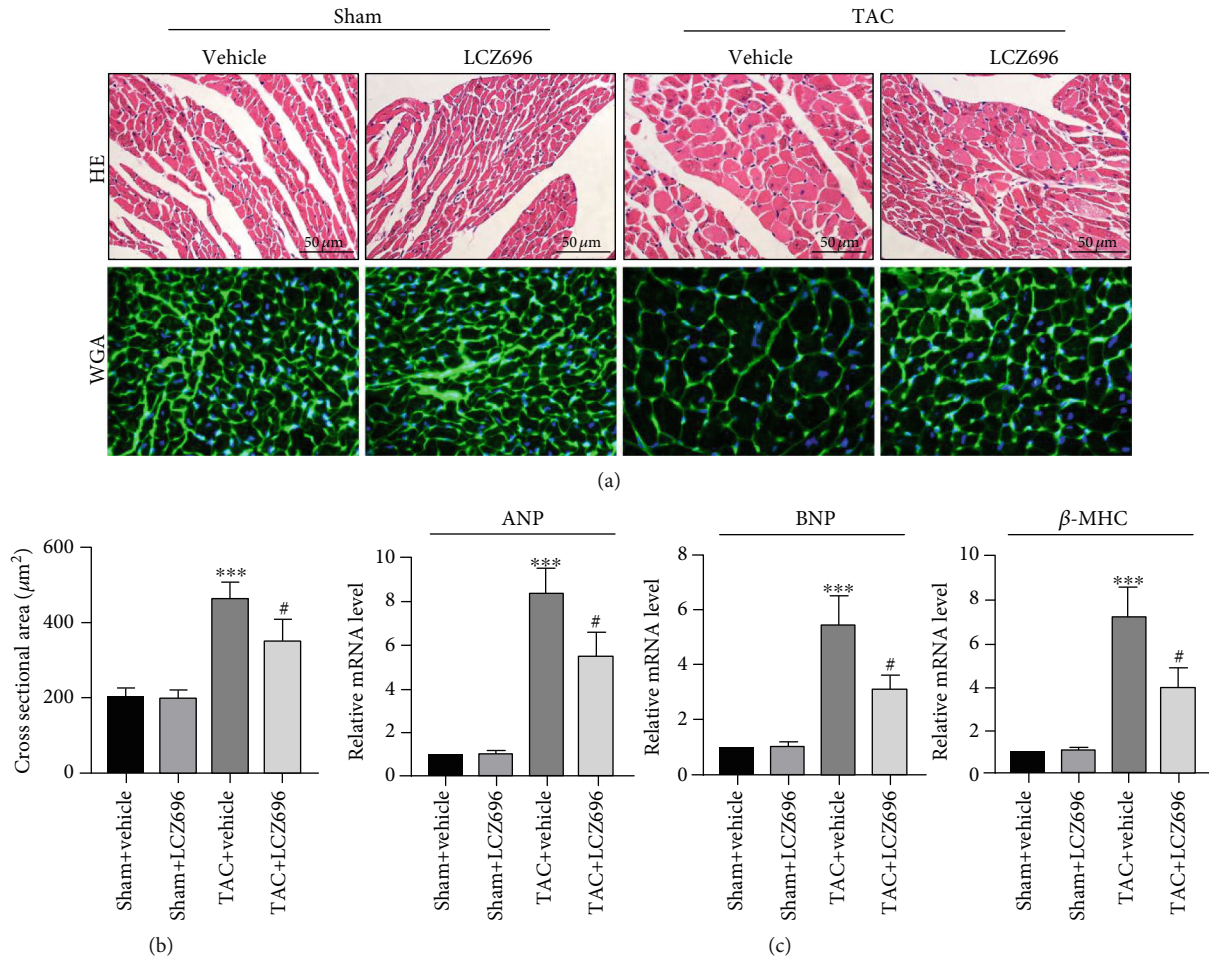(b)   (c)

FIGURE 2: LCZ696 treatment mitigated TAC-induced pathological cardiac hypertrophy. (a) Representative cross-sectional HE staining images and WGA staining images for the sham or TAC mouse hearts treated with vehicle or LCZ696 for 4 weeks. (b) Statistics analysis of cross-sectional areas of cardiomyocytes based on HE staining ($n > 100$ cells per group). (c) mRNA levels of ANP and BNP in different treatment groups. mRNA levels are normalized to the GAPDH mRNA level and converted to fold change relative to the sham+vehicle group ($n = 6$ mice per group). Data are presented as mean ± SEM. ***$p < 0.001$ vs. the sham+vehicle group, #$p < 0.05$ vs. the TAC+vehicle group. ANP: atrial natriuretic peptide; BNP: brain natriuretic peptide; WGA: wheat germ agglutinin; β-MHC: myosin heavy chain β.

level of Sirt3 and MnSOD. Consistent with the abovementioned results (Figure 5), hypertrophic stimuli inhibited Sirt3 and MnSOD expressions following PE treatment. With that, we introduced small interfering RNA (siRNA) to knock down the Sirt3 expression. LCZ696 did not upregulate the expression of MnSOD after the Sirt3 knockdown (Figure 7(c)). We then determined the cellular localization of Sirt3 in cardiomyocytes. Sirt3 was colocalized with mitochondrial marker COX IV and decreased in response to PE stimulation (Figure 7(e)). LCZ696 upregulated Sirt3 expression following PE treatment. Notably, LCZ696 did not upregulate the level of Sirt3 basal expression.

3.6. Sirt3 Knockdown Abolishes the Protective Effect of LCZ696 on Cardiomyocyte Hypertrophy.
Sirt3 deficiency impaired the cardioprotective effect of LCZ696 in alleviating hypertrophic response of cardiomyocytes following PE treatment (Figure 8(a)). In addition, LCZ696 did not influence the expression of Bax and Bcl-2 under Sirt3 deficiency conditions

(Figures 8(c) and 8(d)). Furthermore, Sirt3 knockdown abolished the alleviation of oxidative stress mediated by LCZ696 (Figure 8(e)). To verify the involvement of Sirt3 in the LCZ696-induced antioxidant property, we performed Mito-SOX staining to examine the generation of superoxide by the mitochondria. Sirt3 deficiency aggravated PE-induced oxidative stress and abrogated the protective effect of LCZ696 in mitochondrial ROS generation. Phenylephrine (PE) stimulation decreased the ratio of p-AMPK/AMPK, which was reversed by LCZ696. However, Sirt3 knockdown impeded this process, indicating that the cardioprotective effect of LCZ696 was partly involved in the upregulation of phospho-AMPK.

4. Discussion

In recent decades, heart failure-associated deaths have increased drastically, prompting researchers to focus on conducting studies that can solve the problem. Nevertheless, heart
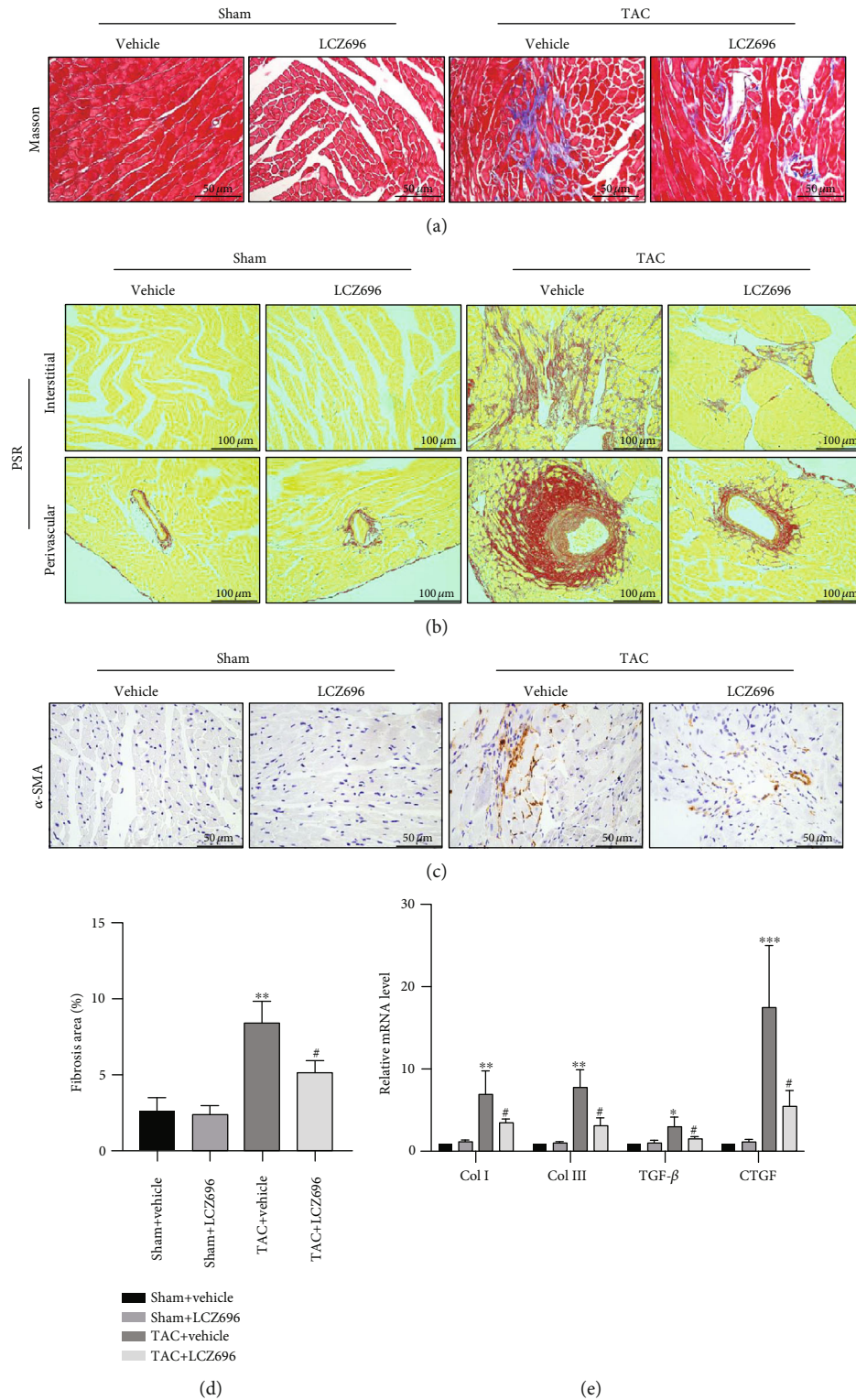
(a)

(b)

(c)

(d)

(e)

FIGURE 3: LCZ696 treatment attenuated TAC-induced cardiac fibrosis. (a) Representative images of Masson trichrome staining in different treatment groups. (b) Representative images of Picric Sirius red (PSR) staining of cardiac interstitial and perivascular regions in different treatment groups. (c) Representative immunohistochemical staining of α-SMA for myofibroblasts. (d) Quantification of the percentage of left ventricular fibrosis area from (b) ($n = 6$ mice per group). (e) mRNA levels of collagen I, collagen III, TGF-β, and CTGF in the indicated groups ($n = 6$ mice per group). The results are normalized against GAPDH and converted to fold change relative to the sham+vehicle group ($n = 6$ mice per group). Data are presented as mean ± SEM. ***$p < 0.001$ vs. the sham+vehicle group, #$p < 0.05$ vs. the TAC+vehicle group.
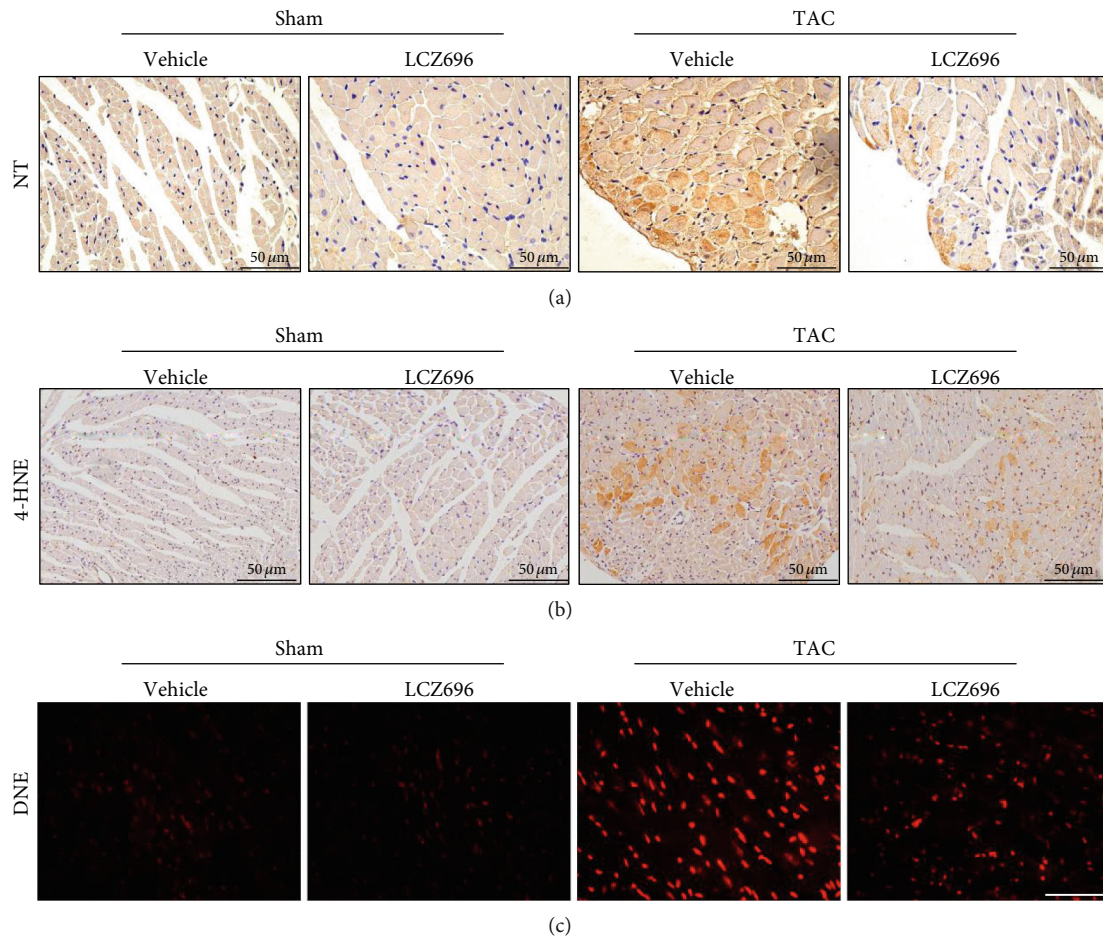
(a)

(b)

(c)

FIGURE 4: LCZ696 treatment mitigated TAC-induced oxidative stress. (a) Representative immunohistochemical staining images of nitrotyrosine (NT) performed to assess myocardial nitrotyrosine production in different groups. (b) Representative immunohistochemical staining images of 4 hydroxynonenal (4-HNE) performed to assess myocardial lipid peroxidation. (c) Representative immunofluorescence staining images of dihydroethidium (DHE) performed to assess myocardial ROS accumulation.

failure is the last battlefield in cardiovascular therapy and has always been challenging to tackle [25, 26]. Many pathological conditions, such as acute myocardial infarction, chronic uncontrolled hypertension, and diabetes, can contribute to the occurrence of heart failure. Among them, cardiac hypertrophy, which is usually caused by pressure or volume overload, is the most common cause of heart failure [1, 2, 27].

LCZ696, also referred to as sacubitril/valsartan, is currently the standard treatment option against the progression of heart failure with reduced ejection fraction [4–7]. Numerous studies have examined the cardioprotective effects of LCZ696 on left ventricular remodeling after myocardial infarction. LCZ696 improves cardiac function by attenuating cardiac fibrosis and MMP-9 expression after ischemia-reperfusion (IR) injury [22, 28, 29]. Moreover, LCZ696 can attenuate cardiac remodeling and cardiac inflammation by alleviating dynamin-related protein 1 (Drp-1) expression in a doxorubicin-induced cardiomyopathy animal model [30]. Although there are several reports on the basic mechanisms underlying the effectiveness of LCZ696, candidate mechanisms responsible for

the direct protective effect of LCZ696 against cardiomyocyte hypertrophy remain unexplored.

Several studies have confirmed that reactive oxygen species (ROS) can cause adverse effects by oxidizing proteins, lipids, and nucleic acids. Cardiac hypertrophy and oxidative stress are mutually causal, forming a vicious circle. Therefore, breaking the vicious circle could be a vital breakthrough in the treatment of heart failure. However, antioxidant therapy has not been developed. Recent studies have confirmed that impairment of catalase, a major antioxidant enzyme, can aggravate diabetes-induced cardiac toxicity. On the contrary, cardiac-specific overexpression of catalase alleviated aging-related cardiac dysfunction and cardiac hypertrophy [31, 32]. Superoxide dismutases (SOD) are the major antioxidant enzymes responsible for the scavenger of superoxide in the mitochondria. Among them, manganese SOD (MnSOD, SOD2) in the mitochondria plays a pivotal role in redox homeostasis [33]. Manganese superoxide dismutase (MnSOD) is a major superoxide-scavenging enzyme, converting superoxide to hydrogen peroxide, which is in turn hydrolyzed to water by catalase [34].
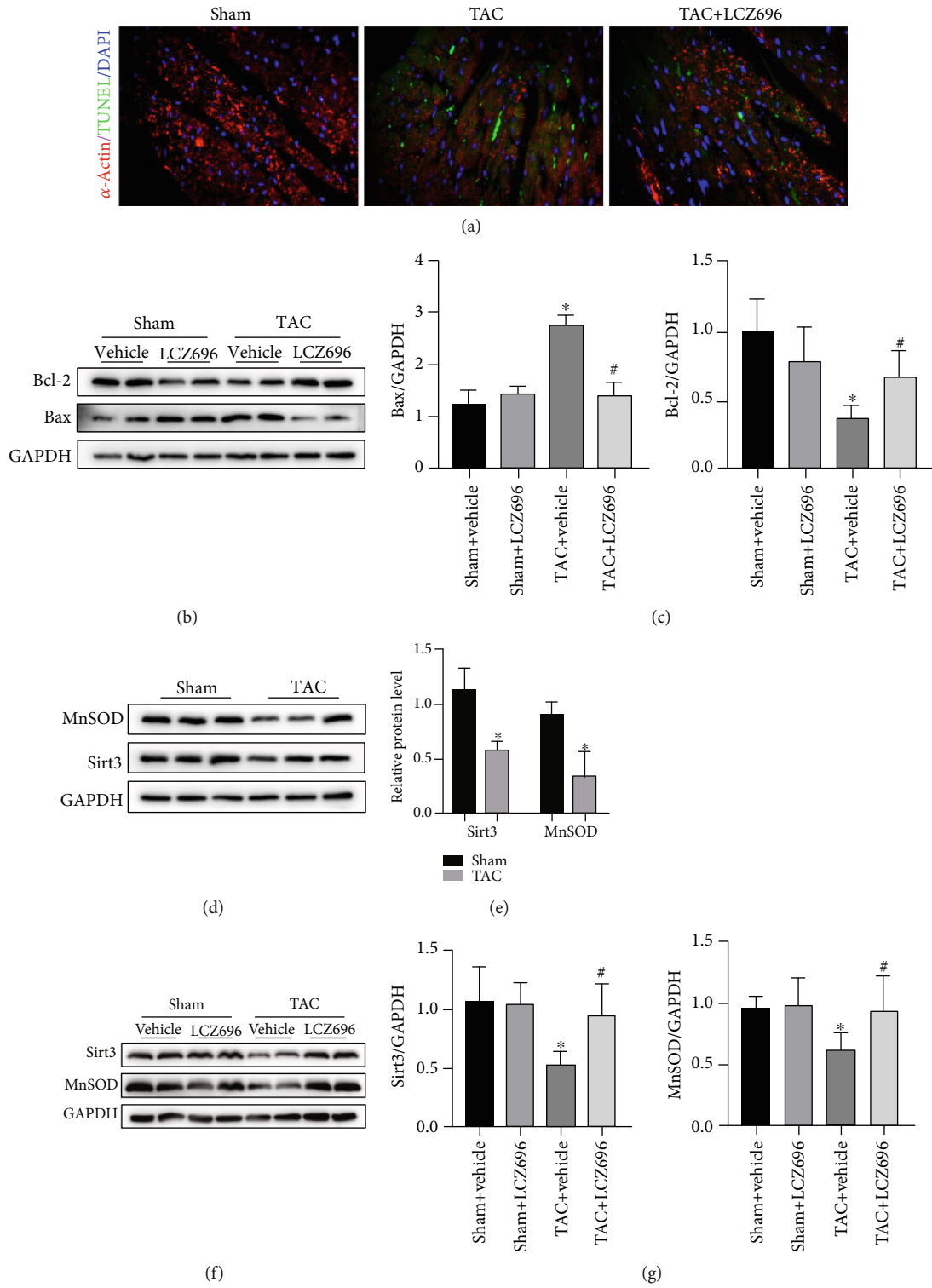
(a)

(b)

(c)

(d)

(e)
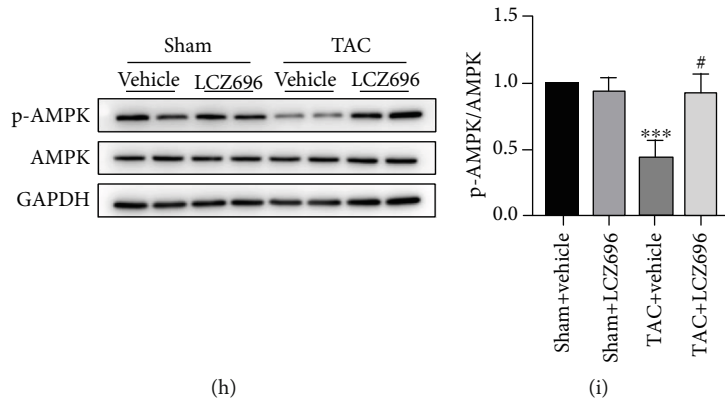

(f)

(g)

Figure 5: Continued.

(h)

(i)

FIGURE 5: LCZ696 treatment alleviated TAC-induced myocardial apoptosis. (a) Representative TUNEL staining images performed to assess myocardial apoptosis in mouse hearts in different groups. (b, c) Western blot analysis and quantitative analysis of Bcl-2 and Bax protein levels in different cardiac homogenates. (d) The protein expression of Sirt3 and MnSOD levels as detected by Western blot. (e) Histograms showing the quantitative expression of Sirt3 and MnSOD, $n = 3$. (f) Expression levels of Sirt3 and MnSOD in hearts from different groups. (g) Histogram of the quantitative analysis of the data in (f), after normalization to the expression of GAPDH, $n = 3$. (h) Western blot analysis of p-AMPK and AMPK protein levels in different cardiac homogenates. (i) Quantitative analysis of the ratio of p-AMPK/AMPK, $n = 3$. $^{*}p < 0.05$ vs. the sham+vehicle group, $^{***}p < 0.001$ vs. the sham+vehicle group, $^{#}p < 0.05$ vs. the TAC+vehicle group.

Sirt3 belongs to CLASS III histone deacetylases (HDACs) and localizes to the mitochondrial matrix, where it may function as a primary stress-responsive protein deacetylase [35]. Many studies have focused on examining the cardioprotective role of Sirt3 in cardiac hypertrophy and heart failure [36]. For example, Sirt3 knockout mice exhibited severe cardiac hypertrophy and fibrosis induced by TAC, and nevertheless, cardiomyocyte-specific overexpression of Sirt3 resisted cardiac fibrosis and oxidative damage following angiotensin II infusion [20]. A study also reported that Sirt3-deficient mice developed dilated cardiomyopathy, and Sirt3 knockout mice exacerbated angiotensin II-induced cardiac hypertrophy [19]. SIRT3 deficiency can aggravate diabetic cardiomyopathy by inactivating Foxo3A-mediated mitophagy and accelerate hypertensive cardiac remodeling by impairing angiogenesis [35, 37]. Besides, Sirt3 silencing can abolish the protective effects of NaHS to reverse Ang II-induced cardiomyocyte hypertrophy and mitochondrial dysfunction as a result of the decline in FOXO3a and SOD2 expression [38, 39]. Studies have shown that many small molecules with Sirt3-activating property can protect against cardiac hypertrophy and heart failure. Honokiol increases Sirt3 activity, thereby alleviating the severity of cardiac hypertrophy [40]. It also reduces oxidative stress induced by melatonin and improves cardiac function by interacting with the Sirt3-dependent pathway [41, 42]. Resveratrol, known as a potent activator of SIRT1, also ameliorates cardiac fibrosis by slightly activating Sirt3 [43]. Sirt3 plays an anticarcinogenic role and functions as a tumor suppressor protein [44]. Clinical studies have shown that the Sirt3 level decreases by 40% in 65-year-old people [45], which may be closely related to the occurrence of many multiple senile diseases, such as hypertension, atherosclerosis, and heart failure.

Given that Sirt3 can play such a crucial role in pathological cardiac remodeling by deacetylating MnSOD [20, 44, 46], we hypothesized that LCZ696 might regulate the expression of Sirt3, mitigate oxidative stress, and thus improve cardiac hypertrophy and heart failure. To verify our hypothesis, we conducted an *in vivo* experiment with transverse aortic constriction, as described earlier. Laparoscopic Transabdominal Cerclage (TAC) mice exhibited deteriorated cardiac dysfunction as evidenced by echocardiography and the ratios of HW/BW, HW/TL, and LW/TL (Figure 1). Moreover, TAC markedly promoted the fibrosis deposition and transdifferentiation from fibroblast to myofibroblast, and as a result, cardiac distensibility declined. Fortunately, LZC696 alleviated myocardium hypertrophy and fibrosis, thereby improving cardiac function. With that, we investigated the mechanisms underlying the role of LCZ696 in cardiac hypertrophy. Pressure overload repressed the expression level of Sirt3 and MnSOD, whereas LCZ696 rescued the decline of Sirt3 and MnSOD. Also, we found that LCZ696 upregulated the phosphorylation of AMPK, whose deficiency could aggravate pressure overload-induced cardiac hypertrophy. Therefore, we hypothesized that LCZ696 might exert an antihypertrophic effect by modulating Sirt3 in an AMPK-dependent manner. To verify this hypothesis, we conducted *in vitro* experiments. Phenylephrine (PE) was used to stimulate neonatal rat cardiomyocytes (NRCMs) to imitate an *in vitro* cardiac hypertrophy model. As explained earlier, LCZ696 blocked the hypertrophic response and alleviated oxidative stress and apoptosis in NRCMs following PE stimulation. In addition, LCZ696 upregulated Sirt3 and MnSOD expression, as well as the ratio of p-AMPK/AMPK. However, Sirt3 silencing abolished the ability of LCZ696 to reverse the PE-induced cardiomyocyte hypertrophy, mitochondrial oxidative stress, and apoptosis, along with the decline in MnSOD expression. Also, Sirt3 deficiency hampered the capacity of LCZ696 to activate the phosphorylation of AMPK. Collectively, these results demonstrate that Sirt3 could be an endogenous negative regulator of cardiac hypertrophy, which protects hearts by suppressing cellular levels of ROS. In addition, LCZ696 might exert antihypertrophic effect by ameliorating oxidative stress via the Sirt3/MnSOD pathway.
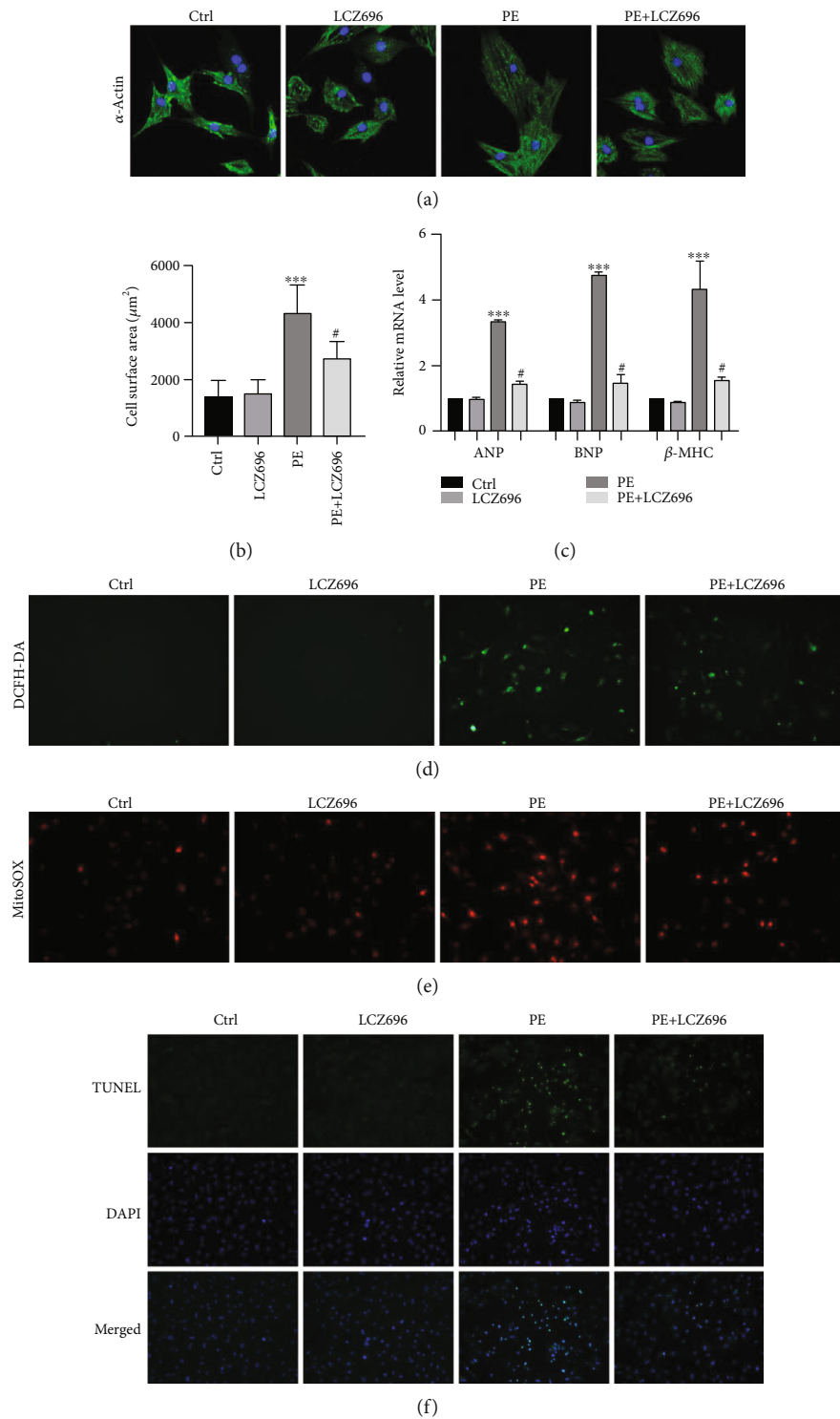
(a)

(b)

(c)

(d)

(e)

(f)

FIGURE 6: LCZ696 blocked the hypertrophic response in NRCMs. (a) Immunofluorescence staining of sarcomeric alpha-actinin (α-actinin) in primary neonatal rat cardiomyocytes (NRCMs) in the indicated treatment groups. (b) The cell surface area of the indicated groups ($n > 50$ cells per experimental group). (c) mRNA levels of *ANP*, *BNP*, and *β-MHC* in different treatment groups. The results were normalized against *GAPDH* and converted to fold change relative to the ctrl group. (d) Intracellular ROS levels in primary cardiomyocytes were quantified with DCFH-DA staining. (e) Mitochondrial ROS levels in primary cardiomyocytes were measured by MitoSOX staining. (f) Representative TUNEL staining of primary cardiomyocytes in different treatment groups. Data are presented as mean ± SEM. ***$p < 0.001$ vs. the control group, #$p < 0.05$ vs. the PE treatment group.

(a)

(b)

(c)

(d)
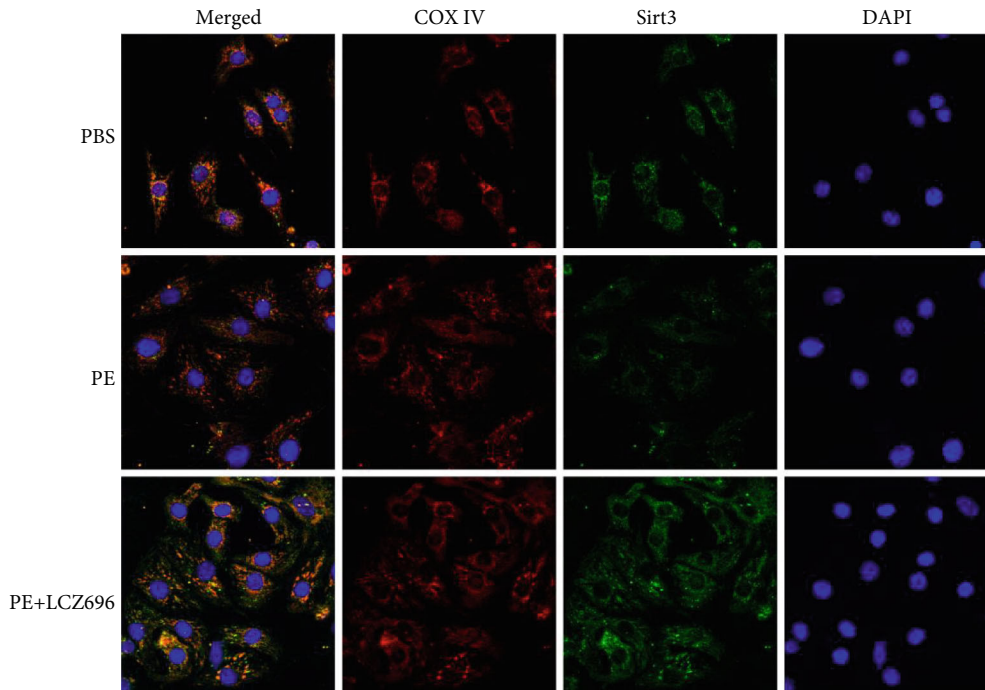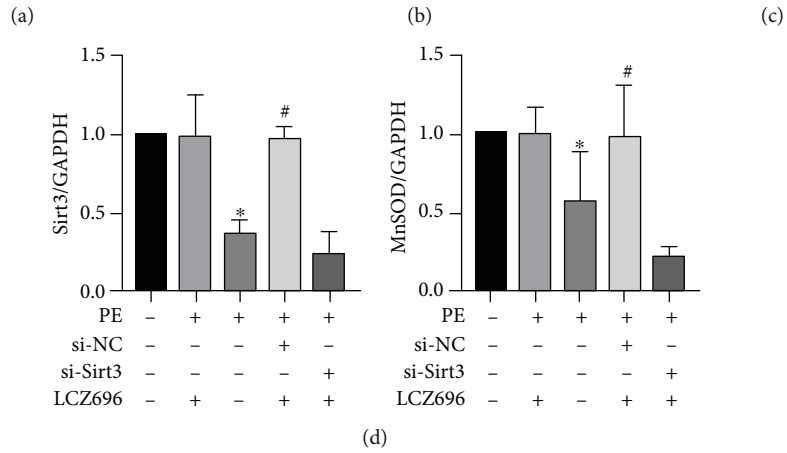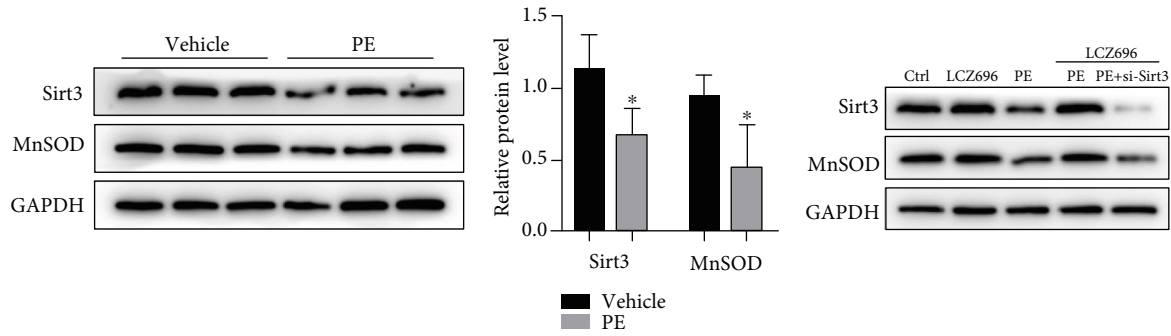
(e)

FIGURE 7: LCZ696 upregulated Sirt3 expression. (a) NRCMs were treated with 50 μM PE for 24 h, and the expression of Sirt3 and MnSOD were detected by Western blotting. (b) Histograms showing the quantitative analysis of Sirt3 and MnSOD, $n = 3$. (c) NRCMS were transfected with small interfering RNA targeting Sirt3 (si-Sirt3, 50 nM) of scramble small interfering RNA (si-NC, 50 nM) for 48 h and then treated as indicated. The expression of Sirt3 and MnSOD was determined with immunoblotting. (d) Histogram of the quantitative analysis of the data in (c), after normalization to the GAPDH levels, $n = 3$. (e) Representative images of immunofluorescence staining for Sirt3 and mitochondrial marker (COX IV) in NRCMs. *$p < 0.05$ vs. the control group, #$p < 0.05$ vs. the PE treatment group.

(a)

(b)

(c)

(d)

(e)

(f)

(g)

(h)
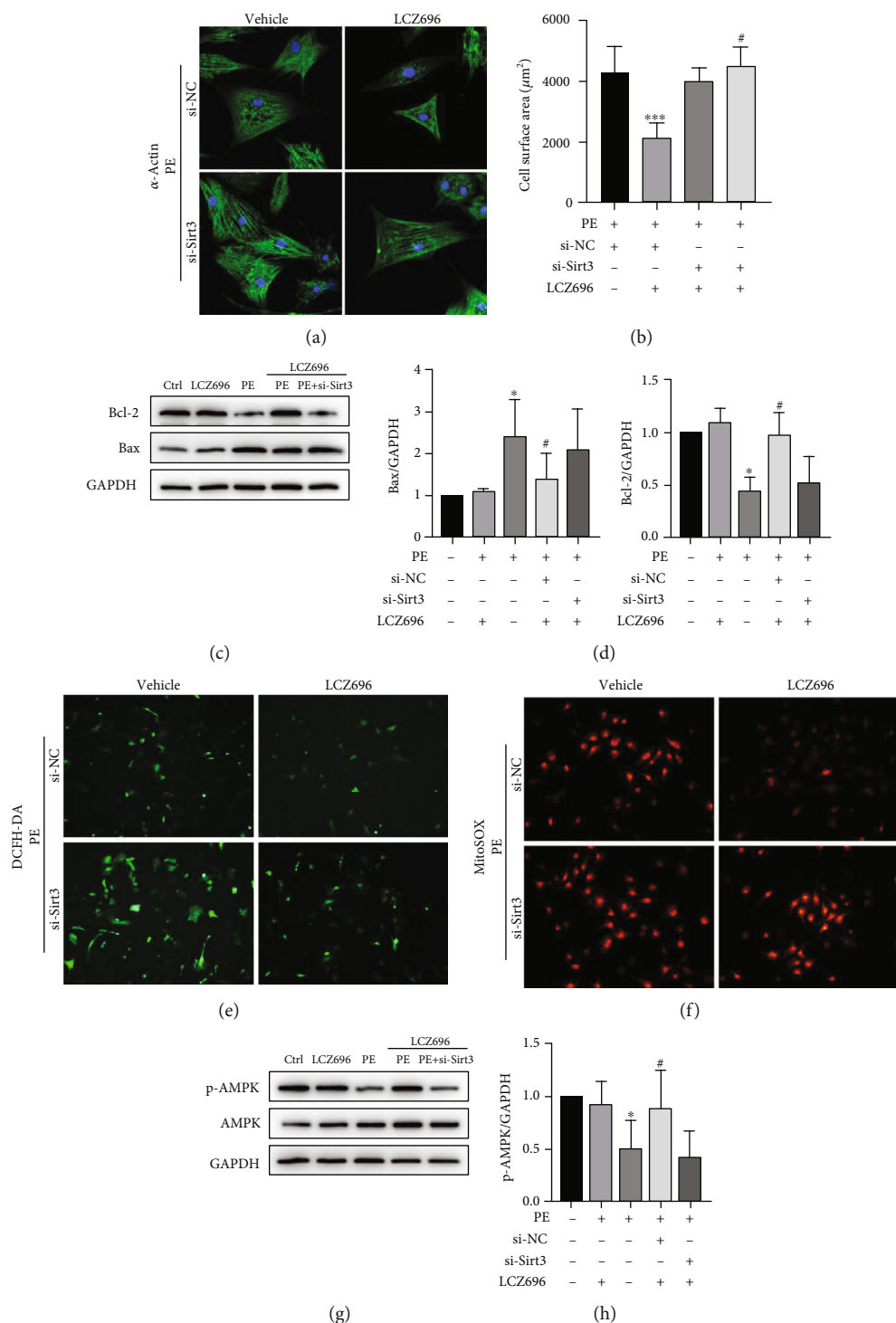
Figure 8: Sirt3 knockdown abolished the antihypertrophic effect of LCZ696 in PE-induced cardiomyocyte hypertrophy. (a) Immunofluorescence staining of α-actinin in primary neonatal rat cardiomyocytes (NRCMs) in the indicated groups. (b) The cell surface area in the indicated groups ($n > 50$ cells per experimental group), ***$p < 0.001$ vs. the si-NC+vehicle group, #$p < 0.05$ vs. the si-NC+LCZ696 treatment group. (c, d) Western blot analysis and quantitative analysis of Bcl-2 and Bax protein levels from different treatment groups. (e) Representative images of DCFH-DA staining in NRCMs. (f) Representative images of MitoSOX staining in NRCMs. (g, h) Western blot analysis of p-AMPK and AMPK protein levels in different treatment NRCMs and quantitative analysis of the ratio of p-AMPK/AMPK, $n = 3$. *$p < 0.05$ vs. control group, #$p < 0.05$ vs. PE treatment group.

5. Conclusion

Our results show that Sirt3 can act as a therapeutic target in the treatment of heart failure. Also, the application of specific small molecules for activating Sirt3 can be a novel strategy to hinder the progression of pathological hypertrophy into heart failure. These findings provide new insights into the molecular mechanism of LCZ696 and its novel therapeutic role in the treatment of pathological cardiac remodeling and heart failure.

Data Availability

The data used to support the findings of this study are available from the corresponding author upon request.

Conflicts of Interest

The authors declare that they have no conflicts of interest.

Authors' Contributions

Shi Peng, Xiao-feng Lu, and Yi-ding Qi contributed equally to this work.

Acknowledgments

Supplementary Materials

Supplementary Table S1: mouse primer sequences for qRT-PCR. Supplementary Table S2: rat primer sequences for qRT-PCR. Supplementary Table S3: sequences of siRNAs for Sirt3. Supplementary Table S4: primary and secondary antibodies used in the Western blot. Supplementary Figure S1: the effect of different small interference sequences for Sirt3 knockdown. As shown in the figure, sequence 1 (Si-1) and sequence 3 (Si-3) effectively knockdown Sirt3 expression and Si-3 works best. As a result, we used Si-3 in our following experiments. Supplementary Figure S2: cell viability assay of different concentrations of LCZ696 in primary cardiomyocytes. Neonatal rat cardiomyocytes were seeded onto a 96-well plate overnight, and different concentrations of LCZ696 (0, 20, 30, 40 μM) were added into culture medium for 24 h. Then, cell viability was measured using a commercial Cell Counting Kit-8 (CCK-8, MedChemExpress, Monmouth Junction, NJ, USA). The concentration of LCZ696 used in our *in vitro* experiment is 20 μM. (Supplementary Materials)

References

[1] D. Lazzeroni, O. Rimoldi, and P. G. Camici, "From left ventricular hypertrophy to dysfunction and failure," *Circulation journal : official journal of the Japanese Circulation Society*, vol. 80, no. 3, pp. 555–564, 2016.

[2] A. M. Katz and E. L. Rolett, "Heart failure: when form fails to follow function," *European Heart Journal*, vol. 37, no. 5, pp. 449–454, 2016.

[3] M. Packer, "The future treatment of heart failure?," *European Heart Journal*, vol. 39, no. 1, pp. 5–7, 2018.

[4] J. J. V. McMurray, M. Packer, A. S. Desai et al., "Angiotensin-neprilysin inhibition versus enalapril in heart failure," *The New England Journal of Medicine*, vol. 371, no. 11, pp. 993–1004, 2014.

[5] A. S. Desai, J. J. V. McMurray, M. Packer et al., "Effect of the angiotensin-receptor-neprilysin inhibitor LCZ696 compared with enalapril on mode of death in heart failure patients," *European Heart Journal*, vol. 36, no. 30, pp. 1990–1997, 2015.

[6] S. D. Solomon, J. McMurray, I. S. Anand et al., "Angiotensin-neprilysin inhibition in heart failure with preserved ejection fraction," *The New England Journal of Medicine*, vol. 381, no. 17, pp. 1609–1620, 2019.

[7] M. Packer, J. McMurray, A. S. Desai et al., "Angiotensin receptor neprilysin inhibition compared with enalapril on the risk of clinical progression in surviving patients with heart failure," *Circulation*, vol. 131, no. 1, pp. 54–61, 2015.

[8] J. McMurray, M. Packer, A. Desai et al., "A putative placebo analysis of the effects of LCZ696 on clinical outcomes in heart failure," *European Heart Journal*, vol. 36, no. 7, pp. 434–439, 2015.

[9] H. N. Siti, Y. Kamisah, and J. Kamsiah, "The role of oxidative stress, antioxidants and vascular inflammation in cardiovascular disease (a review)," *Vascular Pharmacology*, vol. 71, pp. 40–56, 2015.

[10] M. N. Sack, F. Y. Fyhrquist, O. J. Saijonmaa, V. Fuster, and J. C. Kovacic, "Basic biology of oxidative stress and the cardiovascular system: part 1 of a 3-part series," *Journal of the American College of Cardiology*, vol. 70, no. 2, pp. 196–211, 2017.

[11] A. K. Dhalla, M. F. Hill, and P. K. Singal, "Role of oxidative stress in transition of hypertrophy to heart failure," *Journal of the American College of Cardiology*, vol. 28, no. 2, pp. 506–514, 1996.

[12] M. Seddon, Y. H. Looi, and A. M. Shah, "Oxidative stress and redox signalling in cardiac hypertrophy and heart failure," *Heart*, vol. 93, no. 8, pp. 903–907, 2007.

[13] E. Takimoto and D. A. Kass, "Role of oxidative stress in cardiac hypertrophy and remodeling," *Hypertension*, vol. 49, no. 2, pp. 241–248, 2007.

[14] A. Doroszko, P. Dobrowolski, A. Radziwon-Balicka, and R. Skomro, "New insights into the role of oxidative stress in onset of cardiovascular disease," *Oxidative Medicine and Cellular Longevity*, vol. 2018, Article ID 9563831, 2 pages, 2018.

[15] A. Belló-Klein, N. Khaper, S. Llesuy, D. V. Vassallo, and C. Pantos, "Oxidative stress and antioxidant strategies in cardiovascular disease," *Oxidative Medicine and Cellular Longevity*, vol. 2014, Article ID 678741, 2 pages, 2014.

[16] R. S. Balaban, S. Nemoto, and T. Finkel, "Mitochondria, oxidants, and aging," *Cell*, vol. 120, no. 4, pp. 483–495, 2005.

[17] A. Fukushima and G. D. Lopaschuk, "Acetylation control of cardiac fatty acid β-oxidation and energy metabolism in obesity, diabetes, and heart failure," *Biochimica et Biophysica Acta*, vol. 1862, no. 12, pp. 2211–2220, 2016.

[18] A. H. H. Tseng, S.-S. Shieh, and D. L. Wang, "SIRT3 deacetylates FOXO3 to protect mitochondria against oxidative damage," *Free Radical Biology & Medicine*, vol. 63, pp. 222–234, 2013.

[19] C. Koentges, K. Pfeil, T. Schnick et al., "SIRT3 deficiency impairs mitochondrial and contractile function in the heart," *Basic Research in Cardiology*, vol. 110, no. 4, p. 36, 2015.

[20] N. R. Sundaresan, M. Gupta, G. Kim, S. B. Rajamohan, A. Isbatan, and M. P. Gupta, "Sirt3 blocks the cardiac hypertrophic response by augmenting Foxo3a-dependent antioxidant defense mechanisms in mice," *The Journal of Clinical Investigation*, vol. 119, no. 9, pp. 2758–2771, 2009.

[21] L. Xu, Y. Su, Y. Zhao et al., "Melatonin differentially regulates pathological and physiological cardiac hypertrophy: crucial role of circadian nuclear receptor RORα signaling," *Journal of Pineal Research*, vol. 67, no. 2, p. e12579, 2019.

[22] M. Ishii, K. Kaikita, K. Sato et al., "Cardioprotective effects of LCZ696 (sacubitril/valsartan) after experimental acute myocardial infarction," *JACC Basic Transl Sci*, vol. 2, no. 6, pp. 655–668, 2017.

[23] J. Torrado, C. Cain, A. G. Mauro et al., "Sacubitril/valsartan averts adverse post-infarction ventricular remodeling and preserves systolic function in rabbits," *Journal of the American College of Cardiology*, vol. 72, no. 19, pp. 2342–2356, 2018.

[24] S. Peng, L. W. Xu, X. Y. Che et al., "Atorvastatin inhibits inflammatory response, attenuates lipid deposition, and improves the stability of vulnerable atherosclerotic plaques by modulating autophagy," *Frontiers in Pharmacology*, vol. 9, p. 438, 2018.

[25] E. Braunwald, "The war against heart failure: the Lancet lecture," *Lancet*, vol. 385, no. 9970, pp. 812–824, 2015.

[26] J. O. Mudd and D. A. Kass, "Tackling heart failure in the twenty-first century," *Nature*, vol. 451, no. 7181, pp. 919–928, 2008.

[27] T. Oka and I. Komuro, "Molecular mechanisms underlying the transition of cardiac hypertrophy to heart Failure," *Circulation Journal*, vol. 72, SupplementA, pp. A13–A16, 2008.

[28] Y. Suematsu, S. I. Miura, M. Goto et al., "LCZ696, an angiotensin receptor-neprilysin inhibitor, improves cardiac function with the attenuation of fibrosis in heart failure with reduced ejection fraction in streptozotocin-induced diabetic mice," *European Journal of Heart Failure*, vol. 18, no. 4, pp. 386–393, 2016.

[29] T. G. von Lueder, B. H. Wang, A. R. Kompa et al., "Angiotensin receptor neprilysin inhibitor LCZ696 attenuates cardiac remodeling and dysfunction after myocardial infarction by reducing cardiac fibrosis and hypertrophy," *Circulation. Heart Failure*, vol. 8, no. 1, pp. 71–78, 2015.

[30] Y. Xia, Z. Chen, A. Chen et al., "LCZ696 improves cardiac function via alleviating Drp1-mediated mitochondrial dysfunction in mice with doxorubicin-induced dilated cardiomyopathy," *Journal of Molecular and Cellular Cardiology*, vol. 108, pp. 138–148, 2017.

[31] W. Cong, D. Ruan, Y. Xuan et al., "Cardiac-specific overexpression of catalase prevents diabetes-induced pathological changes by inhibiting NF-κB signaling activation in the heart," *Journal of molecular and cellular cardiology*, vol. 89, no. Part B, pp. 314–325, 2015.

[32] D. F. Dai, L. F. Santana, M. Vermulst et al., "Overexpression of catalase targeted to mitochondria attenuates murine cardiac aging," *Circulation*, vol. 119, no. 21, pp. 2789–2797, 2009.

[33] H. He, H. Tao, H. Xiong et al., "Rosiglitazone causes cardiotoxicity via peroxisome proliferator-activated receptor γ-independent mitochondrial oxidative stress in mouse hearts," *Toxicological Sciences*, vol. 138, no. 2, pp. 468–481, 2014.

[34] T. Kim and Q. Yang, "Peroxisome-proliferator-activated receptors regulate redox signaling in the cardiovascular system," *World Journal of Cardiology*, vol. 5, no. 6, pp. 164–174, 2013.

[35] T. Wei, G. Huang, J. Gao et al., "Sirtuin 3 deficiency accelerates hypertensive cardiac remodeling by impairing angiogenesis," *Journal of the American Heart Association*, vol. 6, no. 8, 2017.

[36] J. Wu, Z. Zeng, W. Zhang et al., "Emerging role of SIRT3 in mitochondrial dysfunction and cardiovascular diseases," *Free Radical Research*, vol. 53, no. 2, pp. 139–149, 2019.

[37] W. Yu, B. Gao, N. Li et al., "Sirt3 deficiency exacerbates diabetic cardiac dysfunction: role of Foxo3A-Parkin-mediated mitophagy," *Biochimica et Biophysica Acta - Molecular Basis of Disease*, vol. 1863, no. 8, pp. 1973–1983, 2017.

[38] G. Meng, J. Liu, S. Liu et al., "Hydrogen sulfide pretreatment improves mitochondrial function in myocardial hypertrophy via a SIRT3-dependent manner," *British Journal of Pharmacology*, vol. 175, no. 8, pp. 1126–1145, 2018.

[39] J. Zhang, J. Yu, Y. Chen et al., "Exogenous hydrogen sulfide supplement attenuates isoproterenol-induced myocardial hypertrophy in a sirtuin 3-dependent manner," *Oxidative Medicine and Cellular Longevity*, vol. 2018, Article ID 9396089, 17 pages, 2018.

[40] V. B. Pillai, S. Samant, N. R. Sundaresan et al., "Honokiol blocks and reverses cardiac hypertrophy in mice by activating mitochondrial Sirt3," *Nature Communications*, vol. 6, no. 1, p. 6656, 2015.

[41] M. Zhai, B. Li, W. Duan et al., "Melatonin ameliorates myocardial ischemia reperfusion injury through SIRT3-dependent regulation of oxidative stress and apoptosis," *Journal of Pineal Research*, vol. 63, no. 2, p. 63(2), 2017.

[42] L. Yu, B. Gong, W. Duan et al., "Melatonin ameliorates myocardial ischemia/reperfusion injury in type 1 diabetic rats by preserving mitochondrial function: role of AMPK-PGC-1α-SIRT3 signaling," *Scientific Reports*, vol. 7, no. 1, p. 41337, 2017.

[43] T. Chen, J. Li, J. Liu et al., "Activation of SIRT3 by resveratrol ameliorates cardiac fibrosis and improves cardiac function via the TGF-β/Smad3 pathway," *American Journal of Physiology. Heart and Circulatory Physiology*, vol. 308, no. 5, pp. H424–H434, 2015.

[44] R. Tao, M. C. Coleman, J. D. Pennington et al., "Sirt3-mediated deacetylation of evolutionarily conserved lysine 122 regulates MnSOD activity in response to stress," *Molecular Cell*, vol. 40, no. 6, pp. 893–904, 2010.

[45] I. R. Lanza, D. K. Short, K. R. Short et al., "Endurance exercise as a countermeasure for aging," *Diabetes*, vol. 57, no. 11, pp. 2933–2942, 2008.

[46] P. Li, J. Ge, and H. Li, "Lysine acetyltransferases and lysine deacetylases as targets for cardiovascular disease," *Nature Reviews. Cardiology*, vol. 17, no. 2, pp. 96–115, 2020.

Research Article

Impact of Modality and Intensity of Early Exercise Training on Ventricular Remodeling after Myocardial Infarction

Diego Fernando Batista,[1] Bertha Furlan Polegato,[1] Renata Candido da Silva,[1]
Renan Turini Claro,[1] Paula Shmidt Azevedo,[1] Ana Angélica Fernandes,[2] Katashi Okoshi,[1]
Sergio Alberto Rupp de Paiva,[1] Marcos Ferreira Minicucci,[1]
and Leonardo Antônio Mamede Zornorff [ID][1]

[1]Internal Medicine Department, Botucatu Medical School, São Paulo State University (UNESP), Botucatu, Brazil
[2]Chemistry and Biochemistry Department, Institute of Biosciences of Botucatu, São Paulo State University (UNESP), Botucatu, Brazil

Correspondence should be addressed to Leonardo Antônio Mamede Zornorff; leonardo.zornoff@unesp.br

The objective of this study was to analyze the impact of different modalities and intensities of exercise training on cardiac remodeling started early after experimental myocardial infarction (MI). Male Wistar rats, weighing 200–250 g, were subjected to experimental MI. After 5 days, the animals were allocated into three experimental groups and observed for three months: S (sedentary control animals), C (animals subjected to continuous low-intensity training), and HIT (animals subjected to high-intensity interval training). Low-intensity exercise training was performed at a treadmill speed corresponding to 40% VO_2 max, which was kept unchanged throughout the entire session (i.e., continuous low-intensity training). High-intensity interval training was performed in such a way that rats run during 3 min at 60% VO_2 max, followed by 4-minute intervals at 85% VO_2 max (i.e., high-intensity interval training). After the follow-up period, we studied hypertrophy and ventricular geometry, functional alterations *in vivo* and *in vitro*, oxidative stress, apoptosis, and cardiac energetic metabolism. Our data showed that both high-intensity interval and continuous low-intensity modalities improved cardiac energetic metabolism variables in comparison with sedentary infarcted animals. In addition, high-intensity interval training decreased cardiac oxidative stress, associated with improved diastolic function. On the other hand, the continuous low-intensity group showed impairment of cardiac function. Therefore, altogether, our data suggest that high-intensity interval training could be the best modality for early physical exercise after MI and should be better studied in this clinical scenario.

1. Introduction

After myocardial infarction (MI), ventricular remodeling is associated with poor outcomes, mainly due to increased risk for ventricular dysfunction and cardiovascular death. Therefore, strategies to attenuate this process are fundamental tools in the management of patients with coronary occlusion, including reperfusion therapy, beta-blockers, and inhibitors of the renin-angiotensin system [1–4].

Exercise training started late after experimental MI is accepted as a strategy to attenuate the remodeling process [5–9]. However, the best time to start a training program

after a coronary occlusion remains to be elucidated. Indeed, during the healing phase, a number of factors may stimulate the progressive dilation of the heart by increasing ventricular wall stress. Importantly, it is postulated that early exercise might act as a parietal stressor, increasing the left ventricular dimensions [1]. In fact, in a previous study, our group showed that delayed exercise might be better than early exercise following coronary occlusion [10].

We must consider, however, that the remodeling process starts at very early stages after coronary occlusion. Thus, strategies initiated early could have greater repercussions in mitigating ventricular remodeling after MI. In addition, in
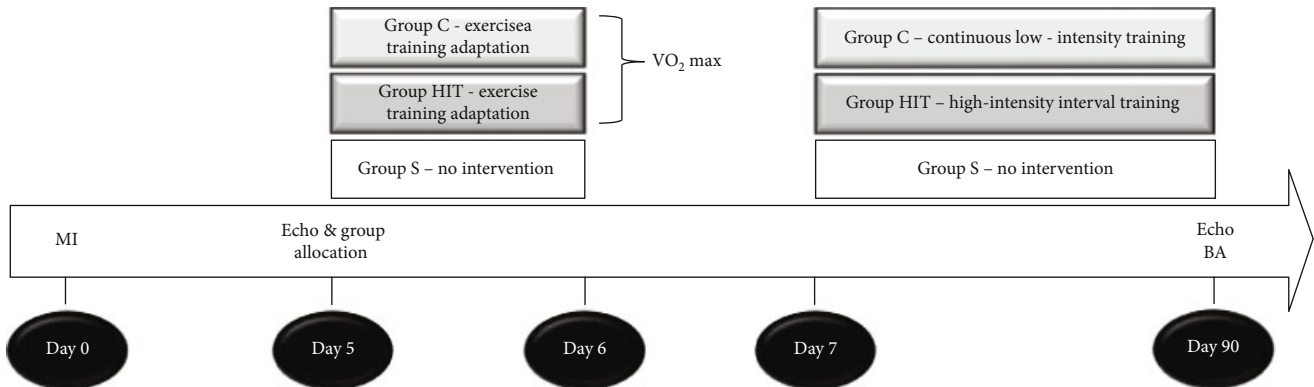
FIGURE 1: Experimental timeline. MI: myocardial infarction; echo: echocardiogram; VO_2 max: maximum oxygen uptake; BA: biochemical analysis.

recent years, new modalities of physical exercise have been introduced in different models with promising results, including interval training. Importantly, it remains unknown if modality and intensity of early exercise training, after MI, could also influence the remodeling process. Therefore, the objective of this study was to analyze the impact of different modalities and intensities of exercise training on cardiac remodeling started early after experimental MI.

2. Material and Methods

All experiments and procedures were performed in concordance with the National Institute of Health's Guide for the Care and Use of Laboratory Animals and were approved by the Animal Ethics Committee of our institution.

2.1. Experimental Groups.
The experimental timeline is shown in Figure 1. Male Wistar rats, weighing 200-250 g, were subjected to experimental MI, according to the method described previously [11, 12]. We selected only the animals with an infarct size greater than 35% as assessed by histologic analysis because we considered that animals with small infarct size do not undergo cardiac remodeling [13].

After 5 days of performing the surgical procedure of infarction induction, an initial echocardiographic study was performed to evaluate systolic and diastolic areas, fraction area changes, and infarct size, to guarantee homogeneity between the groups (data not shown).

After the initial echocardiographic study, the animals were allocated into three experimental groups and observed for three months: S (sedentary control animals), C (animals subjected to continuous low-intensity training), and HIT (animals subjected to high-intensity interval training).

2.2. Exercise Training Protocols.
Exercise training protocols started 5 days after surgical procedures. The speed started at 6 m/min and was increased by 3 m/min every 3 min until the rats could not run. The same protocol was also used to measure the maximum oxygen uptake (VO_2 max). The animals were placed inside a metabolic chamber (airflow inside the chamber (3.500 mL/min)). Low-intensity exercise training was performed at a treadmill speed corresponding to

40% VO_2 max, which was kept unchanged throughout the entire session (i.e., continuous low-intensity training). High-intensity interval training was performed in such a way that rats run during 3 min at 60% VO_2 max, followed by 4-minute intervals at 85% VO_2 max (i.e., high-intensity interval training), which was repeated seven times, so each HIT session lasted for 49 min. Similar to continuous low-intensity training, this protocol was kept unchanged throughout the entire session. Continuous low-intensity and HIT protocols were of matched volume, meaning that total running distances in each session of either continuous low-intensity training or HIT were identical [14]. The protocols were performed at 15° inclination, 5 days per week, over 3 months.

2.3. Echocardiographic Analysis.
At the end of the three-month follow-up, echocardiography was performed. The cardiac structures were measured according to previous methods in an infarcted rat model [15, 16]. The systolic (SA) and diastolic areas (DA) were measured in two dimensions through planimetry. The left ventricle (LV) function was assessed by calculating the fractional area change ($FAC = (DA - SA)/DA \times 100$), the posterior wall shortening velocity (PWSV), the Tei index, the E wave deceleration time (EDT), the isovolumetric relaxation time normalized to the heart rate ($IRT/RR^{0.5}$), and the S' wave and A' wave, assessed by tissular echocardiogram.

2.4. In Vitro Left Ventricular Function Analysis.
The procedures and measurements for assessing left ventricular function were performed following a previously described method [17]. The LV systolic function was assessed by the maximum systolic pressure (PS) and the maximum rate of ventricular pressure rise (+dP/dt). The LV diastolic function was assessed by the decreased maximum rate of ventricular pressure rise (-dP/dt).

2.5. Cardiac Energy Metabolism and Oxidative Stress.
By spectrophotometry, LV samples of approximately 200 mg were homogenized in sodium phosphate buffer (0.1 M, pH 7.0) and centrifuged at 10,000 rpm for 15 minutes at 4°C. The supernatant was used to determine the

TABLE 1: Echocardiographic data.

Variables	S ($n = 15$)	C ($n = 16$)	HHIT ($n = 15$)
LVDD (mm)	10.4 ± 0.9	10.6 ± 1.1	10.3 ± 1.2
LVSD (mm)	7.85 ± 1.0	8.21 ± 1.4	8.53 ± 0.2
EF (%)	0.57 ± 0.1	0.53 ± 0.1	0.50 ± 0.1
FAC (%)	36.5 ± 11.1	30.7 ± 13.4	33.9 ± 14.5
Tei index	0.56 (0.47-0.65)	0.69 (0.59-0.84)*	0.60 (0.55-0.66)
LVWT (mm/s)	29.7 ± 5.7	$19.3. \pm 6.7$	27.9 ± 7.4
EDT	43.3 ± 7.6	47.4 ± 8.7	$37.3 \pm 10.8^{\#}$
IRT/RR$^{0.5}$	$57.3 \pm 8.8^{\#}$	66.2 ± 9.1	$57.2 \pm 14.3^{\#}$
S'	3.10 ± 0.48	2.79 ± 0.35	3.09 ± 0.56
A'	3.29 ± 1.19	3.46 ± 0.86	$4.69 \pm 1.15^{*\#}$

S: sedentary control animals; C: continuous moderate intensity training; HIT: high-intensity interval training; LVDD: left ventricular diastolic diameter; LVSD: left ventricular systolic diameter; LVWT: posterior wall shortening velocity; FAC: fractional area change; IRT/RR$^{0.5}$: isovolumetric relaxation time normalized to the heart rate. Data are expressed as mean ± SD or medians (including the lower quartile and upper quartile). $^{*}P < 0.05$ versus S; $^{\#}P < 0.05$ versus C.

concentrations of protein, lipid hydroperoxide, and antioxidant enzymes and energy metabolism. The activities of the enzymatic complexes of the mitochondrial respiratory chain were determined after resuspension of the pellet in phosphate buffer containing 0.1 M sodium, 250 mM sucrose, and 2 mM ethylenediaminetetraacetic acid (EDTA) and centrifugation (10,000 rpm, 5 minutes, 4°C) according to an adapted technique [18].

The activities of lactate dehydrogenase (LDH), citrate synthase, β-hydroxyacyl-CoA dehydrogenase (β-OH-acyl-CoADH), phosphofructokinase (PFK), pyruvate dehydrogenase complex (PI-DH), NADH dehydrogenase (complex I), succinate dehydrogenase (complex II), and ATP synthase were measured by the method described previously [18].

Oxidative stress was assessed by determining the concentration of lipid hydroperoxide (LH). Glutathione peroxidase (GSH-Px) and catalase (CAT) activities were assessed as previously specified [19].

2.6. Statistical Analysis. The data were expressed as mean ± standard deviation (for normal distribution) or median with the 25th and 75th percentiles (for nonnormal distribution). Continuous variables were tested for normality; continuous variables with normal distribution were compared by ANOVA, completed by the Holm-Sidak test, while nonnormal continuous variables were compared by Kruskal-Wallis test, completed by the Dunn test. Data analysis was performed with SigmaStat for Windows v2.03 (SPSS, Inc., Chicago, IL, USA). The significance level was 5%.

3. Results

We subjected 140 animals to coronary occlusion. After 5 days, 50 rats died. In addition, 20 animals were discarded for having an infarct size of <35%. Therefore, our groups were composed of the following animals: S = 25, C = 25, and HIT = 22.

TABLE 2: Isolated heart data.

Variables	S ($n = 8$)	C ($n = 8$)	HIT ($n = 8$)
+dP/dt (mmHg/s)	1825 ± 496	1541 ± 557	1750 ± 337
−dP/dt (mmHg/s)	1375 ± 423	1208 ± 437	1200 ± 357
SP (mmHg)	100 ± 23.5	80 ± 12.1	93 ± 14.1

S: sedentary control animals; C: continuous moderate intensity training; HIT: high-intensity interval training; +dP/dt: maximum LV pressure development rate; −dP/dt: maximum LV pressure decrease rate; SP: systolic pressure. Data are expressed as mean ± SD. $P > 0.05$.

TABLE 3: Cardiac oxidative stress enzyme activity.

Variables	S ($n = 8$)	C ($n = 8$)	HIT ($n = 8$)
LH (nmol/mg of tissue)	251 ± 30.9	249 ± 55.7	$186 \pm 39.9^{*\#}$
CAT (μmol/g)	80.4 ± 11.5	86.5 ± 9.7	$119 \pm 15.7^{*\#}$
GSH-Px (nmol/mg)	22.5 ± 4.9	$33.1 \pm 2.9^{*}$	$41.1 \pm 7.7^{*\#}$

S: sedentary control animals; C: continuous moderate intensity training; HIT: high-intensity interval training; LH: lipid hydroperoxide; CAT: catalase; GSH-Px: glutathione peroxidase. Data are expressed as mean ± SD. $^{*}P < 0.05$ versus S; $^{\#}P < 0.05$ versus C.

There were no differences in body weight between the groups at the beginning of the experiment (S = 232 ± 28 g, C = 226 ± 18 g, and HIT = 229 ± 15 g; $P > 0.05$) or after 3 months (S = 504 ± 39 g, C = 483 ± 54 g, and HIT = 459 ± 11 g; $P > 0.05$).

There was no difference in infarct size between the groups (S = 47 ± 3.6%, C = 46 ± 4.2%, and HIT = 48 ± 2.5%; $P > 0.05$). Likewise, in the period of 3 months after the infarction, there was no difference in the mortality between the groups (S = 10, C = 7, and HIT = 7; $P > 0.05$).

The results of the echocardiographic study are shown in Table 1. The C group presented higher values of EDT than the HIT group and higher values of the Tei index than the S group. In addition, the C group presented higher values

TABLE 4: Cardiac energy metabolism.

Variables	S ($n = 8$)	C ($n = 8$)	HIT ($n = 8$)
Pyruvate dehydrogenase complex (nmol/g)	198 ± 39.5	165 ± 20.1	$217 \pm 35.4^{\#}$
Lactate dehydrogenase (nmol/g)	101 ± 9.4	$89.6 \pm 9.5^{*}$	$80.4 \pm 8.0^{*}$
β-Hydroxyacyl coenzyme-A dehydrogenase (nmol/mg)	18.1 ± 4.1	19.5 ± 4.6	$24.2 \pm 4.8^{*\#}$
Citrate synthase (nmol/g)	27.0 ± 7.0	35.4 ± 9.0	$74.7 \pm 9.9^{*\#}$
Complex I (NADH dehydrogenase) (nmol/mg)	3.2 (1.8-4.1)	5.1 (4.3-6.4)*	5.1 (3.9-6.0)*
ATP synthase (nmol/mg)	33.5 ± 7.2	$60.1 \pm 8.1^{*}$	$61.8 \pm 6.8^{*}$

S: sedentary control animals; C: continuous moderate intensity training; HIT: high-intensity interval training. Data are expressed as mean ± SD or medians (including the lower quartile and upper quartile). $^{*}P < 0.05$ versus S; $^{\#}P < 0.05$ versus C.

of IRT/RR$^{0.5}$ in comparison to groups HIT and S. The animals of the HIT group presented higher values of A' than the other groups. There was no difference in the other variables between the groups. Likewise, in the study of the isolated heart, we did not find differences among the groups (Table 2).

In relation to the results of oxidative stress, the animals of the HIT group presented higher values of the antioxidant enzymes catalase and glutathione peroxidase. As a consequence, intense interval exercise showed a decrease in oxidative stress, assessed by LH concentrations. Importantly, this phenomenon did not occur with the group of animals subjected to continuous exercise (Table 3).

Considering the data on energy metabolism, both trained groups presented a decrease in lactate dehydrogenase activity and increased ATP synthase and mitochondrial complex I activity. On the other hand, only the HIT group showed increased activity of β-hydroxyacyl coenzyme-A dehydrogenase, citrate synthase, and pyruvate dehydrogenase (Table 4).

4. Discussion

The objective of this study was to analyze the impact of different modalities and intensities of exercise training on cardiac remodeling started early after experimental MI. Our data showed that both high-intensity interval and continuous low-intensity modalities improved cardiac energetic metabolism variables in comparison with sedentary infarcted animals. In addition, high-intensity interval training decreased cardiac oxidative stress, associated with improved diastolic function. On the other hand, the continuous low-intensity group showed impairment of cardiac function.

As discussed earlier, the beneficial effects of late physical training after MI are unquestionable [5–9]. On the other hand, when physical exercise is started early after coronary occlusion, the results in the remodeling process are not uniform. In rats with large infarctions of the anterior wall, physical exercise started less than one week after coronary occlusion resulted in an increase in infarct expansion with dilation of the left ventricular cavity. The authors hypothesized that early physical exercise could increase parietal stress and stimulate the remodeling process [20–23]. In contrast, in mice and rats, nonintense physical exercise started one week after infarction of different sizes attenuated the remodeling

process or had no morphological repercussion [24–27]. Therefore, we can conclude that the effects of physical exercise after infarction depend on different variables, including infarct size, and the exercise protocol used. Importantly, the role of modality and intensity of early exercise training in ventricular remodeling after MI remains to be elucidated.

Our study showed that high-intensity interval training improved diastolic function. On the other hand, the continuous low-intensity group showed impairment of cardiac function, assessed by the Tei index and IRT/RR$^{0.5}$ ratio. Importantly, early exercise after MI did not improve systolic function. We have to consider that the beneficial effects of exercise initiated late after the experimental infarction are consensual, including improved systolic function. Therefore, our data reinforce the concept that, at least so far, late physical exercise protocols after infarction could be better than early physical exercise, regardless of the modality or intensity.

Reactive oxygen species and oxidative stress play a critical role in cardiac remodeling following several cardiac injuries [28, 29]. To protect against oxidative stress, a well-organized system of antioxidants works in a coordinated manner. In our study, both modalities increase antioxidant enzymes, but only the high-intensity interval training protocol decreased oxidative stress, assessed by LH. Therefore, considering the redox system, we can conclude that HIT was superior to continuous low-intensity training.

Another potential mechanism involved in the action of exercise training on cardiac remodeling is related to cardiac energy metabolism [30]. The remodeled heart exhibits several changes in energy metabolism, including a fuel preference shift, decreased fuel amount, mitochondrial abnormalities, and impaired transport of energy from mitochondria to the site of utilization. Data on energy metabolism suggest that, despite some specific differences, in general, high-intensity interval training increased the energy substrate and mitochondrial phosphorylation activity, more evident than continuous low-intensity training.

Finally, our data showed that the evident benefits in oxidative stress and cardiac energy metabolism in the high-intensity interval training group did not result in improved systolic function, which is a critical variable in the assessment of cardiac remodeling. However, we must understand that the temporal evolution of the remodeling process could

explain these apparently discrepant results. In fact, the first event in this process is a stimulus to the heart, including hemodynamic overload, loss of myocytes, cardiac inflammation, genetic changes, and toxic injuries. As a consequence, fetal genes are reexpressed. This phenomenon, in turn, results in deleterious cardiac responses in different pathways, including inflammatory systems, cell death, collagen accumulation, energy metabolism deficit, and oxidative stress. Finally, as a result of these events, the remodeling process is associated with changes in cardiac morphological and functional variables [1–4]. Therefore, with a longer follow-up time, we believe that the beneficial biochemical changes induced by high-intensity interval training in this study would result in cardiac systolic functional improvement.

In conclusion, both high-intensity interval and continuous low-intensity modalities improved cardiac energetic metabolism variables. In addition, the high-intensity interval modality decreased cardiac oxidative stress, associated with improved diastolic function. On the other hand, a continuous low-intensity training group showed impairment of cardiac function. Therefore, altogether, our data suggest that high-intensity interval training could be the best modality for early physical exercise after MI and should be better studied in this clinical scenario.

Data Availability

The authors confirm that the data supporting the findings of this study are available within the article.

Conflicts of Interest

The authors declare that there is no conflict of interest regarding the publication of this paper.

Authors' Contributions

DFB conceived the experiments, contributed to research data, and drafted the manuscript. BFP, RCS, RTC, PSA, and AAF contributed to research data and data analysis. SARP and MFM supervised the analysis and revised the manuscript. LAMZ designed the experiments, revised the manuscript, and supervised the analysis. All authors read and approved the final manuscript.

Acknowledgments

References

[1] M. A. Pfeffer and E. Braunwald, "Ventricular remodeling after myocardial infarction: experimental observations and clinical implications," *Circulation*, vol. 81, no. 4, pp. 1161–1172, 1990.

[2] L. A. M. Zornoff, S. A. R. Paiva, D. R. Duarte, and J. Sparado, "Ventricular remodeling after myocardial infarction: concepts and clinical implications," *Arquivos Brasileiros de Cardiologia*, vol. 92, no. 2, pp. 157–164, 2009.

[3] J. N. Cohn, R. Ferrari, and N. Sharpe, "Cardiac remodeling-concepts and clinical implications: a consensus paper from an international forum on cardiac remodeling," *Journal of the American College of Cardiology*, vol. 35, no. 3, pp. 569–582, 2000.

[4] P. S. Azevedo, B. F. Polegato, M. F. Minicucci, S. A. Paiva, and L. A. Zornoff, "Cardiac remodeling: concepts, clinical impact, pathophysiological mechanisms and pharmacologic treatment," *Arquivos Brasileiros de Cardiologia*, vol. 106, no. 1, pp. 62–69, 2016.

[5] D. M. Guizoni, S. A. Oliveira-Junior, S. L. R. Noor et al., "Effects of late exercise on cardiac remodeling and myocardial calcium handling proteins in rats with moderate and large size myocardial infarction," *International Journal of Cardiology*, vol. 221, pp. 406–412, 2016.

[6] Z. Daliang, Y. Lifang, F. Hong et al., "Netrin-1 plays a role in the effect of moderate exercise on myocardial fibrosis in rats," *PLoS One*, vol. 14, no. 2, article e0199802, 2019.

[7] M. A. Garza, E. A. Wason, J. R. Cruger, E. Chung, and J. Q. Zhang, "Strength training attenuates post-infarct cardiac dysfunction and remodeling," *The Journal of Physiological Sciences*, vol. 69, no. 3, pp. 523–530, 2019.

[8] M. Donniacuo, K. Urbanek, A. Nebbioso et al., "Cardioprotective effect of a moderate and prolonged exercise training involves sirtuin pathway," *Life Sciences*, vol. 222, pp. 140–147, 2019.

[9] N. Naderi, M. Hemmatinafar, A. A. Gaeini et al., "High-intensity interval training increase GATA4, CITED4 and c-Kit and decreases C/EBPβ in rats after myocardial infarction," *Life Sciences*, vol. 221, pp. 319–326, 2019.

[10] D. F. Batista, A. F. Gonçalves, B. P. Rafacho et al., "Delayed rather than early exercise training attenuates ventricular remodeling after myocardial infarction," *International Journal of Cardiology*, vol. 170, no. 1, pp. e3–e4, 2013.

[11] J. M. Pfeffer, P. V. Finn, L. A. Zornoff, and M. A. Pfeffer, "Endothelin-A receptor antagonism during acute myocardial infarction in rats," *Cardiovascular Drugs and Therapy*, vol. 14, no. 6, pp. 579–587, 2000.

[12] S. A. R. Paiva, R. Novo, B. B. Matsubara et al., "β-Carotene attenuates the paradoxical effect of tobacco smoke on the mortality of rats after experimental myocardial infarction," *Journal of Nutrition*, vol. 135, no. 9, pp. 2109–2113, 2005.

[13] M. F. Minicucci, P. S. Azevedo, P. F. Martinez et al., "Critical infarct size to induce ventricular remodeling, cardiac dysfunction and heart failure in rats," *International Journal of Cardiology*, vol. 151, no. 2, pp. 242-243, 2011.

[14] J. B. N. Moreira, L. R. G. Bechara, L. H. M. Bozi et al., "High- versus moderate-intensity aerobic exercise training effects on skeletal muscle of infarcted rats," *Journal of Applied Physiology*, vol. 114, no. 8, pp. 1029–1041, 2013.

[15] P. S. Azevedo, M. F. Minicucci, F. Chiuso-Minicucci et al., "Ventricular remodeling induced by tissue vitamin A deficiency in rats," *Cellular Physiology and Biochemistry*, vol. 26, no. 3, pp. 395–402, 2010.

[16] M. F. Minicucci, P. S. Azevedo, S. A. Oliveira Jr et al., "Tissue vitamin A insufficiency results in adverse ventricular remodeling after experimental myocardial infarction," *Cellular Physiology and Biochemistry*, vol. 26, no. 4-5, pp. 523–530, 2010.

[17] R. A. C. Silva, A. F. Gonçalves, P. P. dos Santos et al., "Cardiac remodeling induced by all-trans retinoic acid is detrimental in

normal rats," *Cellular Physiology and Biochemistry*, vol. 43, no. 4, pp. 1449–1459, 2017.

[18] H. B. Assalin, B. P. Rafacho, P. P. . Santos et al., "Impact of the length of vitamin d deficiency on cardiac remodeling," *Circulation Heart Failure*, vol. 6, no. 4, pp. 809–816, 2013.

[19] A. F. Gonçalves, B. F. Polegato, A. A. Fernandes et al., "Zinc supplementation attenuates cardiac remodeling after experimental myocardial infarction," *Cellular Physiology and Biochemistry*, vol. 50, no. 1, pp. 353–362, 2018.

[20] P. Gaudron, K. Hu, R. Schamberger, M. Budin, B. Walter, and G. Ertl, "Effect of endurance training early or late after coronary artery occlusion on left ventricular remodeling, hemodynamics, and survival in rats with chronic transmural myocardial infarction," *Circulation*, vol. 89, no. 1, pp. 402–412, 1994.

[21] M. Jain, R. Liao, S. Ngoy, P. Whittaker, C. S. Apstein, and F. R. Eberli, "Angiotensin II receptor blockade attenuates the deleterious effects of exercise training on post-MI ventricular remodelling in rats," *Cardiovascular Research*, vol. 46, no. 1, pp. 66–72, 2000.

[22] R. A. Kloner and J. A. Kloner, "The effect of early exercise on myocardial infarct scar formation," *American Heart Journal*, vol. 106, no. 5, pp. 1009–1013, 1983.

[23] H. Hammerman, F. J. Schoen, and R. A. Kloner, "Short-term exercise has a prolonged effect on scar formation after experimental acute myocardial infarction," *Journal of the American College of Cardiology*, vol. 2, no. 5, pp. 979–982, 1983.

[24] M. C. de Waard, J. van der Velden, V. Bito et al., "Early exercise training normalizes myofilament function and attenuates left ventricular pump dysfunction in mice with a large myocardial infarction," *Circulation Research*, vol. 100, no. 7, pp. 1079–1088, 2007.

[25] V. Bito, M. C. de Waard, L. Biesmans et al., "Early exercise training after myocardial infarction prevents contractile but not electrical remodelling or hypertrophy," *Cardiovascular Research*, vol. 86, no. 1, pp. 72–81, 2010.

[26] X. Xu, W. Wan, L. Ji et al., "Exercise training combined with angiotensin II receptor blockade limits post-infarct ventricular remodelling in rats," *Cardiovascular Research*, vol. 78, no. 3, pp. 523–532, 2008.

[27] X. Xu, W. Wan, A. S. Powers et al., "Effects of exercise training on cardiac function and myocardial remodeling in post myocardial infarction rats," *Journal of Molecular and Cellular Cardiology*, vol. 44, no. 1, pp. 114–122, 2008.

[28] P. F. Martinez, C. Bonomo, D. M. Guizoni et al., "Modulation of MAPK and NF-KB signaling pathways by antioxidant therapy in skeletal muscle of heart failure rats," *Cellular Physiology and Biochemistry*, vol. 39, no. 1, pp. 371–384, 2016.

[29] P. F. Martinez, C. Bonomo, D. M. Guizoni et al., "Influence of N-acetylcysteine on oxidative stress in slow-twitch soleus muscle of heart failure rats," *Cellular Physiology and Biochemistry*, vol. 35, no. 1, pp. 148–159, 2015.

[30] P. S. Azevedo, M. F. Minicucci, P. P. Santos, S. A. R. Paiva, and L. A. M. Zornoff, "Energy metabolism in cardiac remodeling and heart failure," *Cardiology in Review*, vol. 21, no. 3, pp. 135–140, 2013.